

PALACKÝ UNIVERSITY OLOMOUC
Faculty of Science
Department of Biochemistry



Genetic Control of Pluripotency
in Plants

Ph.D. Thesis

Author: **Mgr. Ivona Kubalová**
Study program: P1416 Biochemistry
Supervisor: **Yoshihisa Ikeda Ph.D.**
Date: 2019

I hereby declare that this Ph.D. thesis has been written solely by me. All the sources cited in this thesis are listed in the “Reference” section. All published results included in this work are approved by co-authors.

October 01, 2018

.....

Acknowledgment

I would like to thank my supervisor Dr. Yoshihisa Ikeda for teaching me everything I know about plant science, his help, advice, and patience when explaining the tangled genetic-framework.

This thesis would not have been completed without encouragement from my brother-like colleague David Zalabák. Thank you for keeping me sane in every moment of hysteria, for a daily portion of inside jokes, and endless disputes including green tea ☺

Special thanks go to an incredible “Chromosome Structure and Function” group of Prof. Andreas Houben at IPK, Gatersleben Germany. I spent there memorable moments with amazing people. Many thanks, Andreas for the opportunity you gave me. I want to thank Jörg, my paradigm of a cool scientist, for hours he spent by sorting my numerous samples; Veit for the super-resolution microscopy and consultation; Katrin and Oda for the great technical work; and the rest members of the group for making this such an awesome place to work every day! Especially, I would like to thank Celia; I really enjoyed our conversation and chocolate.

I want to acknowledge Petr Vojta who performed RNA-seq and analysis, Andreas, Veit, David, and Tomáš for reading my thesis and suggestions which improved its quality.

I'd like to give another special thank to my family; my mom and dad, for their support over the years; my sister Veronika for never-ending WhatsApp chat.

I thank my fellow labmates from Molecular Biology Department for the help and the fun; particularly Alžbeta, Eva, Karolina, and Míša for all voucher and other sessions; Kerolajna for inappropriate jokes and great office company; Kristýna for her inspiring life energy; Pepa for his excellent knowledge and wonderful character; and Veronika for her hilarious stories that made me laugh every time.

I am also grateful

to Katka Holubová for her trying to teach me to socialize and for each life advice, I have never listened to.

to Maja Janíková for the lifts and asylum.

to Lucia and Tomáš for bike trips and every cake, I ate them.

to Ivan for gossiping about *Arabidopsis*.

to Petra, fellow-fighter in teaching.

to my friends who accompanied me through all my studies for being on my side no matters what, especially Meggie, my old friend.

to all amazing people, I had the chance to meet during my Ph.D. study, particularly, a person who made me stronger than ever.

In the end, I would like to thank my high-school biology teacher, Iveta Letková, for showing me the beauty of Biology.

Bibliografická identifikácia:

Meno a priezvisko autora	Mgr. Ivona Kubalová
Názov práce	Genetická kontrola rastlinnej pluripotencie
Typ práce	Dizertačná
Pracovisko	Centrum regionu Haná pro biotechnologický a zemědělský výzkum, PřF UP
Vedúci práce	Yoshihisa Ikeda, Ph.D.
Rok obhajoby práce	2019

Abstrakt

Nesmrtelnost' spojená s obnovou starých a poškodených tkanív fascinovala ľudí od nepamäti. Žiarivým príkladom regenerácie sú rastliny. Ich schopnosť nahrádzať staré orgány novými bunkami a pletivami stojí dlhodobo v značnej pozornosti vedy. Len pred niekoľkými desaťročiami odhalilo štúdium zamerané na molekulárne mechanizmy podmieňujúce regeneračný proces WUSCHEL proteín ako kľúčový komponent.

V tejto práci sme rozvinuli WUSCHEL nezávislú dráhu, ktorá prispieva k správne umiestneniu a udržovaniu apikálneho meristému stonky. Navrhli sme ETHYLENE RESPONSIVE FACTOR (ERF) transkripčné faktory ako nové komponenty regulujúce túto dráhu. Štvornásobný *wus;erf4-1;8;9-1;10;11-2;12* mutant dokázal produkovať apikálny meristém stonky počas vegetatívnej fázy rastu aj napriek chýbajúcemu WUS. Tiež sme analyzovali expresný profil *CUC1*, *STM*, *ESR1* a *ESR2* génov v *erf4-1;8;9-1;11-2;12* a *erf4-1;8;9-1;10;12* mutantnej línii a zistili sme zvýšenú relatívnu expresiu meristemických regulátorov.

Následne sme ukázali, že ERF4 lokalizuje v euchromatíne v rámci jadra a je vylúčený z heterochromatínu. ERF4 nie je umiestnený v jadrových telieskach. Tiež sme zistili, že ERF4 môže ovplyvniť acetylačný stav rozličných lyzínových rezíduí na históne 3. Optimálna aktivita tejto dráhy závisí od vzniku a zániku ERF proteínov. Ubikvitínom sprostredkovaná proteínová degradácia je pravdepodobne krok, ktorý limituje funkciu ERF proteínov.

Zároveň sme rozšírili súčasnú problematiku regulácie *WUSCHEL* a ukázali sme dôležitosť komunikácie z plastidov do jadra a jej vplyv na expresiu *WUSCHEL*. Stanovili sme novú metódu na rýchlu kvantifikáciu chlorofylu z jedného koreňového odrezku. Analýzou rozličných mutančných línií v biosyntéze tetrapyrolu sme identifikovali hem ako možnú kandidátnu molekulu retrográdnej signalizácie.

Kľúčové slová *Arabidopsis thaliana*, ERF, WUS, transkripčné represory, pletivové kultúry, regenerácia výhonov, sub-celulárna lokalizácia, super-rezolučná mikroskopia, acetylácia histónov, chlorofyl, retrográdna signalizácia

Počet strán 160

Počet príloh 2

Jazyk Anglický

Bibliographical identification:

Author's first name and last name	Mgr. Ivona Kubalová
Title	Genetic Control of Pluripotency in Plant
Type of thesis	Ph.D.
Department	Centre of the Region Haná for Biotechnological and Agricultural Research, Faculty of Science, Palacký University
Supervisor	Yoshihisa Ikeda, Ph.D.
The year of presentation	2019

Abstract

People were fascinated by immortality accompanied by renewal of old and sick tissue since ancient times. Plants are a shining example of regeneration ability. Their competence to produce new cells, tissues and thus replenish the old organs throughout plant lifespan is of great interest in science. Just a few decades ago the molecular mechanisms behind these processes started to be unveiled and WUSCHEL being found as the key player.

Here we elaborated a WUSCHEL-independent pathway of shoot apical meristem (SAM) positioning and maintenance and proposed ETHYLENE RESPONSIVE FACTOR (ERF) transcriptional repressors as novel components regulating this pathway. The quintuple *wus;erf4-1;8;9-1;10;11-2;12* could restore the SAM formation throughout the vegetative growth in *wus* mutant background. The expression profile of *CUC1*, *STM*, *ESR1*, and *ESR2* in *erf4-1;8;9-1;11-2;12* and *erf4-1;8;9-1;10;12* mutants was also investigated. The elevated relative expression of these SAM regulators was detected.

Further, we showed that ERF4 is predominantly localized in nuclear euchromatin and it is excluded from heterochromatin. ERF4 did not localize in nuclear bodies. Also, we have found out that ERF4 might influence the acetylation status of various lysine residues at histone 3

Turnover of ERF proteins is essential for the accurate activity of this pathway. Ubiquitin-mediated protein degradation seems to be the limiting step regulating the ERF's function.

Additionally, we extended our recent knowledge of *WUSCHEL* regulation as we showed the importance of plastid-to-nucleus communication on nuclear *WUSCHEL* expression. Therefore, we established a new high-throughput method for chlorophyll quantification from a single root explant. Using different mutants in tetrapyrrole biosynthesis we hypothesize Heme as a plausible candidate molecule of retrograde signaling.

Keywords *Arabidopsis thaliana*, ERF, WUS, transcriptional repressors, tissue culture, shoot regeneration, subcellular localization, super-resolution microscopy, histone acetylation, chlorophyll, retrograde signaling

Number of Pages 160

Number of Appendices 2

Language English

Table of Contents

Acknowledgment.....	iii
Bibliografická identifikácia:	iv
Bibliographical identification:	vi
Table of Contents	viii
Aims of Work	1
Introduction.....	2
PART I – Placing ERF transcriptional repressors into genetic framework regulating Shoot Apical Meristem development	4
1 Introduction.....	5
1.1 Totipotency, pluripotency, multipotency, and unipotency.....	5
1.2 Tissue culture	5
1.3 Shoot apical meristem.....	8
1.4 Root apical meristem	13
1.5 ETHYLENE RESPONSIVE FACTORS.....	14
1.6 Protein degradation	17
1.7 Histone acetylation, transcriptional repression, and development.....	20
1.8 HDA-facilitated transcriptional repression	23
2 Material and Methods	27
2.1 Plant material	27
2.2 Growth conditions.....	27
2.3 Plant selection	28
2.4 Genomic DNA isolation and PCR genotyping	28
2.5 RNA extraction and cDNA synthesis	31
2.6 Semi-quantitative RT-PCR	31
2.7 Quantitative RT-PCR analysis (qRT-PCR)	32
2.8 Shoot regeneration assay.....	33
2.9 Constructs preparation	33
2.10 Constructs preparation for CRISPR/Cas9.....	41
2.11 RNA-seq	43
2.12 Yeast two-hybrid assay (Y2H).....	43
2.13 Chemical treatment	44
2.14 Whole-mount immuno-fluorescence.....	44
2.15 Nuclei isolation and sorting	45

2.16	Immunostaining	45
2.17	Microscopic analysis of co-immunostained nuclei and whole-mount immunostained seedlings	47
2.18	Live-cell imaging	47
3	Results.....	48
3.1	Selection of T-DNA insertion lines of <i>ERF</i> and <i>BPM</i> genes.....	48
3.2	Proteolysis is essential for the correct development	55
3.3	<i>ERF</i> proteins can interact with <i>BPM</i> adaptor proteins of E3 ligase.....	56
3.4	Direct candidate target genes of <i>ERF4</i>	58
3.5	Evaluation of shoot regeneration in higher-order mutants.....	63
3.6	Phenotypic characterization of <i>erf4-1;8;9-1;12</i> quadruple mutant.....	67
3.7	Quadruple mutant in <i>ERF</i> genes could partially rescue aberrant SAM in <i>wuschel</i> mutant 68	
3.8	Higher-order <i>erf</i> mutants show opposite relative <i>ESR1</i> and <i>ESR2</i> gene expression 69	
3.9	Higher-order <i>erf</i> mutants display alteration in relative <i>CUC1</i> and <i>STM</i> gene expression	71
3.10	Expression pattern and sub-cellular localization of <i>ERF4</i>	73
3.11	<i>ERF4</i> is more often associated with the active than with the inactive RNAPoIII variant 75	
3.12	The impact of <i>ERF4</i> on the acetylation of histone H3.....	77
4	Discussion.....	88
4.1	Proper proteolysis of transcriptional factors is essential for correct plant development.....	88
4.2	<i>WUSCHEL</i> -independent pathway.....	90
4.3	Role of <i>ERF4</i> in gene expression regulation.....	95
4.4	<i>ERF4</i> affects histone acetylation.....	97
4.5	Can mutation in <i>ERF</i> repressors cause enlargement of SAM?	98
PART II – Chlorophyll Measurement as a Quantitative Method for the Assessment of Cytokinin-Induced Green Foci Formation in Tissue Culture		
5	Abstract.....	101
6	Introduction.....	102
7	Materials and methods	103
7.1	Plant material and growth conditions.....	103
7.2	Semi-quantitative RT-PCR analysis	104
7.3	Chlorophyll extraction, measurement, and statistical analysis	104
8	Results.....	106

8.1	Employment of bead disruption for efficient and consistent chlorophyll extraction from cultured tissue.....	106
8.2	Validation of chlorophyll measurement as an objective greening phenotype analysis method in tissue culture	107
9	Discussion.....	110
PART III – Mutations in Tetrapyrrole Biosynthesis Pathway Uncouple Nuclear		
<i>WUSCHEL</i> Expression from <i>de novo</i> Shoot Development in <i>Arabidopsis</i>		
10	Abstract.....	112
11	Introduction.....	113
12	Materials and Methods.....	115
12.1	Plant material	115
12.2	Growth conditions.....	116
12.3	Chlorophyll measurement	116
12.4	Shoot regeneration assay.....	116
12.5	Quantitative RT-PCR analysis (qRT-PCR)	116
13	Results.....	118
13.1	WUS expression and <i>de novo</i> SAM formation are coupled in altered cytokinin response mutants.....	118
13.2	WUS expression is uncoupled from <i>de novo</i> SAM formation in mutants defective in tetrapyrrole biosynthesis	119
14	Discussion.....	123
Conclusions.....		124
References.....		127
Abbreviations		139
Curriculum vitae.....		143
Supplements.....		146
	A) Chlorophyll Measurement as a Quantitative Method for the Assessment of Cytokinin-Induced Green Foci Formation in Tissue Culture	146
	B) Mutations in Tetrapyrrole Biosynthesis Pathway Uncouple Nuclear <i>WUSCHEL</i> Expression from <i>de novo</i> Shoot Development in <i>Arabidopsis</i>	153

Aims of Work

- literature review
- preparation of higher-order mutants and evaluation of their shoot regeneration efficiency phenotype
- placing ERF transcriptional repressors into the regulatory network of the shoot apical meristem development
- subcellular localization of ERF4 and monitoring the acetylation status of histone H3 in cells overexpressing *ERF4*
- establishment of a high-throughput method for chlorophyll measurements from single root explants
- study of WUSCHEL regulation in tetrapyrrole mutants

Introduction

Plants as sessile organisms had to evolve an effective system of how to cope with changing environmental cues. In contrast to animals, that usually lack the pluripotent stem cells after the establishment of their body; plants retain them through their whole lifespan. The pluripotent stem cells can replenish any given type of plant cells and therefore develop new organs and tissues. They are located in a specialized microenvironment called stem cell niche, which is a part of a meristem, a place where all new organs and tissues are established. There are three different meristem types in plant body: shoot, root, and vasculature meristems. Shoot and root meristems are situated at opposite ends of the plant body, therefore known as a shoot apical meristem (SAM) and a root apical meristem (RAM) (Heidstra and Sabatini, 2014).

Phytohormones play an eminent role in mediating responses to the external and internal stimuli as well as in coordinating plant development. The key players in this process are auxin and cytokinins. An effective and broadly used approach to study plant development, including regeneration and gene expression profiling, is an *in vitro* tissue culture system manipulated by phytohormones (Sugimoto et al., 2010). The employment of this tool helps us to better understand the pluripotency and regeneration programs *in planta*. The *Arabidopsis* model plant was used in this work to discover the shoot regeneration mechanism. Because *de novo* shoot development starts from lateral root primordia (LRP) (Sugimoto et al., 2010), we investigated this phenomenon using explants prepared from *Arabidopsis* roots in combination with an *in vitro* tissue culture system.

Master key regulator of this process is the transcription factor WUSCHEL (WUS) and its regulation seems to be crucial for a correct SAM development (Laux et al., 1996). The proper spatial-temporal gene expression plays an important role during plant development.

Gene expression is controlled by a plethora of transcription factors which can act in a positive or negative manner. Negative regulators, so-called transcriptional repressors, often form complexes with co-repressors and thus moderate the expression of the target genes. Fine-tuning of gene expression is mediated by epigenetic modification of chromatin, including conformational changes (chromatin remodeling)

or chemical modification of DNA (methylation) or histones (histone acetylation, methylation, and phosphorylation) (Reynolds et al., 2013; Wang et al., 2016). Additionally, the non-coding RNAs were shown to contribute to epigenetic regulation of gene transcription as well (Heo and Sung, 2011; Deforges et al., 2019).

Increasing evidence strongly implies the existence of parallel WUSCHEL-independent pathways regulating SAM positioning and maintenance. In this study, we analyzed ETHYLENE RESPONSIVE FACTOR (ERF) transcriptional repressors and placed them into the regulation network leading to shoot development. We propose ERF transcriptional factors being novel key players in a WUSCHEL-independent pathway that contributes to SAM maintenance.

Despite the fact that the WUS-dependent pathway is of main interest for several decades (Clark et al., 1993; Laux et al., 1996; Baurle, 2005; Meng et al., 2017; Snipes et al., 2018), the WUS regulation is still not completely understood. *De novo* shoot regeneration is induced by a higher concentration of cytokinins. It is well known that cytokinins affect plant development in three aspects 1) by promoting shoot regeneration, 2) by etioplast to chloroplast transition, and 3) by changing nuclear gene expression. To further investigate the relationship between these three aspects we have asked whether plastid-to-nucleus communication has an impact on SAM development.

Although it was previously shown that plastid-to-nucleus signalization controls the expression of genes involved in photosynthesis (Susek et al., 1993; Woodson et al., 2011) little is known whether and how plastid-to-nucleus signaling is involved in the regulation of genes responsible for the SAM development. In this work, we focused on answering this question by using mutants in tetrapyrrole biosynthesis (Terry and Smith, 2013). To effectively evaluate the chlorophyll content we established a high-throughput method for chlorophyll measurements from a single root explant.

Here we report that the plastid-to-nucleus communication influences the expression of the master key regulator *WUSCHEL*.

**PART I – Placing ERF transcriptional
repressors into genetic framework regulating
Shoot Apical Meristem development**

1 Introduction

1.1 Totipotency, pluripotency, multipotency, and unipotency

The adult body consists of stem cells sustaining different levels of regeneration capacity. The classification based on animal stem cell research recognizes totipotent, pluripotent, multipotent, and pluripotent stem cells. By definition, the totipotent stem cells are able to regenerate the whole new body including embryo. On the other hand, pluripotent stem cells can proliferate and consecutively differentiate into three germ cell layers but not into the embryonic tissue. Multipotent stem cells can give rise to any tissues from the same germline while unipotent stem cells can produce only the same type of cells (Dua et al., 2003; Serafini and Verfaillie, 2006). Definition of plant stem cells is taken from the animal terminology; hence it does not fit perfectly. Meristematic plant stem cells can give rise to all cell types of above-ground tissue and root but their behavior resembles more multipotent animal stem cells (Gaillochot and Lohmann, 2015). Verdail et al. (2007) proposed an extended plant stem cell concept. In accordance with this concept, single somatic cells can de-differentiate to a totipotent embryonic cell under certain conditions. Thus, a totipotent cell can lead to the whole plant body through somatic embryogenesis (Verdeil et al., 2007).

However, not all plant cells sustain the same regeneration capacity. There are cells capable to re-enter the cell cycle and thus they can produce new shoots and roots without previous induction of pluripotency (Atta et al., 2009). This is called direct regeneration. If such cells are missing, indirect regeneration is required (Atta et al., 2009; Duclercq et al., 2011).

1.2 Tissue culture

Tissue culture under controlled sterile conditions represents an elegant system for studying plant regeneration. Excised plant tissues are cultivated on a growth medium with a defined composition supplemented with phytohormones that determine the subsequent plant cell fate (Kumar and Loh, 2012). In principle, the plant cell identity can be manipulated by changing the ratios of two major plant hormones; auxin (AUX) and cytokinin (CK). The tissue culture system became a powerful tool for studying plant development since its establishment in the 1950s (Valvekens et al., 1988).

In most cases, regeneration of the plant body is a two-step procedure involving different types of media. Plant explants are placed firstly on a callus induction medium (CIM) containing a high concentration of both auxin and cytokinin. During this period, plant cells acquire competence to respond to signals leading to the production of shoots. Stimulated cells start to proliferate and form a callus. The term callus describes a mass of unorganized, growing plant cells. Subsequently, explants can be transferred onto shoot induction medium (SIM) containing a high ratio of cytokinin to auxin to induce a shoot formation, or onto a root induction medium (RIM) with a high auxin to cytokinin ratio to produce roots (Figure 1) (Skoog and Miller, 1957; Valvekens et al., 1988; Ikeuchi et al., 2013).

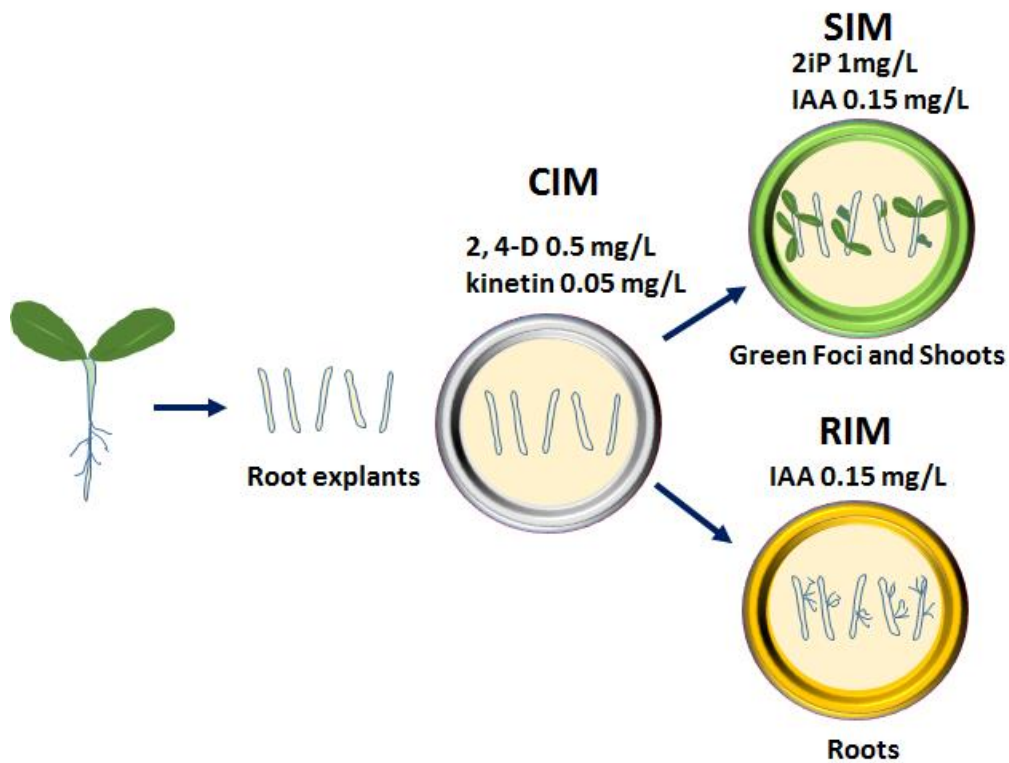


Figure 1 Tissue culture system. Plants explants are pre-incubated on callus induction (CIM) medium containing higher auxin (2-4D) to cytokinin (kinetin) ratio. Cells acquire competence to respond to signals leading to organ development. After 4 days explants are transferred onto shoot induction medium (SIM) with high cytokinin content (iPA); cells lose their root commitment and adopt shoot cell fate program; green foci are formed after few days incubation; finally, new green shoots are developed. Alternatively, explants are transferred onto the root induction medium (RIM) with auxin (IAA) only; new roots are developed from explants.

Pericycle cells of intact roots are a source of lateral root formation and are arrested in the G1 phase of the cell cycle. It has been shown that pericycle cells in the root explants

start to proliferate and differentiate, and stop to express the pericycle cell-specific marker genes. Cells acquire competence to produce green callus after 1 day of pre-incubation on CIM, without undergoing cell divisions. Two to three days-long incubation on CIM is necessary to acquire competence to produce shoots. However, root explants can still produce roots when transferred back to hormone-free medium even after 4 days on CIM. They lose their root commitment only when transferred to the SIM (Dubrovsky et al., 2000; Cary et al., 2002; Che et al., 2007).

Atta et al. (2009) showed that shoots can regenerate from the pericycle cells adjacent to xylem poles. Interestingly, xylem pericycle, but not phloem pericycle, could give rise to shoots without prior CIM incubation, when grown on CK rich medium (Atta et al., 2009). This indicates that pericycle cells sustain pluripotency. Moreover, pericycle cells retain a diploid status and do not undergo multiple rounds of endoreduplication. This attribute allows them to re-enter the cell cycle and to regenerate meristems (Atta et al., 2009). The protuberances emerging from the root and hypocotyl explants cultivated on CIM resemble a lateral root meristem (LRM). After transfer to SIM, the LRM-like structures develop into shoots. Thus the authors proposed that SAM regeneration during shoot regeneration process is a result of re-determination of LRM-like primordia and not de-differentiation process (reprogramming process back to an undifferentiated stage) (Atta et al., 2009).

Because plants are able to regenerate new organs not only from roots or hypocotyls, it was uncertain whether callus derived from different tissues has the same regenerative properties and the same mechanisms to drive the regeneration itself. Sugimoto et al. (2010), used cotyledons and petals to produce calli and found out that these calli also show features of the root tip. They employed the pericycle marker line J0121 (GAL4-GFP enhancer trap line) (Laplaze et al., 2005) to investigate pericycle-like cells in aerial organs. They observed strong GFP expression around the vasculature tissue. On the molecular level, calli derived from cotyledons and petals are enriched in root tip-specific genes but not in elongation and maturation zone-expressed genes. Taken together, callus formation from various organs occurs *via* lateral root initiation program and it is not a process of reprogramming to an undifferentiated state. The pericycle and pericycle-like cells, present in the organs, undergo differentiation toward root meristem-like tissue (Sugimoto et al., 2010).

The molecular mechanisms beyond competence acquisition were examined only in recent years. Global analyses of gene expression pattern during shoot *in vitro* regeneration showed that the expression of the majority of genes remains unchanged. Only a small set of genes undergo transient expression during this process, especially transcription factors and signaling components (Che et al., 2002). WUSCHEL (WUS), ARABIDOPSIS RESPONSE REGULATOR (ARR) 15 and POLYGALACTURONASE INHIBITING PROTEIN (PGIP) 2 are upregulated on SIM but all require initial CIM pre-incubation. ARR15 and PGIP2 are developmental markers for competency acquisition to form callus tissue, whereas WUS is connected with the ability to set shoots (Che et al., 2007).

1.3 Shoot apical meristem

The shoot apical meristem (SAM) is a source of all above-ground tissue and therefore its functionality through the plant lifespan is essential. It is localized at the shoot apex and resembles a dome-shaped structure. SAM is organized into several functionally distinct zones. The central zone (CZ), with very low cell division rate, comprises the stem cell niche and organizing center (OC). OC is responsible for the maintenance of the stem cells and also provides signals to stop differentiation. The peripheral zone (PZ) surrounds CZ from both sides of SAM and contains dividing cells destined to generate leaf and flower primordia. CZ and PZ are composed of three distinct clonal tissue monolayers marked L1, L2, and L3. The L1 layer is an outer layer and gives rise to the epidermis, the L2 layer provides cells for sub-epidermal tissue, and the internal L3 layer produces cells for internal tissue. L1 and L2 layers divide mostly anticlinally, whereas L3 divides in all directions. The most underlying rib-zone produces cells for the inner tissue of the stem (Figure 2). Whether cells after division remain stem cells or undergo differentiation depends on their position. Only cells displaced into PZ can differentiate and give rise to new organs. Each zone is specified by a different composition of hormones and regulatory components. The key development regulators are discussed below (Satina et al., 1940; Gross-Hardt and Laux, 2003; Gordon et al., 2009; Aichinger et al., 2012).

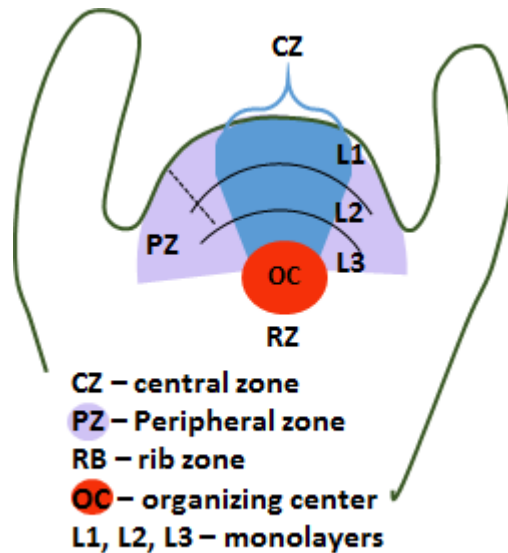


Figure 2: Schematic representation of the shoot apical meristem (SAM). The SAM consists of the central zone (CZ) harboring the stem cell niche and organizing center (purple square); peripheral zone (PZ), the source of leaf and flower primordia; and rib-zone (RZ), provides an inner tissue of stem. CZ and PZ are composed of three clonal distinct monolayers L1 – L3.

The ability to maintain a balance between the differentiated and stem cells requires precise control. Key components of this process are two homeobox-containing transcription factors *WUSCHEL* and *SHOOT MERISTEMLESS (STM)*.

WUSCHEL

WUSCHEL encodes a homeodomain-containing transcription factor and is a founder member of the *WUSCHEL-RELATED HOMEOBOX (WOX)* gene subfamily (Mayer et al., 1998; Haecker et al., 2004). Loss of function mutation of *WUS* leads to the developmental defects in the shoot and floral meristems (Laux et al., 1996). *WUS* is specifically expressed in OC and is responsible for maintaining the stem cell niche (Mayer et al., 1998). *WUS* protein acts cell-non-autonomously and moves to stem cells where it triggers the so-called *CLAVATA (CLV)* pathway which restricts *WUS* expression. The *WUS* – *CLV* negative feedback has an important impact on maintaining SAM size and stem cell number (Yadav et al., 2011).

WUS recognizes and binds to the *CLAVATA3 (CLV3)* promoter element and triggers the gene expression. *CLV3* encodes a secretory protein acting as a peptide hormone. The 96-amino acid precursor protein is post-translationally processed and then cleaved in 12 amino acid peptide with two hydroxylated prolines (*CLV3p12*) (Kondo, 2006), Alternatively, a 13 amino acid-long glycopeptide carrying arabinosylated

hydroxyproline residue is released (CLV3p13) (Ohyama et al., 2009). It was presumed that only CLV3p13 has physiological significance but a recent study showed that both CPV3p12 and CLV3p13 peptides are actively involved in WUS – CLV signaling (Kim et al., 2017). Hormone peptides are secreted from stem cell to the extracellular space and transported apoplastically (Rojo et al., 2002; Xu et al., 2013). Subsequently, they are perceived by various receptors localized on plasma membrane: the leucine-rich repeat (LRR) receptor kinase CLAVATA1 (CLV1) homomers (Clark et al., 1993); the receptor-like protein CLAVATA2 (CLV2), lacking intracellular kinase domain (Kayes and Clark, 1998; Guo et al., 2010); the membrane-localized kinase CORYNE/SUPPRESSOR OF LLP1 2 (CRN/SOL2) heteromers (Müller et al., 2008); and the receptor kinase RECEPTOR-LIKE PROTEIN KINASE 2/TOADSTOOL2 (RPK2/TOAD2) (Kinoshita et al., 2010). and triggers the cascade contributing to shoot development.

A recent study proposed putative mechanisms of CLV3p/CLV1 mediated WUS repression. Chou et al. (2016) showed that the CLV3p/CLV1 ligand-receptor interaction may elevate a second messenger Ca^{2+} concentration through the cyclic nucleotide-activated Ca^{2+} -conducting channels and further activate a signaling transduction cascade resulting in WUS repression (Chou et al., 2016). Except for the above-described receptors, expressed in the central zone of SAM, CLV3p is perceived also by CLV1-related BARELY ANY MERISTEM (BAM) 1, BAM2, and BAM3 receptor-like kinases, expressed within differentiated tissues (DeYoung et al., 2006). CLV1 and BAM1 are considered as primary receptors of arabinosylated CLV3p whereas CLV2/CRN and RPK2 are incapable to directly bind CLV3p, therefore they act rather as co-receptors (Shinohara and Matsubayashi, 2015). Recently, it was shown that perception of CLV3p by CLV1/BAM1 leads to the activation of mitogen-activated protein kinases (MAPKs) and that their activation correlates with WUS repression (Lee et al., 2019).

Apart WUS – CLV pathway, cytokinin and auxin also significantly contribute to the regulation of SAM maintenance and integrity. In *Arabidopsis*, cytokinin signaling pathway is mediated by histidine kinase transduction via His-Asp-His-Asp phosphorelay, which resemble bacterial histidine kinase two-component phosphorelay. Cytokinin signal is perceived by histidine kinase receptor and then transduced by phosphotransfer proteins AHPs to two types of transcription factors. ARR type-A are

negative regulators whereas ARR type-B positive regulators of cytokinin signaling (To et al., 2004; To and Kieber, 2008).

A recent study unveiled 148 direct target genes of WUS (Leibfried et al., 2005). Of these, 44 genes were repressed, including four members of type-A *ARR* genes – *ARR5*, *ARR6*, *ARR7*, and *ARR15* (Leibfried et al., 2005). Direct interaction between *ARR7* and WUS was proven by employing chromatin immunoprecipitation and mobility-shift assays. WUS directly binds to TAAT elements situated approximately 1 000 bp upstream from the transcription start site of *ARR7*. TAAT elements are crucial for WUS binding. At the same time, *ARR7* negatively regulates *WUS* expression in a negative feedback manner (Leibfried et al., 2005). It was shown that the CYTOKININ RESPONSE 1/ARABIDOPSIS HISTIDINE KINASE 4 (*CRE1/AHK4*), one of the three *Arabidopsis* cytokinin receptors, shares its expression domain with *WUS* and therefore cytokinin could induce *WUS* expression especially in the cells with high *CRE1/AHK4* abundance. The auxin pretreatment in the tissue culture system resulted in *CRE1/AHK4* up-regulation (Gordon et al., 2009). Additionally, auxin mediates inhibition of *ARR7* and *ARR15* expression (Zhao et al., 2010). On the other hand, recent studies proved that cytokinins contribute to SAM maintenance through direct activation of *WUS* by ARR type-B transcriptional activators (Meng et al., 2017; Zhang et al., 2017), the positive regulators of cytokinin signaling (Argyros et al., 2008; Romanov et al., 2018). *ARR1*, *ARR10*, and *ARR12* bind to *WUS* promoter and thus directly control *WUS* expression (Meng et al., 2017; Zhang et al., 2017). Recently, the B-ARR-6-BA (AGATHY) primary binding motif for ARRs type B was identified within the *WUS* promoter sequence (Xie et al., 2018).

Besides the DNA-binding homeodomain, WUS comprises important conserved C-terminal domains; an acidic region, a WUS-box, and an EAR-like motif (ERF-associated Amphiphilic Repression). Kieffer et al. (2006) showed that both the WUS-box and the EAR-like motif interact with co-repressor proteins. Thus, WUS recruits the co-repressor complex via these motifs to suppress the expression of genes promoting differentiation (Kieffer et al., 2006). On the contrary, another study showed that WUS can activate the expression of *AGAMOUS* gene through the interaction of its acidic domain (Ikeda et al., 2009). Altogether, WUS can act as a transcription activator

as well as a transcriptional repressor tightly controlling the expression of direct downstream genes involved in development.

SHOOT MERISTEMLESS (STM)

STM is a member of the class I *KNOTTED1*-like homeobox (*KNOX*) gene family. Unlike *WUS*, which is expressed only in a distinct zone, the *STM* is expressed all over the SAM (Long et al., 1996). *STM* is a small protein moving from cell to cell. Even though there is no difference between mRNA and *STM* protein tissue localization, the protein movement has been proved to be essential for its proper function to maintain meristem and to define the meristem-organ boundary zone (Balkunde et al., 2017). The authors have demonstrated that down-regulation of *CUP-SHAPED COTYLEDON (CUC) 1* occurred in plants with immobile *STM* (Balkunde et al., 2017). *CUC1* is a transcription factor and together with *CUC2* and *CUC3* specify the meristem-organ boundary zone. Neither *cuc1* nor *cuc2* mutant display aberrant SAM, while the double mutant *cuc1;cuc2* completely lacks SAM; indicating their redundancy (Aida, 1997). During the embryogenesis, *CUC* genes are expressed over the SAM, later they are restricted to meristem-organ boundary zone. It was shown that *STM* can induce *CUC* expression. Whereas *STM* directly binds to and strongly activates the *CUC1* promoter, the expression of *CUC2* and *CUC3* by *STM* is indirect (Spinelli et al., 2011). Likewise, *CUC1* binds to the *STM* promoter and stimulates its expression in an intermediate fashion. This mutual regulation creates a positive transcriptional feedback loop (Scofield et al., 2018). Additionally, *STM* induces the expression of the microRNA *MIR164c* in SAM that attenuates *CUC1* expression (Scofield et al., 2018). A model was proposed in which *CUC1* expression is restricted to the meristem-organ boundary zone due to the attenuation by *MIR164c*. Accumulation of *MIR164c* is highest in CZ just as for *STM*. The low accumulation of *MIR164c* in the meristem-organ boundary zone is insufficient to repress *CUC1*. Attenuation by *MIR164c* and movement of *STM* may explain the differential expression pattern of both genes despite the positive feedback loop (Scofield et al., 2018). Except for *CUC* genes regulation, *STM* further maintains SAM through positive modulation of cytokinin signaling as demonstrated by Yanai et al. (2005). The authors have shown that *STM* induces expression of *ISOPENTYLTRANSFERASE 7*, a cytokinin biosynthetic enzyme (Yanai et al., 2005).

1.4 Root apical meristem

The plant root is built in a radial pattern and the root meristem is centered at the tip of the growing root. The root meristem consists of three zones: a meristematic, an elongation, and a differentiation zone. The stem cell niche lies in the meristematic zone. The rarely dividing quiescence center (QC), which occupies the center of the niche, resembles the OC in SAM. QC controls the surrounding stem cells which are a source for all differentiated cell files located in three sectors: distal – columella; lateral – epidermis, lateral root cap; proximal – stele (a vascular tissue), cortex, and endodermis (Figure 3) (Sarkar et al., 2007; Aichinger et al., 2012).

Stem cells proliferate in an asymmetric manner. Daughter cell attached to the QC remains as stem cell, whereas the second cell, without direct contact to QC, undergoes several rounds of cell division and the new cell is differentiated (van den Berg et al., 1997; Zhang and Yu, 2014). The quiescence center is determined by *SCARECROW* (*SCR*) expression, which is also important for sustaining the population of stem cells (Sabatini et al., 2003). *SCR* was shown to be a positively regulated direct target gene of the *SHORTROOT* (*SHR*) transcription factor (Levesque et al., 2006). Both, *SCR* and *SHR* are members of the GRAS transcription factor family. Moreover, *SCR* can also activate its own promoter and therefore *SCR* is regulated by an *SHR/SCR*-dependent positive feedback loop. The *SHR* gene is expressed in the stele, whereas the *SHR* protein was found also in the endodermis, endodermis/cortex initial cell, and QC. Due to physical interaction between *SHR* and *SCR*, *SHR* is sequestered to the nucleus and prevented from another movement (Cui et al., 2007).

Further key players in the maintenance of RAM are *PLETHORA* (*PLT*) genes *PLT1* and *PLT2* encoding APETALA2/ETHYLENE-RESPONSIVE ELEMENT BINDING PROTEIN (AP2/EREBP) transcription factors that are specifically expressed in root stem cells (Aida et al., 2004). In parallel with the *SCR/SHR* pathway, *PLT* provides a signal for correct QC and stem cells positioning (Aida et al., 2004).

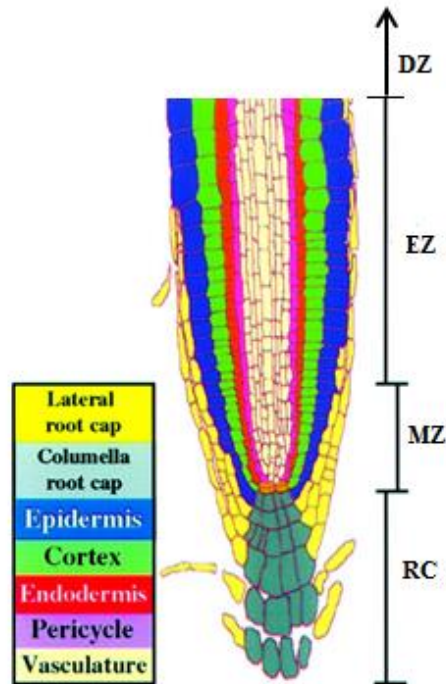


Figure 3: Schematic representation of the root apical meristem. RC – root cap, M – meristematic zone, EZ – elongation zone, DZ – differentiation zone. Adapted from (Marchant et al., 1999).

Expression of *WOX5*, a member of the *WOX* gene family, in QC is crucial for the organization of the distal meristem (Haecker et al., 2004). In *wox5-1* mutant plants, columella stem cells (CSC) are enlarged with accumulated starch-granule-containing organelles, which is a sign of differentiation. So *WOX5* is required for keeping CSC in an undifferentiated state in a non-cell-autonomous manner. In the proximal stem cells, *WOX5* has a redundant function together with the *SHR/SCR* and *PLT* (Sarkar et al., 2007).

1.5 ETHYLENE RESPONSIVE FACTORS

Members of the ETHYLENE RESPONSIVE FACTOR (ERF) gene family create a big group of transcription factors. They are part of the APETALA2/ETHYLENE RESPONSIVE FACTOR (AP2/ERF) superfamily. Each member contains at least one copy of the AP2/ERF, a DNA binding domain, at the N-terminus that recognizes CGGCGG cis-element (GCC-box) in the sequence of the target loci (Ohme-Takagi and Shinshi, 1995; Nakano et al., 2006). In early classification, the AP2/ERF superfamily was divided into four subfamilies and these were subdivided into 12 groups. However,

this classification did not provide information about locus identifiers (Sakuma et al., 2002).

Nakano et al. (2006) reevaluated the AP2/ERF superfamily and proposed a new classification. According to Nakano's classification, *Arabidopsis* has 147 genes, of these 146 are divided into three families: the ERF family (122 genes), the AP2 family (18 genes), and the RAV (RELATED TO ABI3/VP1) family (6 genes). The remaining At4g13040 gene is considered as a soloist gene. This classification is based on functional motifs, which besides the AP2 domain, are conserved within the gene sequence. The ERF superfamily consists of 12 groups (Nakano et al., 2006).

The aim of this work was to clarify the role of ERF transcription factors, belonging to group VIII, in development. Therefore, this group is described in more detail. Members of the group VIII split into two subgroups, the subgroup VIIIa and subgroup VIIIb (Figure 5).

Classification	Group	No.
AP2 family	Double AP2/ERF domain	14
	Single AP2/ERF domain	4
ERF family	Groups I to IV	57
	Groups V to X	58
	Groups VI-L and Xb-L	7
At4g13040		1
RAV family		6
	Total	147

Figure 4 Classification of the AP2/EAR superfamily according to Nakano et al. 2006. AP2 family consists of 18 genes; four of them contain a single AP2/ERF domain instead of two domains but are more similar to AP2 family than ERF family. ERF family consists of 122 genes divided into 11 groups. RAV family consists of 6 genes and one gene is a soloist.

The subgroup VIIIa is composed of eight members with phylogenetically related pairs: *ERF10/ERF11*; *ERF4/ERF8*; *ERF3/ERF7*; and solitary *ERF9* and *ERF12*. Each member contains in its C-terminal region a conserved $^L/_F\text{DLN}^L/_F(\text{x})\text{P}^1$ motif (abbreviated as CMVIII-1), also known as an ERF-associated Amphiphilic Repression (EAR) motif (Nakano et al., 2006). This motif was shown to be responsible for the

¹ Symbols in square brackets mean one of amino acids on place, x mean any amino acid

repression of target gene transcription (Ohta et al., 2001). Hence, the members of this subgroup are considered as transcriptional repressors. Besides CMVIII-1, five of these members further contain another repressor motif CMVIII-2 (Nakano et al., 2006). So far, the research on VIIIa members focused mainly on their function in various stress-related responses such as biotic stress (McGrath et al., 2005; Maruyama et al., 2013) and abiotic stress (Tian et al., 2015), Their role was also proved in stress-related hormone signaling pathways of ethylene, abscisic acid, and jasmonic acid (Yang et al., 2005), as well as in senescence (Koyama et al., 2013; Ogata et al., 2013).

The second subgroup, VIIIb, comprises seven genes, some of them carry a CMVIII-3 motif at the C-terminus (Nakano et al., 2006). The well-studied members of this subgroup are ENHANCER OF SHOOT REGENERATION (ESR) 1 and ESR2 which are capable to enhance shoot regeneration in vitro (Banno et al., 2001; Matsuo et al., 2011) and to positively regulate gene expression of CUC1 (Ikeda et al., 2006). Other members were also shown to participate in plant development (Chandler and Werr, 2017; Chandler, 2018). Thus, members of this subgroup are considered as transcription activators (Banno et al., 2001).

A better understanding of the biological relevance of the ERF transcriptional repressors in the development and *de novo* regeneration still remains elusive. Based on the fact, that the VIIIb subgroup play a key roles in the regulation of SAM and plant development (Banno et al., 2001; Ikeda et al., 2006; Matsuo et al., 2011; Chandler and Werr, 2017; Chandler, 2018), similar important function can be presumed for the members of the neighbor subgroup VIIIa. Nevertheless, to prove this hypothesis the experimental evidence is needed.

Group VIII

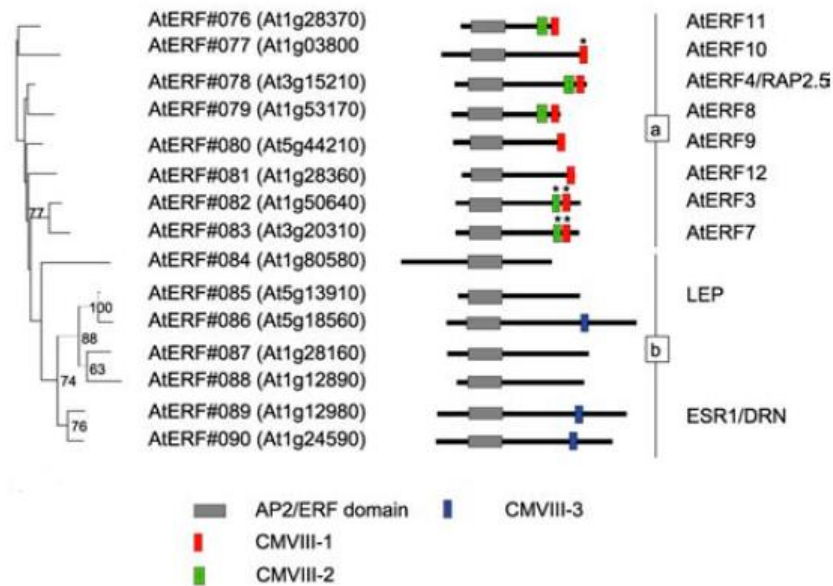


Figure 5 Group VIII of the ERF transcription factor superfamily. Members containing the EAR repressor motif (CMVIII-1) belong to the subgroup VIIIa, remaining members compose the subgroup VIIIb, the positive regulator of transcription. Both subgroups share the same DNA binding domain, AP2/ERF, and compete for the target loci. Adopted from (Nakano et al., 2006).

1.6 Protein degradation

Proper development requires maintenance of an internal environment of the organism in a balanced state. This process is known as homeostasis and includes also a mechanism specialized for proteins, referred to as proteostasis. It includes protein synthesis, folding, trafficking, interaction, and proteolysis. There are two ways of how proteins can be degraded. While long-living proteins tend to be degraded in the lysosomes, short-living proteins are eliminated through the Ubiquitin-26 Proteasome System (UPS) (Jackson and Hewitt, 2016).

Among these proteins are also TFs which control genes involved in the regulation of development. UPS contributes to fine-tune gene expression and thus TFs can trigger expressional programs only at a proper time. Briefly, proteins marked by polyubiquitination (polyUBQ) are targeted to the 26S proteasome, where they are proteolytically processed. Firstly, the ubiquitin (UBQ) molecule is activated by the E1 ubiquitin-activating enzyme and then UBQ is transferred to the E2 ubiquitin-conjugating enzyme. Further, E2 with bound UBQ is recognized by E3 ubiquitin ligase, which also recognizes the target protein and thus comprises substrate

specificity. After the E2+UBQ+E3 complex recognizes the substrate, the UBQ is transferred from E2 to the substrate molecule (Figure 6) (Vierstra, 2009). This target specification allows the precise regulation of different biological processes.

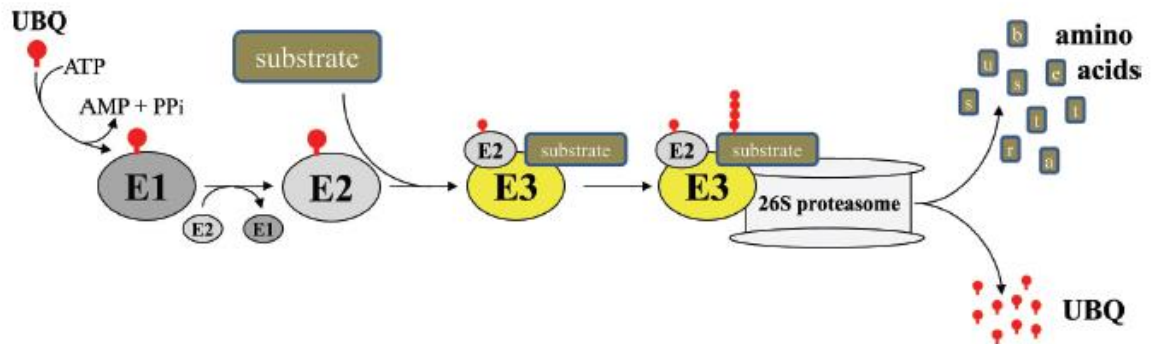


Figure 6: Schematic model of the polyubiquitination mediated proteasomal degradation. UBQ is activated by the E1 ubiquitin-activating enzyme using energy from ATP, then UBQ is transferred to the E2 ubiquitin-conjugating enzyme. E2 loaded with Ub binds the E3 ubiquitin ligase, which also provides substrate specificity. Binding of E3+UBQ to its target leads to the transfer of UBQ from E2 to the substrate molecule. The polyubiquitinated substrate is targeted for degradation by the 26S proteasome. The substrate is cleaved into short peptides and amino acids. Released UBQ is reused in the new round of polyubiquitination. UBQ – ubiquitin; ATP – adenosine triphosphate; AMP – adenosine monophosphate; PPi – pyrophosphate. Adopted from (Chen and Hellmann, 2013).

In the plant kingdom, there are several types of E3 ligases. Basically, E3s are classified upon their subunits and the mechanism of action into four subfamilies – single subunit E3s HOMOLOGOUS TO THE E6AP CARBOXYL TERMINUS (HECT); REALLY INTERESTING NEW GENE (RING) and U-box; and multisubunit CULLIN – RING ligases (CRLs) (Vierstra, 2009). HECT E3 ligases possess a unique ubiquitination mechanism. The UBQ is transferred from E2 to the HECT domain of E3 ligase creating a thiol-ester intermediate and afterward, UBQ is transmitted to the substrate. On the other hand, the RING and U-box containing E3 ligases bind E2 with attached UBQ. The UBQ molecule is then directly transferred from E2 to the substrate without any additional step in transferring process (Vierstra, 2009; Shu and Yang, 2017).

The multimeric CRLs is comprised of the RING-box1 (RBX1) protein responsible for E2 binding, CULLIN protein, which forms a bridge between RBX1 and specialized subunit for target protein recognition. There are four CRLs families: CUL1 based S PHASE KINASE-ASSOCIATED PROTEIN1 – CULLIN1– F-BOX (SCF); CUL3 based BRIC-A-BRAC – TRAMTRACK – BROADCOMPLEX/POX VIRUS and ZINC FINGER (BTB/POZ); CUL4-based DNA DAMAGE-BINDING (DDB); and

ANAPHASE PROMOTING COMPLEX/CYCLOSOME (APC) (Vierstra, 2009; Chen and Hellmann, 2013; Shu and Yang, 2017).

So far, the best-described family among the CRL superfamily is CUL1-based SCF E3s with its shining example of auxin mediated degradation of AUXIN/INDOLE ACETIC ACID (AUX/IAA) transcriptional repressors (Gray et al., 2001). AUX/IAAs possess an EAR motif and thus bring the co-repressor machinery to the promoter region of *AUXIN RESPONSE FACTORS* (ARFs). The ARFs are transcription factors that control auxin response genes (Szemenyei et al., 2008). Auxin facilitates binding of the SCF containing F-box protein TRANSPORT INHIBITOR RESISTANT1/AUXIN SIGNALING F-BOX (TIR1/AFB) – SCF^{TIR1/AFB} E3 ligase to AUX/IAA proteins. Consequently, AUX/IAAs are targeted for protein degradation *via* UPS. ARFs are accessible for transcription and auxin response gene can be expressed (Salehin et al., 2015).

In recent years, few studies tried to shed light on the role of CUL3 – RING E3s complex (Mazzucotelli et al., 2006; Chen et al., 2013). In *Arabidopsis*, there are two *CUL3* genes with redundant function, *CUL3A*, and *CUL3B*. They share 88 % similarity and at least one gene is required for proper embryo development. Mutation in either *CUL3A* or *CUL3B* does not result in phenotype changes. On the other hand, loss of function mutation of both genes is embryonic-lethal (Figuroa et al., 2005). CUL3 interacts *via* its C-terminal region with RBX1. Also, CUL3 is a target for RUB (Related to Ubiquitin) modification. The N-terminus is responsible for binding BTB/POZ domain-containing proteins (Figuroa et al., 2005; Gingerich et al., 2005). This domain is localized at the C-terminal end of the protein and additionally can serve for BTBs assembling into homo- or heterodimers. Moreover, BTB proteins can contain additional domains or motifs at the N-terminus, which act as a substrate-specific adaptor (Figure 7A). Together, they form twelve subgroups. One of these groups contains the MEPRIN and TRAF (TUMOR NECROSIS FACTOR RECEPTOR-ASSOCIATED FACTOR) HOMOLOGY (MATH) at the N-terminus (Gingerich et al., 2007). In *Caenorhabditis elegans* was shown that the BTP/POZ-MATH containing protein CeMel-26 interacts with CUL3 (Xu et al., 2003).

Based on the conserved homology among BTB/POZ-containing proteins, Weber et al. (2005) focused their work on finding related BTB/POZ-MATH (BPM) proteins in *Arabidopsis*.

Arabidopsis possesses six genes expressing BPM proteins (BPM1-6). Phylogenetically, they can be divided into four subgroups: BPM1 and BPM2 in the first group; BPM5 and BPM6 in the second; and BPM3 with BPM4 in their own individual groups (Weber et al., 2005). All BPMs, except BPM4, were localized in the nucleus. BPM4 was exclusively found only in the cytoplasm (Weber and Hellmann, 2009). In the same study, the authors showed for the first time that the members of a group I AP2/ERF TFs are recognized and bound by BPMs *via* the MATH domain. This interaction directs TFs towards UPS and represents a novel transcription regulation pathway (Figure 7B). Another study from 2013 confirmed the interaction of AP2/ERF TFs with BPMs. Furthermore, the interaction of BPM1 with ERF1 from group IX and BPM1 with ERF4 from group VIII has been observed in this study (Chen et al., 2013).

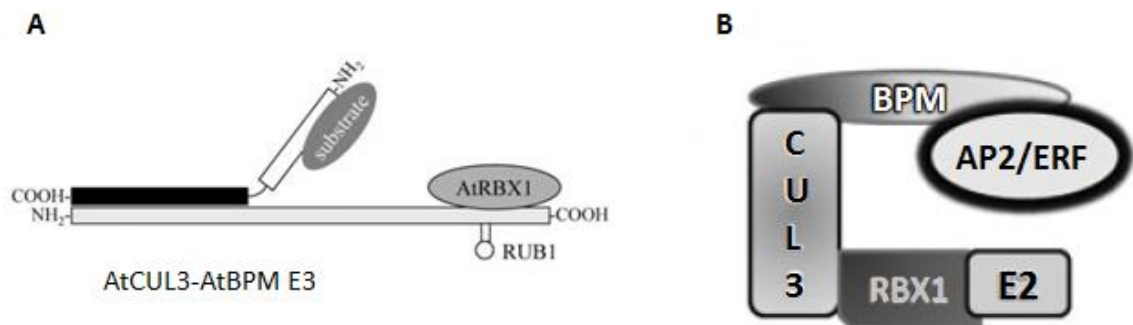


Figure 7: Schematic model of CUL3 based E3 ligase degradation of AP2/ERF proteins. A) CUL3 (grey bar) binds to BPMs *via* its N-terminal end; the C-terminal end associates with RBX and it is also a site RUB modification. BPM protein associates with CUL3 *via* its C-terminal end (black bar); N-terminal (white bar) end binds to ERF/AP2 substrates. B) Model of multimeric CRL with its components. E2 binds to CUL3 *via* RBX1. Substrate selection is arranged by BPM proteins that bind to AP2/ERF proteins. RBX1 – RING-box1 protein; RUB1 – Related to ubiquitin. Modified from (Weber and Hellmann, 2009).

1.7 Histone acetylation, transcriptional repression, and development

Even though every single cell of the plant body possesses the same genetic information stored in genomic DNA of the nucleus, not all the cells face the same developmental fate. Each cell lineage has to produce a different spectrum and amount of compounds at the right time and right place. These variations are generated in response to internal or

external stimuli and the mechanism behind is the differential gene expression. Gene expression might be controlled in several ways and one of these is the epigenetic control. The term epigenetics describes all the changes in gene expression, which are not caused by altering DNA sequence but still can be passed during mitosis or meiosis. DNA methylation, histone modification (Pikaard and Scheid, 2014), chromatin remodeling factors (Ojolo et al., 2018), and small RNAs contribute to epigenetic control of gene expression (Borges and Martienssen, 2015).

In the last years, the organization of chromatin gained attention as an important player of gene expression thereby influencing cellular differentiation and plant development (Ikeuchi et al., 2015). Due to the extreme size of the genomic DNA of the cell, it needs to be compacted and stored in the nucleus in highly organized structures called chromosomes. These structures are formed by DNA-protein complexes termed chromatin. Based on the condensation state, chromatin can form tightly-packed heterochromatin or loose euchromatin (Naumova et al., 2013; Fyodorov et al., 2018). The basic organizing unit of the chromatin structure is nucleosome. The protein core of the nucleosome comprises the histone octamer, which contains two copy of each core histone protein H2A, H2B, H3, and H4. Approximately 147 bp of DNA strand is wrapped around each octamer and such a structure is further stabilized by histone H1 working as a linker (Maeshima et al., 2014, 2019). The amino-terminal tail emerging from the core nucleosomes provides several residues that can be post-translationally modified by acetylation, methylation, phosphorylation, ubiquitination, or ADP-ribosylation. These modifications act as a so-called histone code and indirectly affect the expression of genes and other elements such as rRNA, miRNA, etc. (Jenuwein and Allis, 2001; Liu et al., 2014).

Since histone proteins are positively charged and they have a naturally strong affinity for negatively charged DNA. Acetylation of lysine at the histone N-terminus neutralizes the positive charge, and thus histone-DNA binding is weakened and chromatin is loosened. The relaxed chromatin structure allows to easy access the transcription machinery components, such as RNA polymerase II, to promoter regions of the genes. Highly acetylated histones are associated with actively transcribed genes, whereas hypoacetylated histones mark transcriptionally silent loci. Several sites of histone H3 are known to be acetylated at lysine residues K9, K14, K18, K23, K27, and K36. The

acetylation pattern of *Arabidopsis* histone H4 is also well described and involves residues of K5, K8, K12, K16, and K20 (Mahrez et al., 2016). Two groups of enzymes control histone acetylation in the opposite manner. Histone acetyltransferases (HATs) add the acetyl group to lysine residues while histone deacetylases (HDAs) remove them. The genome of *Arabidopsis thaliana* encodes 12 HATs and 18 HDAs (Pandey et al., 2002). Phylogenetically, histone deacetylases can be clustered into three families: REDUCED POTASSIUM DEPENDENCY 3/HISTONE DEACETYLASE 1 (RPD3/HDA1); HISTONE DEACETYLASE 2 (HD2); and the SILENT INFORMATION REGULATOR 2 (SIR2)-like RPD3/HDA1 family. The most studied RPD3/HDA1 family contains 12 members divided into three classes I-III and one more unclassified group (Hollender and Liu, 2008). This system was revised based on a broad phylogenetic analysis comparing histone deacetylase orthologues of 6 plant species, yeasts, *Drosophila*, *Caenorhabditis elegans*, and human. Sequential homology and evolutionary conservation gave rise to three distinct classes; I, II, and IV (Alinsug et al., 2009). Members of Class I, HDA6, 7, 9, 10, 17 and 19, belong to RPD3 group of proteins (Alinsug et al., 2009). The significance of these group members was clearly demonstrated in several works. Unique position in this group has HDA6 as it is involved in a plethora of processes affecting plant development. It is involved in root epidermis formation (Li et al., 2015), ethylene and jasmonic acid signaling (Zhu et al., 2011). Furthermore, HDA6 deacetylate negative regulator of flowering FLOWERING LOCUS D and thus promote flowering. This flowering control is conducted via crosstalk with histone demethylation pathway. It was shown that HDA6 directly interact with histone demethylase. Moreover, HDA6 can impact transposons expression (Yu et al., 2011). Additionally, it can also modulate DNA methylation of CpG islands (Hristova et al., 2015). Another member, HDA19, was shown to enhance seed germination due to its presence in BES1-TPL-HDA19 co-repressor complex which attenuates abscisic acid signaling (Ryu et al., 2014). Moreover, HAD19 influences root cortex development via its interaction with SCR (Chen et al., 2019). The enzymes HDA10 and HDA17 lack catalytic domain and therefore are considered to be inactive (Hartl et al., 2017).

Members of Class II are categorized as an HDA1 group of protein. Here belongs HDA 5, 8, 14, 15, and 18. HDA18 is indirectly involved in patterning of root epidermis via regulation of phosphorelay kinase genes (Liu et al., 2013). Recently, it was shown that

HDA14 preferentially localize to chloroplasts where contributes to RUBISCO activity control (Hartl et al., 2017).

The class IV (not III, to distinguish it from sirtuin deacetylases) contains only HDA2 with its isoforms and represents the solitary HDA class *unique* for plant kingdom (Alinsug et al., 2009).

1.8 HDA-facilitated transcriptional repression

The mechanism by which HDAs facilitate transcriptional repression is complex. TFs, specifically recognizing cis-regulating elements in their target genes, interact with co-repressor proteins which in turn bind to HDA and thus recruit deacetylation machinery to the target loci (Kagale and Rozwadowski, 2011).

Co-repressors are incapable of binding directly to the DNA; hence they need to interact with DNA-binding transcription factors to mediate transcriptional repression (Hong, 2016). The broad family of co-repressors called GROUCHO/TRANSDUCIN-LIKE ENHANCER OF SPLIT (GRO/TLE) is conserved across animal species (Kaul et al., 2014; Agarwal et al., 2015). The GRO was discovered in *Drosophila* (Jiménez et al., 1997) and its homolog TLE in vertebrates (Stifani et al., 1992). Functionally similar co-repressors, called TUP, were found also in *Saccharomyces* (Williams and Trumbly, 1990).

In *Arabidopsis*, the GRO/TUP like co-repressors family consists of 13 members. Best described are LEUNIG (LUG), LEUNIG HOMOLOG (LUH), TOPLESS (TPL), TOPLESS-RELATED (TPR), and WUSCHEL-INTERACTING PROTEINS (WSIPs) (Liu and Karmarkar, 2008). Based on a phylogenetic study they can be divided into two subclades LUG/LUH and TPL/TPR/WSIP (Liu and Karmarkar, 2008). Although LUG and LUH share similarities on the sequential level their function in distinct developmental processes can vary. On the one hand, they show redundant function in embryo development where double *lug/luh* mutant is embryonic lethal. On the other hand, *luh* mutation does not impact floral development as severe as *lug* mutation. *luh-1* single mutant exhibits normal flowering but germination rate is significantly reduced as

well as its overall growth when compared to WT. Moreover, *luh-1* can enhance flower defects in *lug* mutant. Interestingly, both *LUG* and *LUH* display similar expression patterns during development but when responding to environmental stresses these patterns are opposite (Sitaraman et al., 2008).

Members of subclade TPL/TPR/WSIPs are involved in apical-basal fate determination of the embryo (Long et al., 2006; Liu and Karmarkar, 2008; Lee and Golz, 2012). An important role of the TPL co-repressor in SAM development was discovered in the thermosensitive mutant *tpl-1*. The embryonic apical (shoot) pole was transformed into a second root pole. This resulted in the double-root seedling when grown at higher, non-permissive, temperature (29°C). At lower temperature embryos were defective in proper SAM development and a broad range of phenotypes were observed displaying cotyledons fused to some degree (Long et al., 2002). The same group identified the *tpl-1* mutation as a dominant-negative mutation (gain-of-function allele) caused by a substitution of asparagine to histidine at position 176 (Long et al., 2006). Noteworthy, no mutant phenotype was observed in the case of the loss-of-function mutation of TPL gene (*tpl-2*). The *tpl-1* like phenotype occurred only when additional TOPLESS-RELATED (TPR) genes were mutated. The *tpl-1* phenotype was further enhanced by introducing an additional mutation in *HDA19* even when grown at a lower temperature (24°C). In contrast, a single *hda19-1* mutation displayed some *tpl-1* like phenotype only at a higher temperature (29°C) (Long et al., 2006). Mutation in the histone acetyltransferase *GCN1* gene (*HAG1*) rescued the *tpl-1* phenotype independent of temperature. *HAG1* acts as a transcription activator of root-specific gene expression in the apical part of the embryo. This result confirmed the hypothesis that TPL is a co-repressor of gene transcription working in concert with histone-modifying enzymes (Long et al., 2006). Taken together, TPL and TPR proteins have a big impact on proper embryo development when shoot and root commitment takes place. They allow root-determining genes to be repressed and thus the shoot establishing program can be triggered in the apical half of the embryo. TPL and TPRs conduct their role in development in co-operation with histone deacetylases (Long et al., 2006).

Semi-in vivo pull-down assays showed the interaction of TPL with *HDA19* (Krogan et al., 2012) and *HDA6* (Wang et al., 2013). Nevertheless, it is still not clear if there is direct binding or it is facilitated by some adaptor proteins (Kagale and Rozwadowski,

2011; Yamamuro et al., 2016). On the other hand, the closest TPL homolog, TPR1, can interact with HDA19 *in vivo* (Zhu et al., 2010).

Transcription factors containing the repressor domain such as EAR motif have been shown to interact with co-repressor proteins (Causier et al., 2012). Kagale et al. (2010) employed a genome-wide bioinformatic analysis to identify all members of the EAR repressor network. They found 219 EAR-containing proteins, belonging to 21 different TF families. From these, 72% contain an LxLxL EAR motif and 22% a DLNxxP EAR motif while 6% of these proteins contain both motifs (Kagale et al., 2010). Conserved leucine residue within EAR motif was shown to be essential for repressor activity as its mutation caused a significant reduction of repression (Tiwari, 2004). Oh et al. (2014) tested interaction of TPL with EAR-containing transcription factor brassinazole resistant 1 by employing the site-directed mutagenesis. Substitution of conserved leucine residue in the core EAR motif to alanine or deletion of whole EAR motif completely impaired interaction between transcription factor and TPL (Oh et al., 2014).

Additionally, Song *et al.* (2005) showed the interaction of ERF7, member of the group VIII AP2/ERF transcription factors, with SIN3-like (SWI/SNF-INDEPENDENT3) protein. This is an orthologue of mammalian co-repressor component SIN3, that is known to form an active complex with HDA *in vitro* and *in vivo* (Zhang et al., 1997). SIN3 could interact both with ERF7 and HDA19 in a yeast two-hybrid system. Co-expression of *ERF7*, *SIN3*, and *HDA19* resulted in reduced expression of a reporter gene fused with a GCC box (Song et al., 2005). Moreover, ERF3 and ERF4, other members of group VIII AP2/ERF transcription factors, interacted with the SIN-associated polypeptide 18 (SAP18), an orthologue of human SAP18 working as an adaptor protein (Song and Galbraith, 2006). SAP18 directly interacts with SIN3 and together with HDAs acts in co-repressor complex in human (Zhang et al., 1997). These findings suggest that the interaction of ERFs with HDAs may be mediated by some adaptor protein.

Based on the current knowledge, Kagale and Rozwadowski (2011) proposed a model of transcriptional repression mediated by the EAR motif-containing repressors. In this model, ERF TFs specifically bind to the GCC-box localized in the promoter of the target gene and recruit the co-repressor complex through their EAR motif.

Consequently, HDAs deacetylate histones which become again positively charged and thus can tightly bind DNA molecule. Finally, chromatin is condensed and transcription of the target loci is inhibited (Figure 8).

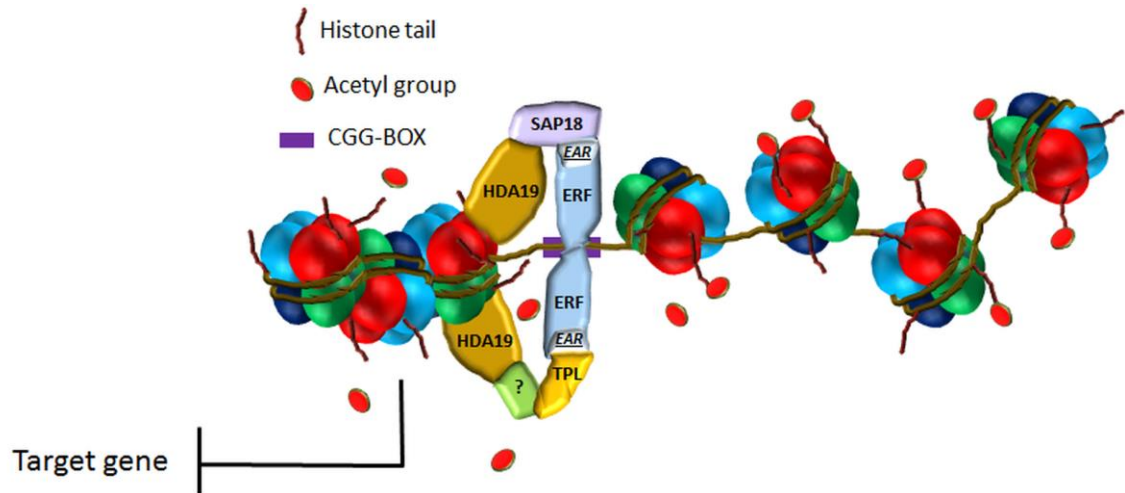


Figure 8: Model of EAR and HDA mediated repression of a target locus. Transcriptional repressor upon different signals binds to its target locus and conducts transcriptional repression through its EAR motif. A) Repressor binds through EAR motif to SAP18 and thus recruits co-repressor complex to the target loci. SAP 18 directly interacts with HDA19 which deacetylates histones. As a result, chromatin is closed and transcription is stopped. B) Repressor binds through EAR motif to TPL which indirectly interacts with HDA19 through the putative adaptor. HDA deacetylates histones and gene expression is stopped.

2 Material and Methods

2.1 Plant material

Arabidopsis thaliana accession Columbia-0 (Col-0) was used as wild-type. Seeds described below are obtained from the European Nottingham Arabidopsis Stock Centre (NASC) and have been previously described; AT2G17950 *wus-101* (Gabi Kat 870_H12) (Zhao et al., 2017); AT5G63110 *hda6-6* (Yu et al., 2011; Hristova et al., 2015); AT3G15210 *erf4-1* (SALK_073394) (Koyama et al., 2013; Liu et al., 2017); AT5G44210 *erf9-1* (SALK_043407) (Maruyama et al., 2013; Van den Broeck et al., 2017); AT1G28370 *erf11-1* (SALK_116053) (Zhou et al., 2016; Van den Broeck et al., 2017); seeds of AT1G53170 *erf8* (FLAG_157D10) (Koyama et al., 2013; Van den Broeck et al., 2017) were obtained from National Institute for Agricultural Research, France (INRA). Another seeds used in this study obtained from NASC: AT5G44210 *erf9* (GK-371H03); AT1G03800 *erf10* (GK-61A9, GK-170C2); AT1G28360 *erf12* (Sail_873_D11); AT5G19000 *bpm1* (Salk_31057; Salk_125026); AT3G06190 *bpm2* (GK-391E4); AT2G39760 *bpm3* (GK-436E12, Salk_72848). The original *erf8* FLAG_157D10 was Wassilewskija (Ws) accession. The position of T-DNA insertion was confirmed by sequencing. The mutant lines were backcrossed at least 3 times with Col-0. The AT2G01830.2 *cre1-2* mutant was kindly provided by Tatsuo Kakimoto at Osaka University (Inoue et al., 2001).

2.2 Growth conditions

The *Arabidopsis* plants and *in vitro* tissue culture were grown in a photoperiod of 16 h light (approximately 60 $\mu\text{mol m}^{-2} \text{s}^{-1}$) and 8 h dark at 21 °C with 70 % humidity. The conditions for seed surface sterilization and growth on MS plates, CIM pre-incubation, and subsequent SIM culture were described in (Kubalová and Ikeda, 2017). Briefly, *Arabidopsis* seeds were surface sterilized, firstly with 70 % ethanol and then with sterilization mixture containing 10 % sodium hypochlorite (VWR Chemicals), 70 % ethanol, and water (5:1:4) up to 10 minutes. Sterilized seeds were washed with sterile water 3 times and stored for 3 days at 4° C in the dark. Subsequently, seedlings were grown on MS medium (1x Murashige and Skoog (MS) basal salt; 1 % saccharose; 0.05 % MES; pH 5.7) containing 0.57 % or 1.0 % Gellan Gum (GG) (Thermo Fisher Scientific) in a horizontal or vertical orientation, respectively. For tissue culture

experiments, roots from 5-day-old seedlings, after the germination, were excised into segments of approximately 8 mm in length without RAM and hypocotyl (Figure 9). Prepared root explants were transferred onto CIM (1x Gamborg B5 medium; 2 % glucose; 0.05 % MES; 2, 4-D 0.5 mg/L; kinetin 0.05 mg/L; pH 5.7) and incubated for 4 days. Subsequently, root explants pre-incubated on CIM were then transferred onto SIM (MS medium containing isopentenyl adenosine [2ip] 1mg/L and IAA 0.15 mg/L) or onto RIM (IAA 0.15 mg/L) for indicated period and subjected to chlorophyll extraction, shoot regeneration assay, phenotype evaluation or RNA extraction.



Figure 9: Preparation of root explants. Roots of 5 days-old seedling were cut into approximately 8 mm long explants in the sterile condition. The segments did not contain RAM or root caps.

2.3 Plant selection

To select T-DNA insertion mutant lines, seeds were incubated onto medium containing: kanamycin (75 mg/L) for SALK lines, phosphinothricin (16 mg/L) for Sail lines, or sulfadiazine (2 mg/L) for GABI-Kat lines.

2.4 Genomic DNA isolation and PCR genotyping

Single fresh leave of tested young seedling was collected into tube containing gDNA extraction buffer (200mM Tris-HCl, 20mM EDTA, 250mM NaCl, 0.5 % SDS), Chloroform:Isoamyl alcohol (24:1), and a tungsten carbide bead (3 mm QIAGEN). Tissue was disrupted by Mixer Mill (Retsch MM 400) at 25 Hz for 20 seconds. The homogenate was centrifuged at 14000 g for 3 minutes and supernatant was transferred into a new Eppendorf tube, then gDNA was precipitated by 1.5 volume of 96 % ethanol.

Two sets of primers were designed for PCR genotyping of T-DNA insertion mutants using GoTaq[®] DNA Polymerase (Promega) (Table 1a, 1b). The first primer combination detects the T-DNA insertion, while the second one detects the WT allele. Thus, the homozygous, heterozygous and WT plants can be easily identified. The PCR program: initial denaturation 60s at 95°C followed by 36 cycles of denaturation at 95°C, 20s, annealation at 57°C, 20s, and amplification at 72°C for 60s. Final amplification step was done at 72°C, 7 minutes. Amplicons were loaded onto 1.75 % agarose gel with ethidium bromide and visualized by Gel Doc EZ imaging system (Bio-Rad).

Gene	T-DNA Insertion	Primers for Genotyping	Sequence 5' → 3'
ERF4	<i>erf4-1</i> SALK_073394	ERF4_F3060	GCTCGTGTATCAGATCCCGATG
		ERF4_R3760	GTGGTAACGATAGAAAAGGAAAGCC
		LBa1m	GGTTCACGTAGTGGGCCATCGCCCTG
ERF8	<i>erf8</i> FLAG_157D10	ERF8F_1846	GTGATTTGTGCAGTCTTTGTTACAAAGG
		ERF8_RFsel	CTCGGCCGGCCTTCCGCCGGAGGAGCTAAG
		FLAG_LB4	CGTGTGCCAGGTGCCCACGGAATAGT
ERF9	<i>erf9-1</i> SALK_043407	ERF9_F2Ascl	TTTGGCGCGCCATGGCTCCAAGACAGGCGAACGG
		ERF9_R3244	CCAGGTTTAGTTCTCTTCTCGGTTTC
		LBa1m	GGTTCACGTAGTGGGCCATCGCCCTG
ERF9	<i>erf9</i> GK-371H03	ERF9_F2Ascl	TTTGGCGCGCCATGGCTCCAAGACAGGCGAACGG
		ERF9_R3244	CCAGGTTTAGTTCTCTTCTCGGTTTC
		GK L8760	GGGCTACACTGAATTGGTAGCTC
ERF10	<i>erf10</i> GK-170C2	ERF10_F2890	TGTAAGCTGCGAATGGAACCG
		ERF10_R3119	ACGTCAACACGAAATCCATTGG
		GK L8760	GGGCTACACTGAATTGGTAGCTC
ERF10	<i>erf10</i> GK-61A09	ERF10_F1900	TTTCTAAGTACTTGTATTATCAGATTCTCAG
		ERF10_RFsel	ATCGGCCGGCCGGGACTTGC GTT GAGGTC
		GK L8760	GGGCTACACTGAATTGGTAGCTC
ERF11	<i>erf11-1</i> SALK_116053	ERF11_F1849	ATATAAATTGTTTCCATGCAAAGCC
		ERF11_RFsel	AATGGCCGGCGTTCTCAGGTGGAGGAGGGAA
		LBa1m	GGTTCACGTAGTGGGCCATCGCCCTG
ERF11	<i>erf11-2</i> Cr2657	ERF11_F2591	AACGGAGTCCGTTACAGAGG
		ERF11_R2569	GTTACCTTCGTTGGTTTTGACGGC
ERF12	<i>erf12</i> Sail_873_D11	ERF12_F2804	TTTTTCTCCGAACCGGTGTGC
		ERF12_R3066	ATAGAAAAGTAGGCAAAACGGCG
		Sail LB3m	CTGAATTTTCATAACCAATCTCGATACAC
BPM1	<i>bpm1</i> SALK_31057 SALK_125026	BPM1_F606	AGCTTCTCTAGCTGCCCAAACCTCTG
		BPM1_R1103	TTTAGCGAGAGAGTACCCACAGATC
		LBa1m	GGTTCACGTAGTGGGCCATCGCCCTG
BPM1	<i>bpm1</i> Cr1070	BPM1_F606	AGCTTCTCTAGCTGCCCAAACCTCTG
		BPM1_R1290	TCTGATCCACAAGCGTGAGC
BPM2	<i>bpm2</i> GK-391E4	BPM2_F1170	TGCGAGTTTTAGATCATGGCTCCTG
		BPM2_R1999	TCCCATTTAAGTCACAACCATCAGC
		GK L8760	GGGCTACACTGAATTGGTAGCTC
BPM3	<i>bpm3</i> GK-436E12	BPM3_F2167	GCTAGTGCTTCTCTGTGTCAGAAGC
		BPM3_R2531	TCAGAGGTTTCTAAAGCTGATCG
		GK L8760	GGGCTACACTGAATTGGTAGCTC
BPM3	<i>bpm3</i> SALK_7284	BPM3_F3106	TGGCAACAACACTTGC GTT TGG
		BPM3_R3541	AGGCAGATGATCCTTCATACAAG
		LBa1m	GGTTCACGTAGTGGGCCATCGCCCTG

Table 1a: List of primers used for PCR genotyping of selected mutant lines.

Gene	T-DNA Insertion	Primers for Genotyping	Sequence 5' → 3'
<i>WUS</i>	<i>wus-101</i> GK-870H12	WUS_F2418	CACGGTGTTCATGCAGAGACC
		WUS_R2526	TCACCGTTATTGAAGCTGGGATATGG
		GK_L8760	GGGCTACACTGAATTGGTAGCTC
<i>HDA6</i>	<i>hda6-6</i>	HDA6_F3144	GTTTCTGTTGCCTCATCGCAGACTGC
		hda6-6dREcoRV	GACCATAAAAATGGAAAGTAGGAGATGATA

Table 1b: List of primers used for PCR genotyping of selected mutant lines. To identify homozygous mutant lines two sets of primers were used; in the first set both primers anneal to gDNA sequence; in the second set one primer anneals to gDNA sequence and other is specific for T-DNA insertion. Primers highlighted in blue were used in both sets.

2.5 RNA extraction and cDNA synthesis

Total RNA was extracted from root explants cultured 5 days on SIM (described above) by RNeasy phenol-free total RNA isolation kit following the manufacturer's instructions (Ambion). Extracted RNA was treated with TURBO DNase (Ambion) to avoid gDNA contamination and precipitated by LiCl. The RNA integrity was tested by electrophoresis in 1.75 % agarose gel. Complementary DNA (cDNA) was synthesized using RevertAid H Minus First Strand cDNA Synthesis Kit (Thermo Scientific) with oligo(dT)18 (Sigma-Aldrich).

2.6 Semi-quantitative RT-PCR

For semi-quantitative reverse transcription PCR (semi-quantitative RT-PCR) the ordinary PCR program for PCR genotyping was used (see PCR genotyping). Primers for semi-quantitative RT-PCR are listed in Table 2. A number of cycles was adjusted for each target gene separately. Loading of template cDNA from mutant lines and WT was normalized to *TUBULIN3*. PCR amplicons were analyzed by electrophoresis in 1.75% agarose gel.

Gene	Primers for semi-q RT-PCR	Sequence 5' → 3'
<i>ERF4</i>	ERF4_F3060	GCTCGTGTATCAGATCCCGATG
	ERF4_RFsel	GTTAGGCCGGCCGGCCTGTTCCGATGGAGGAG
<i>ERF8</i>	ERF8_FAscl	CTAGGCGCGCCATGCCCAACATCACCATG
	ERF8_RFsel	CTCGGCCGGCCTTCCGCCGAGGAGCTAAG
<i>ERF9</i>	ERF9_F2Ascl	TTTGGCGCGCCATGGCTCCAAGACAGGCGAACGG
	ERF9_R3244	CCAGGTTTAGTTCTTCTCTCGGTTC
<i>ERF10</i>	ERF10_FAscl	CCAGGCGCGCCATGACCACAGAAAAAGA
	ERF10_RFsel	ATCGGCCGGCCGGGACTTGC GTTGAGGTC
<i>ERF11</i>	ERF11F_Ascl	TTGGGCGCGCCATGGCACCAGAGTTAAAAC
	ERF11R_Fsel	AATGGCCGGCCGTCTCAGGTGGAGGAGGGAA
<i>ERF12</i>	ERF12_F2595	TACGACGGCGCTGCTCGTTTCC
	ERF12_RFsel	GTTGGCCGGCCAAGCCAAAGCGGCGGAGGCTC
<i>BPM1</i>	BPM1_FNdel	TTGCATATGGGCACAAC TAGGGTCTG
	BPM1_RBamHI	CTCGGATCCTCAGTGCAACCGGGGCT
<i>BPM2</i>	BPM2_FNdel	TGTCATATGGACACAATTAGGGTTTC
	BPM2_RBamHI	ATTGGATCCTAATGTAACCGTTGCTT
<i>BPM3</i>	BPM3_FNdel	GAGCATATGAGTACCGTCCGAGGTAT
	BPM3_RBamHI	TAAGGATCCTAAGACACTGCTCGCAC
<i>HDA6</i>	HDA6_F2957	GTCAAGGGTACACGCTGATTGC
	HDA6_R3870	GCCACCACGACATGAGTAACC
<i>WUS</i>	WUS_F2814	CACGGTGTTCATGCAGAGACC
	WUS_R3476	CGTCGATGTTCCAGATAAGCATCG
<i>Tubulin3</i>	tubulin U51	GGACAAGCTGGGATCCAGGTCTG
	tubulin U52	CATCGTCTCCACCTTCAGCAC
<i>ER</i>	F_Fsel_Myc	AAAGGCCGGCCTGAACAGAAATTAATCTCTG
	R_Spel_Myc	TCTAGAACTAGTTTAAAGGTCTTCTTCAGAG

Table 2: List of primers used for semi-quantitative RT-PCR.

2.7 Quantitative RT-PCR analysis (qRT-PCR)

Quantitative real-time PCR reactions were performed using gb SG PCR Master Mix (Generi Biotech) on a StepOnePlus™ Real-Time PCR System (Life Technologies). Primers for detecting *CUC1* by qRT-PCR were described in (Lee et al., 2016), for *ESR1* and *ESR2* in (Iwase et al., 2017) and for *STM* in (Spinelli et al., 2011) (Table 3). Relative gene expression was normalized to *TUBULIN3* and *ELONGATION FACTOR 1α (EF1 α)* as reported (Vandesompele et al., 2002).

Gene	Primer Efficiency	Primers for qPCR	Sequence 5' → 3'
<i>EF1α</i>	98,5 %	EF1aF	GTTTTGAGGCTGGTATCTCTAAG
		EF1aR	GTGGTGGCATCCATCTTGTTAC
<i>TUBULIN3</i>	97,3 %	TUB3F	TGTTGACTGGTGCCCAACTG
		TUB3R	TACATACAGCTCTCTGAACC
<i>CUC1</i>	99,93 %	CUC1_HX1693F	ACATTTCCCTCCTCCGCTAAGGATG
		CUC1_R3693	AGAGGAGAACTCTCCGGTGACG
<i>STM</i>	99,73%	STM_F_Spinelli	GAAGCTTACTGTGAAATGCTCG
		STM_R_Spinelli	AACCACTGTACTTGCGCAAGAG
<i>ESR1</i>	105,90 %	ESR1_IWASE_F	ACAGCTGTCATTATGCCTGAACCA
		ESR1_IWASE_R	GGTAGAGGAATCTAACGGTAGAGA
<i>ESR2</i>	106,62 %	ESR2_IWASE_F	GCTGACTTCCATGTCTGAAGGA
		ESR2_R5265	CGTTCTGCTGCATCTTAGC

Table 3: List of primers used for quantitative RT-PCR.

2.8 Shoot regeneration assay

Roots of 5-day-old seedlings grown on 1 x MS (0.8 % Gellan Gum) in vertical orientation were dissected to the appropriate length of 5 – 8 mm and place on CIM medium for 4 days. Subsequently, root explants were transfer onto SIM and time-course analysis of phenotype was carried out. To statistically evaluate shoot regeneration efficiency, nascent shoots developing true leaves were counted under a stereomicroscope at indicated time points as described previously (Li et al., 2011).

2.9 Constructs preparation

To prepare constructs harboring various coding regions the conventional cloning techniques requiring restriction digestion and ligation were used. The coding sequence of the desired genes was PCR amplified from *Arabidopsis* Col-0 gDNA or cDNA using Phusion DNA polymerase (NEB).

The PCR program initial denaturation 30s at 98°C followed by 35 cycles of denaturation at 98°C, 10s, annealing at 57°C, 20s, and amplification at 72°C 30s per kb. Final amplification step was done at 72°C, 7 minutes. PCR product was purified by NucleoSpin® Gel and PCR Clean-up (Macherey-Nagel) and digested overnight with restriction enzymes (NEB) at 37°C along with acceptor vector. Both, vector and PCR product were again purified using the above-mentioned kit and subsequently ligated

together with T4 DNA ligase (Thermo Scientific) for 1h at room temperature. Competent cells *E. coli* TOP 10 strain (NEB), were electroporated with the ligation mixture and plated on solid LB plates containing proper antibiotic selection. Positive clones were selected using colony PCR and prepared constructs were confirmed by sequencing (Seqme). The sequences of primers used for the vector preparation are listed in Table 4.

2.9.1 Editing of pBlueScriptSK+ vector

The original pBlueScriptSK+ vector was digested at BamHI and XbaI restriction sites and the polylinker carrying additional AscI and FseI sites was inserted into the original vector. The modified vector was denoted as pBlueScriptSK+MCS.

2.9.2 Cloning of ERF genes for protein – protein interaction study

Genomic DNA of *Arabidopsis* WT Col-0 was used as a template for PCR amplification of *ERF4*, *ERF8*, *ERF9*, *ERF10*, *ERF11*, and *ERF12* genes. Forward and reverse primers contained restriction sites for AscI and FseI, respectively. The PCR products were subcloned into the modified pBlueScriptSK+MCS vector. The ORFs of *ERF* genes were subcloned into a pGBKT7 plasmid using BamHI and NotI restriction sites. The pGBKT7 construct harboring *ERF4* coding region was used for sub-cloning *ERF4* into pGADT7 between BamHI and SacI restriction sites. To sub-clone remaining *ERF* genes into pGADT7, the *ERF4* coding region was replaced by the other *ERF* ORFs by AscI and FseI restriction enzymes.

2.9.3 Cloning BPM constructs for protein – protein interaction assay

The *Arabidopsis* WT Col-0 cDNA was used as a template for PCR amplification of *BPM1*, *BPM2*, *BPM3*, *BPM4*, *BPM5*, and *BPM6* genes. Forward and reverse primers contained NdeI and BamHI restriction sites, respectively, in the case of *BPM1* – *BPM5*. While for cloning of *BPM6* the primers contained NcoI and BamHI restriction sites. Prepared PCR products were subcloned into pGADT7 in between NdeI and BamHI restriction sites (*BPM1* – *BPM5*) or between NcoI and BamHI restriction sites (*BPM6*). Next, the ORF of *BPM* genes were subcloned from prepared pGADT-BPM constructs into pGBKT7 vector by using BamHI and NdeI restriction sites.

Gene/Construct	Primers for cloning	Sequence 5' → 3'
<i>ERF4</i> AT3G15210	ERF4FAscI	ATCTGCGGCCGCATGGCCAAGATGGGCTTGA
	ERF4_R2FseI	TAAGGCCGGCCAGCTTGTTCCGATGGAG
<i>ERF8</i> AT1G53170	ERF8_FAscI	CTAGGCGCGCCATGCCCAACATCACCATG
	ERF8_RFseI	CTCGGCCGGCCTTCCGCCGGAGGAGCTAAG
<i>ERF9</i> AT5G44210	ERF9_F2AscI	TTTGGCGCGCCATGGCTCCAAGACAGGCGAACGG
	ERF9_RFseI	AAAGGCCGGCCAACGTCCACCACCGGTGG
<i>ERF10</i> AT1G03800	ERF10_FAscI	CCAGGCGCGCCATGACCACAGAAAAAGA
	ERF10_RFseI	ATCGGCCGGCCGGGACTTGCGTTGAGGTC
<i>ERF11</i> AT1G28370	ERF11F_AscI	TTGGGCGCGCCATGGCACCCGACAGTTAAAAC
	ERF11R_FseI	AATGGCCGGCCGTTTCTCAGGTGGAGGAGGGAA
<i>ERF12</i> AT1G28360	ERF12_FAscI	AGAGGCGCGCCATGGCGTCAACGACGTGTGCA
	ERF12RFseI	GTTGGCCGGCCAAGCCAAAGCGGCGGAGGCTC
<i>BPM1</i> AT5G19000	BPM1_FNdeI	TTGCATATGGGCACAACCTAGGGTCTG
	BPM1_RBamHI	CTCGGATCCTCAGTGCAACCGGGGCT
<i>BPM2</i> AT3G06190	BPM2_FNdeI	TGTCATATGGACACAATTAGGGTTTC
	BPM2_RBamHI	ATTGGATCCTAATGTAACCGTTGCTT
<i>BPM3</i> AT2G39760	BPM3_FNdeI	GAGCATATGAGTACCGTCGGAGGTAT
	BPM3_RBamHI	TAAGGATCCTAAGACTGCTCGCAC
<i>BPM4</i> AT3G03740	BPM4F_NdeI	TGTCATATGAAATCTGTCAATTTTCAC
	BPM4_RBamHI	TTTGGATCCTCAATCTTCTAGTTCTGC
<i>BPM5</i> AT5G21010	BPM5_FNdeI	ACGCATATGTCAGAATCAGTGATTCA
	BPM5_RBamHI	TTGGGATCCTAGGTGGTTTCGTTGTCT
<i>BPM6</i> AT3G43700	BPM6_FNcoI	TTCCATGGAGATGTCAAAGCTAATGACC
	BPM6_RBamHI	AAGGGATCCTAAGTGGTTTCGCTGCCT

Table 4: List of primers used for cloning genes for protein-protein interaction assay

2.9.4 Cloning of *mCherry* gene into *pBlueScriptSK+MCS*

The coding region of *mCherry* was PCR amplified from plasmid purchased from Clontech (Plasmid WAVE 6R *mCherry*) with primers containing HindIII and SpeI restriction sites and sub-cloned into *pBlueScriptSK+MCS*.

2.9.5 Cloning of *ERF4* gene and its mutant variants

Genomic DNA of *Arabidopsis* WT Col-0 was used as a template for PCR amplification of *ERF4* open reading frame (ORF) using primers containing ApaI, AscI restriction sites in the forward primer and FseI in the reverse primer. The PCR product was sub-cloned into *pDRIVE* using QIAGEN PCR cloning kit (QIAGEN). In the next step, a positive clone was used as a template for PCR amplification of *ERF4* with the same primer set. Subsequently, the PCR product was sub-cloned into *pBlueScriptSK+MCS* already containing *mCherry* between ApaI and FseI restriction sites. To obtain mutant variants of the native *ERF4* gene the PCR reaction with specific primers as indicated in

Figure 10 and Table 5 and 6 was employed. A mutant form of the *ERF4* lacking AP2/ERF DNA binding domain (*dAP2*) and mutant lacking central domain (*dC*) was prepared by inverse PCR with pBlueScriptSk+MCS_ERF4-mCherry as a template, followed by enzymatic digestion with EcoRI or XmaI, respectively, and self-ligation. The mutant variant, missing the repressor domain at a C-terminal end (*dEAR*), was PCR amplified and sub-cloned into pBlueScriptSK+MCS_mCherry. In-frame fused sequence of *ERF4* (full length) and *mCherry* was sub-cloned into the pBIB-UAS-tNOS plasmid (kindly provided by Dr. Kenji Nakajima, Nara Institute of Science and Technology, Japan) at ApaI and SpeI restriction sites (Figure 11). Mutant variants were sub-cloned into pBIB-ERF4-mCherry-tNOS at AscI and SpeI restriction sites by replacement of *ERF4* ORF. As a control *mCherry-only* sequence was sub-cloned in the same vector at HindIII and SpeI restriction sites. Prepared constructs were transformed into *Agrobacterium tumefaciens* GV3101 strain and the *Arabidopsis* ERF4GAL4 enhancer trap line (Gardner et al., 2009) was transformed using floral dip method (Zhang et al., 2006). Thus, all the constructs were driven under the control of native *ERF4* enhancer (Figure 12). Positive plants were selected on 1 x MS medium containing Carbenicillin (100 mg/L) and Hygromycin b (25 mg/L).

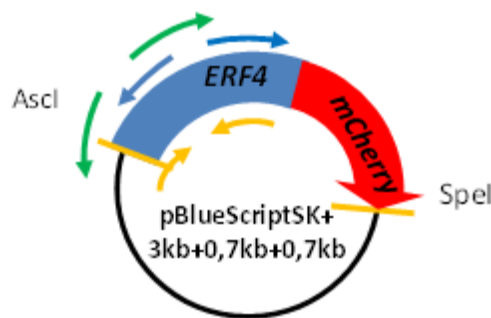


Figure 10: Cloning strategy of *ERF4* mutant forms. Different sets of primers were used to PCR amplify mutant variants of *ERF4* gene from *pBluescriptSK+ERF4-mCherry*. The variants *dAP2* and *dC* were prepared by inverse PCR using green and blue primer pair, respectively. The amplicons were digested with EcoRI or XmaI, respectively, and self-ligated. The *dEAR* variant was amplified using reverse primer lacking EAR motif. Next, the PCR product was digested at AscI and FseI restriction sites and original *ERF4* sequence in *pBluescriptSK+ERF4-mCherry* was replaced.

Name of construct	Used enzyme	Deletion	Primers
<i>dAP2</i>	EcoRI	1-19 Δ 81-222	FdAP2EcoRI RdAP2EcoRI
<i>dC</i>	XmaI	1-80 Δ 201-222	FdCXmaI RdCXmaI
<i>dEAR</i>	AscI, FseI	1-210 Δ	FdRAscI RdRFseI

Table 5: Overview of the cloning strategy of *ERF4* mutant variants.

Gene/Construct	Primers for cloning	Sequence 5' → 3'
<i>ERF4dEAR</i>	ERF4dRD_FApaIAscI	AATGGGCCCCGGCGCGCCATGGCCAAGATGGGCTTG
	ERF4dRD_RFseI	TTAGGCCGGCCATCTAACAGCTGAGATCTCTTC
<i>ERF4dC</i>	ERF4dC_FXmaI	TTTCGACCCGGGGATGGAGAAGAGATCT
	ERF4dCR_XmaI	GAAAACCCGGGAAATTGGTCTTAGCC
<i>ERF4dAP2</i>	ERF4dAP2_FEcoRI	GACCGAATTCCCAACTTTTCTCGAGC
	ERF4dAP2_REcoRI	AACGGAATTCTTTGGCATTATTGTGG
<i>ERF4N-ESR2C</i>	ESR2FAscI	CTTAGGCGCGCCATGGAAGAAGCAATCATGAG
	ESR2R_FseI	ACAGGCCGGCCATAATCATCATGAAAGCAATAC
	M13_F	TGTAAAACGACGGCCAGTG
	M13_R	GGAAACAGCTATGACCATGA
	ESR2C_FBamHISnaBI	TCGAGGATCCTACGTATACCCAATGCCT
	ERF4N_RPstiDraI	GAGCTGCAGTTTAAAATTGGTCTTAGC
<i>mCherry</i>	mC_FHindIIIFseI	TTTAAGCTTGGCCGGCCTATGTTGAGCAAGGGCGAGG
	mC_RSpeI	AGTACTAGTTTACTTGTACAGCTCGTCCATGC
<i>MCS linker</i>	MCS5'	GATCCGGCGCGCCTTTAATTAAGCCGGCCTTACTAGTT
	MCS3'	CTAGAACTAGTAAGGCCGGCCTTAATTAAAGGCGCGCCG
<i>HPT</i>	HPT_FSpeI	ATCCACTAGTATGAAAAAGCCTGAAC
	HYG_cas_RHindIII	AGCGGCATGCAAGCTTTTCGAGGG

Table 6: List of primers used for cloning mutant variants of *ERF4* gene, the active form of *ERF4* and plasmids modification

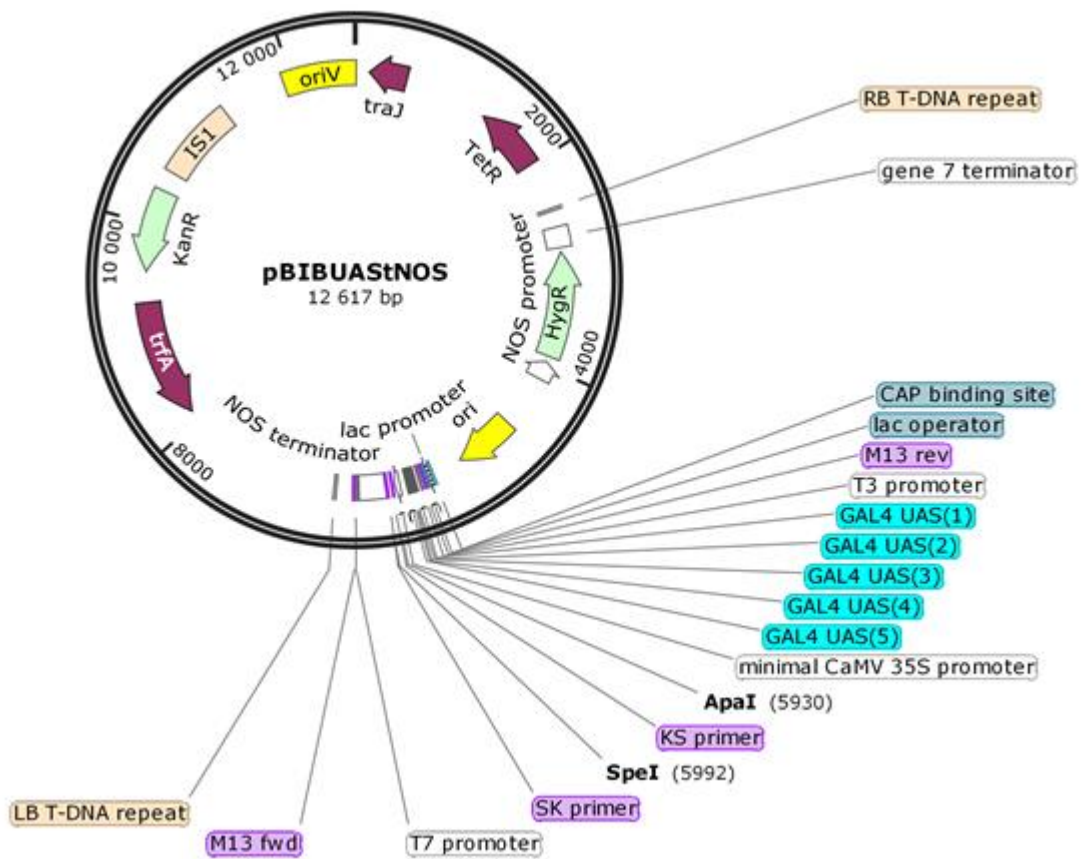


Figure 11: DNA plasmid map of the binary vector pBIB-UAS-tNOS with indicated restriction sites, *ApaI* and *SpeI*.

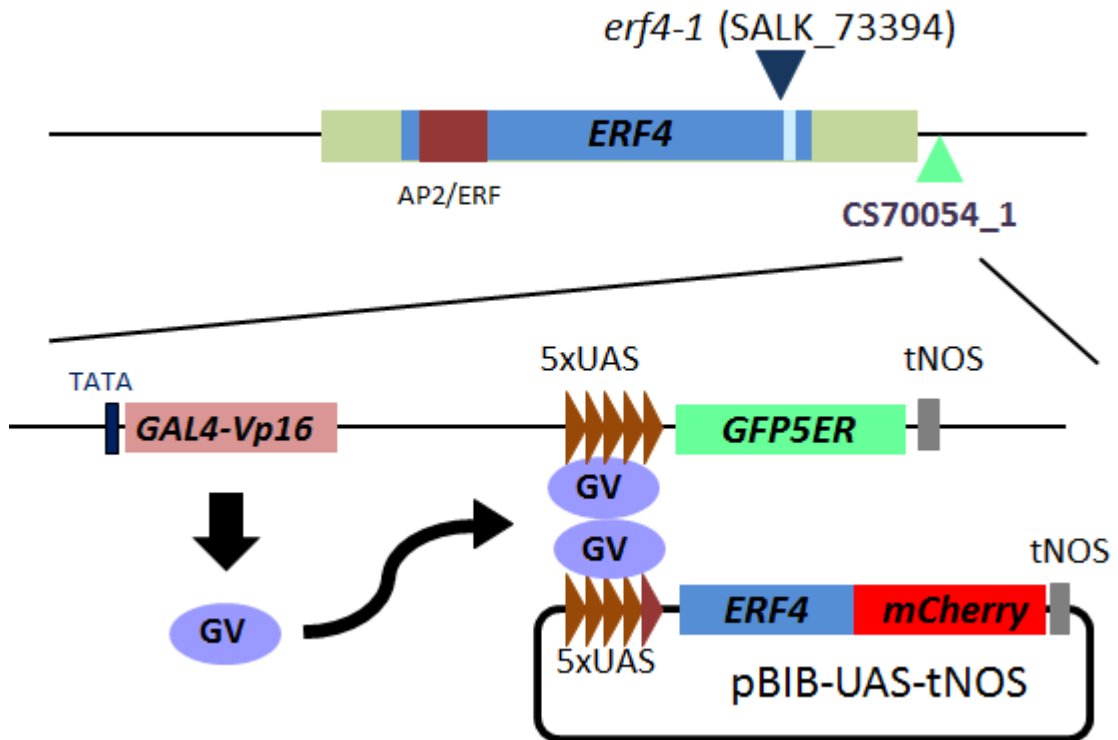


Figure 12: Schematic description of ERF4GAL4 enhancer trap line and *pBIB-UAS-ERF4-mCherry-tNOS* construct. T-DNA insertion line *erf4-1* harbors transcriptional cassette CS70054_1 controlled by native ERF4 enhancer. Transcribed trans-activating transcription factor GV recognizes 5xUAS sequence. The specific binding to 5xUAS triggers transcription of the downstream transcriptional unit; endoplasmic reticulum localized green fluorescent protein (GFP5ER). In the presence of *pBIB-UAS-ERF4-mCherry-tNOS* construct, GV binds also to the 5xUAS sequence of the construct and triggers expression of *ERF4-mCherry*.

2.9.6 Preparation of ERF4 active form

A transcription-active form of ERF4 was prepared by fusing *ERF4* nucleotide sequence corresponding to 1 – 81 amino acids (AP2/ERF DNA binding domain) with an *ESR2* nucleotide sequence corresponding to 113 – 307 amino acids (transactivation domain), resulting in *N4C2*. Firstly, the ORF of *ESR2* was PCR amplified from cDNA using forward and reverse primer containing AscI and FseI, respectively, and subcloned into pDRIVE using QIAGEN PCR cloning kit (QIAGEN). Subsequently, C-terminal region of *ESR2* was PCR amplified from *pDRIVE-ESR2* using forward primer containing BamHI restriction site and M13 reverse. The PCR product was then subcloned into pBlueScript+MSC between BamHI and FseI. N-terminal region of *ERF4* was PCR amplified from pBluescriptSK+MCS using M13 forward primer and DraI reverse primer, the PCR product was digested with AscI and DraI restriction enzymes and subcloned into pBlueScriptSK+*ESR2C* digested with AscI and SnaBI. Thus prepare

construct was subcloned into pKSEM50 (Figure 13) binary vector between AscI and FseI restriction sites. Stop codon of *ESR2* was deleted and instead, hormone-binding domain of *ESTRADIOL RECEPTOR* fused with 4xMyc tag (*EM*) was fused in frame with *N4C2*, resulting in *N4C2-ER*, under the control of a constitutive *CaMV35S* promoter (Figure 14). Analogically, the negative control *GFP* as well as the positive control *ESR2* was PCR amplified using forward and reverse primers containing AscI and FseI, respectively, and subcloned into pKSEM50 at AscI and FseI restriction sites. Prepared constructs were transformed into *Agrobacterium tumefaciens* strain GV3101 and then in *Arabidopsis* WT Col-0 using floral dip (Zhang et al., 2006). Transgenic plants were selected on 1x medium containing carbenicillin (100 mg/L) and Kanamycin (75 mg/L).

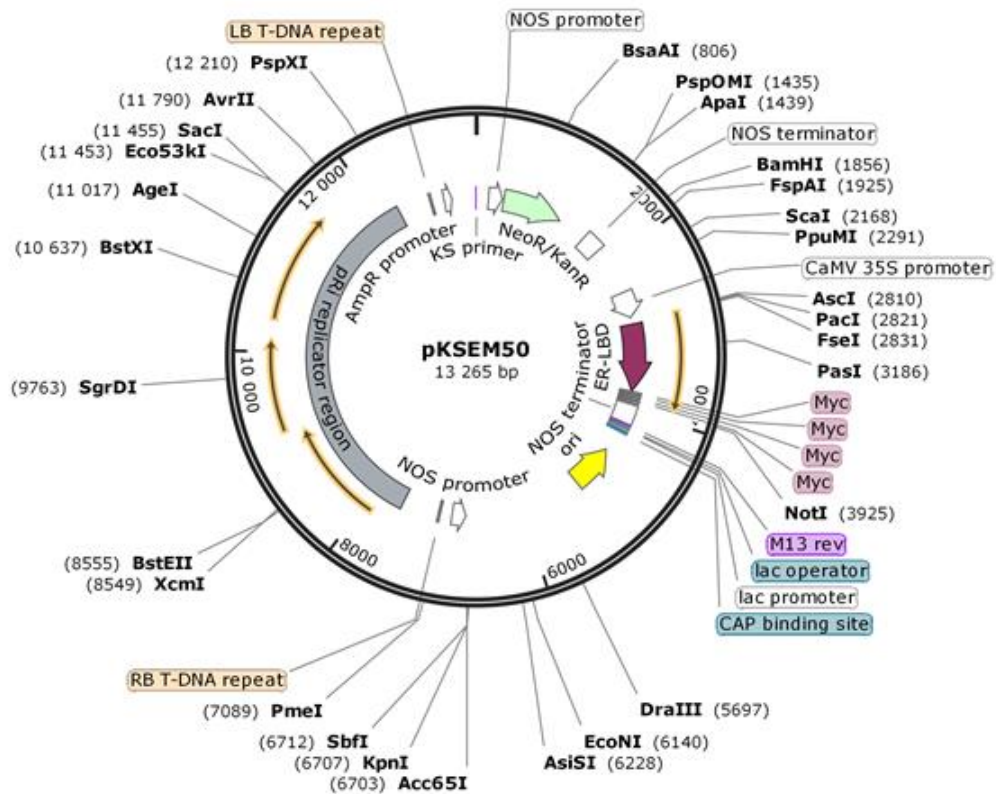


Figure 13: DNA plasmid map of the binary vector used for estradiol translocation system.

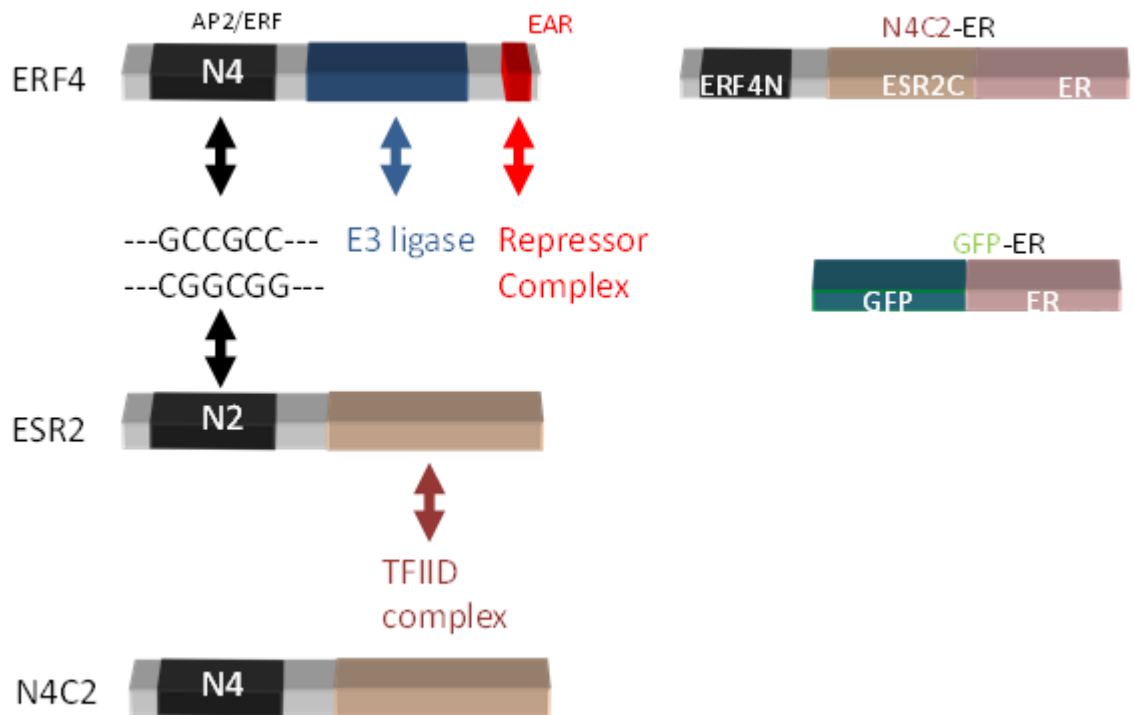


Figure 14: Schematic description of preparation active form of ERF4. The ERF4 protein contains DNA-binding domain AP2/ERF at the C-terminal end, similar to the ESR2 transcription activator. The repression domain at the N-terminal end of ERF4 was replaced with N-terminal end of ESR2, which was fused to ER – estradiol binding receptor motif. As a control, GFP-ER fusion was prepared.

2.10 Constructs preparation for CRISPR/Cas9

To introduce a mutation in *ERF11* gene CRISPR/Cas9 technique was employed. Two sets of protospacers named Cr2606 (1) and Cr2657 (1) carrying sites for unique restriction enzymes, BsaI or PmlI (highlighted in blue) were subcloned first into pEn-Chimera vector using BbsI restriction site and then sub-cloned into pDE-Cas9 using Gateway™ LR Clonase II (Invitrogen). The protospacers were designated to be adjacent to the PAM (protospacer adjacent motif) presented in the DNA, showed in red (1), (2). Both pEn-Chimera plasmid and pDE-Cas9 plasmid were kindly provided by Prof. Puchta (Karlsruhe Institute of Technology, Germany) (Fauser et al., 2014). Phosphinothricin resistance cassette was replaced by Hygromycin b resistance cassette (HPT) using SpeI and HindIII restriction sites. The HPT region was amplified from pER8 plasmid (Zuo et al., 2000).

Prepared constructs were transformed into *Agrobacterium tumefaciens* strain GV3101 and then delivered into *Arabidopsis* quadruple mutant *erf4-1;8;9-1;12* by using floral dip (Zhang et al., 2006). Transgenic plants were selected on 1x MS medium containing Carbenicillin (100 mg/L) and Hygromycin b (25 mg/L).

(1)

Cr2606

	BsaI		gDNA	BsaI	PAM
F	5'	attgGAGGAGTGAGGAAGAGACCA	3'	5'	GAGGAGTGAGGAAGAGACCATGG ^{3'}
R	3'	CTCCTCACTCCTTCTCTGGTcaaa	5'	3'	CTCCTCACTCCTTCTCTGGTACC ^{5'}
				5'	GAGGAGUGAGGAAGAGACCANNN ^{3'}
					sgRNA

(2)

Cr2657

	PmlI		gDNA	PmlI	PAM
F	5'	attgCTTTCAAGAAGTCACGTGTC	3'	5'	CTTTCAAGAAGTCACGTGTC ^{3'}
R	3'	GAAAGTTCTTCAGTGACACAGcaaa	5'	3'	GAAAGTTCTTCAGTGACACAGACC ^{5'}
				5'	CUUUCAAGAAGUCACGUGUCNNN ^{3'}
					sgRNA

Similar to *ERF11*, CRISPR/Cas9 system was employed to produce complete null allele of *BPM1* gene. Two sets of protospacers named Cr1070c (3) and Cr1224 (4) were designed carrying unique EcoRI and NheI restriction sites, respectively (in blue). After subcloning the protospacers into the original binary vector the WT Col-0 plants were transformed by *Agrobacterium*, as described above. Transgenic plants were selected on 1x MS medium containing Carbenicillin (100 mg/L) and Phosphinothricin (16 mg/L).

The cleaved amplified polymorphic sequence (CAPS) analysis (Konieczny and Ausubel, 1993) was carried out to identify single nucleotide polymorphism caused by CRISPR/Cas9. DNA from transgenic plants was PCR amplified in the region of protospacers and digested with restriction enzyme as indicated in protospacers (1), (2), (3), and (4). Plants showing different profile from WT were sequenced.

(3)

Cr1070c

```

                                     EcoRI
R 5' attgACCCACAGATCTTGAATTCA 3'
F 3' TGGGTGTCTAGAACTTAAGTcaaa5'
                                     sgRNA
3' NNNACUUAAGUUCUAGACACCCA5'
5' GGTGGAATTCAAGATCTGTGGGT3'
3' CCAACTTAAGTTCTAGACACCCA5'
                                     PAM EcoRI
gDNA
```

(4)

Cr1224

```

                                     NheI
F 5' attgTTCATAGCTCTTGCTAGCGA 3'
R 3' AAGTATCGAGAACGATCGCTcaaa5'
                                     gDNA NheI PAM
5' TTCATAGCTCTTGCTAGCGAAGG3'
3' AAGTATCGAGAACGATCGCTTCC5'
5' UUCAUAGCUCUUGCUCUAGCGANNN3'
                                     sgRNA
```

2.11 RNA-seq

Root explants from 3 independent T3 homozygous lines harboring *35S::N4C2ER*, *35S::ESR2ER* (positive control), and *35S::GFPER* (negative control) grown on B5 hormone-free medium (1x Gamborg B5 medium, 2 % glucose, 0.05 % MES, pH 5.7) were prepared, pre-treated on CIM for 3 days. Expression of the transgene was then induced by application of 10 μ M β -estradiol overnight. After 1-hour of 30 μ M cycloheximide (CHX) treatment (Ikeda et al., 2006) total RNA was extracted and subjected to RNA-seq analysis. The RNA-seq procedure was performed as described previously (Vojta et al., 2016).

2.12 Yeast two-hybrid assay (Y2H)

To investigate the protein-protein interaction, yeast two-hybrid assay Matchmaker[®] Gold *Yeast Two-Hybrid System* (Clontech), based on split GAL-4 transcription factor into DNA binding domain (BD) in plasmid pGBKT7 and activation domain (AD) in plasmid pGADT7, was employed. Chemo-competent cells, *Saccharomyces cerevisiae* strain Y2HGold Yeast, were simultaneously transformed with both pGBKT7 and pGADT7

vectors, harboring translation fusion of BD with ERFs and AD and with BPMs and *vice versa*. Positive transformants were selected on solid SD medium without tryptophan (Trp) and leucine (Leu). Two positive colonies for each protein-protein combination were chosen and inoculated onto liquid SD -Trp, -Leu medium, and incubated overnight. Subsequently, each culture was dropped on the solid SD selection medium lacking tryptophan, leucine, histidine, and adenine. Incubation was carried out at 28°C. The growth of colonies was observed only if the interaction of proteins took a place.

2.13 Chemical treatment

β-estradiol

4-days-old *Arabidopsis pER10-ERF4Myc* seedlings harboring ERF4Myc fusion (Zuo et al., 2000) under the control of estradiol-inducible promotor were treated overnight with 10 μM β-estradiol to induce transgene expression.

MG132

4-day-old *Arabidopsis* seedlings were treated overnight with 50 μM proteasome inhibitor MG132. For tissue culture studies, MG132 was directly added into solid medium to obtain a final concentration of 50 μM.

2.14 Whole-mount immuno-fluorescence

Arabidopsis seedlings were fixed with ice-cold 4 % paraformaldehyde in 1 x PBS (phosphate-buffered saline) for 5 minutes under the vacuum. Seedlings were kept in ice-cold fixation solution for another 5 hours. After fixation, material was washed twice with ice-cold 1 x PBS for 3 minutes and treated with enzymatic cocktail [(1 % pectolyase (Sigma-Aldrich); 0.7 % cellulase (Calbiochem); 0.7 % cellulase R10 (Duchefa); 1 % cytohelicase (Sigma-Aldrich) dissolved in 1 x PBS] for 30 – 60 minutes in wet chamber at 37°C. Next, seedlings were washed four times with ice-cold 1 x PBS for 5 minutes, incubated for 1 hour at 4°C in membrane penetration solution (10 % DMSO; 3 % NP-40 in 1 x PBS), and again four times washed with ice-cold 1 x PBS for 5 minutes. Samples were incubated with a primary antibody, anti-c-Myc (9E10), mouse monoclonal, **1:500** (Santa Cruz, sc-40) diluted in antibody-solution (2 % BSA; 1 x PBS; 0.1 % Triton X-100), overnight at 4°C. Primary antibody was washed out four times with ice-cold 1 x PBS for 5 minutes and material was immediately incubated with secondary antibody, donkey anti-mouse Alexa 488, **1:200** (Dianova, 715-546-151) diluted in antibody-solution, for 3 hour at 37°C and following four times wash with

ice-cold 1 x PBS for 5 minutes. Material was post-fixed with ice-cold 4 % paraformaldehyde 5 minutes under the vacuum; washed four times with ice-cold 1 x PBS for 5 minutes; and stained with DAPI.

2.15 Nuclei isolation and sorting

5-day-old *Arabidopsis* seedlings were fixed in 4 % formaldehyde on ice for 20 minutes. After washing three times with Tris-buffer (10 mM Tris; 10mM Na₂EDTA; 100 mM NaCl; 0.1 % Triton X-100; pH 7.5) the tissue was chopped with a razor blade in nuclear isolation solution LB01 (15 mM Tris; 2 mM Na₂EDTA; 0.5 mM spermine tetrahydro-chloride; 80 mM KCl; 20 mM NaCl; 0.1% Triton X-100; pH7.5) (Doležel et al., 1989) and filtered through the 50 µm filter CellTrics[®] (SYSMEX). Isolated nuclei were sorted according to the ploidy using the high-speed cell sorter BD INFLUX. Fraction containing 8C nuclei was embedded in a saccharose buffer (10 mM Tris; 50mM KCl; 2 mM MgCl₂; 5 % saccharose; 0.05 % Tween20; pH 7.5) on microscopic slide. For long-term storage, slides were kept at 20°C, while for a short time period at 4°C.

2.16 Immunostaining

Slides with embedded nuclei were three times washed with 1 x PBS (137 mM NaCl; 2.7 mM KCl; 10 mM Na₂KHPO₄·2H₂O; 1.8 mM KH₂PO₄; pH 7.4) and incubated for 1 hour with blocking solution (5 % BSA; 1 x PBS; 0.3 % Triton X-100). Subsequently, primary antibodies were added and samples were incubated overnight at 4°C.

Primary antibodies were diluted in antibody-solution (1 % BSA; 1 x PBS; 0.1 % Triton X-100) as followed:

Anti-Histone H3 (acetyl K9), rabbit polyclonal, **1:500** (Novus Biological, NBP2-44095)

Anti-Histone H3 (acetyl K14), rabbit polyclonal, **1:1000** (MerckMillipore, 07-353)

Anti-Histone H3 (acetyl K18), rabbit polyclonal, **1:1500** (Abcam, ab1191 ChIP Grade)

Anti-Histone H3 (acetyl K23), rabbit polyclonal, **1:100** (Abcam, ab46982)

Anti-Histone H3 (acetyl K9 + K14 + K18 + K23 + K27), rabbit polyclonal, **1:500** (Abcam, ab47915 ChIP Grade)

Anti-RNAPIISer2ph (active; phosphorylated at Ser2), rat monoclonal, **1:200** (MerckMillipore, 04-1571)

Anti-RNAPII inactive, mouse monoclonal, **1:300** (Abcam, ab817)

Anti-c-Myc (9E10), mouse monoclonal, **1:500** (Santa Cruz, sc-40)

Anti-RFP, rat monoclonal, **1:1000** (Chromotek, 5f8-20)

Slides with nuclei specimen were then washed three times in 1x PBS and incubated with secondary antibodies 1 hour at 37°C.

Secondary antibodies were diluted in antibody-solution as followed:

Goat anti-mouse Alexa 488, **1:200** (Invitrogen, A-11001)

Donkey anti-mouse Alexa 488, **1:200** (Dianova, 715-546-151)

Goat anti-rat Alexa 488, **1:200** (Jackson ImmunoResearch, 112-545-167)

Goat anti-rabbit DyLight 594, **1:500** (Abcam, ab96885)

Goat anti-rat DyLight 594 **1:500** (Abcam, ab98388)

Finally, nuclei were dehydrated in 70 %, 85 %, and 96 %

ethanol gradient. Dehydrated nuclei were counterstained with DAPI (1 µg/ml) (Molecular Probes, D1306) diluted in Vectashield mounting medium (Linaris, H-1000) (Schubert et al., 2013).

2.17 Microscopic analysis of co-immunostained nuclei and whole-mount immunostained seedlings

Immunostained samples were analyzed using an epifluorescence microscope (BX61; Olympus, <https://www.olympus.com>) equipped with a cooled charge-coupled device (CCD) camera (Orca ER; Hamamatsu, <http://www.hamamatsu.com>).

To observe epigenetic marks, ERF4Myc fusion protein and its co-localization with RNAPolIII more in detail at a resolution of ~120 nm (super-resolution achieved with a 488 nm laser) structured illumination microscopy (SIM) was performed with a 63×/1.4 Oil Plan-Apochromat objective of an Elyra PS.1 microscope system and the software ZENblack (Carl Zeiss GmbH). Images were captured separately for each fluorochrome using the 642, 561, 488, and 405 nm laser lines for excitation and appropriate emission filters (Weisshart et al., 2016).

2.18 Live-cell imaging

Prior to sub-cellular localization analysis of ERF4 protein, 8-days-old transgenic *Arabidopsis* seedlings of T2 or T3 generation were briefly checked for the strongest fluorescence signal using the epifluorescence microscope (BX61; Olympus, <https://www.olympus.com>). Namely, 10 lines of *pBIB-UAS-ERF4-mCherry-tNOS*, 9 lines of *pBIB-UAS-dAP2-mCherry-tNOS*, 6 lines of *pBIB-UAS-dC-mCherry-tNOS*, 8 lines of *pBIB-UAS-dR-mCherry-tNOS*, and 3 *pBIB-UAS-mCherry-only-tNOS* were tested. Two best lines per each genotype were chosen for further analysis using laser scanning confocal microscopy (LSCM) LSM 780 (Carl Zeiss GmbH) equipped with C-Apochromat 40x/1.20 W Korr FCS M27 objective. Images taken by the T-PMT camera were processed in ZEN software Black edition (Carl Zeiss GmbH) Settings for laser beam were similar to (Dreissig et al., 2017).

3 Results

3.1 Selection of T-DNA insertion lines of *ERF* and *BPM* genes

To shed a light on the role of ERF transcriptional repressors in developmental processes different mutant lines of *ERF* and *BPM* genes were used. A genetic approach was used to create higher-order mutant lines. *Arabidopsis* lines mutated in *ERF* and *BPM* genes obtained from NASC were three times backcrossed with wild-type (WT) plants of Col-0 ecotype to remove additional non-specific mutations. After backcrossing plants were grown on a particular selection medium (2.3 Plant selection), positive seedlings were transferred to the soil and self-pollinated. Each line was genotyped and then sequenced to identify the exact position of T-DNA insertion. The structure of *ERF* genes is simpler than the one of *BPM* genes. *ERF* genes consist of one exon; the introns are missing. Positions of T-DNAs are indicated in Figure 15. In the case of *erf4-1*, *erf9-1*, and *erf12* the T-DNA is inserted in the coding region. These alleles were considered as strong alleles because T-DNA lying within the exons is very likely resulting in complete knock-out of the gene. The weak alleles usually contain the T-DNA in the promoter region or in the 5'UTR or 3'UTR e.g. in the case of *erf8*, *erf10*, and *erf11*. Two T-DNA insertion lines carrying weak alleles of *BPM1* were selected both carrying an insertion in the promoter region, SALK_31057 and SALK_152026. For *BPM2* one T-DNA insertion line was chosen and the T-DNA was confirmed in the last exon. In the case of *BPM3*, two independent insertion lines were examined. Line SALK_72848 contains T-DNA in the introns, therefore there was a chance that gene disruption is not complete. Line GB-436E12 harbors T-DNA in the second exon, considered again as a strong allele (Figure 16).

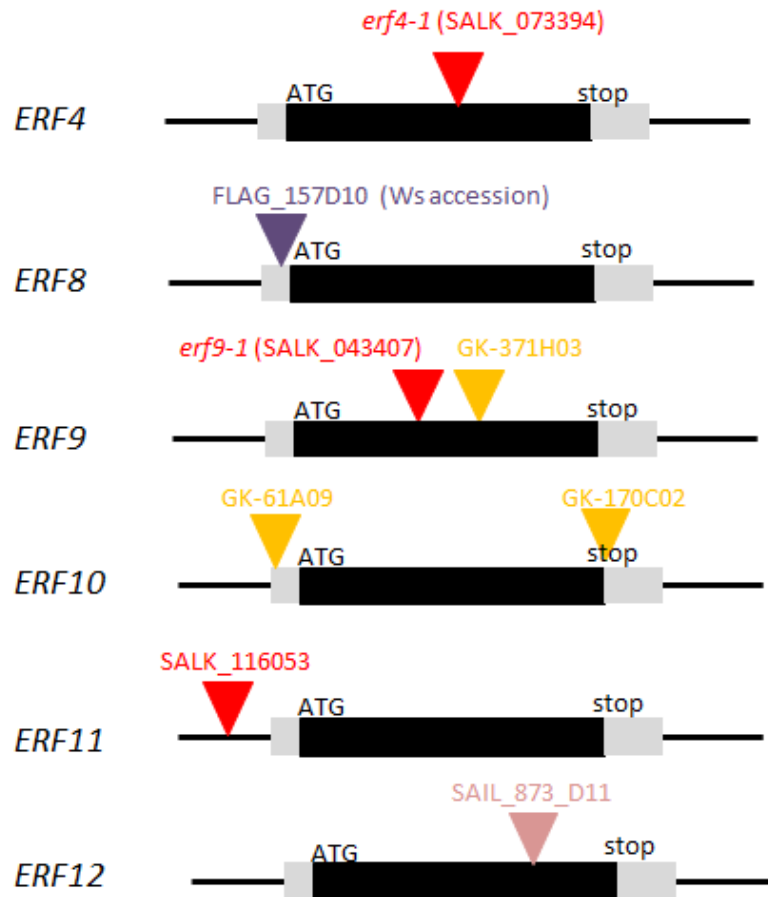


Figure 15: Schematic representation of T-DNA position in the particular *ERF* genes. Arrowheads indicate the confirmed position of T-DNA in the DNA sequence. Grey boxes represent 5'UTR or 3'UTR while black boxes depict exon.

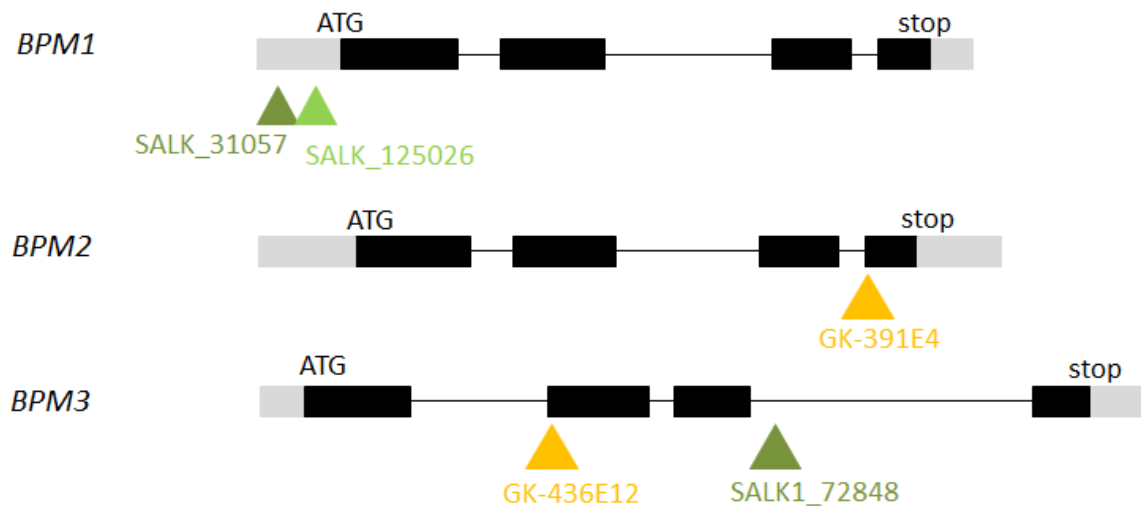


Figure 16: Schematic representation of T-DNA position in the particular *BPM* genes. Arrows heads indicate the concrete position of T-DNA in the DNA sequence. Grey boxes – 5'UTR or 3'UTR; black boxes – exons; lines – introns.

The expression status of the gene was estimated using semi-quantitative RT-PCR. Endogenous control *TUBULIN3* was used to normalize the amount of cDNA template used in the reaction. The number of PCR cycles was optimized for each target gene. No PCR product was detected in most of the analyzed *erf* mutant lines, thus no transcript of the target genes was present in these mutants. Therefore these *erf* T-DNA insertion lines; namely *erf4* (SALK_073394), *erf9*, *erf9*, *erf10*, *erf11*, and *erf12*; were considered as a complete knock-out (Figure 17). In the case of *erf8* mutant, the amount of *ERF8* transcript was significantly decreased. Based on this result the *erf8* is considered as a knock-down mutant line. Surprisingly, the expression of *ERF10* in *erf10* (GK-61A09) mutant was increased when compared to WT Col-0. This is most likely due to the T-DNA position in the promoter region (Figure 15). On the contrary, no mRNA was detected in *erf11* SALK_116053 mutant line even though the T-DNA insertion lies in the promoter region. This result may not exclude partial *ERF11* expression which was beyond the detection limit of the method. Mutant lines of *erf4* (SALK_073394) denoted as *erf4-1*, *erf8* (FLAG_157D10), *erf9* (SALK_043407) denoted as *erf9-1*, *erf10* (GK-170C02), *erf11* (SALK116053) denoted as *erf11-1*, and *erf12* (SAIL_873_D11) were used for further experiments.

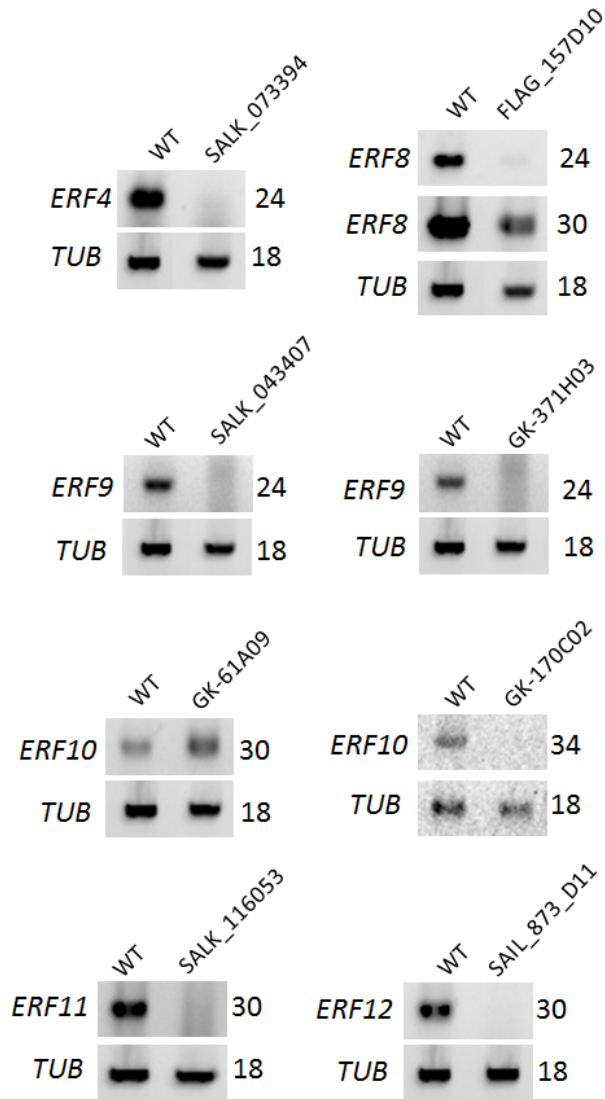


Figure 17: Identification of knock-out T-DNA insertion lines in *ERF* genes. Semi-quantitative RT-PCR confirmed malfunction of indicated *ERF* genes. Numbers of PCR cycles were optimized for each mutant line independently. *TUBULIN3* (TUB) served as an endogenous control.

In the case of *BPM* genes, *bpm1* SALK_125026 and SALK_31057 lines were shown not to be knock-out lines. Interestingly, based on semi-quantitative RT-PCR, the SALK_31057 line appeared to be an overexpressor. On the other hand, *bpm2* GK-391E4 and *bpm3* GB-436E12 mutant lines were confirmed to be a complete knock-out; and *bpm3* SALK_72848 line as a knock-down line (Figure 18).

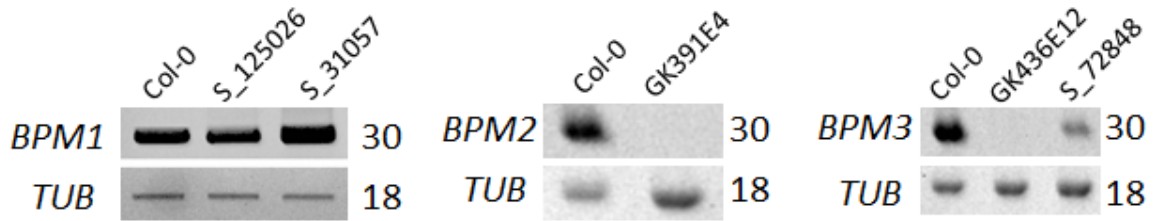


Figure 18: Identification of knock-out T-DNA insertion lines in *BPM* genes. Semi-quantitative RT-PCR confirmed malfunction of indicated *ERF* genes. Numbers of PCR cycles were determined for each mutant line independently. *TUBULIN3* (TUB) served as an endogenous control.

Higher-order mutant combinations were obtained by crossing individual single mutants followed by self-pollination. Due to the linkage of *ERF11* (At1g28370) and *ERF12* (At1g28360) genes, it was impossible to obtain double mutant using traditional crossing approach. To overcome this issue, CRISPR/Cas9 system was employed to engineer the *ERF11* gene. Two sets of protospacers were designed to disrupt *ERF11* gene. Since *erf12* T-DNA knock-out line carries SAIL_873_D11, *erf12* hetero- or homozygous plants confer phosphinothricin resistance and the original pDe-Cas9 vector also contains the same resistance cassette. Therefore, the phosphinothricin acetyltransferase gene (BlpR) was replaced with aminoglycoside phosphotransferase (HygR). Thus after quadruple *erf4-1;erf8;erf9-1;erf12* mutant was transformed the positive transformants were selected on hygromycin. More than 20 transgenic hygromycin resistant plants were obtained and at least 8 individual lines were sequenced. One line was selected for further experiments as recognizable deletion was possible to detect using simple sequence length polymorphism analysis (SSLP) marker. A number of pDe-Cas9 integrations appeared to be single by hygromycin resistance. The integrated T-DNA, *pDe-Cas9*, segregated out in the following T2 generation and the lack of *pDe-Cas9* was confirmed by PCR. Figure 19 shows the SSPL analysis, the 32 bp deletion was confirmed by sequencing. Since *ERF11* does not contain introns such deletion affects the coding region and results in truncation of ERF11 protein at 25 amino acids position which is likely to be non-functional. The resulting homozygous mutant can be considered as a null allele (Figure 20). The new mutated line was designed as *erf11-2*. The homozygous state of remaining *ERF* genes was confirmed by PCR, thus obtaining quintuple *erf4-1;8;9-1;11-2;12* mutant line.

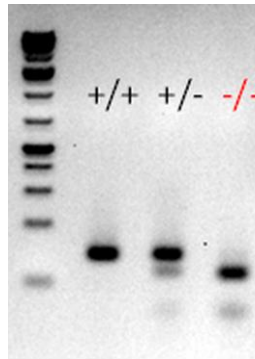


Figure 19: SSPL analysis of T2 *erf11-2* transgenic plants. Simple sequence length polymorphism analysis revealed the 32 bp deletion caused by CRISPR/Cas9 system. The heterozygous plants (+/-) show two bands, the upper band corresponds to WT allele, the lower band represents 32 bp deletion. The line highlighted in red indicates a homozygous individual (-/-).

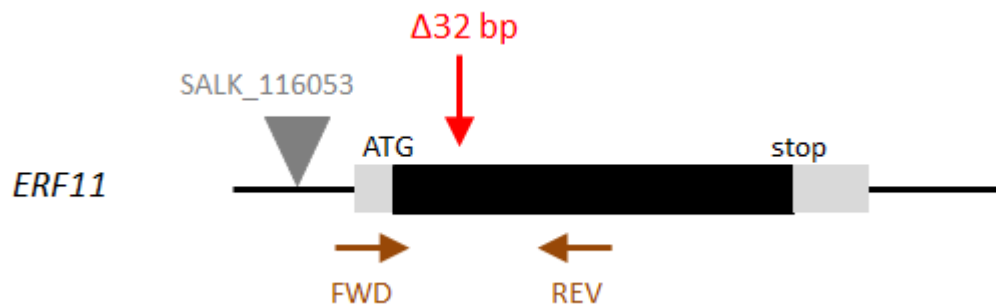


Figure 20: Schematic representation of *erf11-2* mutant obtained using CRISPR/Cas9 system. T-DNA insertion line SALK_116053 carries T-DNA insertion in 5'UTR and might not be a complete knock-out mutant. To obtain mutation in the coding region, CRISPR/Cas9 system was employed. Sequencing analysis of *erf11-2* T1 plants revealed 32 bp deletion in the coding region.

Because *bpm1* SALK_31057 and *bpm1* SALK_125026 mutant lines did not display complete gene disruption the CRISPR/Cas9 system was employed to create complete knock-out in *BPM1* gene. No obvious deletion/insertion was observed in T1 transgenic plants after the PCR amplification of the sequence with the putative mutated site. The CAPS analysis did not reveal any change in sensitivity to cleavage by selected restriction enzymes. Sequencing of selected plants did not unveil clear modification in the nucleotide sequence, assuming the chimeric state. The CAPS analysis of T2 generation revealed plants partially resistant to cleavage by EcoRI (Cr1070c protospacer) (Figure 21), these plants were propagated to the next generation and sequenced to verify the homozygous state. Sequencing confirmed the one base-pairs insertion (A) in the first exon (Figure 22). The mutation causing frame-shift and thus likely resulting in null mutation was confirmed also at RNA level (Figure 23). The

positive homozygous *bpm1* mutant plant was crossed with *bpm2* and *bpm3* mutant lines to prepare a triple mutant.

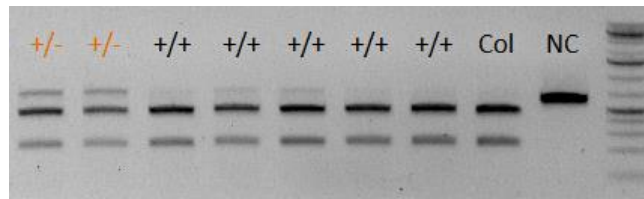


Figure 21: CAPS analysis of T2 *bpm1* transgenic plants. Mutation introduced by CRISPR/Cas9 into protospacer sequence (cr1070) removed EcoRI restriction site and plants were resistant to digestion. Col – WT Col-0; NC – negative control resistant to EcoRI digestion; +/+ WT plants without mutation in EcoRI site, +/- heterozygous plants carrying one mutated allele in *BPM1* gene.



Figure 22: Schematic representation of *bpm1cr1070* mutant obtained by CRISPR/Cas9 system. One base-pair insertion in the first exon of *BPM1* gene resulting in the frame-shift was detected. The addition of an A was confirmed by sequencing.

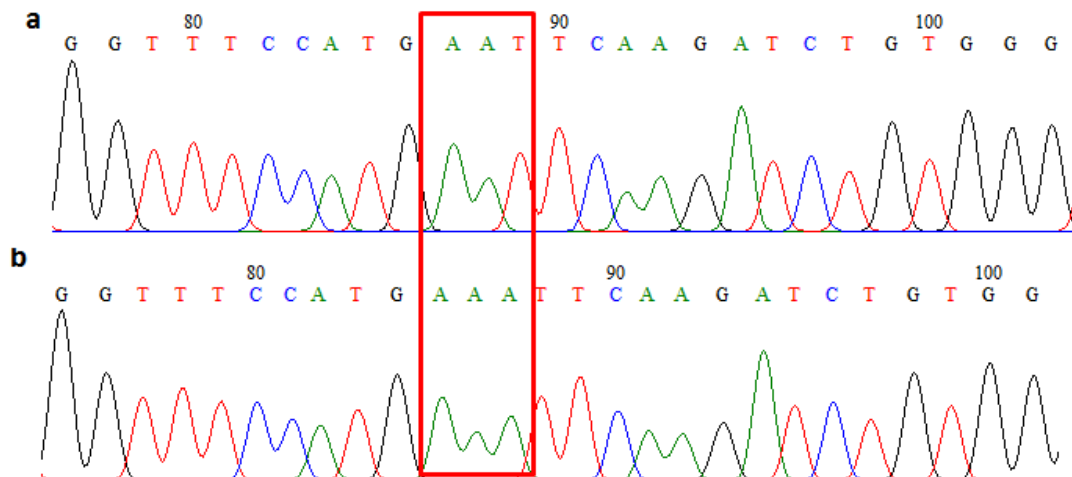


Figure 23: Confirmation of *bpm1cr1070* mutation at the RNA level. a) chromatogram showing *BPM1* WT sequence b) chromatogram showing *BPM1* sequence of *bpm1cr1070*. One adenine insertion in the first exon of *BPM1* was confirmed in cDNA of *bpm1cr1070* mutant line.

3.2 Proteolysis is essential for the correct development

Before the genetic analysis of *erf* and *bmp* higher-order mutant was carried out, the chemical treatment was conducted first to monitor the global impact of proteolysis on development. Root explants prepared from 5-day-old WT Col-0 seedlings were incubated on medium (MS, CIM, SIM) with or without MG132 proteasome inhibitor and the shoot regeneration phenotype was observed (Figure 24a). Explants grown on medium without MG132 started to green and expand their size when transferred on SIM. After 10 days on SIM incubation first shoots started to emerge. From such regenerated explants, new roots penetrated into the medium (Figure 24c). Interestingly, no shoot regeneration was observed when explants were grown on medium with MG132. The explants were yellowish and smaller than explants grown on medium without MG132. Also, the growth was considerably reduced; the size of explants remained similar to the starting size (5 – 8 mm); and roots emerging from explants were very short (Figure 24b). Application of proteasome inhibitor had a clear impact on shoot regeneration and development itself. This result indicates that protein degradation is essential for the proper development of plants.

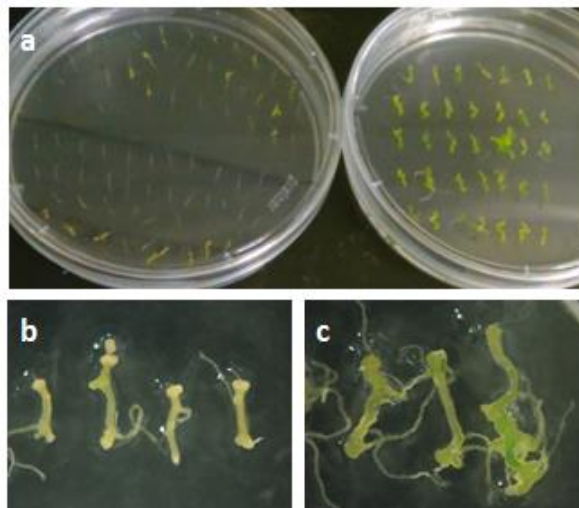


Figure 24: Pharmacological treatment of Col-0 root explants with MG132 reduces *de novo* organogenesis. 5-day-old roots of *Arabidopsis thaliana* seedlings grown on MS were cut in 5 mm pieces and incubated on CIM for 4 days, explants were subsequently transferred onto SIM and phenotype was observed. a) Left, root explants grown on medium supplemented with MG132; right, root explants grown on medium without MG132. b) Detailed view of 10 days WT Col-0 root explants cultivated on SIM with MG132. *De novo* developmental program is inhibited and explants lose their ability to form shoots c) Detailed view of 10 days WT Col-0 root explants cultivated on SIM without proteasome inhibitor. Explants form green foci and then produce new shoots.

BPM proteins mediate the substrate specificity of CUL3 based E3 ligase that targets proteins for degradation *via* 26S proteasome (Gingerich et al., 2007). The previous experiment showed that impaired proteolysis has a severe effect on plant development. To investigate the role of BPM proteins in this process *Arabidopsis bpm* mutant lines were examined in terms of shoot regeneration efficiency. Mutation in a single *BPM* gene did not cause change in phenotype (not shown), indicating gene redundancy. Therefore, the double *bpm1;bpm2* mutant was assessed in the shoot regeneration assay. In the early phase on SIM incubation, explants showed altered phenotype from WT Col-0. Explants were pale, shoot formation frequency was reduced, and explants exhibited also weak lateral root system (Figure 25b). The shoot regeneration capacity was notably reduced. Root explants prepared from WT Col-0 developed normally, including greening, shoot development and large root system (Figure 25a). Double mutant phenotype partially resembled the phenotype of root explants treated with MG132.

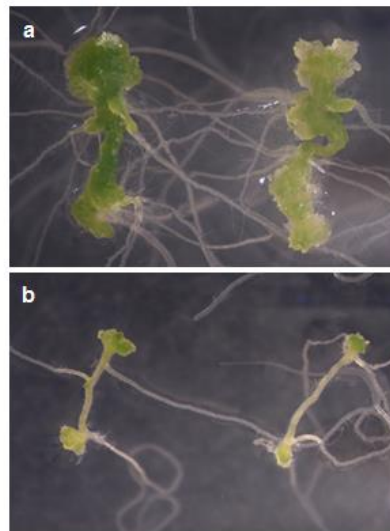


Figure 25: BPM E3-ligases are positive regulators of organogenesis. Shoot regeneration phenotype of root explants from WT Col-0 and *bpm1;bpm2* mutant. 5-day-old roots of *Arabidopsis thaliana* seedlings grown on MS were cut into approximately 5 – 8 mm pieces and incubated on CIM for 4 days, subsequently explants were transferred onto SIM and phenotype was observed. a) WT Col-0 b) *bmp;bpm2* double mutant. Plants mutated in E3 ligase showed reduced regeneration capacity.

3.3 ERF proteins can interact with BPM adaptor proteins of E3 ligase

Another task was to identify key players connecting protein degradation with target gene repression together in developmental processes. BPMs, part of E3 CUL^{BPM}

complex, were shown to be positive regulators of shoot regeneration. Therefore the ERF proteins, negative regulators of gene expression, were tested to be the substrate proteins for BPMs and be targeted for protein degradation *via* 26S proteasome. Analysis of the physical interaction of ERF repressors with E3 substrate-specific E3 ligases BPMs in yeast revealed that only ERF4 and ERF8 were able to interact with BPM1 and BPM3. To further investigate the key domain, responsible for the interaction of ERF with BPM, the mutant variant of the ERF4 protein, lacking the central domain (dC), was prepared. This ERF4dC mutant version was unable to interact with E3 ligases. Suggesting the central domain of repressors is responsible for binding to E3 ligase. ERF9, ERF10, ERF11, and ERF12 did not associate with any BPMs (Figure 26). BPMs were fused with Gal4-DNA BD and ERFs repressors to DNA AD. A positive interaction was not detected when BPMs were fused with DNA AD and ERFs to DNA BD, probably because of steric masking of BPM N-terminal which is responsible for substrate binding. These results are in contrary with observation reported previously (Chen et al., 2013), where interaction was observed when BPMs were fused to AD and ERFs to BD.

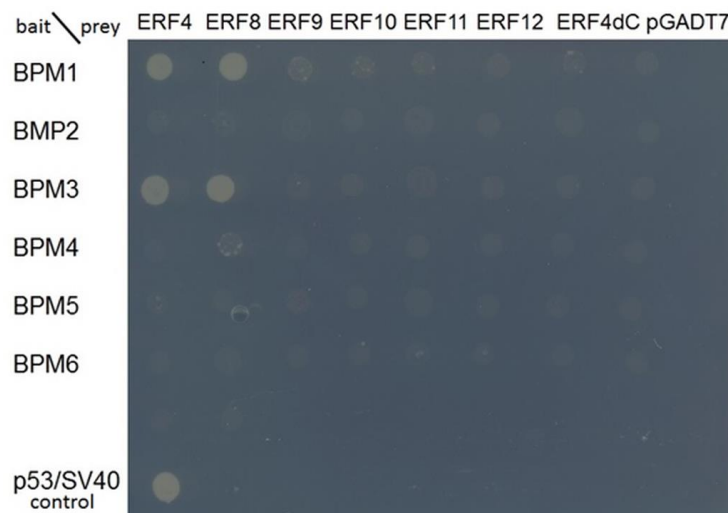


Figure 26: Interaction studies between ERF repressors and BPM E3 ligases by Y2H assays. ERF4 and ERF8, members of the VIII ERFs transcription factors group, interact with E3 ligases BPM1 and BPM3 in the Y2H assay. ERFs were sub-cloned into the prey vector pGADT7 containing the activation domain of GAL4 transcription factor. BPM E3 ligases (1-6) were sub-cloned into the bait vector pGADT7 containing binding domain of GAL4. The interaction between the remaining ERFs and BPMs was not observed. Selection medium for checking interaction: -leucine, -tryptophan, -histidine, -adenine. As a control for positive interaction p53/SV40 was used. As a negative control, ERF4dC without central domain responsible for interaction with E3 ligases was used.

3.4 Direct candidate target genes of ERF4

As a transcription factor, ERF4 recognizes and binds to certain loci in the genome. Considering its negative effect on shoot regeneration, ERF4 acts as a transcriptional repressor. A classical approach to study the effect of transcriptional activators *in planta* is to follow the transcript level of putative target genes upon the activator overexpression. In contrast to transcriptional activators, this approach can be hardly used to study the transcriptional repressors. The main reason is that the transcript abundance might not be significantly changed even after massive overexpression of repressor. Therefore repressor function was changed from gene repression to activation while its DNA binding specificity was maintained. This approach allows for the easy study of ERF target genes. To investigate direct downstream target genes of ERF4 the repressor EAR domain was replaced with the activation domain (AD) of positive regulator ESR2 and fused with estradiol-binding receptor domain, creating *N4C2-ER* (Figure 14). Upon β -estradiol treatment, the nuclear translocation took place and *N4C2-ER* moved to the nucleus where it bound to the direct downstream loci and due to the presence of ESR2 AD it activated the gene expression. The cycloheximide (CHX, an inhibitor of proteosynthesis) treatment was conducted to accumulate only primary mRNA transcripts and thus avoid indirect activation of further downstream genes. The root explants from T2 transgenic plants harboring *35S::N4C2-ER*, *35S::ESR2-ER* and *35S::GFP-ER* were after 3 days incubation on CIM transferred onto RIM + 10 μ M β -estradiol. The phenotype of five independent lines *35S::N4C2-ER* was examined. Lines no. 5, 9, 14, and 15 produced green calli, line 13 showed similar phenotype as a control *35S::GFP-ER*. Figure 27 shows the greening phenotype of 11 days old explants.

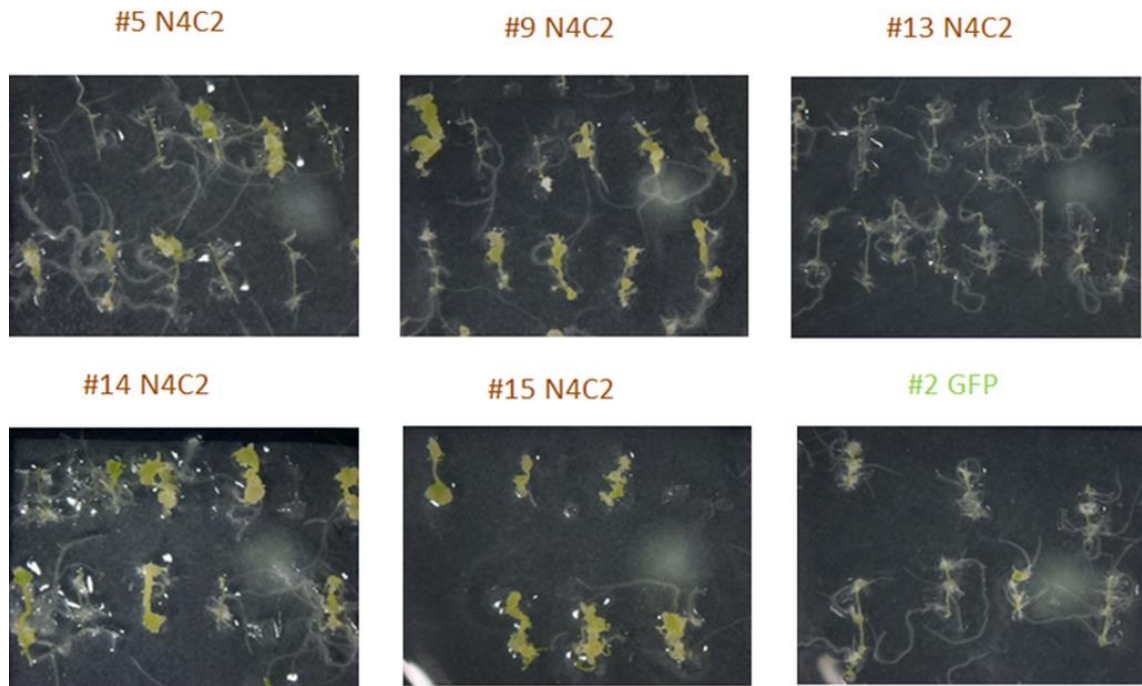


Figure 27: Greening and calli formation of T2 N4C2 plants after nuclear translocation caused by β -estradiol. Root explants of five independent transgenic lines *35S::N4C2-ER* were grown for 11 days on RIM + 10 μ M β -estradiol and then evaluated for the phenotype. Lines no. 5, 9, 14, and 15 formed green calli whereas line 13 was defective in green calli production same as control root explants from *35S::GFP-ER* line.

Lines showing strong phenotype were propagated to T3 generation and checked again for the phenotype after β -estradiol treatment. Line no. 15 exhibited reduced phenotype from phenotype observed in a T2 generation, suggesting the transgene silencing might take a place. Therefore three independent homozygous lines no. 5, 9, and 14 with stable phenotype were selected for RNA-seq analysis (Figure 28). Analogically, three independent homozygous lines of *35S::ESR2-ER* and *35S::GFP-ER* were used. Total RNA was extracted from root explants grown 3 days on CIM and 3 days on B5 Gamborg hormone-free medium. Nuclear translocation was induced with 10 μ M β -estradiol and primary mRNA transcripts were accumulated. To suppress translation of further downstream target genes CHX was also applied together with β -estradiol.

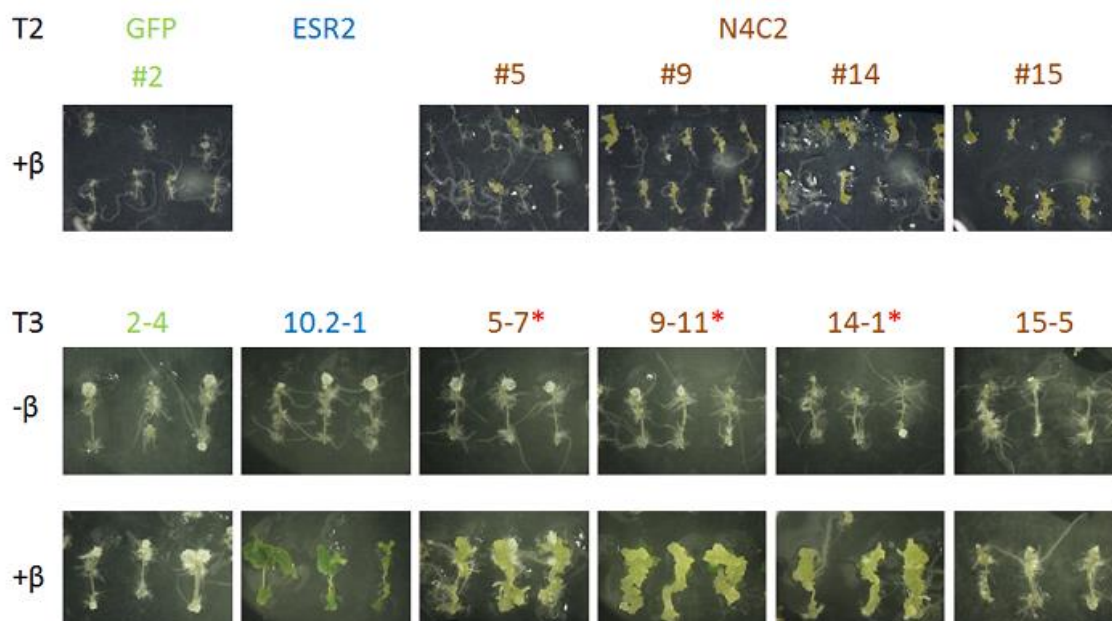


Figure 28: Greening and calli formation of T3 N4C2 explants after nuclear translocation caused by β -estradiol. For RNA-seq analysis three independent T3 homozygous lines of *35S::N4C2-ER* were selected based on constant phenotype (marked with an asterisk), as a positive control *35S::ESR2-ER*, as a negative control *35S::GFP-ER* were used.

Because ERF4 and ESR2 recognize the same cis-regulation element in target loci RNA-seq was carried out for both mutant lines harboring *35S::N4C2-ER* and *35S::ESR2-ER*, respectively. Transcript abundance was compared between *35S::N4C2-ER* and *35S::GFP-ER* then between *35S::ESR2-ER* and *35S::GFP-ER*. Transcripts showing at least 2-fold change are listed in Table 7 for *35S::N4C2-ER* and in Table 8 for *35S::ESR2-ER*.

RNA-seq analysis (performed by Dr. Vojta) revealed upregulation of 16 candidate direct-downstream target genes of *N4C2-ER* showing at least 2-fold change. Since the *N4C2-ER* is the active form of ERF4 repressor it can be assumed that these upregulated genes represent the target genes repressed by canonical ERF4. One-third of these genes are members of the AP2/ERF transcription factor family, including *ERF4*, *ERF8*, *ERF9*, and *ERF12*.

In the root explants harboring *35S::ESR2-ER*, a set of 30 genes showed at least 2-fold change; including *ERF8*, *ERF9*, and *ERF12*. The SAM marker gene *CUC1* was upregulated 2.3-fold. In comparison, the Affymetrix *Arabidopsis* GeneChips analysis showed 3-fold upregulation of *CUC1* in *35S::ESR2-ER* (Ikeda et al., 2006). It is likely that ESR2 directly activates *CUC1* gene.

Gene ID	Fold Change	SE	<i>p</i> -value	Gene Name	Description
AT4G30230	2.,977	0.328	1.14E-19	N/A	Unknown protein
AT4G37670	2.880	0.235	1.58E-34	NAGS2	N-ACETYL-L-GLUTAMATE SYNTHASE 2
AT1G26290	2.680	0.323	1.19E-16	N/A	Hypothetical protein
AT1G53170	2.619	0.242	2.79E-27	ERF8	AP2/ERF transcription factor
AT4G25490	2.581	0.336	1.49E-14	DREB1B	AP2/ERF transcription factor
AT3G48520	2.542	0.255	1.75E-23	CYP94B3	Jasmonoyl-isoleucine-12-hydroxylase
AT5G44210	2.447	0.316	8.84E-15	ERF9	AP2/ERF transcription factor
AT4G11140	2.357	0.344	7.39E-12	CRF1	AP2/ERF transcription factor
AT1G80590	2.332	0.344	1.18E-11	WRKY66	Member of WRKY transcription factor
AT1G49620	2.301	0.31	1.09E-13	KRP7	Cyclin-dependent kinase inhibitor family protein
AT2G39980	2.199	0.17	2.63E-38	N/A	HXXXD-type acyl-transferase family protein
AT3G62410	2.155	0.287	5.70E-14	CP12-2	CP12 domain-containing protein 2
AT5G04310	2.076	0.31	2.18E-11	N/A	Pectin lyase-like superfamily protein
AT3G54820	2.058	0.279	1.56E-13	PIP2-5	PLASMA MEMBRANE INTRINSIC PROTEIN 2D
AT3G15210	2.053	0.218	4.34E-21	ERF4	AP2/ERF transcription factor
AT1G28360	2.042	0.276	1.50E-13	ERF12	AP2/ERF transcription factor

Table 7: Direct downstream target genes of ERF4

Fold change of transcript accumulation between *35S::NAC2-ER* and *35S::GFP-ER* root explants.

SE Standard error for the comparison

p -value for the comparison

Gene ID	Fold Change	SE	p-value	Gene Name	Description
AT4G37670	3.934	0.235	5.21E-63	NAGS2	N-ACETYL-L-GLUTAMATE SYNTHASE 2
AT3G48520	3.062	0.255	2.52E-33	CYP94B3	Jasmonoyl-isoleucine-12-hydroxylase
AT1G19630	2.775	0.32	4.26E-18	CYP722A1	Cytochrome P450
AT2G31380	2.665	0.3	2.56E-19	BBX25	B-BOX DOMAIN PROTEIN 25
AT5G44210	2.643	0.315	5.47E-17	ERF9	AP2/ERF transcription factor
AT5G55090	2.454	0.2	1.92E-34	MAPKKK15	mitogen-activated protein kinase kinase kinase 15
AT5G62730	2.448	0.349	2.48E-12	NPF4.7	Major facilitator superfamily protein
AT1G80100	2.407	0.279	7.10E-18	AHP6	Histidine phosphotransfer protein 6
AT1G28360	2.381	0.276	6.82E-18	ERF12	AP2/ERF transcription factor
AT1G53170	2.354	0.242	2.49E-22	ERF8	AP2/ERF transcription factor
AT3G15200	2.338	0.254	3.31E-20	N/A	Tetratricopeptide repeat (TPR)-like superfamily protein
AT1G49620	2.334	0.31	4.39E-14	KRP7	Cyclin-dependent kinase inhibitor family protein
AT3G15170	2.312	0.329	NA	NAC054	CUC1; cup-shaped cotyledon1 protein
AT5G67430	2.311	0.308	6.28E-14	N/A	GCN5-related <i>N</i> -acetyltransferase (GNAT) (HLSL)
AT5G04310	2.233	0.31	5.94E-13	N/A	Pectin lyase-like superfamily protein
AT3G54820	2.191	0.279	3.90E-15	PIP2-5	Plasma membrane intrinsic protein 2;5
AT3G59435	2.184	0.334	5.96E-11	N/A	Hypothetical protein
AT1G07260	2.177	0.214	2.32E-24	UGT71C3	UDP-glucosyl transferase 71C3
AT4G30230	2.17	0.329	4.13E-11	N/A	Unknown protein
AT1G80710	2.169	0.292	1.09E-13	DRS1	DROUGHT SENSITIVE 1 (WD40 repeat family protein)
AT2G34340	2.168	0.288	5.35E-14	N/A	Proteins of unknown function
AT4G11140	2.162	0.344	3.33E-10	CRF1	AP2/ERF transcription factor
AT1G30840	2.137	0.344	5.24E-10	PUP4	Purine permease 4
AT1G70210	2.134	0.225	2.65E-21	CYCD1-1	D-type cyclin
AT5G39420	2.082	0.349	2.55E-09	CDC2C	cyclin-dependent protein serine/threonine kinase
AT4G29310	2.072	0.298	3.68E-12	N/A	Proteins of unknown function
AT2G46990	2.071	0.347	2.42E-09	IAA20	Indole-3-acetic acid inducible 20
AT5G66440	2.064	0.245	3.97E-17	N/A	tRNA-methyltransferase non-catalytic subunit
AT5G54040	2.044	0.224	7.64E-20	N/A	Cysteine/Histidine-rich C1 domain family protein
AT4G36850	2.028	0.338	2E-09	N/A	PQ-loop repeat family protein / transmembrane family protein

Table 8: Direct downstream target genes of ESR2

Fold change of transcript accumulation between *35S::ESR2-ER* and *35S::GFP-ER* root explants.

SE Standard error for the comparison

p -value for the comparison

Based on the results obtained from RNA-seq, semi-RT PCR was carried out to show changed expression of selected *ERF* genes. The cDNA prepared from five replicates of root explants harboring *35S::NAC2-ER*, *35S::ESR2-ER*, and *35S::GFP-ER* treated with β -estradiol and CHX was used. From five tested genes only *ERF9* and *ERF12* responded to ERF4 and ESR2 accumulation (Figure 29). No changes in *ERF 4, 10, and 11* transcript accumulation were observed among *35S::GFP-ER*, *35S::NAC2-ER*, and *35S::ESR2-ER*.

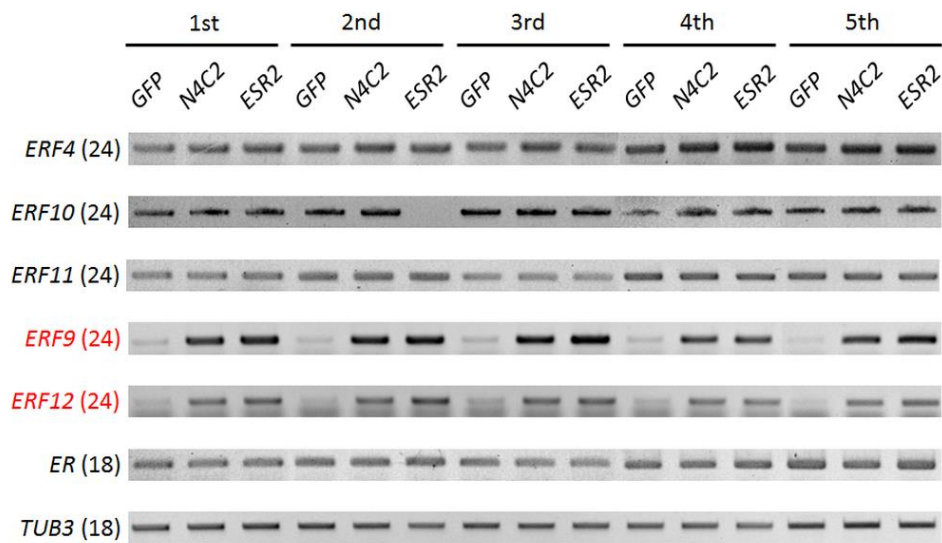


Figure 29: Only *ERF9* and *ERF12* genes respond to ESR2 and ERF4. cDNA from five biological replicates was prepared from root explants harboring *35S::GFP-ER*; *35S::NAC2-ER*; and *35S::ESR2-ER*, treated with β -estradiol and CHX and analyzed by semi-RT PCR to investigate changes in gene expression of *ERF* genes. Only *ERF9* and *ERF12* were responsive to ESR2 and ERF4. No change was detected for *ERF4*, *ERF10*, and *ERF11* gene. The number in parenthesis corresponds to the numbers of PCR cycles. The cDNA loading was normalized to *TUBULIN3*. Primers detecting estradiol receptor (*ER*) were used to show the amount of ER-fused transcripts.

3.5 Evaluation of shoot regeneration in higher-order mutants

Higher-order mutants were subjected to shoot regeneration analysis. Root explants were incubated on SIM and *de novo* developed shoots were counted at indicated time points. First shoots started to emerge after 14 days on SIM incubation in the case of WT Col-0 and sextuple mutant *erf4-1;8;9-1;10;11-2;12*. Over time the shoot regeneration frequency gradually rose and reached up to 84.86 % and 85.14 %, respectively. The mutant in the SAM master regulator, *wus*, could not regenerate shoots in the early time points, after the 26 days on SIM the shoot regeneration frequency remained still below 10 %. The septuple *wus;erf4-1;8;9-1;10;11-2;12* mutant showed a similar shoot regeneration frequency to *wus* (Figure 30).

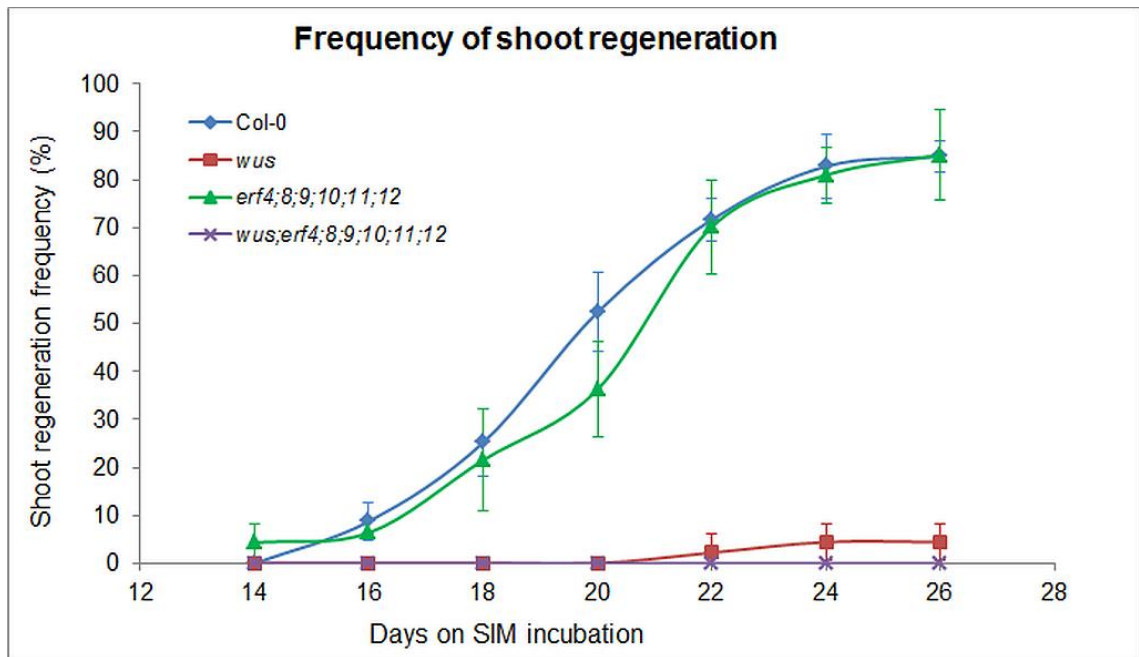


Figure 30: Shoot regeneration frequency of root explants incubated on SIM. Sextuple mutant in *ERF* genes showed no significant differences in shoot developmental process compared to WT Col-0. No rescue phenotype of *wus* mutation was observed in the case of septuple *wus;erf4-1;8;9-1;10;11-2;12* mutant after 26 days of SIM incubation. The values were obtained from three replicates; at least 15 root explants per replicate were evaluated.

To investigate the role of BPMs, the substrate-specific adaptors for E3 ligases, in shoot regeneration *bxami_bpm* (the micro RNA silencing line of *BPM 1 – 6* genes) and the *bpm1;2;3* triple mutant were examined in the shoot regeneration assay. Further, a double mutant in *ERF* transcriptional repressors *erf4-1;8*, the substrate of BPM proteins, and quintuple *erf4-1;8;bpm1;2;3* mutant were tested. Four out of five genotypes started to produce shoot on day 14 on SIM, only *bpm1;2;3* mutant started to regenerate from day 16. The regeneration rate of all above-mentioned genotypes seemed to be same up to day 18 on SIM. Col-0 and *bpm1;2;3* produced more shoots from day 20 than the remaining genotypes with regeneration frequency up to 73 % after 22 days on SIM. *bxami_bpm1;2;3* displayed the slightly reduced number of shoots from Col-0 and *bpm1;2;3* but still produced more shoots than *erf4-1;8* and *erf4-1;8;bpm1;2;3*. Reduced shoot regeneration frequency from Col-0 was observed in *erf4-1;8* and *erf4-1;8;bpm1;2;3* mutant lines. *erf4-1;8* showed significantly decreased shoot regeneration frequency from Col-0 after 22 days on SIM (46.7 %), whereas *erf4-1;8;bpm1;2;3* displayed significantly reduced shoot regeneration frequency after

day 20 on SIM (up to 44.86 % after 22 days on SIM), $p < 0.05$. No significant differences were observed between *erf4-1;8;bpm1;2;3* and *erf4-1;8* (Figure 31).

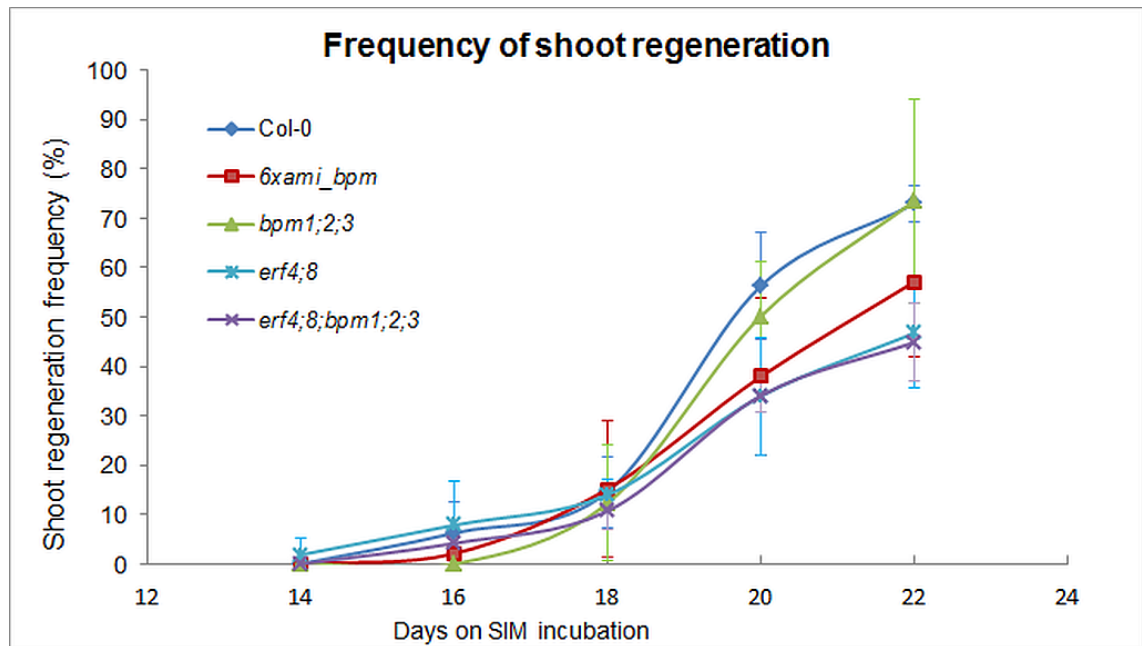


Figure 31: Shoot regeneration frequency of root explants incubated on SIM. Micro RNA silencing line *6xamiBPM* showed slightly reduced shoot regeneration in later time points of SIM incubation, but no statistically significant differences were observed when compared to WT Col-0. Putative triple mutant *bpm1;2;3* produced shoots similarly to WT Col-0. Double mutant *erf4-1;8* produced statistically significant fewer shoots than WT Col-0 from day 22 on SIM incubation. Quintuple *erf4-1;8;bpm1;2;3* mutant showed similar phenotype as double *erf4-1;8* mutant, shoot regeneration frequency was significantly reduced from day 20 on SIM incubation ($p < 0.5$). The values were obtained from three biological replicates; at least 15 root explants per replicate were evaluated.

Next, another negative regulator of gene expression, HDA6, was also examined in shoot regeneration assay to test the impact of histone deacetylation on shoot development. Mutation in histone deacetylase HDA6 positively affected shoot regeneration. *hda6-6* mutant showed higher shoot regeneration efficiency than Col-0, significant differences were observed from day 16 on SIM incubation and the mutant reached up to 91 % regeneration capacity ($p < 0.5$) whereas Col-0 reached up to 73 %. *bpm1;2;3* started to regenerate shoots later (day 16) than remaining genotypes (day 14). The shoot regeneration efficiency from day 18 on SIM was similar to WT Col-0. Quadruple *hda6-6;bpm1;2;3* mutant produced more shoots than *bpm1;2;3* and Col-0 but less than single *hda6-6* mutant (Figure 32).

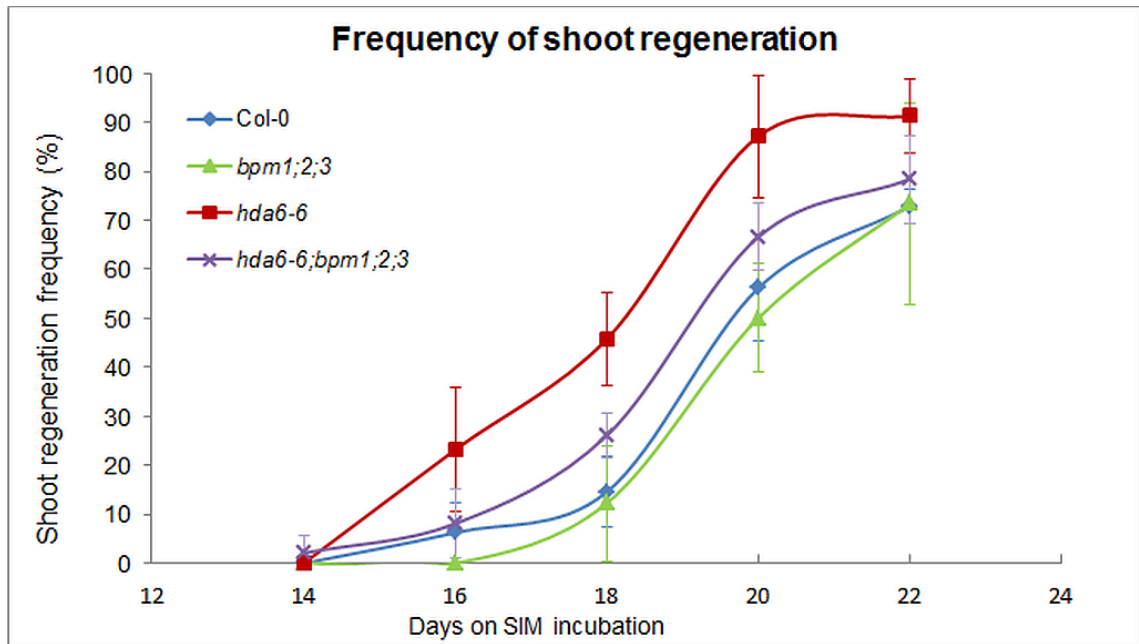


Figure 32: Shoot regeneration frequency of root explants incubated on SIM. Mutation in *HDA6* resulted in a higher frequency of shoot development compared to WT Col-0, statistically significant results were observed from day 16 on SIM incubation ($p < 0.05$). Putative *bpm1;2;3* triple mutant showed no statistically significant changes in phenotype compared to WT Col-0. The mutation in *BPM* genes compromised the *hda6-6* superior phenotype. Statistically significant differences were observed between *hda6-6* and *hda6-6;bpm1;2;3* only in day 18 on SIM incubation ($p < 0.05$). The values were obtained from three biological replicates; at least 15 root explants per replicate were evaluated.

3.6 Phenotypic characterization of *erf4-1;8;9-1;12* quadruple mutant

Since mutation in single *ERF* gene had no effect on phenotype and plants are indistinguishable from WT, the higher-order mutant lines were prepared and analyzed. Quadruple mutant, *erf4-1;8;9-1;12*, displayed increased meristematic activity (Figure 33B) and produced more floral buds than WT Col-0 (Figure 33A). The laser scanning confocal microscopy revealed larger inflorescence meristem of *erf4-1;8;9-1;12* quadruple mutant (Figure 33 D) than inflorescence meristem of WT Col-0.

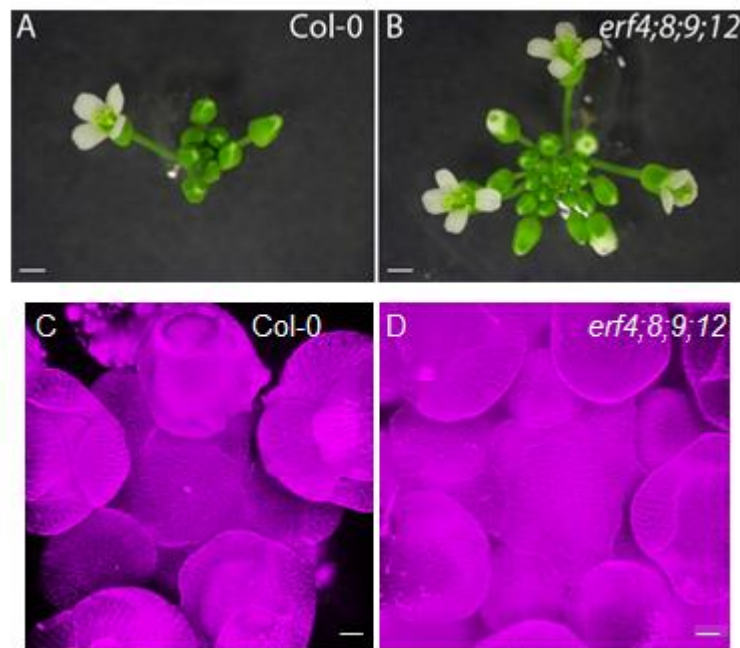


Figure 33: Meristematic activity of *erf4-1;8;9-1;12* quadruple mutant. Mutation in *ERF* genes affected meristematic activity, the quadruple mutant displayed increased meristematic activity resulting in a higher number of flower buds. A) flower roseate of WT Col-0 and B) flower roseate of *erf4-1;8;9-1;12* quadruple mutant. Scale bars represent 1 mm. LSCM of C) WT Col-0 inflorescence meristem D) *erf4-1;8;9-1;12* quadruple mutant inflorescence meristem. Seedlings were stained by propidium iodide. Images C and D were kindly provided by professor Mitsuhiro Aida (Kumamoto University, Japan). Scale bars represent 20 μm .

Additionally to increased meristematic activity, the *erf4-1;8;9-1;12* quadruple mutant displayed disturbed silique arrangement (Figure 34). Siliques aligned in altered angles along the stem when compared to Col-0. In WT Col-0, siliques followed the most abundant pattern, the 137° angle (Hotton, 2003). Interestingly, the phyllotactic change was observed only when *ERF9* and *ERF12* were both mutated.

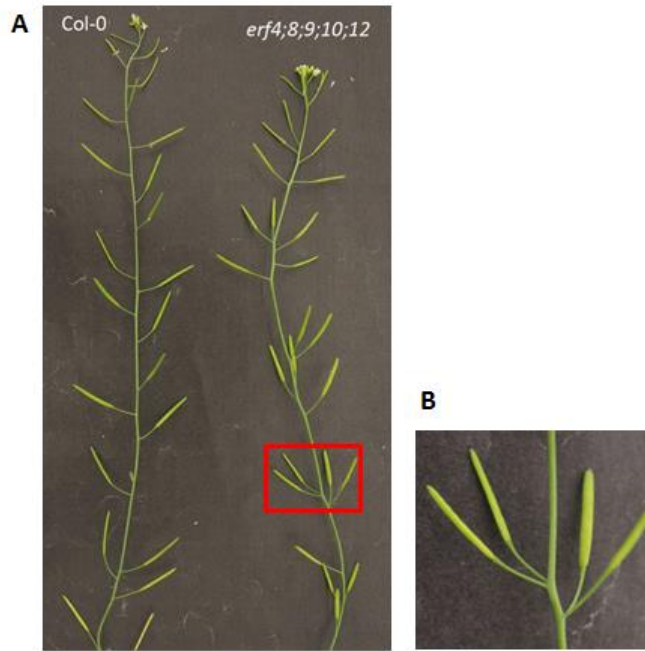


Figure 34: Phyllotaxis of *erf4-1;8;9-1;12* quadruple mutant. A) Comparison of WT Col-0 and *erf4-1;8;9-1;12* quadruple mutant mature plants. The mutant showed changed arrangement of siliques. B) Closed-up view of altered divergence angle of siliques in *erf* multiple mutant.

3.7 Quadruple mutant in *ERF* genes could partially rescue aberrant SAM in *wuschel* mutant

Mutation in *WUS* gene causes aberrant SAM and inflorescence meristem development resulting in plant sterility (Laux et al., 1996). When assessing *wus-101* mutant phenotype, no true leaves development was observed 9 days after germination (d.a.g.) (Figure 35B). The quadruple mutant *erf4-1;8;9-1;12* produced slightly more leaves than WT Col-0 (Figure 35A, C). Despite no significant changes in phenotype were observed in tissue culture system between *wus* single mutant and *wus;erf4-1;8;9-1;10;11-2;12* mutant, in intact seedling the mutation in *ERF4*, *ERF8*, *ERF9*, and *ERF12* gene partially rescued the *wuschel* phenotype in early days of germination (9 d.a.g.) (Figure 35D). This rescue phenotype was observed on SAM maintenance level but not on vegetative to inflorescence transition level, indicating *ERF* repressors act independently from the WUSCHEL pathway in maintenance of SAM.

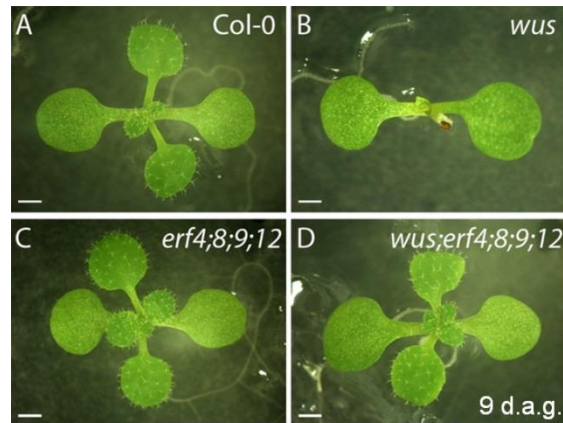


Figure 35: *ERF* repressors act epistatically to *WUSCHEL*. Single mutant in *WUSCHEL* is aberrant in SAM (B), quadruple mutant *erf4-1;8;9-1;12* (C) shows no developmental changes in SAM, similar to WT Col-0 (A). Quintuple mutant *wus;erf4-1;8;9-1;12* could rescue the *wus* phenotype, seedlings developed an intact SAM. Pictures of SAM were taken 9 days after the germination, scale bars represent 1 mm.

3.8 Higher-order *erf* mutants show opposite relative *ESR1* and *ESR2* gene expression

Relative gene expression of *ESR1* and *ESR2* in root explants incubated on SIM at indicated time points showed the opposite effect of ERF transcriptional repressors on *ESR1* and *ESR2* gene expression. Two independent higher-order mutant lines *erf4-1;8;9-1;11-2;12* and *erf4-1;8;9-1;10;12* displayed reduced *ESR1* expression over the time. In the early phase of SIM incubation the *ESR1* expression was slightly reduced to 0.83 and 0.88 in *erf4-1;8;9-1;11-2;12* and *erf4-1;8;9-1;10;12*, respectively, from WT Col-0. After 8 days incubation on SIM, the *ESR1* expression dropped to approximately 0.35 from WT Col-0 in both mutant lines (Figure 36a). In contrast, the expression profile of *ESR2* was opposite to the one of *ESR1* at least in *erf4-1;8;9-1;11-2;12* mutant line. *ESR2* transcripts were gradually accumulated in this mutant line at each tested time point with 8 times higher relative gene expression compared to WT Col-0 after day 8 on SIM. On the other hand, *erf4-1;8;9-1;10;12* mutant line did not follow this trend and *ESR2* expression decreased from 4.24 (day 5) to 1.96 (day 8) (Figure 36b). *ESR1* gene lacks GCC-box in the promoter region and therefore ERF transcriptional repressors have little impact on its repression, whereas *ESR2* contains GCC-box and therefore ERF repressors can bind to this cis-regulation element and thus attenuate transcription of *ESR2*.

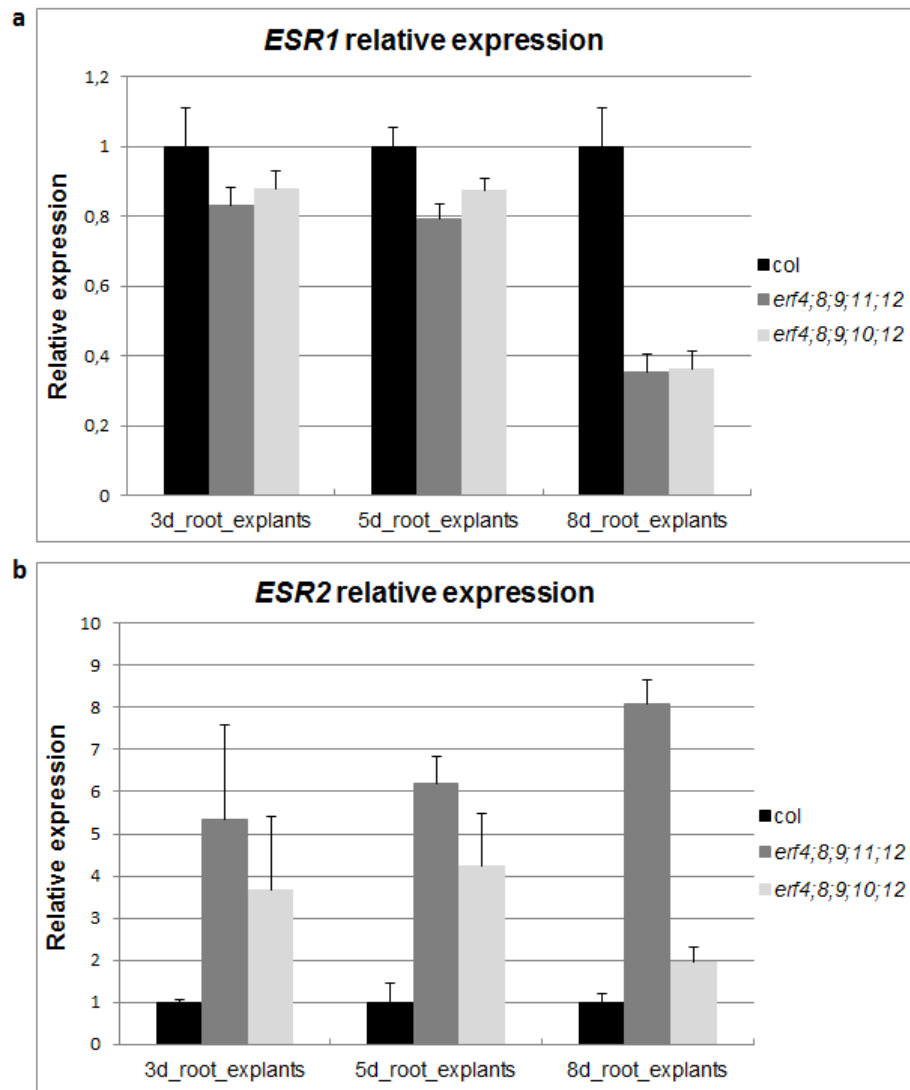


Figure 36: Relative gene expression of *ESR1* and *ESR2* is transient in *erf* mutant lines. Relative expression of *ESR1* and *ESR2* genes was analyzed in two quintuple mutants and *erf4-1;8;9-1;10;12* a) *ESR1* gene expression was slightly reduced in root explants incubated on SIM for 3 and 5 days in both mutants. On day 8 strong reduction of *ESR1* transcript was observed in both mutants. The expression pattern of different mutants remained similar at each indicated time point. b) Relative gene expression of *ESR2* gene displayed also a transient pattern. In the case of *erf4-1;8;9-1;11-2;12* mutant line, expression slowly increased from day 3 until day 8. The *erf4-1;8;9-1;10;12* mutant line displayed different changes in gene expression of *ERS2*. On day 3 and 5 gene expression was higher than in WT Col-0 but remained similar at both time points, after then the gene expression decreased. Root explants from more than 40 plants were pooled and analyzed together; results are obtained from a single experiment.

3.9 Higher-order *erf* mutants display alteration in relative *CUC1* and *STM* gene expression

To monitor the impact of ERFs on the expression of SAM marker genes, two quintuple mutant lines (*erf4-1;8;9-1;11-2;12* and *erf4-1;8;9-1;10;12*) incubated on SIM, were examined and relative *CUC1* and *STM* gene expression was compared to WT Col-0 (Figure 37).

In both mutant lines, the strongest *CUC1* expression was detected after 3 days on SIM incubation. *erf4-1;8;9-1;11-2;12* mutant line displayed 4.7 times higher relative *CUC1* expression than WT Col-0 whereas *erf4-1;8;9-1;10;12* accumulated *CUC1* transcripts only 3.3 times more than WT Col-0 (Figure 37a). After this time point, the relative *CUC1* expression started to decrease. The *CUC1* relative expression on day 5 on SIM was reduced to 2.8 in *erf4-1;8;9-1;11-2;12* mutant and to 1.9 in *erf4-1;8;9-1;10;12*. On day 8 on SIM, only 1.4 times higher *CUC1* expression was observed in the case of *erf4-1;8;9-1;11-2;12* mutant line and no change of *CUC1* expression, when compared to WT Col-0, was detected in *erf4-1;8;9-1;10;12* mutant line (Figure 37a). Therefore, the aberrant *ERF11* gene has a bigger impact on *CUC1* relative expression than *ERF10*.

In contrast to the *CUC1* expression profile, *STM* seems to oscillate in both quintuple mutants. The *STM* expression was 1.9 times higher in *erf4-1;8;9-1;10;12* mutant line than in WT Col-0 after 3 days incubation on SIM. On day 5, the *STM* expression declined to the WT level (0.9) and on day 8 the relative *STM* expression rose again to 1.3. Similarly to effect on *CUC1* expression, the *erf4-1;8;9-1;11-2;12* mutant line displayed stronger impact on *STM* transcripts accumulation than *erf4-1;8;9-1;10;12* mutant line (Figure 37b).

Time-course analysis of root explants grown on SIM revealed that *erf4-1;8;9-1;11-2;12* mutant line accumulated 3.6 times more *STM* transcripts than WT Col-0 on day 3 on SIM. On day 5, the relative *STM* expression was only 1.6 higher than in WT. Surprisingly, the relative expression of *STM* on day 8 on SIM was 7.3 higher than in WT. According to this qRT-PCR analysis (Figure 37b), it is tempting to speculate that *ERF11* is a negative regulator of putative activator controlling *STM* gene expression.

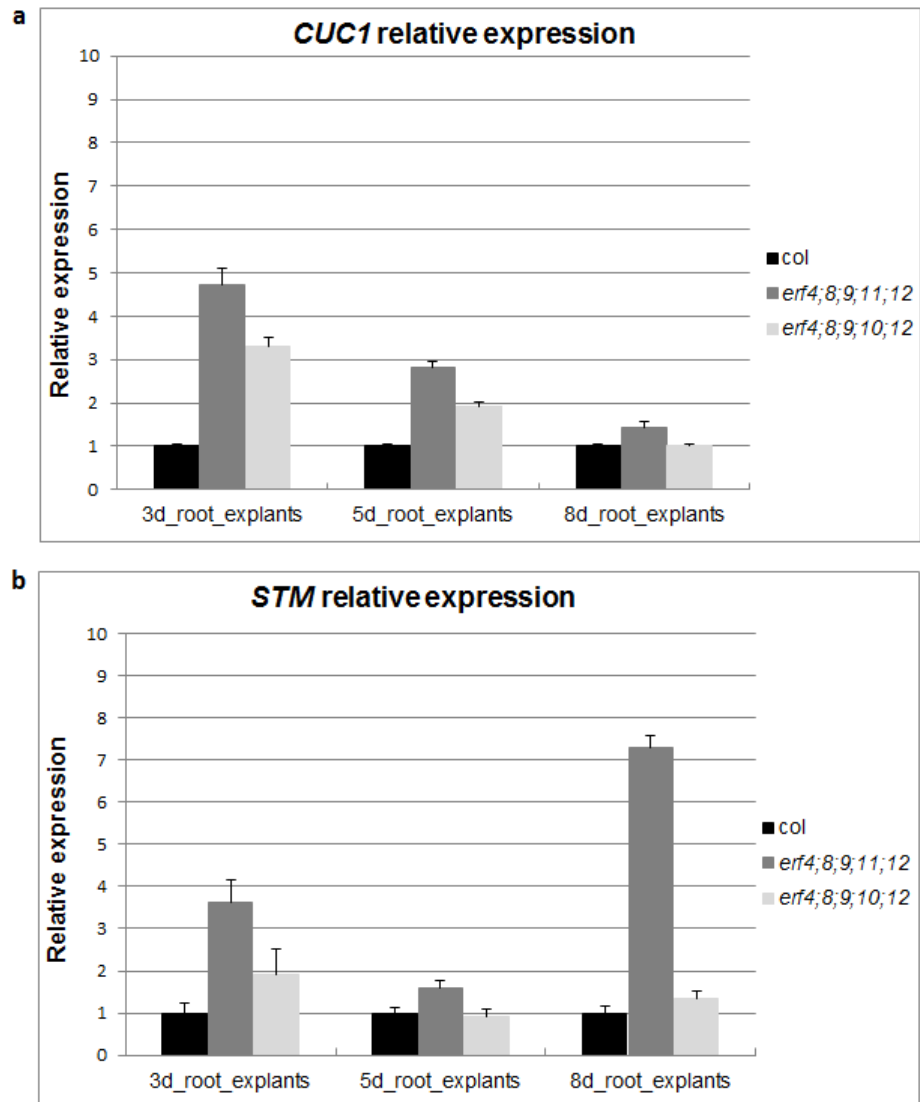


Figure 37: Relative gene expression of *CUC1* and *STM* is transient in *erf* mutant lines. Relative gene expression of *CUC1* and *STM* was analyzed in two quintuple mutants and *erf4-1;8;9-1;10;12*. a) Transient relative expression of *CUC1* gene was observed in root explants incubated on SIM for 3, 5, or 8 days. Quintuple *erf4-1;8;9-1;11-2;12* mutant line displayed a higher accumulation of *CUC1* transcripts than *erf4-1;8;9-1;10;12* quintuple mutant line. In the course of time, the relative *CUC1* expression was reduced in both mutants. b) Transient relative expression of *STM* gene was observed in root explants incubated on SIM for 3, 5, or 8 days. On day 3 both mutants showed higher gene expression than Col-0 WT, quintuple *erf4-1;8;9-1;11-2;12* mutant line accumulated more *STM* transcripts than *erf4-1;8;9-1;10;12* quintuple mutant. On day 5 *STM* relative gene expression decreased, in the case of *erf4-1;8;9-1;10;12* quintuple mutant line, *STM* expression was comparable to Col-0 WT. On day 8, the relative *STM* gene expression was greatly elevated in *erf4-1;8;9-1;11-2;12* mutant line, whereas almost no change was detected in *erf4-1;8;9-1;10;12* quintuple mutant line. Root explants from more than 40 plants were pooled and analyzed together; results are obtained from a single experiment.

3.10 Expression pattern and sub-cellular localization of ERF4

To analyze expression domain of *ERF4*, transgenic plants harboring the *pERF4::ERF4-GUS* construct were analyzed by GUS-staining. Strong signals were observed in pericycle cells and mostly in lateral root primordia (LRP) (Figure 38a). Live-cell imaging of transgenic plants harboring the *pBIB-UAS-ERF4-mCherry-tNOS* construct showed a similar pattern (Figure 38b). Nuclei of LRP were positive for the presence of the ERF4-mCherry fusion protein.

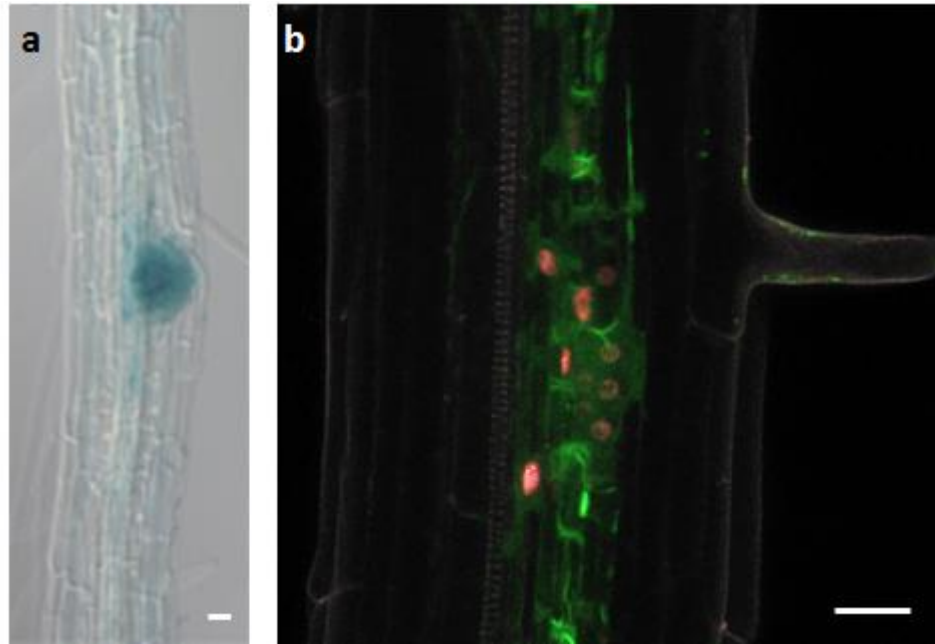


Figure 38: Expression pattern and sub-cellular localization of *ERF4* a) Transgenic plants harboring *pERF4::ERF4-GUS* show the accumulation of the ERF4-GUS fusion protein predominantly in LRP b) Transgenic plants harboring the *pBIB-UAS-ERF4-mCherry-tNOS* construct show a similar pattern. The ERF4-mCherry fusion protein (red) localized mostly in nuclei of LRP. Scale bar represents 20 μm .

To explore the impact of particular ERF4 domains on the ERF4 sub-cellular localization, transgenic plants harboring different *ERF4-mCherry* domain deletion constructs (Figure 10) were investigated by laser scanning confocal microscopy. All constructs transformed into the ERF4GAL enhancer trap line were under the control of the native *ERF4* enhancer together with a green fluorescent protein (GFP5ER) localized at the endoplasmic reticulum (ER) (Figure 12). The ER-localized GFP served as tissue-specific marker. In control plants (*mCherry-only*), the mCherry signal co-localized with GFP in the cytosol and was also detected in nuclei (Figure 39d-f), whereas the full-length ERF4-mCherry localized exclusively in the nuclei (Figure 39a-c). Deletion of the AP2 DNA binding domain changed the sub-cellular localization

of the ERF4-mCherry fusion protein (Figure 39g-i). The signal resembled the control mCherry only (Figure 39d-f). Deletion in the central domain (dC) (Figure 39j-l) and repressor domain (dR) (Figure 39m-o) had no impact on the sub-cellular localization of ERF4-mCherry.

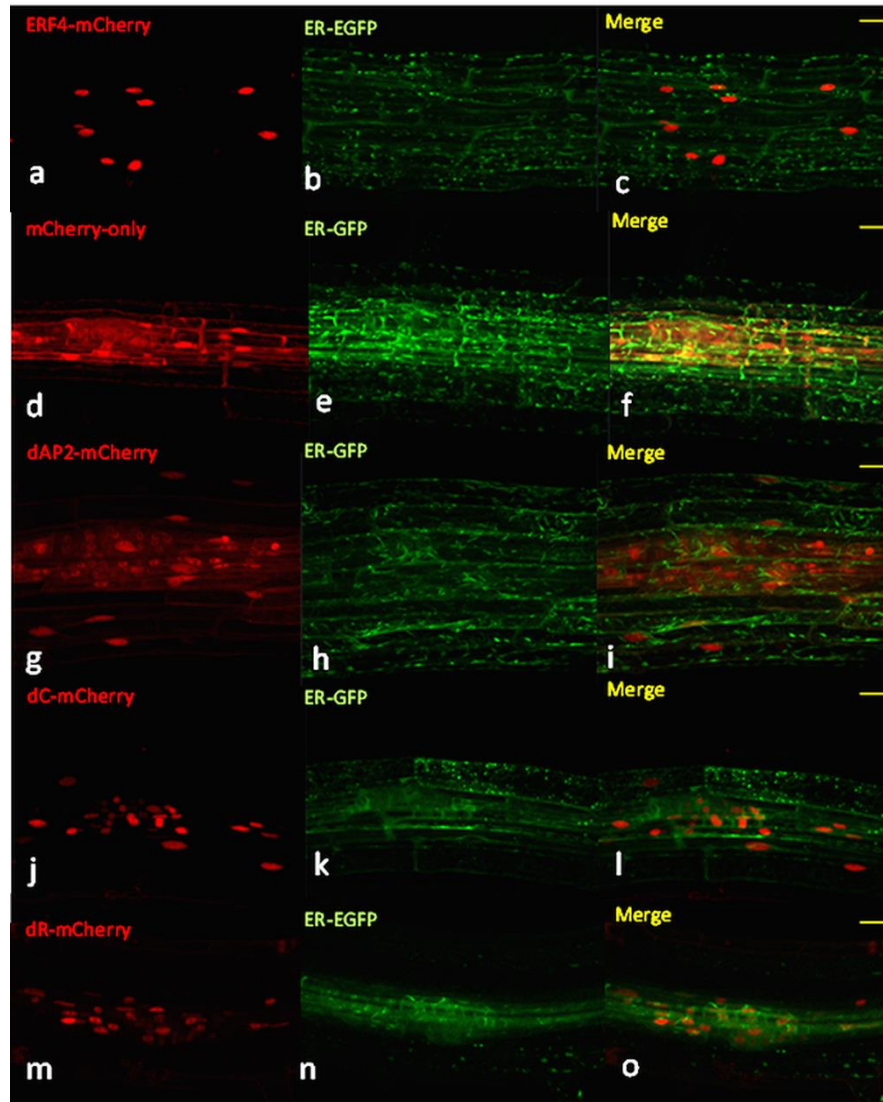


Figure 39: Subcellular localization of ERF4-mCherry fusion protein (*GAL4-ERF4-mCherry-UAS*) in the enhancer-trap line mutant background. The ERF4-mCherry fusion protein is under the control of native ERF4 enhancer. The *A. thaliana* seedlings were grown on MS in a vertical orientation, 5 – 10 days old seedlings were subjected to laser scanning confocal microscopy. The protein of interest fused with mCherry is shown in red while the green channel represents the green fluorescence marker protein (ER-GFP). a) The full-length ERF4 protein fused with mCherry localized exclusively in nucleus; b), e), h), k), n) EGFP localized in the endoplasmic reticulum; c), f), i), l), o) Merge of the red and green channels; d) Free mCherry protein only, without any fusion, did not show a particular localization, it localized in the nucleus and in cytoplasm; g) ERF4dAP2mCherry, the truncated ERF4 protein, lacking a DNA binding domain AP2/ERF, mimicked the subcellular localization of the free mCherry protein; j) ERF4dCmCherry, the truncated ERF4 protein, lacking the central domain, and m) ERF4dRmCherry, the truncated ERF4 protein, lacking the EAR domain, did not show a different localization compared to full-size ERF4. Scale bars represent 20 μ m.

3.11 ERF4 is more often associated with the active than with the inactive RNAPoIII variant

Afterward, widefield life-cell imaging super-resolution microscopy was employed to examine the ERF4 protein distribution inside the nucleus more in detail. In addition, the co-localization of ERF4 with inactive RNAPoIII and the active variant RNAPoIIser2ph (phosphorylated at serine 2) has been quantified. The ERF4-mCherry fusion protein was present in euchromatin but absent from heterochromatin and the nucleolus (Figure 40a, c, d, e, g, h), where also RNAPoIII was localized in a network-like manner (Figure 40b, f). The inactive RNAPoIII formed more compact structures (Figure 41b) when compared to the active variant (Figure 41f). ERF4-mCherry co-localized more often to RNAPoIIser2ph (Figure 41a, b) than to the inactive variant (Figure 41e, f).

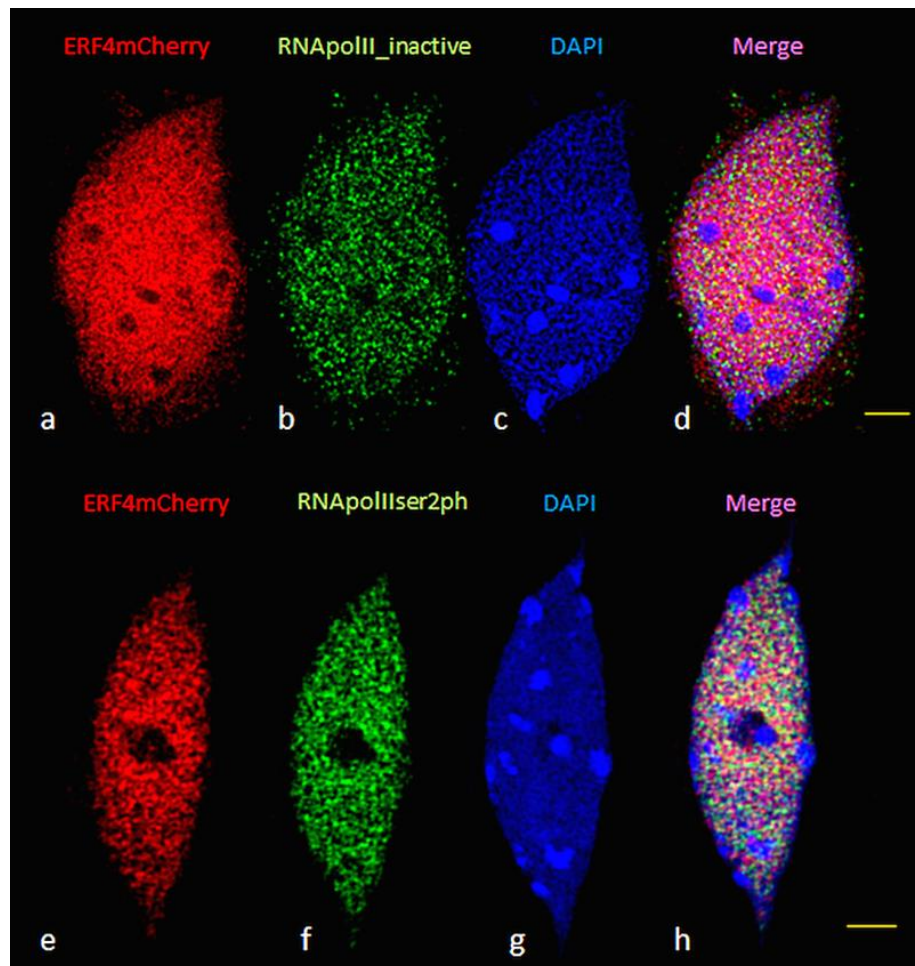


Figure 40: Co-localization of ERF4-mCherry with inactive RNAPoIII and the active variant RNAPoIIser2ph. The 8C fraction of nuclei isolated from 5-day-old seedlings expressing ERF4-mCherry fusion protein was immuno-stained with anti-mCherry antibodies (a, e), anti-RNAPoIII (b), and anti-RNAPoIIser2ph (f), respectively. ERF4-mCherry localized mostly in euchromatin outside of the chromocenters (brighter DAPI-positive spots; c, g). Scale bars represent 2 μ m.

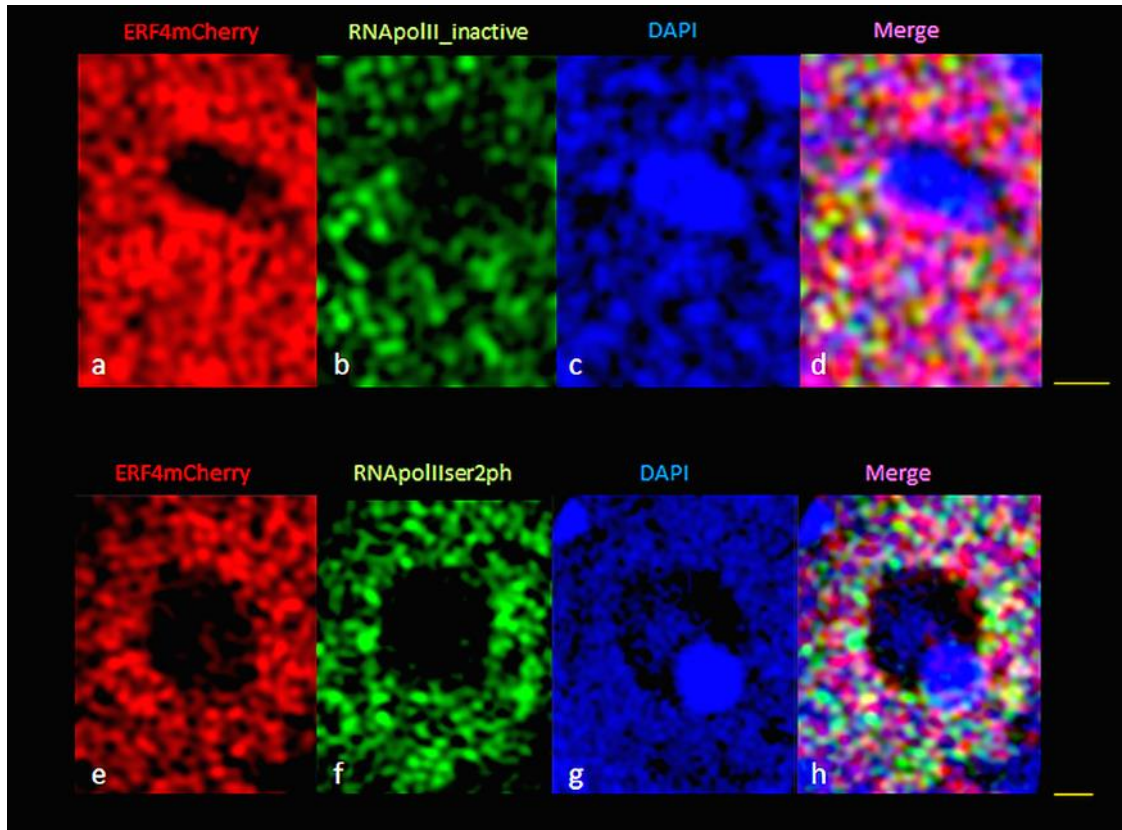


Figure 41: Close-up view of ERF4-mCherry co-localization with the active RNAPolIIs2ph and inactive RNAPolIII. Labeling as in Figure 40. Scale bars represent 0.5 μm .

To quantify the co-localization of ERF4-mCherry with either inactive or active RNAPolIII the voxel intensities of 12 nuclei per each RNAPolIII variant were measured using SIM and the IMARIS 8.0 software. The obtained data were evaluated by Student's *t*-test, and significant differences were found. The frequency of ERF4-mCherry co-localization with the active RNAPolIII was significantly higher (69.8 %) than with the inactive variant (52.8 %) (Figure 42).

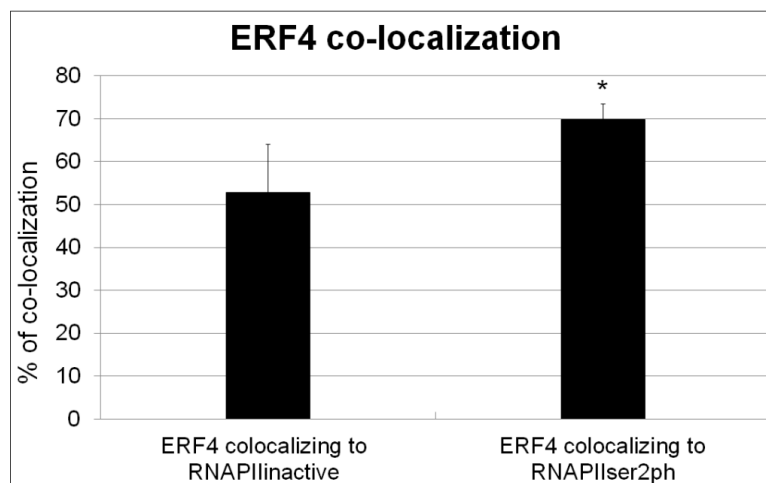


Figure 42: Co-localization of ERF4 to the inactive RNAPoIII and active RNAPoIIser2ph. The 8C fraction of nuclei isolated from *Arabidopsis* seedlings were selected and subjected to immunostaining and super-resolution microscopy. ERF4 co-localized more to active (RNAPoIIser2ph) polymerase (69.8 %) than to inactive (RNAPoIII) polymerase (52.8 %). Co-localization was calculated by Imaris 8.0 software. Data shown represent the mean + SD of 12 individual nuclei and statistical significance was determined by student's *t*-test (* $p < 0.05$).

3.12 The impact of ERF4 on the acetylation of histone H3

Because the expression of ERF4-mCherry under the control of native *ERF4* regulation elements was very low and tissue-specific, plants harboring the *ERF4-Myc* expression cassette under the control of the strong estradiol inducible promoter (XVE) were selected for further analysis. First, the functionality of the construct was tested using β -estradiol treatment. Seedlings treated with β -estradiol showed severe pleiotropic phenotypes, obviously suffering from *ERF4-Myc* overexpression, and were vastly dwarfed when compared to non-treated seedlings (Figure 43a). The overexpressing lines showing the strongest deviating phenotype were selected for further experiments. To detect the fused ERF4-Myc protein Western blot analysis was carried out. Although the construct was driven under the inducible promoter and the expression was supposed to be massive only very weak signal was detected (data not shown). Presumably, this could be due to protein degradation. Western blotting seems not to be sensitive enough to detect such an unstable protein. Instead, the presence of the ERF4-Myc fusion protein was detected using a whole-mount approach (Figure 43b). The ERF4-Myc fusion protein was detected using a specific anti-Myc antibody. The signals were observed in nuclei and no distinct structures within the nucleus were found. Assuming that ERF4 takes part in a co-repressor mediated expression attenuation, the acetylation status of nuclei expressing ERF4-Myc was monitored.

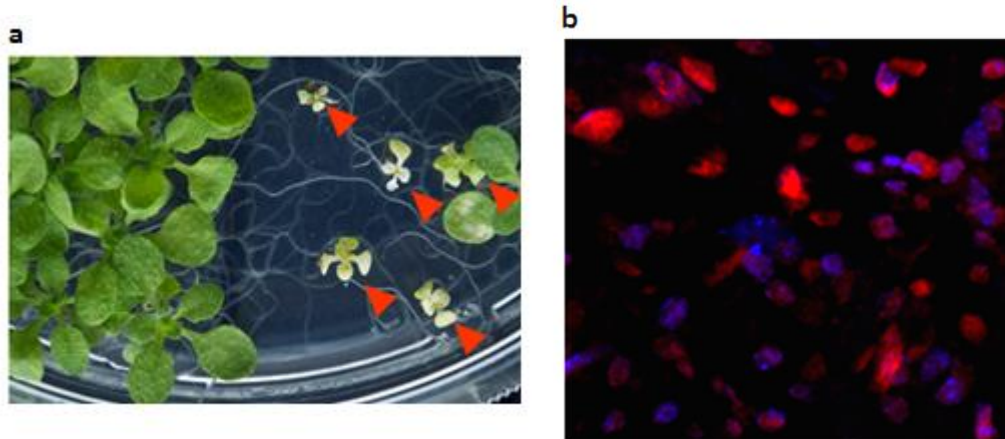


Figure 43: Inducible expression of *ERF4-Myc* after β -estradiol treatment. a) Phenotypic appearance of plants overexpressing *ERF4-Myc* after β -estradiol induction. The seedlings treated with 10 μ M β -estradiol suffered and showed dwarfed phenotypes (red arrowheads). b) Whole-mount nuclei isolated from *A. thaliana* leaves were immuno-stained with anti-Myc antibody. Chromatin was counterstained with DAPI. Nuclei expressing *ERF4-Myc* are shown in red.

To analyze changes in the acetylation status of histone 3 (H3) at different lysine residues (K), transgenic plants harboring an estradiol-inducible *XVE::ERF4Myc* expression cassette were treated with β -estradiol overnight. Nuclei from whole 5-day-old seedlings were isolated and immediately flow-sorted according to their ploidy level. Within the population of isolated nuclei, the nuclei accumulating *ERF4-Myc* fused protein and nuclei without *ERF4-Myc* were found. The 8C fraction of sorted nuclei was subjected to super-resolution microscopy (SIM) analysis to achieve a higher resolution. The fluorescence signals of nuclei expressing the *ERF4-Myc* fusion protein were detected in euchromatin (Figure 44f), similar to the localization pattern observed in nuclei prepared from plants harboring the *pBIB-UAS-ERF4-mCherry-tNOS* construct (Figure 41). No fluorescence signals were observed in the nucleoli and chromocenters (heterochromatin) (Figure 44g). As expected, nuclei without *ERF4-Myc* expression showed no fluorescence signals when detected using anti-Myc antibody (Figure 44j). Similarly, no signals for Myc were detected in the two controls, WT Col-0 (Figure 44b) and plants harboring the empty vector pER10 after β -estradiol treatment (Figure 44n). The fluorescence signals of H3K9 were detected in euchromatin in the whole nucleus and were excluded from the nucleolus and heterochromatin (Figure 44a, e, i, m). A similar signal distribution was observed also for H3K14 (Figure 45), H3K23 (Figure 46), and H3K9, H3K14, H3K23, H3K27 (Figure 47) epigenetic marks.

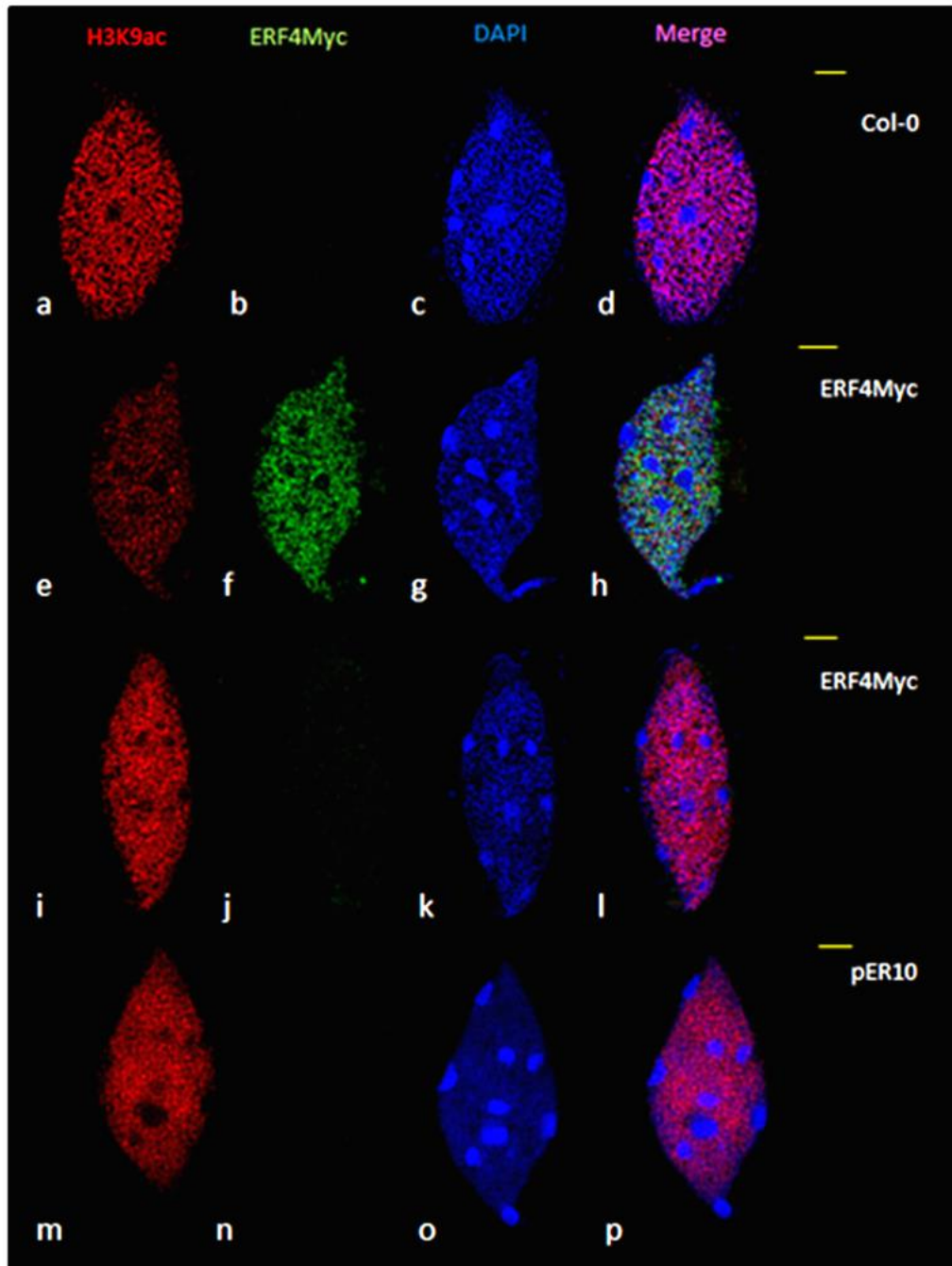


Figure 44: Co-localization of the ERF4-Myc fusion protein with epigenetic markers for histone 3 acetylated at lysine 9 (H3K9). The 8C nuclei, isolated from 5-day-old seedlings, were immune-stained against H3K9ac (a, e, i, and m), and ERF4-Myc fusion protein (b, f, j, and n). The chromatin was stained with DAPI (c, g, k, and o). a), b), c), and d) WT Col-0; e), f), g), h) transgenic plants harboring the *XVE::ERF4-Myc* construct and ERF4-Myc fusion protein is expressed; i), j), k), and l) plants harboring *XVE::ERF4-Myc* construct but ERF4-Myc fusion protein was not detected; m), n), o), and p) transgenic plants harboring *XVE::GFP*. ERF4-Myc fusion protein localized in euchromatin (f), outside from the chromocenters (DAPI-intense stained spots, g). A change in the acetylation intensity of H3K9 of a), i), and m) was observed in nuclei expressing ERF4-Myc (e). Scale bars represent 2 μ m.

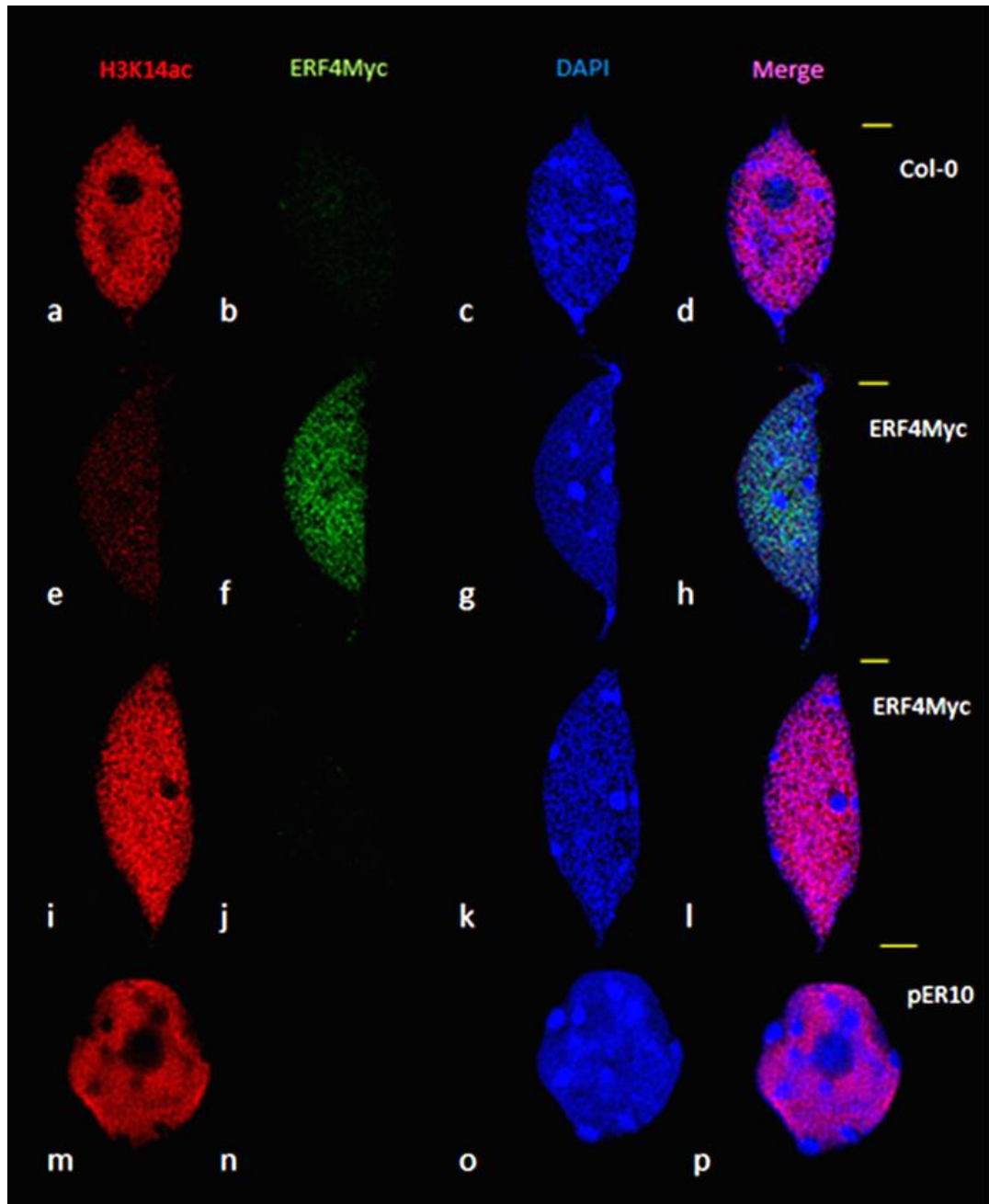


Figure 45: Co-localization of the ERF4-Myc fusion protein with epigenetic markers for histone 3 acetylated at lysine 14 (H3K14). The 8C nuclei, isolated from 5-day-old seedlings, were immune-stained against H3K14ac (a, e, i, and m), and ERF4-Myc fusion protein (b, f, j, and n). The chromatin was stained with DAPI (c, g, k, and o). a), b), c), and d) WT Col-0; e), f), g), h) transgenic plants harboring the *XVE::ERF4-Myc* construct and ERF4-Myc fusion protein is expressed; i), j), k), and l) plants harboring *XVE::ERF4-Myc* construct but ERF4-Myc fusion protein was not detected; m), n), o), and p) transgenic plants harboring *XVE::GFP*. ERF4-Myc fusion protein localized in euchromatin (f), outside from the chromocenters (DAPI-intense stained spots, g). A change in the acetylation intensity of H3K14 of a), i), and m) was observed in nuclei expressing ERF4-Myc (e). Scale bars represent 2 μ m.

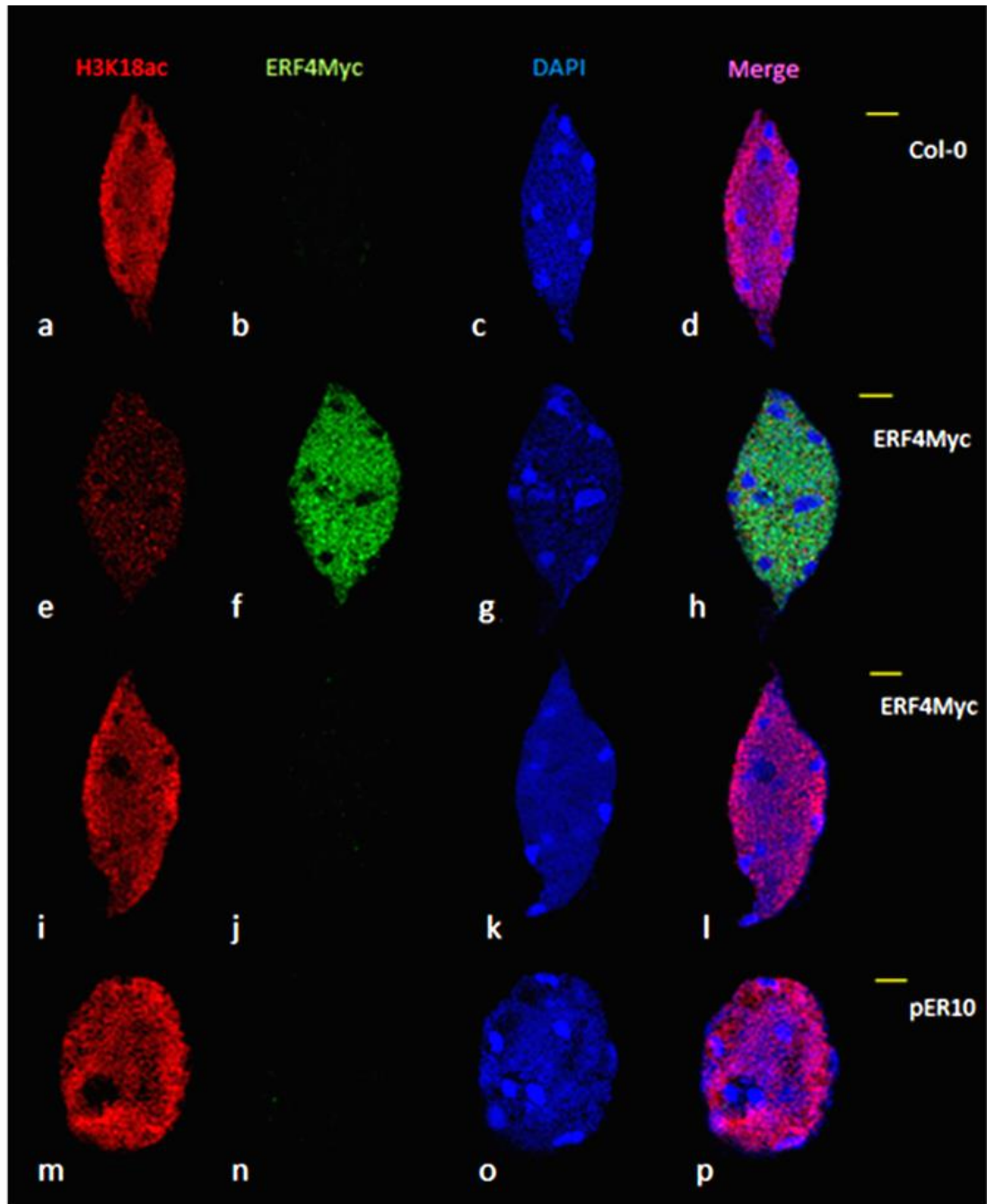


Figure 46: Co-localization of the ERF4-Myc fusion protein with epigenetic markers for histone 3 acetylated at lysine 18 (H3K18). The 8C nuclei, isolated from 5-day-old seedlings, were immune-stained against H3K18ac (a, e, i, and m), and ERF4-Myc fusion protein (b, f, j, and n). The chromatin was stained with DAPI (c, g, k, and o). a), b), c), and d) WT Col-0; e), f), g), h) transgenic plants harboring the *XVE::ERF4-Myc* construct and ERF4-Myc fusion protein is expressed; i), j), k), and l) plants harboring *XVE::ERF4-Myc* construct but ERF4-Myc fusion protein was not detected; m), n), o), and p) transgenic plants harboring *XVE::GFP*. ERF4-Myc fusion protein localized in euchromatin (f), outside from the chromocenters (DAPI-intense stained spots, g). A change in the acetylation intensity of H3K18 of a), i), and m) was observed in nuclei expressing ERF4-Myc (e). Scale bars represent 2 μ m.

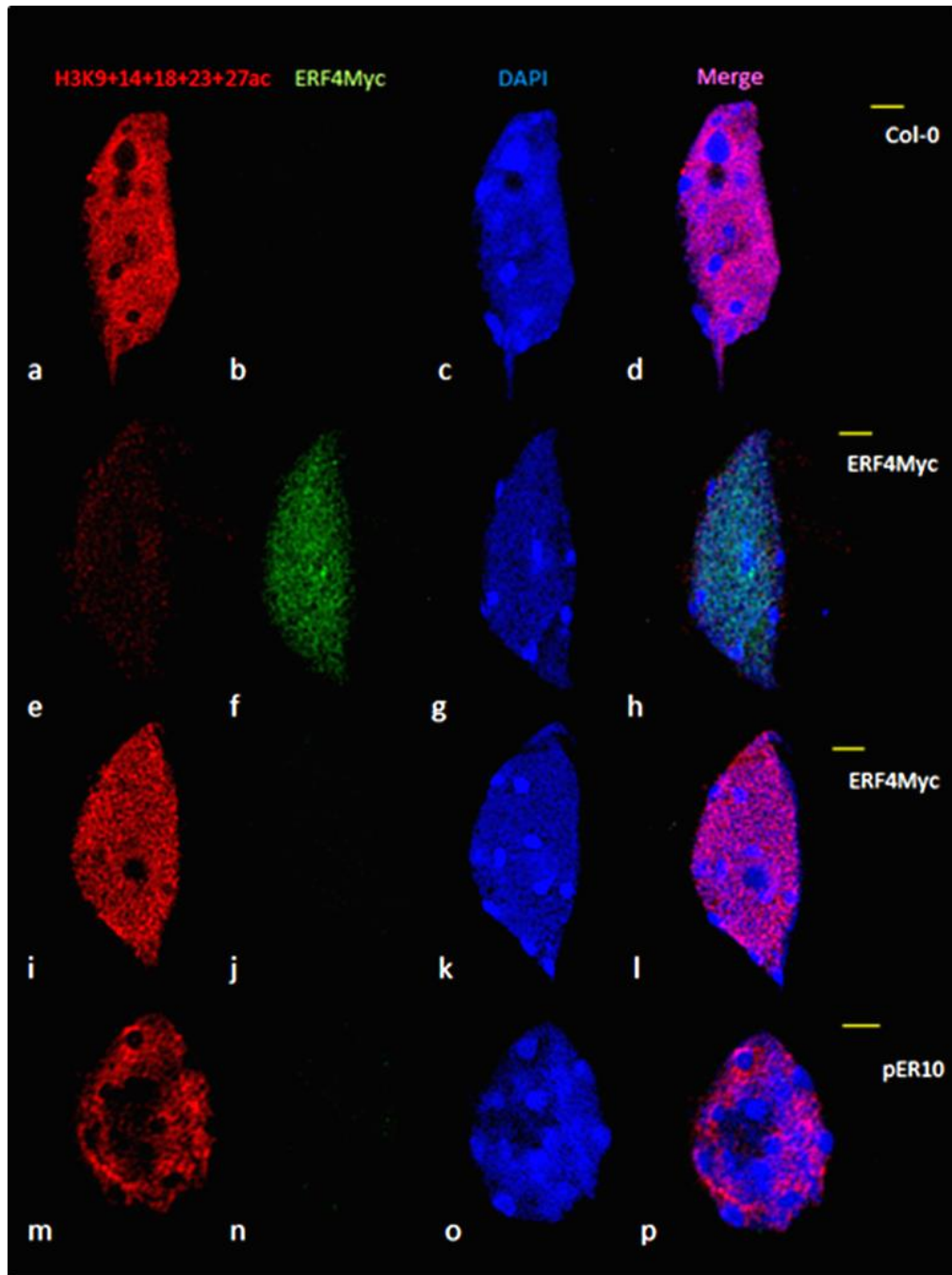


Figure 47: Co-localization of the ERF4-Myc fusion protein with epigenetic markers for histone 3 acetylated at lysine 9, 14, 18, 23, 27 (H3K9+14+18+23+27). The 8C nuclei, isolated from 5-day-old seedlings, were immune-stained against H3K9+14+18+23+27 acetyl (a, e, i, and m), and ERF4-Myc fusion protein (b, f, j, and n). The chromatin was stained with DAPI (c, g, k, and o). a), b), c), and d) WT Col-0; e), f), g), h) transgenic plants harboring the *XVE::ERF4-Myc* construct and ERF4-Myc fusion protein is expressed; i), j), k), and l) plants harboring *XVE::ERF4-Myc* construct but ERF4-Myc fusion protein was not detected; m), n), o), and p) transgenic plants harboring *XVE::GFP*. ERF4-Myc fusion protein localized in euchromatin (f), outside from the chromocenters (DAPI-intense stained spots, g). A change in the acetylation intensity of H3K9+14+18+23+27 acetyl of a), i), and m) was observed in nuclei expressing ERF4-Myc (e). Scale bars represent 2 μ m.

Although the analyzed nuclei displayed no changes in the acetylation pattern of H3K9, differences in the intensity of the fluorescence signals were observed. The intensity of H3K9 acetylation was clear and strong in the control nuclei (Col-0, pER10), and also in nuclei without the detection of ERF4-Myc (Figure 44 – 47a, i, m). Interestingly, some ERF4-Myc-positive nuclei exhibited an altered signal intensity of H3K9. The fluorescence signals were apparently weaker, and in some nuclei, only background noise was visible (Figure 44 – 47e). This suggests that the acetylation of H3K9 was specifically reduced. This decrease was predominantly visible in nuclei with ERF4-Myc expression. To classify nuclei showing various acetylation intensities three distinct categories were created. The first category denotes the nuclei with the lowest H3K9 fluorescence signals (Figure 48a), the second category represents intermediate intensities (Figure 48b), and the third one stands for the strongest signals observed in nuclei without ERF4-Myc expression (Figure 48c). No negative correlation between ERF4-Myc expression and the H3K9 fluorescence signal intensity was observed. Nuclei from all three categories were found among nuclei showing strong ERF4-Myc fluorescence signals as well as among nuclei showing weak ERF4-Myc fluorescence signals.

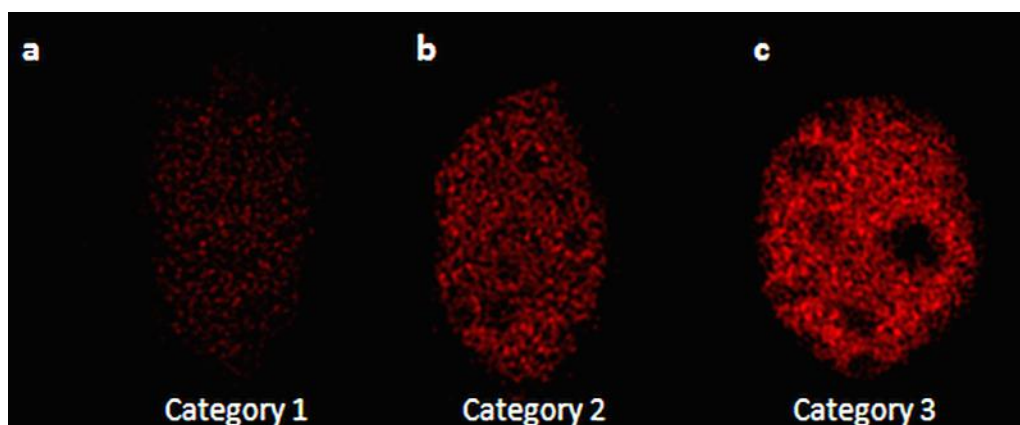


Figure 48: Categories of nuclei showing altered histone H3 acetylation intensity. a) category 1 shows the reduced intensity b) category 2 shows an intermediate intensity c) category 3 shows the strongest histone H3 acetylation. Category 3 was dominant in the nuclei without ERF4-Myc expression.

Figures 49–52 describe the proportion of nuclei in the three different H3 acetylation intensity categories. Among 8C nuclei expressing ERF4-Myc, the categories 1 and 2 of the H3K9 acetylation intensities (27 % and 37 %, respectively) were more abundant than in the control samples WT Col-0 and pER10-GPF. Here both categories reached only 5 %. The majority of nuclei in control samples fitted to category 3 (95 %), whereas

the 8C fraction of ERF4-Myc nuclei contained only 43 % of category 3 (Figure 49). To investigate whether this acetylation variation was caused by the ploidy level, or whether it is a global phenomenon, a mixture of isolated (not flow-sorted) nuclei was used to count the number of nuclei belonging into the three distinct categories. No significant differences between the mixed and the flow-sorted nuclei were detected. The obtained values were almost identical (Figure 49).

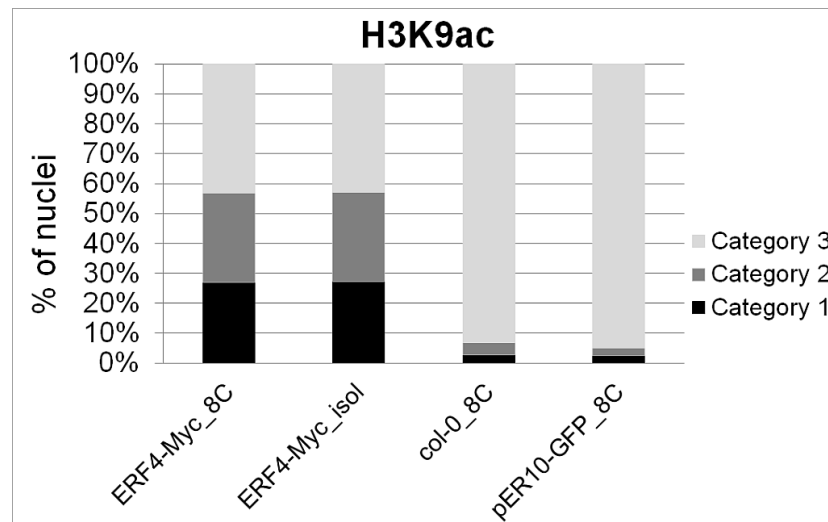


Figure 49: Proportion of nuclei belonging to the three distinct categories of H3K9. The 8C fraction of nuclei isolated from seedlings harboring the *pER10-ERF4-Myc* construct showed an elevated number of nuclei with a changed acetylation pattern of H3K9 when compared to the control samples WT Col-0 and plants harboring *pER10-GFP*. Similar results were obtained when a non-sorted nuclei mixture was analyzed.

Similar trends were found for acetylated H3K14; H3K18; and H3K9, H3K14, H3K18, H3K23, H3K27, where categories 1 and 2 were more abundant in ERF4-Myc positive nuclei than in the control samples (Figures 50–52).

The acetylation intensities of H3K14 in 8C ERF-4Myc positive nuclei were 34 %, 27 % and 39 % for the categories 1, 2 and 3, respectively. The mixture of isolated ERF4-Myc positive nuclei samples contained most nuclei in category 1 (41 %). Category 2 had 27 %, while 32 % of the nuclei represented the strongest acetylation intensity category 3. In both control samples, the most abundant category was again category 3 with more than 92 % of analyzed nuclei (Figure 50).

In the case of H3K18 acetylation, the 8C ERF4-Myc nuclei exhibited 23 % of category 1, 37 % of category 2, and 40 % of category 3. The mixture of isolated nuclei contained almost two times more nuclei of category 1 (41 %) than 8C. Category 2 and 3 were proportionally divided into 30 % and 29 %, respectively. The control sample (Col-0) displayed the similar distribution of nuclei as previously described, the pER10-GFP nuclei contained slightly more nuclei from category 1 and 2 but still, the dominant category was number 3 with 90 % of observed nuclei (Figure 51).

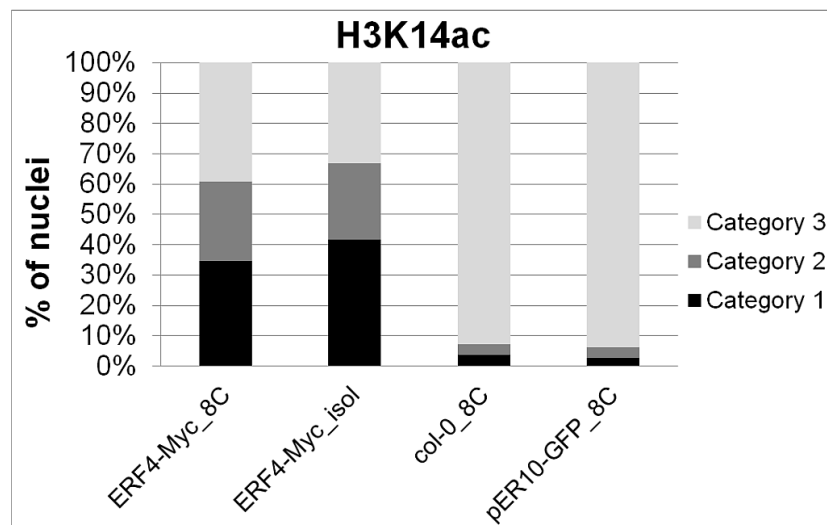


Figure 50: Proportion of nuclei categorized into three distinct intensity categories of histone H3 acetylation at lysine 14. For details see figure 49.

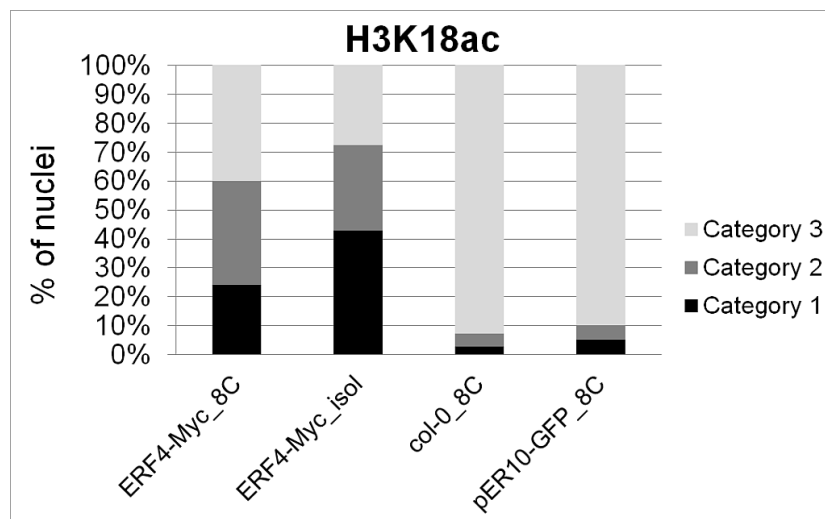


Figure 51: Proportion of nuclei categorized into three distinct intensity groups of histone H3 acetylation at lysine 18. For details see figure 49.

The abundance of nuclei in category 1 and 2, 21 % and 29 %, respectively, was slightly reduced in the ERF4-Myc nuclei immuno-stained with pan-acetylated H3K9+K14+K18+K23+K27 antibody, whereas category one was represented by 50 % of all analyzed nuclei. Isolated nuclei displayed a shifted ratio of fluorescence intensity categories 1, 2 and 3 with 39 %, 22 %, and 39 %, respectively. The control samples contained again more than 90 % of category 3 (Figure 52). The calculation for each assessed antibody was done from at least five independent measurements with at least 400 scored nuclei per genotype.

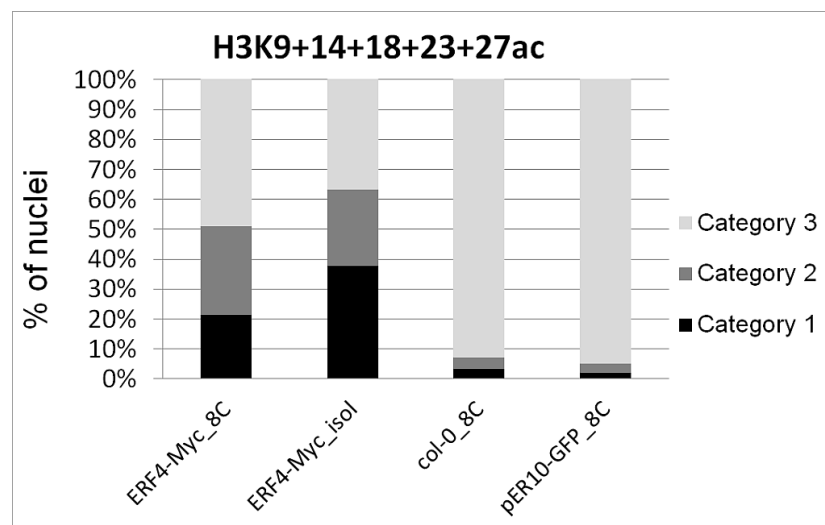


Figure 52: Proportion of nuclei categorized into three distinct intensity groups of histone H3 acetylation at lysine 9, 14, 18, 23, and 27. For details see figure 49.

After the examination of the acetylation pattern at different lysine residues, one example (H3K14) was chosen for voxel intensity measurement by Imaris 8.0 software. Individual nuclei positive for ERF4-Myc signal and belonging to the first category were selected and compared with nuclei lacking the ERF4-Myc expression. Significant differences proved the reduction of H3 acetylation in nuclei where *ERF4* was overexpressed. Nuclei from the first category displayed more than two-times reduced fluorescence intensity of H3K14ac (Figure 53).

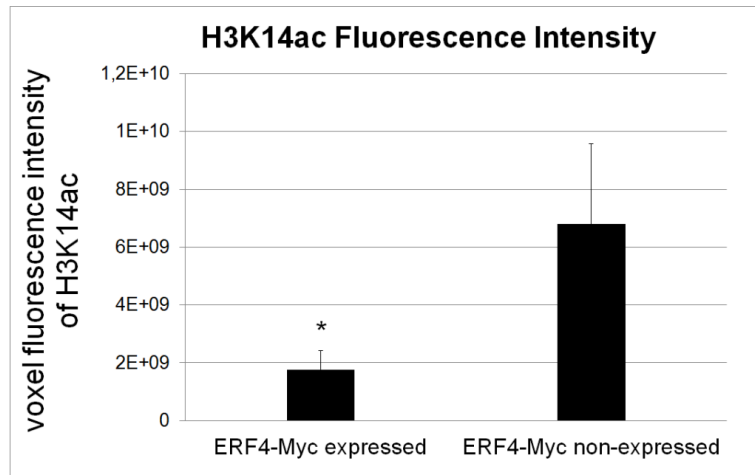


Figure 53: Nuclei expressing ERF4 showed a reduced H3K14 acetylation pattern. Nuclei from *A. thaliana* seedlings were isolated and sorted according to the ploidy level. The 8C fraction was selected and subjected to immunostaining and super-resolution microscopy. Voxel intensities were calculated by Imaris 8.0 software. Nuclei expressing ERF4 showed reduce H3K14ac pattern when compared to nuclei without ERF4 expression. Data shown are the mean + SD of 12 individual nuclei and statistical significance was determined by student's *t*-test (* $p < 0.05$).

4 Discussion

4.1 Proper proteolysis of transcriptional factors is essential for correct plant development

The impaired proteolysis causing severe plant defects clearly shows that not only the proteosynthesis but also protein degradation play an essential role in normal plant growth and development (Sonoda et al., 2007; Gallois et al., 2009). Except for the pharmacological treatment, we affirmed the crucial role of proteolysis on the development of shoots by employing a genetic approach. WT Col-0 root explants treated with the proteasome inhibitor MG132 were defective in shoot development, while control root explants treated with DMSO were able to regenerate the shoots normally (Figure 24). This pharmacological experiment proved the essential role of the proteasome in normal shoot development. A *bpm1;2 Arabidopsis* double mutant in genes encoding the E3 ligases *BPM1* and *BPM2*, which are key elements of proteasome-mediated protein degradation machinery, exhibited also reduced shoot regeneration efficiency. We expected an even stronger shoot regeneration deficient phenotype in a *bpm1;2;3* triple mutant. Surprisingly, this mutant did not display such phenotype (Figure 31). How could this be explained? It is important to mention that for both experiments two different solidifiers were used to prepare plant cultivation media that might affect these results. First, the solidifier Phytigel (Sigma-Aldrich) was used for the *bpm1;2* double mutant experiment, while the Gellan Gum solidifier (Thermo Fisher Scientific) was used for *bpm1;2;3* triple mutant. This might be one reason why the differences between the two mutants were observed. We also observed that in general, explants cultivated on medium solidified with Gellan Gum started to regenerate later when compared to the media solidified with Phytigel. No obvious differences in greening among the genotypes were detected in the early phases of explants incubation on SIM media (8 – 12 days). Testing the *bpm1;2* double mutant was a preliminary experiment. For all remaining experiments, we used Gellan Gum as solidifier.

Nevertheless, the phenotype of the *bpm1;2;3* triple mutant seems to be relevant as we found out that the *bpm1* mutant allele actually causes overexpression of *BPM1* rather than the expected gene disruption. This is due to the T-DNA insertion in the *BPM1* promoter region. In the future, another shoot regeneration assay is required to confirm the importance of the BPM adaptor protein in the development of SAM. The weak

penetrance of the phenotype in *bpm* mutants is likely due to the incomplete inactivation of BPM1. Similarly, the *6xami_bpm* silencing mutant line produced fewer shoots than WT. However, the phenotype was not as severe as originally expected for the mutations in all six *BPM* genes (Figure 31). Most likely, this mutant is not a complete knock-out but rather a knock-down of *BPMs* caused by micro RNA silencing. Therefore, we edited the *BPM1* gene by CRISPR/Cas9 technology and prepared a new *bpm1* mutant line named *bpm1cr1070*. This line carries an extra A insertion mutation in the first exon of the *BPM1* gene (Figure 21 – 22), causing a frame-shift that was further confirmed based on cDNA analysis (Figure 23). This newly confirmed mutant line was crossed with the previously prepared *bpm1;2;3* T-DNA insertion triple mutant to obtain a complete triple *bpm1;2;3* mutant. So far, more than 120 plants were analyzed but any triple mutant was found. Moreover, the *bpm1*^{S_{31057/cr1070}}; *BPM2/bpm2;bpm3/bpm3* mutant which is trans-heterozygous for *bpm1*, heterozygous for *bpm2* and homozygous for *bpm3* alleles showed an aberrant seed development. The defective seeds were arrested in the torpedo stage of embryo development. This observation strongly indicates that the complete *bpm1;2;3* triple mutation results in embryonic lethal. To prove this hypothesis, further experiments are needed.

Next, we elucidated the role of ERF repressors in the maintenance and specification of SAM as well as their impact on *CUC1* and *STM* gene expression. We also showed that the inhibition of the proteasome degradation pathway reduces the shoot regeneration capacity. A general feature of transcriptional repressors is their fast degradation, usually mediated *via* 26S proteasome activity (Gray et al., 2001; Patra et al., 2013). Such a tightly controlled regulation allows for the prompt and transient accumulation of repressor and thus is essential for its proper function. Malfunction of components of the proteasome might cause accumulation of cellular proteins including transcriptional repressors such as ERFs. This assumption is greatly supported by positive protein-protein interaction results provided in this work. Although only ERF4 and ERF8 could interact with the components of the E3 CUL^{BPM} ligase complex (Figure 26), the ERF interaction with other E3 ligases cannot be completely excluded. To this, protein-protein interaction analysis in yeast showed the interaction of BPM1 and BPM3 with both ERF4 and ERF8. In the case of BPM2, ambiguous results were obtained. Hence, in the future pull-down assay should be carried out to prove the previous findings *in planta*.

Our results on BPMs and ERFs are pointing out the importance of protein degradation in gene expression regulation mediated by the ERF repressors playing an important developmental role. We assume that the stabilization of ERF repressor proteins leads to a greater rate of co-repressor assembly at actively transcribed loci. As a consequence of this process, adjacent histones undergo deacetylation. Thus, chromatin condenses and the access of the transcription machinery to the promoter is constrained. The employment of the TPL-EAR motif-containing a transcription factor involved in root and shoot meristem development was recently reported (Espinosa-Ruiz et al., 2017).

To prove the link between protein degradation and histone deacetylation leading to chromatin condensation, further shoot regeneration experiments were employed. The shoot regeneration assay revealed an intermediate phenotype of *hda6-6;bpm1;2;3* quadruple mutant from single *hda6-6* mutant and *bpm1;2;3* triple mutant. No significant differences were observed between *hda6-6;bpm1;2;3* and *hda6-6* as well as between *hda6-6;bpm1;2;3* and *bpm1;2;3* (Figure 32). Due to the lack of strong phenotype penetration of the analyzed *bpm1;2;3* triple mutant it is impossible to unambiguously determine components acting up- or down-stream in this genetic framework. Additional experiments are needed to prove this concept.

Because we showed that the ERF repressors can interact with BPM adaptor proteins which are components of E3 CUL^{BPM} ligase, we hypothesize that an impaired BPM synthesis leads to the accumulation of ERF. In turn, ERF can recruit a co-repressor complex to its target loci and thus HDA can execute histone deacetylation. Therefore, we favor the interpretation that HDA6 acts downstream from the BPMs but an opposite role cannot be excluded.

4.2 WUSCHEL-independent pathway

Next objective of this work was to expand the current knowledge on plant development regulation focused on genes playing a key role in shoot regeneration. Plant development is a complex process involving several regulatory pathways. Some are acting synergistically while others antagonistically. These pathways usually consist of particular genes which act up- or downstream from each other and thus create

a complex genetic framework. The best-studied pathway is the WUS/CLV pathway which regulates the specification of stem cells and maintenance of the shoot apical meristem (Baurle, 2005; Busch et al., 2010; Somssich et al., 2016). Apart from this pathway, other independent mechanisms were suggested to take part in SAM regulation.

Besides the WUS-CLV pathway, meristem maintenance is also controlled *via* microRNA (miRNA) and HOMEODOMAIN-LEUCINE ZIPPER Class III (HD-ZIP III) transcription factors. It was shown that miRNA 165/166 negatively regulates HD-ZIP III TFs by directing them for cleavage (Mallory et al., 2004; Jung and Park, 2007). In addition to miRNA-mediated regulation of HD-ZIP III TFs, the ALTERED MERISTEM PROGRAM 1 (AMP1) inhibits HD-ZIP III TFs *via* translation inhibition (Li et al., 2013; Yang et al., 2018).

Five members of the HD-ZIP III transcription factors, PHABULOSA (PHB), PHAVULOTA (PHV), CORONA (CNA), REVOLUTA (REV), and ARABIDOPSIS THALIANA HOMEBOX8 (ATHB8) play a role in SAM development and have overlapping and antagonistic functions (Prigge et al., 2005; Williams et al., 2005). Three members of this TF family PHB, PHV, and CNA are negative regulators of meristem maintenance, whereas REV is a positive regulator (Lee and Clark, 2015). How the HD-ZIP III TFs control plant development is still not clear. Recently Zhang et al. (2017) showed that PHB, PHV, and REV can directly interact with B-type ARR1s. This HD-ZIP III-B-ARR1s complex can bind to and *de novo* activate WUS promoter and thus enhance the regeneration of shoots (Zhang et al., 2017).

On the other hand, *phb/phv/cna* triple mutants displayed a similar phenotype as *clv* mutants suggesting that the PHB/PHV/CNA pathway act antagonistically to the WUS/CLV pathway and thus restricts the meristematic cells within their niche (Lee and Clark, 2015). The same work proposed the existence of another factor “x” that controls the maintenance of SAM. Additionally, the study from 2018 showed that also *ERECTA* family genes, *ERECTA* (*ER*), *ERECTA-LIKE1* (*ERL1*), and *ERL2*, can regulate WUS-independent SAM development. The loss of function mutant *wus er erl1 erl2* was able to restore SAM but moreover, the mutant produced flowers with pistils (Kimura et al., 2018). Our results obtained by the genetic approach and the phenotypic manifestation of a quintuple *wus;erf4-1;8;f9-1;12* mutant, that could partially rescue the

wuschel phenotype (Figure 35), strongly suggest the importance of ERF transcriptional repressors in SAM maintenance acting independently from WUSCHEL. Interestingly, mutants lacking the WUS protein were able to produce recognizable SAM only when ERF repressors were impaired. Similarly to a *wus;phb;phv;cna* quadruple mutant described previously by (Lee and Clark, 2015), the rescue of the *wus* phenotype in a *wus;erf4-1;8;9-1;12* mutant was observed only within the vegetative growth stage. After the floral transition, the *wus;erf4-1;8;9-1;12* mutant showed a phenotype similar to *wus*, resulting in plant sterility. These results imply that ERF TFs are members of some alternative pathway bypassing the main WUSCHEL-dependent SAM maintenance pathway.

Role of the ERF repressor in the regulation of SAM development corroborates the acceleration of meristem activity. This is seen as an enlarged inflorescence meristem and an increased number of floral buds (Figure 33). The altered divergence angle of siliques might be also an attribute of SAM expansion (Figure 34). Lately, Landerain et al. (2015) proved the model previously predicted by (Mirabet et al., 2012) and showed that the meristem size correlates with phyllotaxis. The mutant showing meristem enlargement displayed a higher frequency of permutation in the spiral phyllotaxy than WT (Landrein et al., 2015; Mandel et al., 2016).

On the contrary, we could not observe an enhanced shoot production in *erf4-1;8;9-1;10;11-1;12* sextuple mutant or rescue of the *wus* phenotype in *wus;erf4-1;8;9-1;10;11-1;12* septuple mutant when assessed in an *in vitro* tissue culture system (Figure 30). In *erf4-1;8;9-1;10;11-1;12* sextuple mutant, this might be due to the production of “puff-like” structures which hinder the emergence of shoots and probably arise from the preparation of explants. This idea is supported by the fact, that shoot regeneration efficiency of WT Col-0 was almost 20 % higher than of sextuple mutant after 20 days on SIM but two days later, the shoot regeneration efficiency was same in both genotypes. Another explanation is that the weak phenotype of the *erf4-1;8;9-1;10;11-2;12* mutant might be due to the natural instability of ERF proteins in WT. Therefore the mutation has only very low or no impact on the shoot regeneration. Likewise, no shoot regeneration rescue phenotype was observed in *wus;erf4-1;8;9-1;10;11-2;12*. We assume that the conditions used in our *in vitro* tissue culture system were not ideal for the manifestation of the *wus;erf4-1;8;9-1;10;11-2;12*

phenotype. More biological replicates are needed in the future to exclude false-negative results.

Transcriptional repressors ERFs, along with transcription activators ESR1 and ESR2, recognize the GCC-box in the promoter region of their target genes. Thus, they can compete for binding to this element. Identification of candidate direct target genes of ERF4 using RNAseq revealed that 62 % of genes showing at least 2-fold change were found to be common for *N4C2-ER* and *ESR2-ER*. Likely, ESR2 and ERF4 share similar targets. Using a semi-quantitative RT-PCR, we showed that *ERF* genes with a GCC-box, only *ERF9* and *ERF12* respond to ERF4 and also ESR2 (Table 7). These findings can explain the reduced shoot regeneration efficiency of the *erf4-1;8* and *erf4-1;8;bpm1;2;3* mutant (Figure 21). We found that *ERF9* and *ERF12* are primary target genes of ERF4 and therefore can be repressed by that (Figure 29). In the mutant line with an impaired ERF4 function, *ERF9* and *ERF12* repressors are no longer repressed or their repression is attenuated. Thus, they can exhibit their repression activity with shoot regeneration inhibition as a result. The significance of *ERF9* and *ERF12* in development is also visible in plants with altered phyllotaxis.

The most downregulated gene from *ERFs*, *ERF8*, do not possess GCC-box same as the majority of identified candidate direct target genes. Yang et al., (2009) showed that different ERF TFs can bind to cis-regulation sequence of their target genes also when only a CG-core is present and that flanking region of this cis-regulation element modifies the binding preferences of TFs (Yang et al., 2009). Another study showed that a high portion of TFs recognizes an additional motif which often varies from the primary recognition motif (Franco-Zorrilla et al., 2014). Thus, regulation of *ERF8* transcription might be mediated *via* another unknown cis-element.

Based on our gene expression analysis it can be hypothesized that the SAM development might be indirectly mediated through *CUC1* and *STM* (Figure 37). Mutant lines impaired in ERF repressors displayed an elevated time-dependent *CUC1* gene expression, similar to *STM*. Although *CUC1* does not contain GCC-box in its promoter, the neighboring gene sequence is enriched in the GC content that might mimic the ERF-binding site.

The accumulation of *CUC1* transcripts in the quintuple *erf4-1;8;9-1;11-2;12* and *erf4-1;8;9-1;10;12* can be mediated direct *via* *ESR2* binding and indirectly by ERFs transcriptional repressors. This hypothesis is supported by our finding *in planta*, showing that *CUC1* expression is upregulated 2.3 times by *ESR2* overexpression (Table 8). In *erf* mutants, the activators do not compete for the DNA-binding site. Thus, they can freely bind to and directly activate the expression of target loci. Additionally, another type of indirect gene up-regulation mediated by ERFs was reported by Zhou et al. (2016). The authors showed that ERF11 can indirectly induce gibberellin accumulation *via* inhibition of ethylene biosynthesis genes (Zhou et al., 2016). In agreement with this, the relative gene expression of *ESR2*, containing GCC-box in its promoter, increased gradually over the time in the *erf4-1;8;9-1;11-2;12* mutant line. We do not have an explanation for the sudden decline of *ESR2* expression in *erf4-1;8;9-1;10;12* mutant on day 8 on SIM incubation (Figure 36b). As *CUC1* can bind to the *STM* promoter as well as *STM* can bind to *CUC1* promoter and thus creates a positive transcriptional feedback-loop (Spinelli et al., 2011; Scofield et al., 2018), we assume that the observed stronger relative *STM* expression in mutant lines was mediated by *CUC1* in early time-points. While at later phase of SIM incubation, *CUC2* or *CUC3* could control the *STM* expression.

The reduced accumulation of *ESR1* transcripts might be explained by the negative feedback loop of *ESR1* (Figure 36a). Expression of *ESR1* is transient and starts earlier (1 day after transfer onto SIM) (Banno et al., 2001), than *ESR2* expression (4 days after transfer onto SIM) (Matsuo et al., 2011) in WT. We assume that at the monitored time points the expression of *ESR1* is naturally depleted. The strong *ESR2* gene expression depletion which was observed in both mutants on day 8 on SIM might be mediated through a cascade triggered by ERF TFs, whereas *ESR1* does not contain a GCC-box and seemed not to be a direct target gene of ERF4.

Surprisingly, apparent differences in the relative expression of *CUC1* and *STM* were observed in two mutant lines, *erf4-1;8;9-1;11-2;12* and *erf4-1;8;9-1;10;12* (Figure 37). These unexpected differences in relative *CUC1* and *STM* gene expression might be explained by the distinct spatiotemporal gene expression pattern of individual *ERF* genes in the time course of CIM and SIM incubation. Based on the publicly available data in TAIR database (Che et al., 2002), we analyzed the expression pattern of *ERF*

genes. Expression of *ERF4* was strongest among all studied *ERF* genes (*ERF4*, *ERF8*, *ERF9*, *ERF11*, and *ERF12* expression profile of *ERF10* was not monitored) at day 0 on CIM incubation and was gently decreasing up to day 4 on CIM incubation. After the transfer to SIM, the *ERF4* expression dropped more rapidly. *ERF11* also showed significant changes in the expression. But, in contrast to *ERF4*, the expression declined dramatically even after 2 days on CIM incubation and further decreased following incubation. *ERF8* and *ERF12* showed a very low transcript abundance at the beginning of CIM incubation that increased slowly in time. Although, there is no information on ERF protein abundance it might be assumed that it correlates with the RNA level. The lack of the *ERF11* gene product has a big impact on the expression of *CUC1* as clearly demonstrated by our results obtained with the *erf* quintuple mutants.

Indeed, it is tempting to speculate that the presence or absence of a particular ERF transcription factor at early stages of plant development plays a crucial role for the specification of developmental program in later phases of plant growth. It is important to accumulate more data from additional replicates. Here we hypothesize, that ERF repressors acting on *CUC1* and *STM* might suppress the putative WUSCHEL independent pathway controlling SAM development.

4.3 Role of ERF4 in gene expression regulation

The sub-cellular localization of ERFs was for the first time shown by Yang et al., (2005). The authors overexpressed a *35S::AtERF4-GFP* construct in *Arabidopsis* protoplasts and found the GFP-fluorescence being localized to discrete nuclear bodies. Previously, it was shown that the ABI5 (abscisic acid insensitive 5) protein, a key player in abscisic acid signaling, co-localized also in nuclear bodies when interacting with its negative regulator (Lopez-Molina et al., 2003). Since, the nuclear bodies contained a RING protein, a key component of 26S proteasome, these structures were proposed as sites for the proteasome-mediated protein degradation (Lopez-Molina et al., 2003). This finding inspired us to examine whether ERF repressors undergo proteasome-mediated degradation within nuclear bodies. To test this hypothesis, the transgenic *Arabidopsis* lines expressing an ERF4-mCherry fusion protein were prepared. The localization of the mCherry fluorescence was followed using live-cell confocal microscopy. Interestingly, ERF4-mCherry-specific signals did not co-localize within the nuclear bodies but were

spread all over the nucleus (Figures 39 – 41). The observed pattern seems to be specific since the control line expressing *mCherry-only* displayed red fluorescence signals throughout the cell. The localization pattern of the mCherry protein is in agreement with previously published works using similar enhancer trap line with GAL4-UAS system (Rim et al., 2009, 2011). These studies showed that free mCherry protein is movable and can move from the site of its synthesis to the other root tissues, showing the uniform fluorescence signals over the cells. On the other hand, the ERF4-mCherry signal was exclusively restricted to the nucleus (Figure 39a, c). Our localization studies further proved that the DNA binding domain is essential for ERF4 trafficking into the nucleus; suggesting the nuclear localization signal (NLS) is confined to the AP2 domain (Figure 39d, f).

Because ERF4-mCherry signals did not co-localize within the nuclear bodies but were spread over the nucleus, its accurate localization within the chromatin was further investigated using immunostaining in combination with super-resolution microscopy. This detailed observations revealed that the ERF4-mCherry signal was excluded from the heterochromatin and exclusively localized in euchromatin (Figure 40a, d, e, h). As ERF4 works as transcriptional repressor directly regulating expression of specific target genes, its co-localization with the transcription machinery was tested in this study. Interestingly, the ERF4-mCherry signals co-localized with the active RNAPolIIser2ph better than with inactive RNAPolII variant (Figure 42). The transactivation activity of transcription activators is usually considered to be mediated through recruitment of the Mediator complex into the actively transcribed loci, whereas the transcriptional repressors recruit so-called co-repressor complex (Kagale and Rozwadowski, 2011; Huang et al., 2016). Our findings thus support the recently described novel concept of transcriptional repressor mode of activation; suggesting that repressors are more co-localizing with actively transcribed loci than with the silent loci (summarized in Reynolds et al., 2013). In yeast, it was shown that the RNA polymerase can recruit the histone deacetylase-containing complex to the actively transcribed loci mediating chromatin condensation and consequently blocking re-initiation of the next round of gene transcription. A similar principle might work also for plants (Keogh et al., 2005; Reynolds et al., 2013). The arrangement of transcriptional repressors around actively transcribed loci is convenient for the accurate and quick response to the changing stimuli whereby enabling fine-tuning of transcription. Thus, ERF action depends not

only on binding preferences to the target DNA sequence but also on the ability to recruit the transcription machinery or co-repressor complex.

4.4 ERF4 affects histone acetylation

ERF4 can interact with co-repressor components (Song and Galbraith, 2006). In parallel, we have shown that ERF4 co-localizes with RNAPolIIser2 (Figure 42) which occupies the sites of active gene transcription in the nucleus. Next, ERF4 is capable to recruit histone deacetylases to target loci and through their enzyme activity presumably to repress gene expression. To test this hypothesis, we investigated the acetylation pattern/status of five histone marks in the plant line over-expressing *ERF4-Myc*. We confirmed the localization of ERF4 within the nuclear euchromatin (Figure 44, 45, 46, 47 a, d, e, h, i, l, m, p). This observation is in agreement with our observation with the ERF4-mCherry line (Figure 40a, e). Obtaining identical results using two independent constructs strongly implies that the observed pattern reflects the actual localization of ERF4 *in planta*. We assume that the weaker fluorescence signal of antibodies specific to histone marks mirrors the reduction of acetylation at histone H3 (Figure 48) in response to ERF4 accumulation in the nucleus. Nuclei showing a reduced level of acetylation of histone H3 at different lysine residues were detected in nuclei co-expressing *ERF4-Myc* more often than in control WT samples (Figures 49 – 52).

Recently, differences in the histone acetylation status were observed across the root tissue in *Arabidopsis* root (Rosa et al., 2014). The authors found out that cells with high competence to divide, such as meristematic cells, show a stronger histone acetylation level than differentiated cells, and acetylation affected the histone mobility. The higher acetylation pattern and thus relaxed/loosen chromatin probably allows for the extensive gene transcription needed for rapid cell divisions, typical for this tissue. Furthermore, the cells in the QC zone showed similar properties like the ones in the differentiation zone. Authors of this study concluded that cell specialization e.g. stem cells in the QC or differentiated cells in DZ is important for chromatin dynamics. They also showed that the division rate depends on the histone acetylation level. Importantly, the RAM enlargement induced by hyperacetylation was caused by a reduced differentiation rate in the root meristem zone rather than by the accelerated number of cell divisions (Rosa et al., 2014). This might suggest the role of the histone acetylation changes in cell differentiation and meristem maintenance. In our case, a majority of analyzed nuclei

overexpressing ERF4-Myc and showing a reduced level of acetylation of histone H3 arose from the differentiated and specialized tissue; according to the ploidy level. We hypothesize that depletion of the ERF transcriptional repressors might change the histone acetylation level of their target genes and thus trigger signal cascades leading to regeneration.

Further evidence stressing out the importance of the chromatin structure for the expression of genes comes from the study on the WUSCHEL gene locus. The authors revealed that the formation of chromatin loops (so-called WUS loops) can attenuate the expression of WUS (Guo et al., 2018).

Since the regeneration of the shoot apical meristem initiates from LRP of plant tissue explants (Atta et al., 2009; Rosspopoff et al., 2017), the particular tissue files where ERF repressors execute their function on acetylation status might be identified by crossing *ERF4-Myc* overexpressor lines with root tissue-specific nucleus fluorescent marker lines (Marquès-Bueno et al., 2016). These marker lines allow for simple nuclei purification by flow-sorting as reported earlier (Deal and Henikoff, 2010). Histone acetylation might be then followed in marker lines overexpressing *ERF4-Myc* to reveal the exact role of ERF repressors during shoot regeneration.

4.5 Can mutation in ERF repressors cause enlargement of SAM?

As we showed, no accelerated shoot regeneration was observed in *erf4-1;8;9-1;10;11-1;12* sextuple mutant by using *in vitro* tissue culture system. Apart from the reasons for this result discussed above a new explanation emerged in light of the study by Rosa et al. (2014). The weak phenotype of *erf4-1;8;9-1;10;11-1;12* sextuple mutant in terms of shoot regeneration efficiency might be due to the retarded differentiation rate of the meristem tissue caused by hyperacetylation in the absence of ERF repressors. There are two possible scenarios explaining why we could not detect a higher number of regenerated shoots. 1) A number of *de novo* formed SAM is not affected but its enlargement is enhanced. 2) The number of *de novo* SAM is increased but their function is limited and some cannot develop true leaves. In our shoot regeneration assay, we considered already differentiated true leaves arising from the *de novo* developed SAM, instead of counting a number of all newly formed meristems. This approach, therefore, reflects only fully functional SAMs. Therefore, even though

we could not detect higher shoot regeneration efficiency in *erf4-1;8;9-1;10;11-1;12* mutants when compared to the WT Col-0 using our system, we still cannot exclude the second scenario.

Taking into consideration the above-discussed results; it seems that the first scenario is more likely. In addition, the enlargement of SAM is supported not only by larger florescence meristems observed in the *erf4 1;8;9-1;12* quadruple mutant (Figure 33) but also by the elevated relative gene expression of the SAM marker gene, *STM*, in *erf* mutants (Figure 37b). Although those are just indirect evidence of SAM enlargement there is a strong indication that ERF repressors can regulate the size of SAM. This scenario might also explain why we could observe the formation of SAM in the *wus;erf4-1;8;9-1;12* mutant *in planta*. To further examine this hypothesis, histological section through SAM of *erf* mutants and WT need to be prepared to evaluate the SAM size.

PART II – Chlorophyll Measurement as a Quantitative Method for the Assessment of Cytokinin-Induced Green Foci Formation in Tissue Culture

Ivona Kubalová, Yoshihisa Ikeda

*Center of the Region Haná for Biotechnological and Agricultural Research, Faculty of
Science, Palacký University, Olomouc, Czech Republic*

5 Abstract

Tissue culture systems have long been exploited to study the process of organogenesis. In response to externally applied cytokinins, pluripotent cells proliferate into green calli and subsequently regenerate shoots. Conventionally, the cytokinin-induced greening phenotype has been evaluated by counting numbers of green foci or to present photographic evidence of morphological changes. However, because the structure of calli is disorganized and the development of pigmentation takes place gradually from pale white through yellow to green, adequately defining and counting green foci remains difficult. In this study, we employed chlorophyll measurement as an alternative method to statistically assess the greening phenotype in tissue culture material. We found that N,N-dimethyl-formamide was the most effective solvent for the extraction of chlorophylls from callus tissue and that bead disruption of the structured tissue improved solvent penetration and the consistency of results. The sensitivity of the method facilitated the quantification of chlorophylls in single-cultured root explants and the use of a spectrophotometer increased the efficiency of measuring multiple samples. Our measurements showed that chlorophyll contents from calli of wild-type and altered cytokinin response mutants (*cre1;ahk3*, or cytokinin hypersensitive 2 (*ckh2*)/pickle (*pkl*) were statistically distinguishable, validating the method. Our proposed procedure represents gains in efficiency and precision and leads to more robust standardization than the conventionally used counting of green foci.

6 Introduction

Since the establishment of the *in vitro* tissue culture system by Skoog and Miller in 1957, plant *de novo* organogenesis has been well documented. In principle, plant cell identity is manipulated by the defined cytokinin to auxin ratio in an *in vitro* tissue culture (Skoog and Miller, 1957). The most widely used *in vitro* tissue culture system for *de novo* organogenesis in *Arabidopsis* was developed in 1988 (Valvekens et al., 1988). It is composed of two subsequent steps – the first step involves pre-incubation of explants on auxin-rich callus inducing medium (CIM) to induce a mass of growing cells, termed callus, that emerge from explants. The second step involves the culture of induced callus on shoot-inducing medium (SIM) in which a high cytokinin-to-auxin ratio is applied. This second medium promotes the nascent development of green foci. Live-imaging cell biology for visualizing marker gene expression and transcriptome analyses have shown that callus formation during CIM incubation is the differentiation of xylem pole-associated pericycle or pericycle-like cells toward root meristem-like tissue and that shoot regeneration is cytokinin-induced transdifferentiation of early lateral root meristems into shoot apical meristems (Atta et al., 2009; Sugimoto et al., 2010). These processes are summarized in detail in a number of review articles (Motte et al., 2014b; Perianez-Rodriguez et al., 2014). Lateral organ (shoot) differentiation takes place from the developed green foci in later stages of SIM incubation. An analysis of 88 *Arabidopsis* accessions revealed no correlation between green foci formation and subsequent shoot regeneration efficiencies, indicating that greening and the subsequent differentiation of lateral organs are distinct phenomena that are under genetic control (Motte et al., 2014a). To obtain a better understanding of organogenesis, these two different processes must be evaluated independently.

To study the cytokinin response during organogenesis, two methods are commonly used to evaluate green foci formation. One is to count the number of green foci and the second is to present photographic evidence of morphological changes. The greening takes place gradually and no defined criteria exist. Determination of the number of green foci has largely been a subjective method, based on the observer's determination. Regardless of the chosen determination, the size and the degree of greening are not considered in the results. It is also difficult to count green foci that have developed downward and grown into the medium. A quantitative analysis of the greening phenotype is required to gain insights into cytokinin actions in a tissue culture system.

7 Materials and methods

7.1 Plant material and growth conditions

Arabidopsis thaliana accession Columbia-0 (Col-0) was used as wild-type. Seeds of *long hypocotyl 1 (hyl)* (Gabi Kat034B01), *genome uncoupled 4 (gun4)* (SALK_026911), *pickle-1 (pkl-1)* (WisDsLox407C12), and *arabidopsis histidine kinase 3 (ahk3)* (Gabi Kat 754H09) were obtained from the European Nottingham Arabidopsis Stock Centre (NASC). The *cytokinin response 1-2 (cre1-2)* mutant was kindly provided by Tatsuo Kakimoto at Osaka University. The original *hyl* and *gun4* mutants were backcrossed once, and *pkl-1* and *ahk3* were backcrossed three times with wild-type plants prior to characterization. The primers used for genotyping by PCR are listed in Table 9.

Arabidopsis plants were grown in a photoperiod of 16 h light (approximately 60 $\mu\text{mol m}^{-2} \text{s}^{-1}$) and 8 h dark at 21 °C with 70 % humidity. The conditions for seed surface sterilization and growth on MS plates, CIM pre-incubation and subsequent SIM culture were as previously described (Ikeda and others 2006). In brief, *Arabidopsis* seeds were surface sterilized with 5 % sodium hypochlorite (VWR Chemicals), washed with sterilized water 3 times and stored for 3 days at 4 °C in the dark. Seedlings were grown on MS + 1 % Sucrose (pH 5.7) containing 0.8 % phytagel plate in vertical orientation. Five days after germination, roots were excised into intervals of approximately 8 mm in length and excised root explants that do not contain RAM were transferred onto CIM for 4 days for pre-incubation. Subsequently, root explants were transferred onto SIM for 10 days and subjected to chlorophyll extraction. For the CIM incubation, CIM containing 0.22 μM 2, 4-D and 1.16 μM kinetin was prepared and root explants were cultured for 36 days.

Gene name	T-DNA insertion	Primer name	Sequence (from 5' to 3')
<i>HY1</i>	<i>hy1-3</i> GK-034B01	HY1F	TTTCTATTCCGATCAAACCATGGCG
		HY1R	AACAACATAAGAAATGAGGCAAAGG
		GK_L8760	GGGCTACACTGAATTGGTAGCTC
<i>GUN4</i>	<i>gun4-3</i> SALK_026911	GUN4F	CGGAGATTACTCATTTCAGATATCCG
		GUN4R	TAAACACTCTTTTGTCTGCTCCTAC
		LBa1	GGTTCACGTAGTGGGCCATCGCCCTG
<i>CRE1/AHK4</i>	<i>cre1-2</i> Kazusa	CRE1F	CGTCTACAGGTTTCTAGGGTTTG
		CRE1R	CTGACCTGATCAATTGCAGAAGGG
		pPCVICEn3596	ATAACGCTGCGGACATCTAC
<i>AHK3</i>	<i>ahk3-8</i> GK-754H9	AHK3F	AGCTCGCAAGCTATGGAGAAGAGG
		AHK3R	AAGAAGCTTACTTTCCAGACAGC

Table 9: List of primers used for PCR-genotyping

7.2 Semi-quantitative RT-PCR analysis

Total RNA was extracted from root explants cultured on SIM for 10 days by RNAqueous phenol-free total RNA isolation kit (Ambion). Conditions for RNA extraction, first-strand cDNA synthesis, PCR and agarose gel electrophoresis were described (Ikeda et al., 2006). Primers used for RT-PCR are listed in Table 10. Cycles used for detection of *WUS* or *TUB* are 38 or 18 cycles, respectively.

RT-PCR	Primer name	Sequence (from 5' to 3')
<i>WUS</i>	WUSF	CACGGTGTTCCCATGCAGAGACC
	WUSR	CGTCGATGTTCCAGATAAGCATCG
<i>TUBULIN3</i>	TUB3_U51	GGACAAGCTGGGATCCAGGTCG
	TUB3_U52	CATCGTCTCCACCTTCAGCACC

Table 10: List of primers used for semi-quantitative RT-PCR.

7.3 Chlorophyll extraction, measurement, and statistical analysis

Root explants cultured for either 10 days on SIM or 36 days on CIM were used in chlorophyll extraction experiments. Individual root explants were transferred to 1.5 mL Eppendorf tubes containing 60 µL solvent (80 % acetone, DMF or DMSO) and a tungsten carbide bead (3 mm QIAGEN). Tissue was disrupted by Mixer Mill (Retsch MM 400) at 25 Hz for 20 seconds. Samples were left for 5 min before the centrifugation at 14 000 rpm for 3 min at room temperature. Supernatants were transferred to 8-strip PCR tubes and centrifuged again to remove debris hindering absorptions. Forty

microliters of solution was carefully transferred to wells of a 96-well glass plate (CORNING High Content Imaging Plate Black with 0.2 mm glass bottom cyclin olefin co-polymer). The following equations were used to determine chlorophyll contents 80% acetone: Chl a (mg l^{-1}) = $12.63 [A_{664} - A_{750}] - 2.52 [A_{647} - A_{750}]$; Chl b (mg l^{-1}) = $20.47 [A_{647} - A_{750}] - 4.73 [A_{664} - A_{750}]$ DMF: Chl a (mg l^{-1}) = $12.70 [A_{664} - A_{750}] - 2.79 [A_{647} - A_{750}]$; Chl b (mg l^{-1}) = $20.70 [A_{647} - A_{750}] - 4.62 [A_{664} - A_{750}]$ (Inskeep and Bloom 1985). DMSO: Chl a (mg l^{-1}) = $14.85 [A_{665} - A_{750}] - 5.14 [A_{648} - A_{750}]$; Chl b (mg l^{-1}) = $25.48 [A_{648} - A_{750}] - 7.36 [A_{665} - A_{750}]$ (Barnes et al., 1992). A wavelength of 750 nm was used as a blank. The Gen5 software on the Synergy H4 microplate reader (BioTek) was used for measurements (Warren, 2008). Results obtained from thirty root explants per genotype were subjected to a Student's t-test (http://www.physics.csbsju.edu/stats/t-test_bulk_form.html) with biological triplicates. *p*-values were as presented.

8 Results

8.1 Employment of bead disruption for efficient and consistent chlorophyll extraction from cultured tissue

To compare the extraction efficiency of chlorophylls from root explants, commonly used solvents, such as 80 % acetone, DMF, and DMSO were compared by following the equations for chlorophyll a and chlorophyll b determination as previously described (Inskeep and Bloom, 1985; Barnes et al., 1992). Glass plates were used for the measurements as DMF is an aggressive solvent that is not compatible with commonly used polystyrene plates. For the convenience of cutting roots, seedlings were grown in the vertical orientation on a relatively solid MS medium containing 0.8 % Phytagel. Five days after germination, root explants were excised and transferred onto CIM for 4 days (CIM pre-incubation), followed by transfer onto SIM. In order to prepare the same starting materials, two surgical blades were joined with an 8 mm gap separating the two blades. To consider variations in growth and cytokinin response, 30 root explants per solvent were randomly collected and subjected to chlorophyll extraction on day 10 of the SIM incubation. No lateral organs (shoot regeneration) were observed at this time. In agreement with previous reports (Inskeep and Bloom, 1985; Stiegler et al., 2005), DMF was the most effective solvent for extracting chlorophylls (Figure 54a to 54c). When extracted in 80 % acetone, 30 min incubation was not sufficient to reach equilibrium (Figure 54a), whereas it took around 15 min for DMF or DMSO to reach maximum levels (Figure 54b and 54c). DMF extracted chlorophylls more efficiently than DMSO ($p = 0.0082$ at 5 min). During tissue culture, some root explants spontaneously developed wound-induced callus (Ikeuchi et al., 2013) (Figure 54d), compromising efficient chlorophyll extraction when tissue is not disrupted, resulting in an underestimation of the chlorophyll content. This is particularly the case in *pkl-1* (data not shown). In order to tackle this difficulty, we applied tungsten bead disruption of all root explants. This procedure resulted in a chlorophyll recovery equivalent to the equilibrium of the corresponding solvents examined for the time-course experiments and an improved extraction in the case of 80 % acetone (Figure 54e and compare to Figure 54a), which is an advantage when glass plates are not available. Heat treatment was reported to prevent chlorophyll degradation by inhibiting the chlorophyll hydrolyzing enzyme, chlorophyllase (CLH) (Hu et al., 2013), however, no degradation was observed in our conditions (data not shown). Thus, for all subsequent experiments

extraction of chlorophylls in DMF with bead disruption and no pre-heat treatment was applied.

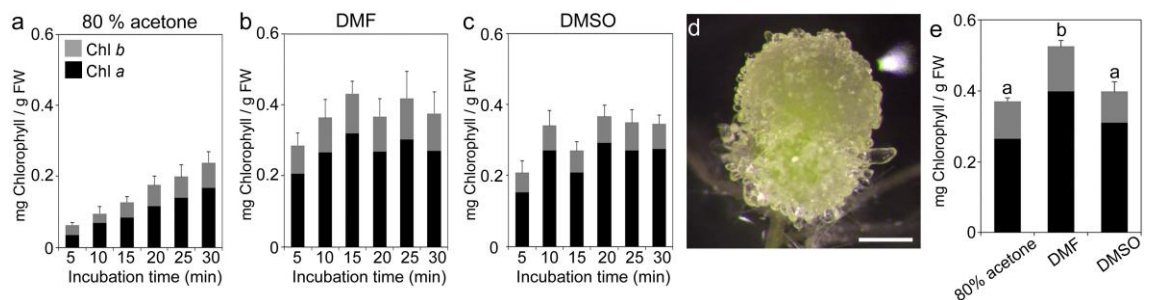


Figure 54: Effect of bead disruption and solvent on chlorophyll extraction from cultured root explants. (a to c) Chlorophyll contents of wild-type root explants cultured on SIM for 10 days extracted by 80 % acetone (a), DMF (b), and DMSO (c) without bead disruption. Chlorophyll a and Chlorophyll b contents were measured at different time points (min) and indicated in black and gray bars, respectively. (d) Wound-induced callus formed at the cutting sites covers green tissue in Col-0 root explant on SIM for 12 days. (e) Chlorophyll contents of wild-type root explants cultured on SIM for 10 days extracted for 5 min with bead disruption in corresponding solvents. Values marked with different letters are significantly different between genotypes ($p \leq 0.01$) as determined by student's t-tests. Data shown are the mean \pm SD of biological triplicates ($n = 30$). Scale bar represents 0.5 mm (d).

8.2 Validation of chlorophyll measurement as an objective greening phenotype analysis method in tissue culture

To verify the reliability and reproducibility of quantifying chlorophylls from cultured root explants as a measure for their greening phenotype, mutants reported having reduced chlorophyll contents were collected (Chory et al., 1989; Peter and Grimm, 2009). They were used as technical negative controls for chlorophyll quantifications. We obtained *hyl* (GK-034B01) and *gun4* (SALK_026911) mutants. GK-034B01 is referred to as *hyl-3* and SALK_026911 as *gun4-3*, respectively. We confirmed the position of the T-DNA insertion of *hyl-3* in the first exon of the annotated At2g26670.1 transcript, a longer version of splice variant. The *gun4-3* appeared to be null as no detectable GUN4 proteins were observed in the mutant (Peter and Grimm, 2009). *HY1* encodes monooxygenase and *GUN4* encodes an adaptor protein positively regulating Mg^{2+} chelatase activity (Davis et al., 1999; Peter and Grimm, 2009). We found that, although the color of mutant calli is paler than that of wild-type (Figure 55a), *hyl-3* and *gun4-3* root explants could form the disorganized structures (Figure 55b and 55c), indicating that tetrapyrrole biosynthesis is not required for cell outgrowth. Therefore cytokinin-induced greening phenotype cannot be assessed by counting green foci or by chlorophyll measurements in these mutants. As expected, chlorophyll amounts extracted

from the *hyl-3* or *gun4-3* root explants were significantly lower than that of wild-type ($p \leq 0.0001$ in both cases, Figure 55d), indicating that our method is able to determine differences in chlorophyll content from a single root explant.

Cytokinin was essential for nascent SAM formation and greening. This suggests that similarly to the *hyl-3* and *gun4-3*, mutants with an altered cytokinin response should have different chlorophyll levels. The *pkl* (*pickle*)/*cytokinin hypersensitive 2* (*chk2*), in which a CHD3 SWI/SNF2 chromatin remodeling factor gene is disrupted, exhibited cytokinin hypersensitivity in tissue culture (Furuta et al., 2011). The *pkl/chk2* was employed as a positive control. As the *cre1-2* and *ahk3* single mutants in the Col-0 background did not exhibit cytokinin-insensitive phenotypes (Riefler et al., 2006), cytokinin receptor double mutant, *cre1-2;ahk3*, was created as a negative control for reduced greening phenotype. We obtained the T-DNA insertion mutant line (Gabi-Kat 754H09), in which a T-DNA was inserted in the second exon of *AHK3*, resulting in no detectable transcript accumulation (data not shown). The GK-754H09 appeared to be a null mutant and we refer to it as *ahk3-8* hereafter. The *cre1-2;ahk3-8* double mutant had reduced green foci formation (Figure 55e), whereas *pkl-1* retained the capacity for pronounced greening phenotype (Figure 55f). We evaluated accumulated chlorophylls per root explant because *pkl-1* exhibited increased growth with root penetrating the agar medium. The increased mass due to pronounced *de novo* root development resulted in the underestimation of chlorophyll accumulation in *pkl-1* when chlorophylls were evaluated per fresh weight (data not shown). Besides, we found it inaccurate to measure the fresh weight of individual 8 mm root explant developing *de novo* roots into the medium (30 roots explants per genotype). Using chlorophyll measurements, we were able to statistically distinguish *cre1-2;ahk3-8* or *pkl-1* from wild-type (in both cases $p \leq 0.0001$, Figure 55g). When the number of green or yellow colored foci developed from *cre1-2;ahk3-8*, and from *pkl-1* were counted, we obtained similar results to those by the chlorophyll measurements (Figure 55h), indicating that chlorophyll measurement can be used as an alternative way to evaluate cytokinin-induced greening phenotype. Since greening tissue does not essentially indicate nascent SAM formation, the expression of *WUSCHEL* (*WUS*), encoding homeodomain transcription factor required for stem cell niche maintenance, was examined. We found a positive correlation of *WUS* expression with chlorophyll accumulation (Figure 55i). The cytokinin-promoted greening of cultured tissue on CIM incubated material was more suitable than the

material from SIM incubation because no lateral organ differentiation took place in the CIM culture. Instead, an outgrowth of calli persisted (Figure 55j-l). Chlorophyll measurements were made on CIM-induced calli for assessing tissue greening stimulated by the higher kinetin to 2, 4-D ratio in CIM. Similar to the SIM incubation, significant differences in chlorophyll contents could be determined between the two mutants and the wild-type ($p \leq 0.0001$ in both cases, Figure 55m).

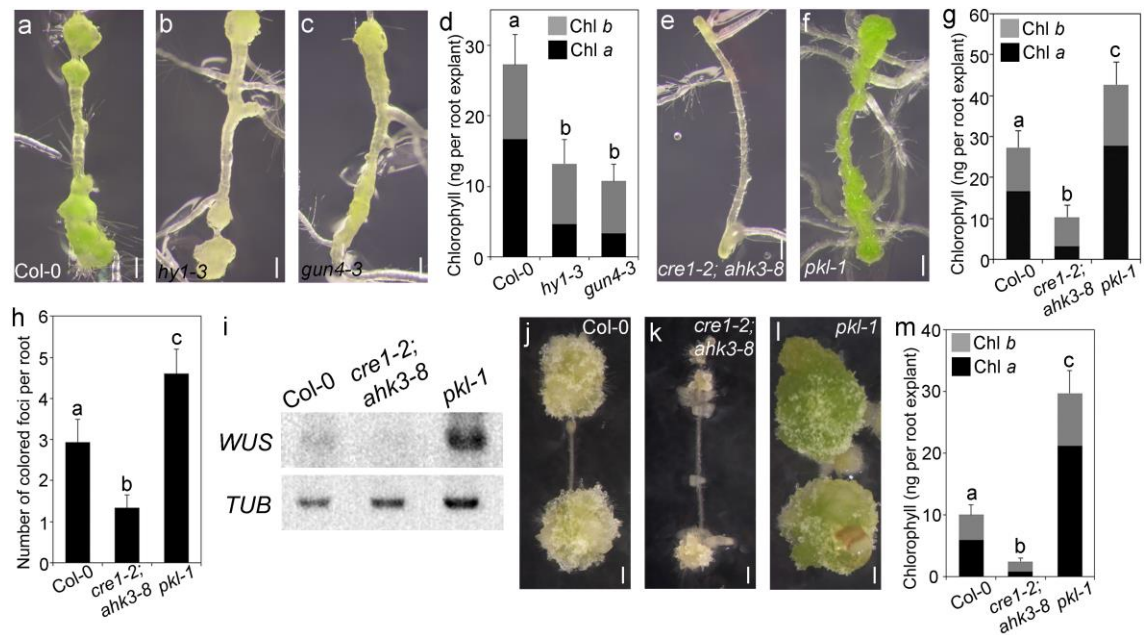


Figure 55: Statistical evaluation of greening phenotype by chlorophyll measurements. (a-c, e, f) Root explant cultured on SIM for 10 days of Col-0 (a), *hy1-3* (b), *gun4-3* (c), *cre1-2;ahk3-8* (e), and *pkl-1* (f). (d) Chlorophyll contents of Col-0, *hy1-3* or *gun4-3* root explants cultured on SIM for 10 days. (g) Chlorophyll contents of Col-0, *cre1-2;ahk3-8* or *pkl-1* root explants cultured on SIM for 10 days. (h) A number of pigmented foci per root explant of Col-0, *cre1-2;ahk3-8* or *pkl-1*. (i) Expression of *WUS* on day 10 SIM incubation. (j - l) Root explant cultured on CIM for 36 days of Col-0 (j), *cre1-2;ahk3-8* (k) or *pkl-1* (l). (m) Chlorophyll contents of Col-0, *cre1-2;ahk3-8*, and *pkl-1* root explants cultured on CIM for 36 days. Chlorophyll a and Chlorophyll b contents are indicated in black and gray bars, respectively (d, g, m). Values marked with different letters are significantly different between genotypes ($p \leq 0.0001$) as determined by student's t-tests. Data shown are the mean \pm SD of biological triplicates ($n = 30$). Bars = 0.5 mm (a-c, e, f, j-l).

9 Discussion

In summary, although chlorophyll accumulation in cultured root explants is not as abundant as it is in leaves and spontaneous wound-induced callus hinders solvent penetration, we developed a method to quantify chlorophylls from a single cultured root explant (8 mm) by applying bead disruption in diverse solvents. Major advantage of our procedure over counting green foci are: 1) chlorophyll levels are a measurable parameter not depending on subjective observations; 2) since the extinction coefficients of chlorophylls are well-defined, the results of different experiments are comparable; 3) considerable number of samples can be measured simultaneously using 96-well glass plates with a conventional microplate reader; 4) the method is sensitive enough to assess a greening phenotype in root explants of 5 mm in length (data not shown), which is helpful for mutants exhibiting a short root phenotype; 5) all green foci are taken into account, including those that develop at sites inaccessible to the eye or image analysis software. Additionally, our methodology does not require parameter setting, which is crucial in the image analysis software when considering pale explants, so objective rather than relative data are obtained. The main disadvantage of our procedure is its destructive nature whereas taking photographs of calli has an advantage in giving insights into morphologic changes over time. Trans-differentiation of RAM into SAM triggered by cytokinins on SIM can be studied by analyzing available SAM-related markers, although introducing the markers in the desired genetic background takes time. Thus, chlorophyll measurements are a concise and sensitive method that combined with complementary approaches such as taking photographs and SAM-related marker analysis for *de novo* SAM development give a whole view of the responsiveness of explants in tissue culture.

**PART III – Mutations in Tetrapyrrole
Biosynthesis Pathway Uncouple Nuclear
WUSCHEL Expression from *de novo* Shoot
Development in *Arabidopsis***

Ivona Kubalová, David Zalabák, Alžbeta Mičúchová, and Yoshihisa Ikeda

*Center of the Region Haná for Biotechnological and Agricultural Research, Faculty of
Science, Palacký University, Olomouc, Czech Republic*

10 Abstract

Plant *de novo* organogenesis in tissue culture systems has long been exploited to study the plasticity of pluripotency. External application of high cytokinin-to-auxin ratio in cultured medium stimulates greening of calli and promotes nascent shoot apical meristem (SAM) formation. The stem cell niche in SAM is maintained by a negative feedback loop between CLAVATA-WUSCHEL (WUS) signaling. Cytokinin being known to induce *WUS* expression, the capacity of *de novo* shoot development is largely dependent on *WUS* activity. However, the molecular mechanism of *WUS* expression remains obscure. Here we provide a novel regulatory mechanism of *WUS* expression during *de novo* SAM formation that is affected by the altered tetrapyrrole metabolism catalyzed in the plastid. Loss-of-function mutations in *HEME OXYGENASE/LONG HYPOCOTYL 1 (hy1)*, *Mg-CHELATASE H (chlh)*, *Mg-CHELATASE II (chli1)*, and the regulator of Mg-CHELATASE, *GENOME-UNCOUPLED 4 (gun4)*, result in elevated *WUS* expression but the shoot regeneration efficiency is decreased whereas loss-of-function mutation in *PROTOPORPHYRIN IX FERROCHELATASE 2 (fc2)* exhibits compromised *WUS* expression with reduced number of shoots when mutant root explants are cultured on shoot induction medium. Our results suggest that plastid-to-nucleus communication takes place to coordinate cytokinin-stimulated etioplast-to-chloroplast transition with *de novo* organogenesis through fine-tuning a nuclear gene expression of the master SAM regulator.

11 Introduction

Since its discovery over 60 years ago, cytokinin, in concert with auxin, has been shown to promote cell division and shoots in an *in vitro* tissue culture system (Miller et al., 1955; Skoog and Miller, 1957). Treatment of cytokinin itself reduces the loss of chlorophylls in detached *Xanthium* leaves (Richmond and Lang, 1957). Cytokinin application renders dark grown plants a series of light-grown traits, such as inhibition of hypocotyl elongation, development of leaves and etioplast-to-chloroplast transition (Chory et al., 1994; Cortleven et al., 2016).

The *in vitro* tissue culture system has been employed to study pluripotency and *de novo* organogenesis. It is composed of two subsequent steps – the first step involves pre-incubation of explants on auxin-rich callus inducing medium (CIM) to induce a mass of growing cells, termed callus (Valvekens et al., 1988). The second step stimulates greening of foci when induced calli are cultured on shoot-inducing medium (SIM) in which a high cytokinin-to-auxin ratio is given. In the late stage of SIM incubation, shoot development takes place from green foci. Recent studies have shown that callus formation during CIM pre-culture is the differentiation of xylem-pole associated pericycle toward root meristem-like tissue and that shoot regeneration is cytokinin-induced transdifferentiation of early lateral root meristem into SAM (Atta et al., 2009; Sugimoto et al., 2010). These processes are summarized in detail in a number of review articles (Motte et al., 2014b; Perianez-Rodriguez et al., 2014). An analysis of 88 *Arabidopsis* accessions revealed no correlation between green foci formation and subsequent shoot regeneration efficiencies, indicating that greening and the subsequent differentiation of lateral organs are distinct phenomena that are under genetic control (Motte et al., 2014a).

External application of cytokinins induces *WUS* expression probably *via* direct activation by B-type *Arabidopsis* RESPONSE REGULATORS (ARR1, ARR2, ARR10, and ARR12), which are involved in primary cytokinin signaling (Meng et al., 2017; Zhang et al., 2017). It appears that *WUS* expression is more tightly linked to shoot regeneration. Given the facts that cytokinin-stimulated phenotypes observed in tissue culture system (greening of tissue, *WUS* expression, and *de novo* SAM development) have been extensively studied, little is known about how these cytokinin-stimulated

phenotypes are co-related together. In this study, we investigate the co-relationship among them by employing loss-of-function mutants defective in cytokinin perception, *wus*, and chlorophyll biosynthesis.

12 Materials and Methods

12.1 Plant material

Arabidopsis thaliana accession Columbia-0 (Col-0) was used as wild-type. Seeds described below are obtained from the European Nottingham Arabidopsis Stock Centre (NASC) and have been previously described; *pk1-1* (Ogas et al., 1997), *ahk3-8* (Gabi Kat 754_H09) (Kubalová and Ikeda, 2017), *wus-101* (Gabi Kat 870_H12) (Zhao et al., 2017), *fc2-1* (Gabi Kat 766_H08) (Woodson et al., 2011), *hyl-3* (Gabi Kat034_B01) (Kubalová and Ikeda, 2017), *gun4-2* (SALK_026911) (Larkin, 2016; Peter and Grimm, 2009), *chli1* (Sail_230_D11) (Huang and Li, 2009; Tsuzuki et al., 2011), *chlh/gun5* (SALK_062726) (Huang and Li, 2009) and *crd1* (SALK_009052) (Mochizuki et al., 2008). The *cre1-2* mutant was obtained from Tatsuo Kakimoto (Inoue et al., 2001). The primers used for genotyping by PCR are listed in Table 11. Transcript levels of *GUN3* in *gun3-3* (SALK_104923) (Cheng et al., 2011) or *CHLD* in *chld* (SALK_048878) T-DNA insertion lines are shown in Figure 59.

Gene Name	T-DNA Insertion	Primer Name	Sequence (from 5' to 3')
<i>FC2</i>	<i>fc2-1</i> GK-766H08	FC2F	CCGGATTTACTTACCAAACCTCG
		FC2R	TCATGGCTGGGCAATTCATTGC
		GK_L8760	GGGCTACACTGAATTGGTAGCTC
<i>GUN3</i>	<i>gun3-3</i> SALK_104923	GUN3F	AATGGCTTTTATCAATGGAGTTTGGG
		GUN3R	AAAAGTTAGCACAGAATATGGGAG
		SALK_LBa1	GGTTCACGTAGTGGGCCATCGCCCTG
<i>CHLI1</i>	<i>chli1</i> Sail_230_D11	CHLI1F	TTATTGATCCAAAGATTGGTGGTG
		CHLI1R	TTCCGGATTTCTGAACCGATC
		SailLB2	TATTATATCTTCCCAAATTACCAATACA
<i>CHLD</i>	<i>chld</i> SALK_048878	CHLDF	TTGAAAATGGCGATGACTCCGG
		CHLDR	AGAGCAGTTTTTATGCCTTCTAC
		SALK_LBa1	GGTTCACGTAGTGGGCCATCGCCCTG
<i>CHLH/GUN5</i>	<i>chlh/gun5</i> SALK_062726	CHLH5F	TTGGTTCTCTGATCTTCGTCGAGG
		CHLH5R	AGACTAAACCGACAACCGTTGCATC
		SALK_LBa1	GGTTCACGTAGTGGGCCATCGCCCTG
<i>CRD1</i>	<i>crd1</i> SALK_009052	CRD1F	GTAACGTATATACTGTTGTCCGG
		CRD1R	AGAGGCTGACATTCTGATCACG
		SALK_LBa1	GGTTCACGTAGTGGGCCATCGCCCTG
<i>WUS</i>	<i>wus-101</i> GK-870H12	WUSF	CACGGTGTCCCATGCAGAGACC
		WUSR	TCACCGTTATTGAAGCTGGGATATGG
		GK_L8760	GGGCTACACTGAATTGGTAGCTC

Table 11: List of primers used for PCR-genotyping

12.2 Growth conditions

The *Arabidopsis* plants and root explants *in vitro* tissue culture were grown in a photoperiod of 16 h light (approximately $60 \mu\text{mol m}^{-2} \text{s}^{-1}$) and 8 h dark at 21 °C with 70 % humidity. The conditions for seed surface sterilization and growth on MS plates, CIM pre-incubation, and subsequent SIM culture were as previously described (Kubalová and Ikeda, 2017). In brief, seedlings were grown on MS + 1 % sucrose (pH 5.7) containing 1.0 % Gellan Gum (Thermo Fisher Scientific) plate in a vertical orientation. Five days after germination, roots were excised into intervals of approximately 8 mm in length and excised root explants were transferred onto CIM and incubated for 4 days. Subsequently, root explants pre-incubated on CIM were transferred onto SIM for indicated period and subjected to chlorophyll extraction or RNA extraction.

12.3 Chlorophyll measurement

In each replicate, at least 12 root explants per genotype, cultured on SIM at indicated time period, were used for measurements. Chlorophyll contents in 8 mm SIM cultured root explant per genotype were determined as described previously (Kubalová and Ikeda, 2017).

12.4 Shoot regeneration assay

As described previously (Li et al., 2011), nascent shoots that could develop true leaves were counted under a stereomicroscope at indicated time points. In each replicate, at least 40 root explants per genotype were examined and the frequency of explants developing shoots was determined.

12.5 Quantitative RT-PCR analysis (qRT-PCR)

Total RNA was extracted from root explants cultured on SIM for 5 days by RNAqueous phenol-free total RNA isolation kit (Ambion). Conditions for RNA extraction and first-strand cDNA synthesis were described (Kubalová and Ikeda, 2017). Using gb SG PCR Master Mix (Generi Biotech), real-time PCR reactions were performed on a StepOnePlus™ Real-Time PCR System (Life Technologies). Primers used for detecting *WUS* by qRT-PCR were described (Lee et al., 2016). Relative gene expression was normalized to *TUBULIN3* and *ELONGATION FACTOR 1 α* as reported

(Vandesompele et al., 2002). Three biological replicates were performed for each experiment. Primers used for quantitative RT-PCR are listed in Table 12.

Gene Name	Primer Name	Sequence (from 5' to 3')
<i>WUS</i>	WUS_qRT_F2	AACCAAGACCATCATCTCTATCATC
	WUS_qRT_R2	CCATCCTCCACCTACGTTGT
<i>TUBULIN3</i>	TUB3_F2426	TGTTGACTGGTGCCCAACTG
	TUB3_R2616	TACATACAGCTCTCTGAACC
<i>EF1a</i>	EF1a_F	GTTTTGAGGCTGGTATCTCTAAG
	EF1a_R	GTGGTGGCATCCATCTTGTTAC

Table 12: List of primers used for semi-quantitative RT-PCR.

13 Results

13.1 WUS expression and de novo SAM formation are coupled in altered cytokinin response mutants

We previously showed that loss-of-function mutants with altered cytokinin responses have a positive correlation among greening of calli, SAM marker expression and *de novo* shoot formation observed in the tissue culture system. Cytokinin receptor double mutant, *cre1-2;ahk3-8*, had reduced sensitivity to cytokinin, thus showing substantially reduced chlorophyll contents, compromised *WUS* expression and reduced shoot regeneration efficiency (Kubalová and Ikeda, 2017). On the contrary, *pickle (pkl)/cytokinin hypersensitive 2 (ckh2)* mutant, in which a CHD3 SWI/SNF2 chromatin remodeler is disrupted, exhibited cytokinin hypersensitivity in CIM (Furuta et al., 2011), as well as in SIM culture (Kubalová and Ikeda, 2017). In this study, we assessed these cytokinin related phenotypes by employing quantitative RT-PCR for examining *WUS* expression and by counting regenerated shoots from day 10 to 22 SIM incubation. *cre1-2;ahk3-8* root explants accumulated 54 % of chlorophyll contents relative to that in wild-type (Figure 56A), reduced *WUS* expression (Figure 56b), and never regenerated shoots during SIM incubation (Figure 56c). On the other hand, *pkl-1* root explants accumulated chlorophylls by 2.1-fold (Figure 56a), had 6.03-fold higher *WUS* expression (Figure 56b), and developed shoots earlier and more effectively (Figure 56c). Thus, we could confirm the positive correlation between cytokinin perception and all cytokinin-related phenotypes observed in SIM culture. Next, we explored the relationship between greening of calli and nascent SAM development by employing *wus-101*. Chlorophyll accumulation was not affected by *wus-101* mutation (Figure 56d). The transcript level of *WUS* in *wus-101* was undetectable (Figure 56e). Consistent with the previous report (Zhang et al., 2017), shoot regeneration efficiency was substantially reduced in *wus-101*, although *wus-101* root explants could regenerate a small number of shoots under our growth conditions (Figure 56f). These results suggest that chlorophyll accumulation is independent of *WUS* activity whereas *WUS* expression and shoot regeneration appear to be more tightly coupled with each other.

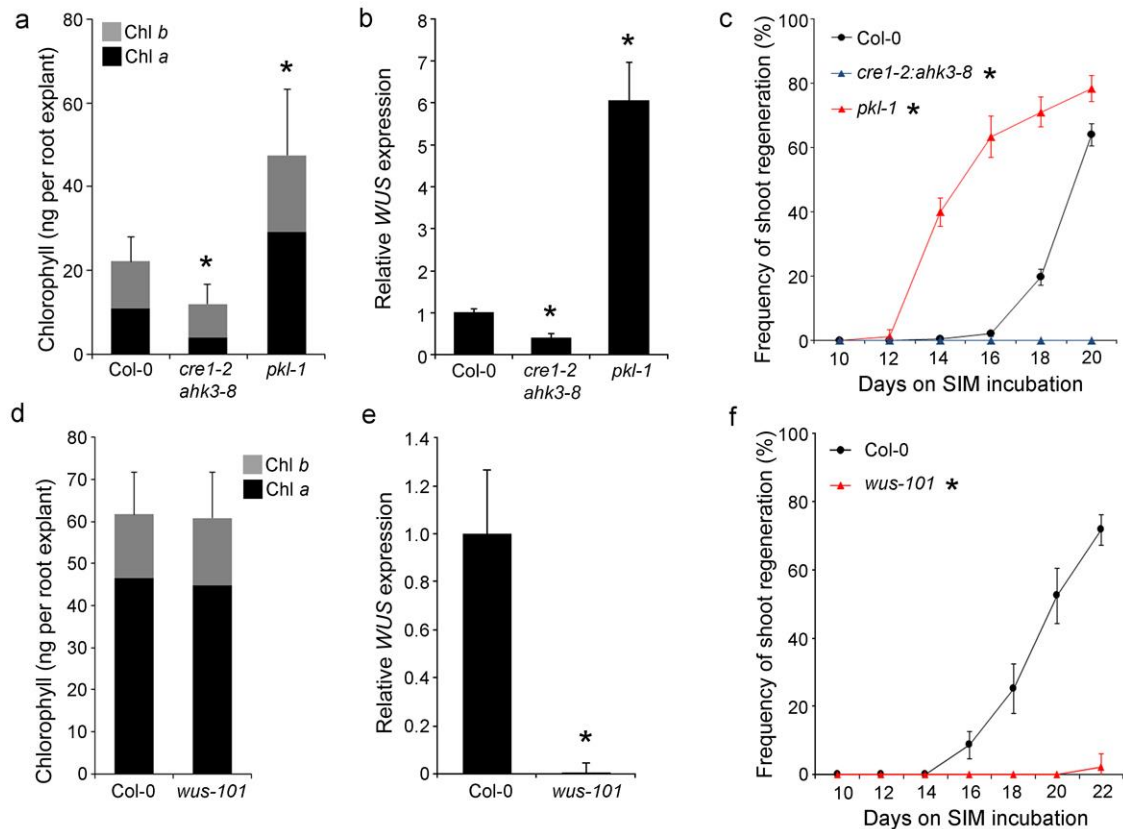


Figure 56: *WUS* expression and *de novo* SAM formation are coupled in altered cytokinin response mutants. (a) Chlorophyll contents of Col-0, *cre1-2;ahk3-8*, and *pkl-1* root explants cultured on SIM for 8 days (b) Relative *WUS* expression in Col-0, *cre1-2;ahk3-8*, and *pkl-1* root explants cultured on SIM for 5 days quantified by qRT-PCR (c) Shoot regeneration frequency in Col-0, *cre1-2;ahk3-8*, and *pkl-1* root explants cultured at indicated time-points on SIM. (d) Chlorophyll contents of Col-0 and *wus-101* root explants cultured on SIM for 12 days (e) Relative *WUS* expression in seven-day-old Col-0 and *wus-101* shoots quantified by qRT-PCR (f) Shoot regeneration frequency in Col-0 and *wus-101* root explants cultured at indicated time-points on SIM. Chlorophyll *a* and *b* contents are indicated in black and gray bars, respectively (a, d). Data shown are the mean \pm SD of biological triplicates and statistical significance was determined by student's *t*-test ($*p < 0.05$).

13.2 *WUS* expression is uncoupled from *de novo* SAM formation in mutants defective in tetrapyrrole biosynthesis

We further explored the relationship between chlorophyll accumulation and *WUS* expression by employing loss-of-function mutants defective in tetrapyrrole biosynthesis; *fc2-1*, *hyl-3*, *gun3-3*, *gun4-2*, *chld*, *chlh*, *chli1*, and *crd1* (Figure 57). FERROCHELATASE 2 (FC2), long hypocotyl 1 (HY1) and GENOME-UNCOUPLED 3 (GUN3) belong to heme/bilin branch. MAGNESIUM CHELATASE-D (CHLD), -H (CHLH), -I1 (CHLI1) subunits, GENOME-UNCOUPLED 4 (GUN4), and COPPER RESPONSE DEFICIENT 1 (CRD1) belong to chlorophyll branch (Figure 57). As reported previously, we found significantly reduced chlorophyll contents in all mutant

root explants, especially those defective in chlorophyll branch (Figure 58a). Surprisingly, the level of *WUS* transcripts in *hy1-3*, *gun4-2*, *chlh*, and *chli1* was elevated (Figure 58b), although the shoot regeneration efficiency is substantially declined (Figure 58c). *fc2-1* was the only mutant examined in this study exhibiting the decreased *WUS* expression with compromised shoot regeneration when the number of developed shoots producing true leaves was counted at various time points during SIM incubation (Figure 58c, d). Shoot regeneration efficiency, as well as an average number of shoots per root explants, were reduced in all tetrapyrrole mutants (Figure 58c-f), suggesting that chlorophyll accumulation appeared to be crucial for sustaining shoot regeneration capacity. Thus, in *hy1-3*, *gun4-2*, *chlh*, and *chli1* mutant root explants the *WUS* expression is not related to shoot regeneration.

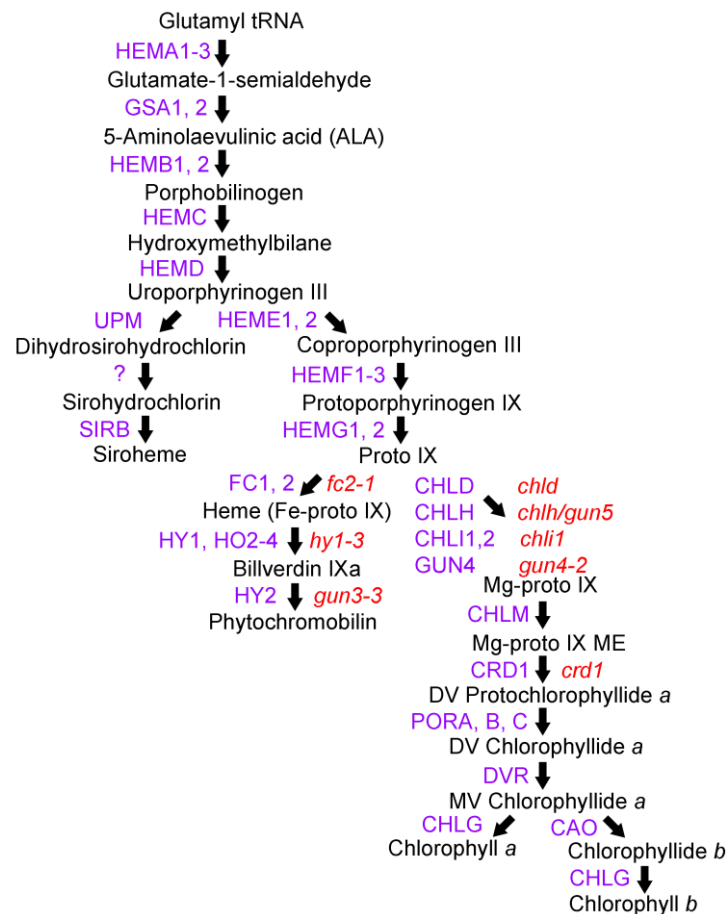


Figure 57: Tetrapyrrole biosynthesis pathway. The tetrapyrrole biosynthesis pathway is adapted from (Tanaka et al., 2011). Names of precursors and end products are indicated with black. Names of enzymes and mutants used in this study are highlighted in purple and red, respectively.

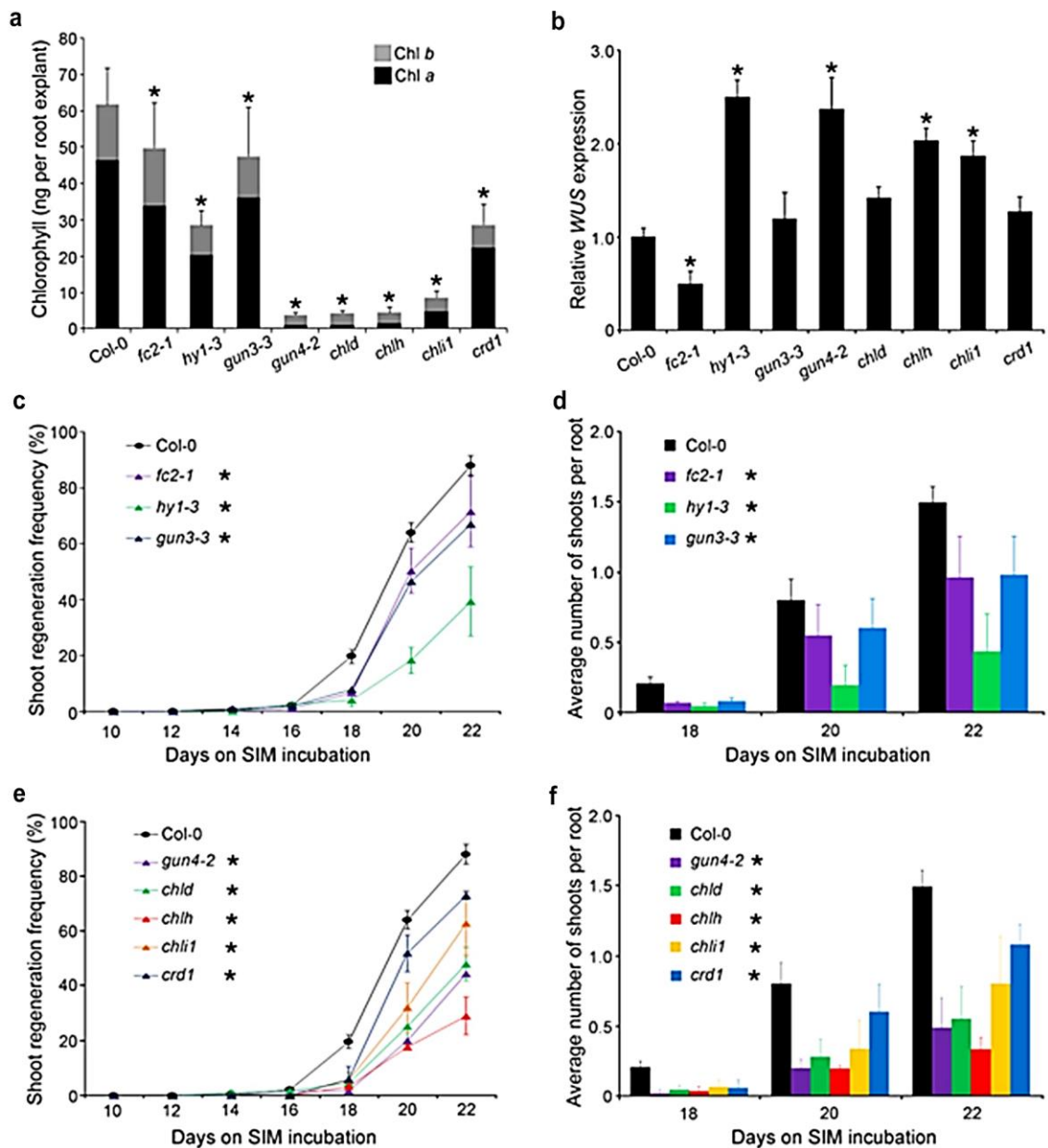


Figure 58: WUS expression and de novo SAM formation are uncoupled in altered tetrapyrrole mutants. (a) Chlorophyll contents of Col-0, *fc2-1*, *hy1-3*, *gun3-3*, *gun4-2*, *chld*, *chlh*, *chli1*, and *crd1* root explants cultured on SIM for 15 days (b) Relative WUS expression in Col-0, *fc2-1*, *hy1-3*, *gun3-3*, *gun4-2*, *chld*, *chlh*, *chli1*, and *crd1* root explants cultured on SIM for 5 days quantified by qRT-PCR (c) Shoot regeneration frequency in Col-0, *fc2-1*, *hy1-3*, and *gun3-3* root explants cultured at indicated time-points on SIM. (d) Shoot regeneration frequency in Col-0, *gun4-2*, *chld*, *chlh*, *chli1*, and *crd1* root explants cultured at indicated time-points on SIM. (e) An average number of shoots per root explant in Col-0, *fc2-1*, *hy1-3*, and *gun3-3*. (f) An average number of shoots per root explant in Col-0, *gun4-2*, *chld*, *chlh*, *chli1*, and *crd1*. Chlorophyll *a* and *b* contents are indicated in black and gray bars, respectively (a). Data shown are the mean \pm SD of biological triplicates and statistical significance was determined by student's *t*-test ($*p < 0.05$).

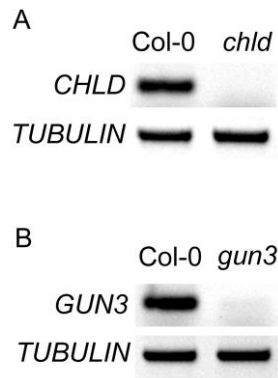


Figure 59: *gun3* and *chld* are null mutants. Transcript levels of A) *GUN3* in *gun3-3* (SALK_104923) T-DNA insertion line B) *CHLD* in *chld* (SALK_048878) T-DNA insertion line.

14 Discussion

Plastid-to-nucleus communication, termed retrograde signaling, has been known to regulate gene expression, RNA turnover and splicing (reviewed in Chan et al., 2016; Larkin, 2016). In the case of *gun* mutant screens, photosynthesis-related nuclear gene expression is monitored when chloroplast biogenesis is blocked by norflurazon treatment (Susek et al., 1993; Mochizuki et al., 2001; Larkin et al., 2003; Woodson et al., 2011). We monitored nuclear *WUS* expression when the etioplast-to-chloroplast transition is stimulated by cytokinin in SIM culture and found that *WUS* expression in *hy1-3*, *gun4-2*, *chlh*, and *chli1* is uncoupled from *de novo* SAM formation (Figure 58b). Although tetrapyrrole biosynthesis is controlled under complex regulation, it is reasonable to assume that precursor molecules accumulate as their further conversion is blocked in mutants where the catalytic enzyme gene is disrupted. Our results imply that the accumulation of either Proto IX or heme (or combination of both) takes place in *hy1-3*, *gun4-2*, *chlh*, and *chli1* mutant root explants to positively regulate *WUS* expression. In fact, the level of Proto IX is reported to be increased in *chlh* (Mochizuki et al., 2001), *fc2-1* (Woodson et al., 2015), and *aci5-3*, a semidominant loss-of-function mutation in *chli1* (Soldatova et al., 2005). However, Proto IX is unlikely to do so due to the fact that *fc2-1* exhibited compromised *WUS* expression (Figure 58b). It is tempting to speculate that heme, which is decreased in *fc2-1* but likely to be accumulated in the rest of above-mentioned mutants, in particular, *hy1-3*, is the plausible candidate molecule controlling *WUS* expression. Note that *hy1-3* exhibited the most contrasting responses to cytokinin (the highest *WUS* expression and the lowest shoot regeneration). This is in agreement with the previous reports revealing the increased steady-state level of non-covalently bound heme in *hy1* (Woodson et al., 2011) and *aci5-3* seedlings (Soldatova et al., 2005) and reduced steady-state level of heme in *fc2-1* (Scharfenberg et al., 2015; Woodson et al., 2015). It is crucial to explore the co-relationship between heme content and mutants with altered *WUS* expression by measuring tetrapyrrole intermediate molecules in the future. Besides, histological studies in nascent SAM in *hy1-3*, *gun4-2*, *chlh*, or *chli1* mutant root explants on SIM culture will give insights into the coordinated *WUS* expression of nascent SAM development modulated by plastid-to-nucleus communication. Novel regulatory mechanism modulating nuclear SAM master regulator gene expression in response to plastid developmental change stimulated by cytokinin during *de novo* organogenesis is proposed in this study.

Conclusions

For many people having weed in their garden is a kind of nightmare, mainly because of its fundamental attribute and that, its ‘immortality’ once it is germinated. This ability may be explained by an outstanding regeneration capacity of weed. Regeneration, by definition, is a capability to renew tissue. *Arabidopsis*, the most popular plant model organism also shares weed characteristics (Meyerowitz, 1989). Thus, for molecular biologists, *Arabidopsis* with its weed characteristics is a gift from heaven to study regeneration. Exploring the molecular mechanisms behind the great regeneration capacity can provide a powerful tool for the applied field in plant science.

Regeneration capacity depends on the ability to replenish old cells by the new ones. This would be impossible without meristem localized stem cells. The function of the meristem must be precisely controlled to avoid an excessive proliferation of meristematic cells, as well as to hinder the loss of stem cells. Proper regulation of these processes is the basis of the plant body plasticity.

WUSCHEL (WUS), the master key regulator of plant development, is studied for years. Its significance in development was shown in numerous studies (Laux et al., 1996; Mayer et al., 1998; Gross-Hardt et al., 2002; Leibfried et al., 2005; Ikeda et al., 2009; Yadav et al., 2011; Meng et al., 2017; Zhang et al., 2017; Snipes et al., 2018). Although new regulatory mechanisms of WUS-dependent pathway controlling SAM are regularly emerging, this puzzle is not completely solved, yet. It is very likely that there are other players controlling WUS-dependent pathway and thus development itself.

As the first, we unveiled that the plastid-to-nucleus communication influences the expression of the master SAM regulator WUSCHEL. With our new high-throughput method for chlorophyll quantification from single root explants we evaluated the correlation between greening and shoot development; and between greening and nuclear gene expression. Based on our results we hypothesize that this new regulation pathway might be mediated by the Heme molecule. We are aware that additional experiments are required to test this hypothesis. However, we consider our findings as an important contribution to the current understanding of the WUSCHEL regulatory network.

Besides the WUS-dependent pathway, we also investigated an alternative WUS-independent pathway. In this work, we showed that ERF transcriptional

repressors from the group VIII can regulate the positioning and maintenance of SAM. We also showed that the quintuple mutant *wus;erf4-1;8;9-1;12* was able to produce SAM *in planta* but, interestingly, failed to establish *de novo* meristems in a tissue culture system. These ambiguous results of SAM controlling through ERF repressors show that the development of a plant is a far more complex process and our understanding of the meristem regulatory network remains still elusive.

Our results help to expand the present model of the SAM regulatory network proposed by Lee and Clark (2015). In our extended regulatory network (Figure 60), we placed ERF repressors up-stream from *CUC* and *STM* genes and independently from the WUS-CLV pathway. Results obtained by our group showed that the double *esr1-1;wus* mutant displays an accelerated *wus* phenotype. This, together with further results presented in this work, strongly implies the existence of an additional pathway regulating the maintenance of SAM. Importantly, this novel pathway, especially ERF repressors; seems to be regulated at the posttranslational level through proteasome-mediated ERF protein degradation, rather than *via* miRNA.

This study focused on the role of ERF repressor in the *de novo* meristem development and maintenance. Discrepancies with hitherto obtained results clearly demonstrate the urgent need for consecutive research in this field. We believe that our work is a novel and significant contribution to our current knowledge of plant development.

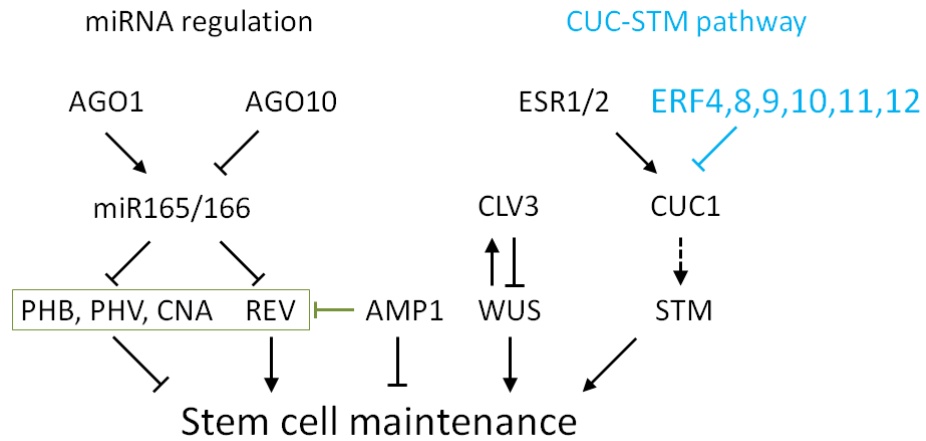


Figure 60: Model of the stem cell regulatory network. Stem cell maintenance is regulated *via* different pathways. 1) miRNA regulation. ARGONAUTE (AGO) proteins 1 and 10 are responsible for processing of precursor miRNA into their mature form and act antagonistically. miR165/166 cleave their targets – HD-ZIP III TFs as PHABULOSA (PHB), PHV (PHAVOLUTA), CORONA (CAN), and REVOLUTA (REV). PHB, PHV, and CNA block stem cell maintenance whereas REV contributes to stem cell production. ALTERED MERISTEM PROGRAM 1 (AMP1) is also involved in miRNA regulation. AMP1 targets HD-ZIP III TFs but in contrast to miR165/166, AMP1 inhibits HD-ZIP III TFs on translation level. 2) WUSCHEL-CLAVATA regulation pathway, where WUS is a positive signal for stem cell maintenance and also induce CLV3 which in turn inhibits *WUS* expression. They act in a negative-feedback loop. 3) CUC-STM pathway. Here WUS-independent pathway CUC1 (CUP-SHAPED COTYLEDON) induce STM (SHOOT MERISTEMLESS) which positively regulates stem cells. CUC1 is positively regulated by ESR1 and ESR2 (ENHANCER OF SHOOT REGENERATION). Adapted from Lee and Clark, (2015). On the other hand, *CUC1* is repressed by ERF transcriptional repressors.

References

- Agarwal, M., Kumar, P., and Mathew, S.J.** (2015). The Groucho/Transducin-like enhancer of split protein family in animal development. *IUBMB Life* **67**: 472–481.
- Aichinger, E., Kornet, N., Friedrich, T., and Laux, T.** (2012). Plant stem cell niches. *Annu. Rev. Plant Biol.* **63**: 615–36.
- Aida, M.** (1997). Genes Involved in Organ Separation in Arabidopsis: An Analysis of the cup-shaped cotyledon Mutant. *PLANT CELL ONLINE* **9**: 841–857.
- Aida, M., Beis, D., Heidstra, R., Willemsen, V., Blilou, I., Galinha, C., Nussaume, L., Noh, Y.-S., Amasino, R., and Scheres, B.** (2004). The PLETHORA Genes Mediate Patterning of the Arabidopsis Root Stem Cell Niche. *Cell* **119**: 109–120.
- Alinsug, M. V., Yu, C.W., and Wu, K.** (2009). Phylogenetic analysis, subcellular localization, and expression patterns of RPD3/HDA1 family histone deacetylases in plants. *BMC Plant Biol.* **9**: 37.
- Argyros, R.D., Mathews, D.E., Chiang, Y.-H., Palmer, C.M., Thibault, D.M., Etheridge, N., Argyros, D.A., Mason, M.G., Kieber, J.J., and Schaller, G.E.** (2008). Type B Response Regulators of Arabidopsis Play Key Roles in Cytokinin Signaling and Plant Development. *PLANT CELL ONLINE* **20**: 2102–2116.
- Atta, R., Laurens, L., Boucheron-Dubuisson, E., Guivarc’h, A., Carnero, E., Giraudat-Pautot, V., Rech, P., and Chriqui, D.** (2009). Pluripotency of Arabidopsis xylem pericycle underlies shoot regeneration from root and hypocotyl explants grown in vitro. *Plant J.* **57**: 626–644.
- Balkunde, R., Kitagawa, M., Xu, X.M., Wang, J., and Jackson, D.** (2017). SHOOT MERISTEMLESS trafficking controls axillary meristem formation, meristem size and organ boundaries in Arabidopsis. *Plant J.* **90**: 435–446.
- Banno, H., Ikeda, Y., Niu, Q.W., and Chua, N.H.** (2001). Overexpression of Arabidopsis ESR1 induces initiation of shoot regeneration. *Plant Cell* **13**: 2609–2618.
- Barnes, J.D., Balaguer, L., Manrique, E., Elvira, S., and Davison, A.W.** (1992). A reappraisal of the use of DMSO for the extraction and determination of chlorophylls a and b in lichens and higher plants. *Environ. Exp. Bot.* **32**: 85–100.
- Baurle, I.** (2005). Regulation of WUSCHEL Transcription in the Stem Cell Niche of the Arabidopsis Shoot Meristem. *PLANT CELL ONLINE* **17**: 2271–2280.
- van den Berg, C., Willemsen, V., Hendriks, G., Weisbeek, P., and Scheres, B.** (1997). Short-range control of cell differentiation in the Arabidopsis root meristem. *Nature* **390**: 287–289.
- Borges, F. and Martienssen, R.A.** (2015). The expanding world of small RNAs in plants. *Nat. Rev. Mol. Cell Biol.* **16**: 727–741.
- Van den Broeck, L., Dubois, M., Vermeersch, M., Storme, V., Matsui, M., and Inzé, D.** (2017). From network to phenotype: the dynamic wiring of an Arabidopsis transcriptional network induced by osmotic stress. *Mol. Syst. Biol.* **13**.
- Busch, W. et al.** (2010). Transcriptional Control of a Plant Stem Cell Niche. *Dev. Cell* **18**: 841–853.
- Cary, A.J., Che, P., and Howell, S.H.** (2002). Developmental events and shoot apical meristem gene expression patterns during shoot development in Arabidopsis thaliana. *Plant J.* **32**: 867–877.
- Causier, B., Ashworth, M., Guo, W., and Davies, B.** (2012). The TOPLESS Interactome: A Framework for Gene Repression in Arabidopsis. *PLANT Physiol.* **158**: 423–438.
- Chan, K.X., Phua, S.Y., Crisp, P., McQuinn, R., and Pogson, B.J.** (2016). Learning the Languages of the Chloroplast: Retrograde Signaling and Beyond. *Annu. Rev. Plant Biol.* **67**: 25–53.
- Chandler, J. and Werr, W.** (2017). DORN RÖSCHEN, DORN RÖSCHEN-LIKE, and PUCHI redundantly control floral meristem identity and organ initiation in Arabidopsis. *J. Exp. Bot.* **68**: 3457–3472.
- Chandler, J.W.** (2018). Class VIIIb APETALA2 Ethylene Response Factors in Plant Development. *Trends Plant Sci.* **23**: 151–162.

- Che, P., Gingerich, D.J., Lall, S., and Howell, S.H.** (2002). Global and hormone-induced gene expression changes during shoot development in Arabidopsis. *Plant Cell* **14**: 2771–2785.
- Che, P., Lall, S., and Howell, S.H.** (2007). Developmental steps in acquiring competence for shoot development in Arabidopsis tissue culture. *Planta* **226**: 1183–1194.
- Chen, L. and Hellmann, H.** (2013). Plant E3 Ligases: Flexible Enzymes in a Sessile World. *Mol. Plant* **6**: 1388–1404.
- Chen, L., Lee, J.H., Weber, H., Tohge, T., Witt, S., Roje, S., Fernie, A.R., and Hellmann, H.** (2013). Arabidopsis BPM proteins function as substrate adaptors to a cullin3-based E3 ligase to affect fatty acid metabolism in plants. *Plant Cell* **25**: 2253–2264.
- Chen, W.-Q., Drapek, C., Li, D.-X., Xu, Z.-H., Benfey, P.N., and Bai, S.-N.** (2019). Histone Deacetylase HDA19 Affects Root Cortical Cell Fate by Interacting with SCARECROW. *Plant Physiol.* **180**: 276–288.
- Cheng, J., He, C.X., Zhang, Z.W., Xu, F., Zhang, D.W., Wang, X., Yuan, S., and Lin, H.H.** (2011). Plastid signals confer Arabidopsis tolerance to water stress. *Zeitschrift für Naturforsch. - Sect. C J. Biosci.* **66 C**: 47–54.
- Chory, J., Peto, C.A., Ashbaugh, M., Saganich, R., Pratt, L., and Ausubel, F.** (1989). Different Roles for Phytochrome in Etiolated and Green Plants Deduced from Characterization of Arabidopsis thaliana Mutants. *Plant Cell* **1**: 867–880.
- Chory, J., Reinecke, D., Sim, S., Washburn, T., and Brenner, M.** (1994). A Role for Cytokinins in De-Etiolation in Arabidopsis (det Mutants Have an Altered Response to Cytokinins). *Plant Physiol.* **104**: 339–347.
- Chou, H., Zhu, Y., Ma, Y., and Berkowitz, G.A.** (2016). The CLAVATA signaling pathway mediating stem cell fate in shoot meristems requires Ca²⁺ as a secondary cytosolic messenger. *Plant J.* **85**: 494–506.
- Clark, S.E., Running, M.P., and Meyerowitz, E.M.** (1993). CLAVATA1, a regulator of meristem and flower development in Arabidopsis. *Development* **119**: 397–418.
- Cortleven, A., Marg, I., Yamburenko, M. V., Schlicke, H., Hill, K., Grimm, B., Schaller, G.E., and Schmülling, T.** (2016). Cytokinin Regulates the Etioplast-Chloroplast Transition through the Two-Component Signaling System and Activation of Chloroplast-Related Genes. *Plant Physiol.* **172**: 464–78.
- Cui, H., Levesque, M.P., Vernoux, T., Jung, J.W., Paquette, A.J., Gallagher, K.L., Wang, J.Y., Blilou, I., Scheres, B., and Benfey, P.N.** (2007). An Evolutionarily Conserved Mechanism Delimiting SHR Movement Defines a Single Layer of Endodermis in Plants. *Science* **316**: 421–425.
- Davis, S.J., Kurepa, J., and Vierstra, R.D.** (1999). The Arabidopsis thaliana HY1 locus, required for phytochrome-chromophore biosynthesis, encodes a protein related to heme oxygenases. *Proc. Natl. Acad. Sci. U. S. A.* **96**: 6541–6546.
- Deal, R.B. and Henikoff, S.** (2010). A simple method for gene expression and chromatin profiling of individual cell types within a tissue. *Dev. Cell* **18**: 1030–1040.
- Deforges, J., Reis, R.S., Jacquet, P., Vuarambon, D.J., and Poirier, Y.** (2019). Prediction of regulatory long intergenic non-coding RNAs acting in trans through base-pairing interactions. *BMC Genomics* **20**: 601.
- DeYoung, B.J., Bickle, K.L., Schrage, K.J., Muskett, P., Patel, K., and Clark, S.E.** (2006). The CLAVATA1-related BAM1, BAM2 and BAM3 receptor kinase-like proteins are required for meristem function in Arabidopsis. *Plant J.* **45**: 1–16.
- Doležel, J., Binarová, P., and Lcretti, S.** (1989). Analysis of Nuclear DNA content in plant cells by Flow cytometry. *Biol. Plant.* **31**: 113–120.
- Dreissig, S., Schiml, S., Schindeler, P., Weiss, O., Rutten, T., Schubert, V., Gladilin, E., Mette, M.F., Puchta, H., and Houben, A.** (2017). Live-cell CRISPR imaging in plants reveals dynamic telomere movements. *Plant J.* **91**: 565–573.
- Dua, H.S., Joseph, A., Shanmuganathan, V.A., and Jones, R.E.** (2003). Stem cell differentiation and the effects of deficiency. *Eye* **17**: 877–885.
- Dubrovsky, J.G., Doerner, P.W., Colón-Carmona, A., and Rost, T.L.** (2000). Pericycle Cell Proliferation and Lateral Root Initiation in Arabidopsis. *Plant Physiol.* **124**: 1648–1657.

- Duclercq, J., Sangwan-Norreel, B., Catterou, M., and Sangwan, R.S.** (2011). De novo shoot organogenesis: from art to science. *Trends Plant Sci.* **16**: 597–606.
- Espinosa-Ruiz, A., Martínez, C., de Lucas, M., Fàbregas, N., Bosch, N., Caño-Delgado, A.I., and Prat, S.** (2017). TOPLESS mediates brassinosteroid control of shoot boundaries and root meristem development in *Arabidopsis thaliana*. *Development* **144**: 1619–1628.
- Fausser, F., Schiml, S., and Puchta, H.** (2014). Both CRISPR/Cas-based nucleases and nickases can be used efficiently for genome engineering in *Arabidopsis thaliana*. *Plant J.* **79**: 348–359.
- Figuroa, P., Gusmaroli, G., Serino, G., Habashi, J., Ma, L., Shen, Y., Feng, S., Bostick, M., Callis, J., Hellmann, H., and Deng, X.W.** (2005). *Arabidopsis* has two redundant Cullin3 proteins that are essential for embryo development and that interact with RBX1 and BTB proteins to form multisubunit E3 ubiquitin ligase complexes in vivo. *Plant Cell* **17**: 1180–1195.
- Franco-Zorrilla, J.M., López-Vidriero, I., Carrasco, J.L., Godoy, M., Vera, P., and Solano, R.** (2014). DNA-binding specificities of plant transcription factors and their potential to define target genes. *Proc. Natl. Acad. Sci.* **111**: 2367–2372.
- Furuta, K., Kubo, M., Sano, K., Demura, T., Fukuda, H., Liu, Y.G., Shibata, D., and Kakimoto, T.** (2011). The CKH2/PKL chromatin remodeling factor negatively regulates cytokinin responses in *Arabidopsis* calli. *Plant Cell Physiol.* **52**: 618–628.
- Fyodorov, D. V., Zhou, B.-R., Skoultchi, A.I., and Bai, Y.** (2018). Emerging roles of linker histones in regulating chromatin structure and function. *Nat. Rev. Mol. Cell Biol.* **19**: 192–206.
- Gailloch, C. and Lohmann, J.U.** (2015). The never-ending story: from pluripotency to plant developmental plasticity. *Development* **142**: 2237–49.
- Gallois, J.-L., Guyon-Debast, A., Lecureuil, A., Vezon, D., Carpentier, V., Bonhomme, S., and Guerche, P.** (2009). The *Arabidopsis* Proteasome RPT5 Subunits Are Essential for Gametophyte Development and Show Accession-Dependent Redundancy. *PLANT CELL ONLINE* **21**: 442–459.
- Gardner, M.J., Baker, A.J., Assie, J.M., Poethig, R.S., Haseloff, J.P., and Webb, A.A.R.** (2009). GAL4 GFP enhancer trap lines for analysis of stomatal guard cell development and gene expression. *J. Exp. Bot.* **60**: 213–226.
- Gingerich, D.J., Gagne, J.M., Salter, D.W., Hellmann, H., Estelle, M., Ma, L., and Vierstra, R.D.** (2005). Cullins 3a and 3b assemble with members of the broad complex/tramtrack/bric-a-brac (BTB) protein family to form essential ubiquitin-protein ligases (E3s) in *Arabidopsis*. *J. Biol. Chem.* **280**: 18810–21.
- Gingerich, D.J., Hanada, K., Shiu, S.-H., and Vierstra, R.D.** (2007). Large-scale, lineage-specific expansion of a bric-a-brac/tramtrack/broad complex ubiquitin-ligase gene family in rice. *Plant Cell* **19**: 2329–2348.
- Gordon, S.P., Chickarmane, V.S., Ohno, C., and Meyerowitz, E.M.** (2009). Multiple feedback loops through cytokinin signaling control stem cell number within the *Arabidopsis* shoot meristem. *Proc. Natl. Acad. Sci. U. S. A.* **106**: 16529–16534.
- Gray, W.M., Kepinski, S., Rouse, D., Leyser, O., and Estelle, M.** (2001). Auxin regulates SCFTIR1-dependent degradation of AUX/IAA proteins. *Nature* **414**: 271–276.
- Gross-Hardt, R. and Laux, T.** (2003). Stem cell regulation in the shoot meristem. *J. Cell Sci.* **116**: 1659–1666.
- Gross-Hardt, R., Lenhard, M., and Laux, T.** (2002). WUSCHEL signaling functions in interregional communication during *Arabidopsis* ovule development. *Genes Dev.* **16**: 1129–38.
- Guo, L., Cao, X., Liu, Y., Li, J., Li, Y., Li, D., Zhang, K., Gao, C., Dong, A., and Liu, X.** (2018). A chromatin loop represses *WUSCHEL* expression in *Arabidopsis*. *Plant J.* **94**: 1083–1097.
- Guo, Y., Han, L., Hymes, M., Denver, R., and Clark, S.E.** (2010). CLAVATA2 forms a distinct CLE-binding receptor complex regulating *Arabidopsis* stem cell specification. *Plant J.* **63**: 889–900.
- Haecker, A., Groß-Hardt, R., Geiges, B., Sarkar, A., Breuninger, H., Herrmann, M., and Laux, T.** (2004). Expression dynamics of WOX genes mark cell fate decisions during early embryonic patterning in *Arabidopsis thaliana*. *Development* **131**: 657–668.
- Hartl, M. et al.** (2017). Lysine acetylome profiling uncovers novel histone deacetylase substrate proteins in *Arabidopsis*. *Mol. Syst. Biol.* **13**: 949.

- Heidstra, R. and Sabatini, S.** (2014). Plant and animal stem cells: Similar yet different. *Nat. Rev. Mol. Cell Biol.* **15**: 301–312.
- Heo, J.B. and Sung, S.** (2011). Vernalization-mediated epigenetic silencing by a long intronic noncoding RNA. *Science* **331**: 76–9.
- Hollender, C. and Liu, Z.** (2008). Histone Deacetylase Genes in *Arabidopsis* Development. *J. Integr. Plant Biol.* **50**: 875–885.
- Hong, J.C.** (2016). General Aspects of Plant Transcription Factor Families. In *Plant Transcription Factors: Evolutionary, Structural and Functional Aspects* (Academic Press), pp. 35–56.
- Hotton, S.** (2003). Finding the center of a phyllotactic pattern. *J. Theor. Biol.* **225**: 15–32.
- Hristova, E., Fal, K., Klemme, L., Windels, D., and Bucher, E.** (2015). HISTONE DEACETYLASE6 Controls Gene Expression Patterning and DNA Methylation-Independent Euchromatic Silencing. *Plant Physiol.* **168**: 1298–1308.
- Hu, X., Tanaka, A., and Tanaka, R.** (2013). Simple extraction methods that prevent the artifactual conversion of chlorophyll to chlorophyllide during pigment isolation from leaf samples. *Plant Methods* **9**: 1–13.
- Huang, P.-Y., Catinot, J., and Zimmerli, L.** (2016). Ethylene response factors in *Arabidopsis* immunity. *J. Exp. Bot.* **67**: 1231–1241.
- Huang, Y.-S. and Li, H. -m.** (2009). *Arabidopsis* CHLI2 Can Substitute for CHLI1. *PLANT Physiol.* **150**: 636–645.
- Ikeda, M., Mitsuda, N., and Ohme-Takagi, M.** (2009). *Arabidopsis* WUSCHEL is a bifunctional transcription factor that acts as a repressor in stem cell regulation and as an activator in floral patterning. *Plant Cell* **21**: 3493–3505.
- Ikeda, Y., Banno, H., Niu, Q.-W., Howell, S.H., and Chua, N.-H.** (2006). The ENHANCER OF SHOOT REGENERATION 2 gene in *Arabidopsis* Regulates CUP-SHAPED COTYLEDON 1 at the Transcriptional Level and Controls Cotyledon Development. *Plant Cell Physiol.* **47**: 1443–1456.
- Ikeuchi, M., Iwase, A., and Sugimoto, K.** (2015). Control of plant cell differentiation by histone modification and DNA methylation. *Curr. Opin. Plant Biol.* **28**: 60–67.
- Ikeuchi, M., Sugimoto, K., and Iwase, A.** (2013). Plant Callus: Mechanisms of Induction and Repression. *Plant Cell* **25**: 3159–3173.
- Inoue, T., Higuchi, M., Hashimoto, Y., Seki, M., Kobayashi, M., Kato, T., Tabata, S., Shinozaki, K., and Kakimoto, T.** (2001). Identification of CRE1 as a cytokinin receptor from *Arabidopsis*. *Nature* **409**: 1060–1063.
- Inskip, W.P. and Bloom, P.R.** (1985). Extinction Coefficients of Chlorophyll a and b in N,N-Dimethylformamide and 80% Acetone. *PLANT Physiol.* **77**: 483–485.
- Iwase, A., Harashima, H., Ikeuchi, M., Rymen, B., Ohnuma, M., Komaki, S., Morohashi, K., Kurata, T., Nakata, M., Ohme-Takagi, M., Grotewold, E., and Sugimoto, K.** (2017). WIND1 Promotes Shoot Regeneration through Transcriptional Activation of ENHANCER OF SHOOT REGENERATION1 in *Arabidopsis*. *Plant Cell* **29**: 54–69.
- Jackson, M.P. and Hewitt, E.W.** (2016). Cellular proteostasis: degradation of misfolded proteins by lysosomes. *Essays Biochem.* **60**: 173–180.
- Jenuwein, T. and Allis, C.D.** (2001). Translating the Histone Code. *Science* **293**.
- Jiménez, G., Paroush, Z., and Ish-Horowicz, D.** (1997). Groucho acts as a corepressor for a subset of negative regulators, including Hairy and Engrailed. *Genes Dev.* **11**: 3072–3082.
- Jung, J.-H. and Park, C.-M.** (2007). MIR166/165 genes exhibit dynamic expression patterns in regulating shoot apical meristem and floral development in *Arabidopsis*. *Planta* **225**: 1327–1338.
- Kagale, S., Links, M.G., and Rozwadowski, K.** (2010). Genome-wide analysis of ethylene-responsive element binding factor-associated amphiphilic repression motif-containing transcriptional regulators in *Arabidopsis*. *Plant Physiol.* **152**: 1109–1134.
- Kagale, S. and Rozwadowski, K.** (2011). EAR motif-mediated transcriptional repression in plants: An underlying

mechanism for epigenetic regulation of gene expression. *Epigenetics* **6**: 141–146.

- Kaul, A., Schuster, E., and Jennings, B.H.** (2014). The Groucho co-repressor is primarily recruited to local target sites in active chromatin to attenuate transcription. *PLoS Genet.* **10**: e1004595.
- Kayes, J.M. and Clark, S.E.** (1998). CLAVATA2, a regulator of meristem and organ development in Arabidopsis. *Development* **125**: 3843–3851.
- Keogh, M.-C. et al.** (2005). Cotranscriptional set2 methylation of histone H3 lysine 36 recruits a repressive Rpd3 complex. *Cell* **123**: 593–605.
- Kieffer, M., Stern, Y., Cook, H., Clerici, E., Maulbetsch, C., Laux, T., and Davies, B.** (2006). Analysis of the transcription factor WUSCHEL and its functional homologue in *Antirrhinum* reveals a potential mechanism for their roles in meristem maintenance. *Plant Cell* **18**: 560–573.
- Kim, H.-J., Wu, C.-Y., Yu, H.-M., Sheen, J., and Lee, H.** (2017). Dual CLAVATA3 peptides in Arabidopsis shoot stem cell signaling. *J. Plant Biol.* **60**: 506–512.
- Kimura, Y., Tasaka, M., Torii, K.U., and Uchida, N.** (2018). ERECTA-family genes coordinate stem cell functions between the epidermal and internal layers of the shoot apical meristem. *Development* **145**.
- Kinoshita, A., Betsuyaku, S., Osakabe, Y., Mizuno, S., Nagawa, S., Stahl, Y., Simon, R., Yamaguchi-Shinozaki, K., Fukuda, H., and Sawa, S.** (2010). RPK2 is an essential receptor-like kinase that transmits the CLV3 signal in Arabidopsis. *Development* **137**.
- Kondo, T.** (2006). A Plant Peptide Encoded by CLV3 Identified by in Situ MALDI-TOF MS Analysis. *Science* **313**: 845–848.
- Konieczny, A. and Ausubel, F.M.** (1993). A procedure for mapping Arabidopsis mutations using co-dominant ecotype-specific PCR-based markers. *Plant J.* **4**: 403–410.
- Koyama, T., Nii, H., Mitsuda, N., Ohta, M., Kitajima, S., Ohme-Takagi, M., and Sato, F.** (2013). A regulatory cascade involving class II ETHYLENE RESPONSE FACTOR transcriptional repressors operates in the progression of leaf senescence. *Plant Physiol.* **162**: 991–1005.
- Krogan, N.T., Hogan, K., and Long, J.A.** (2012). APETALA2 negatively regulates multiple floral organ identity genes in Arabidopsis by recruiting the co-repressor TOPLESS and the histone deacetylase HDA19. *Development* **139**: 4180–4190.
- Kubalová, I. and Ikeda, Y.** (2017). Chlorophyll Measurement as a Quantitative Method for the Assessment of Cytokinin-Induced Green Foci Formation in Tissue Culture. *J. Plant Growth Regul.* **36**: 516–521.
- Kumar, P.P. and Loh, C.S.** (2012). Plant tissue culture for biotechnology. In *Plant Biotechnology and Agriculture* (Academic Press), pp. 131–138.
- Landrein, B., Refahi, Y., Besnard, F., Hervieux, N., Mirabet, V., Boudaoud, A., Vernoux, T., and Hamant, O.** (2015). Meristem size contributes to the robustness of phyllotaxis in Arabidopsis. *J. Exp. Bot.* **66**: 1317–1324.
- Laplaze, L., Parizot, B., Baker, A., Ricaud, L., Martinière, A., Auguy, F., Franche, C., Nussaume, L., Bogusz, D., and Haseloff, J.** (2005). GAL4-GFP enhancer trap lines for genetic manipulation of lateral root development in Arabidopsis thaliana. *J. Exp. Bot.* **56**: 2433–2442.
- Larkin, R.M.** (2016). Tetrapyrrole Signaling in Plants. *Front. Plant Sci.* **7**: 1–17.
- Larkin, R.M., Alonso, J.M., Ecker, J.R., and Chory, J.** (2003). GUN4, a regulator of chlorophyll synthesis and intracellular signaling. *Science* **299**: 902–906.
- Laux, T., Mayer, K.F., Berger, J., and Jürgens, G.** (1996). The WUSCHEL gene is required for shoot and floral meristem integrity in Arabidopsis. *Development* **122**: 87–96.
- Lee, C. and Clark, S.E.** (2015). A WUSCHEL-independent stem cell specification pathway is repressed by PHB, PHV and CNA in Arabidopsis. *PLoS One* **10**: e0126006.
- Lee, D.-K., Parrott, D.L., Adhikari, E., Fraser, N., and Sieburth, L.E.** (2016). The Mobile *bypass* Signal Arrests Shoot Growth by Disrupting Shoot Apical Meristem Maintenance, Cytokinin Signaling, and WUS Transcription Factor Expression. *Plant Physiol.* **171**: 2178–2190.
- Lee, H., Jun, Y.S., Cha, O.-K., and Sheen, J.** (2019). Mitogen-activated protein kinases MPK3 and MPK6 are

- required for stem cell maintenance in the Arabidopsis shoot apical meristem. *Plant Cell Rep.* **38**: 311–319.
- Lee, J.E. and Golz, J.F.** (2012). Diverse roles of Groucho/Tup1 co-repressors in plant growth and development. *Plant Signal. Behav.* **7**: 86–92.
- Leibfried, A., To, J.P.C., Busch, W., Stehling, S., Kehle, A., Demar, M., Kieber, J.J., and Lohmann, J.U.** (2005). WUSCHEL controls meristem function by direct regulation of cytokinin-inducible response regulators. *Nature* **438**: 1172–1175.
- Levesque, M.P., Vernoux, T., Busch, W., Cui, H., Wang, J.Y., Blilou, I., Hassan, H., Nakajima, K., Matsumoto, N., Lohmann, J.U., Scheres, B., and Benfey, P.N.** (2006). Whole-genome analysis of the short-root developmental pathway in Arabidopsis. *PLoS Biol.* **4**: 739–752.
- Li, D.-X., Chen, W.-Q., Xu, Z.-H., and Bai, S.-N.** (2015). HISTONE DEACETYLASE6-Defective Mutants Show Increased Expression and Acetylation of ENHANCER OF TRIPTYCHON AND CAPRICE1 and GLABRA2 with Small But Significant Effects on Root Epidermis Cellular Pattern. *Plant Physiol.* **168**: 1448–58.
- Li, S. et al.** (2013). MicroRNAs inhibit the translation of target mRNAs on the endoplasmic reticulum in Arabidopsis. *Cell* **153**: 562–574.
- Li, W., Liu, H., Cheng, Z.J., Su, Y.H., Han, H.N., Zhang, Y., and Zhang, X.S.** (2011). DNA methylation and histone modifications regulate de novo shoot regeneration in Arabidopsis by modulating WUSCHEL expression and auxin signaling. *PLoS Genet.* **7**: e1002243.
- Liu, C., Li, L.-C., Chen, W.-Q., Chen, X., Xu, Z.-H., and Bai, S.-N.** (2013). HDA18 affects cell fate in Arabidopsis root epidermis via histone acetylation at four kinase genes. *Plant Cell* **25**: 257–269.
- Liu, W., Karemera, N.J.U., Wu, T., Yang, Y., Zhang, X., Xu, X., Wang, Y., and Han, Z.** (2017). The ethylene response factor ATERF4 negatively regulates the iron deficiency response in Arabidopsis thaliana. *PLoS One* **12**: e0186580.
- Liu, X., Yang, S., Zhao, M., Luo, M., Yu, C.W., Chen, C.Y., Tai, R., and Wu, K.** (2014). Transcriptional repression by histone deacetylases in plants. *Mol. Plant* **7**: 764–772.
- Liu, Z. and Karmarkar, V.** (2008). Groucho/Tup1 family co-repressors in plant development. *Trends Plant Sci.* **13**: 137–144.
- Long, J.A., Moan, E.I., Medford, J.I., and Barton, M.K.** (1996). A member of the KNOTTED class of homeodomain proteins encoded by the STM gene of Arabidopsis. *Nature* **379**: 66–69.
- Long, J.A., Ohno, C., Smith, Z.R., and Meyerowitz, E.M.** (2006). TOPLESS Regulates Apical Embryonic Fate in Arabidopsis. *Science* **312**: 1520–1523.
- Long, J.A., Woody, S., Poethig, S., Meyerowitz, E.M., and Barton, M.K.** (2002). Transformation of shoots into roots in Arabidopsis embryos mutant at the TOPLESS locus. *Development* **129**: 2797–2806.
- Lopez-Molina, L., Mongrand, S., Kinoshita, N., and Chua, N.H.** (2003). AFP is a novel negative regulator of ABA signaling that promotes ABI5 protein degradation. *Genes Dev.* **17**: 410–418.
- Maeshima, K., Ide, S., and Babokhov, M.** (2019). Dynamic chromatin organization without the 30-nm fiber. *Curr. Opin. Cell Biol.* **58**: 95–104.
- Maeshima, K., Imai, R., Tamura, S., and Nozaki, T.** (2014). Chromatin as dynamic 10-nm fibers. *Chromosoma* **123**: 225–237.
- Mahrez, W., Trejo Arellano, M.S., Moreno-Romero, J., Nakamura, M., Shu, H., Nanni, P., Köhler, C., Gruissem, W., and Hennig, L.** (2016). H3K36ac is an evolutionary conserved plant histone modification that marks active genes. *Plant Physiol.* **170**: 1566–1577.
- Mallory, A.C., Reinhart, B.J., Jones-Rhoades, M.W., Tang, G., Zamore, P.D., Barton, M.K., and Bartel, D.P.** (2004). MicroRNA control of PHABULOSA in leaf development: Importance of pairing to the microRNA 5' region. *EMBO J.* **23**: 3356–3364.
- Mandel, T., Candela, H., Landau, U., Asis, L., Zelinger, E., Carles, C.C., and Williams, L.E.** (2016). Differential regulation of meristem size, morphology and organization by the ERECTA, CLAVATA and class III HD-ZIP pathways. *Development* **143**: 1612–22.
- Marchant, A., Kargul, J., May, S.T., Muller, P., Delbarre, A., Perrot-Rechenmann, C., and Bennett, M.J.**

- (1999). AUX1 regulates root gravitropism in Arabidopsis by facilitating auxin uptake within root apical tissues. *EMBO J.* **18**: 2066–73.
- Marquès-Bueno, M.M., Morao, A.K., Cayrel, A., Platre, M.P., Barberon, M., Caillieux, E., Colot, V., Jaillais, Y., Roudier, F., and Vert, G.** (2016). A versatile Multisite Gateway-compatible promoter and transgenic line collection for cell type-specific functional genomics in Arabidopsis. *Plant J.* **85**: 320–333.
- Maruyama, Y., Yamoto, N., Suzuki, Y., Chiba, Y., Yamazaki, K. ichi, Sato, T., and Yamaguchi, J.** (2013). The Arabidopsis transcriptional repressor ERF9 participates in resistance against necrotrophic fungi. *Plant Sci.* **213**: 79–87.
- Matsuo, N., Makino, M., and Banno, H.** (2011). Arabidopsis ENHANCER OF SHOOT REGENERATION (ESR)1 and ESR2 regulate in vitro shoot regeneration and their expressions are differentially regulated. *Plant Sci.* **181**: 39–46.
- Mayer, K.F.X., Schoof, H., Haecker, A., Lenhard, M., Jürgens, G., and Laux, T.** (1998). Role of WUSCHEL in regulating stem cell fate in the Arabidopsis shoot meristem. *Cell* **95**: 805–815.
- Mazzucotelli, E., Belloni, S., Marone, D., De Leonardis, A., Guerra, D., Di Fonzo, N., Cattivelli, L., and Mastrangelo, A.** (2006). The e3 ubiquitin ligase gene family in plants: regulation by degradation. *Curr. Genomics* **7**: 509–22.
- McGrath, K.C., Dombrecht, B., Manners, J.M., Schenk, P.M., Edgar, C.I., Maclean, D.J., Scheible, W.R., Udvardi, M.K., and Kazan, K.** (2005). Repressor- and activator-type ethylene response factors functioning in jasmonate signaling and disease resistance identified via a genome-wide screen of Arabidopsis transcription factor gene expression. *Plant Physiol.* **139**: 949–959.
- Meng, W.J., Cheng, Z.J., Sang, Y.L., Zhang, M.M., Rong, X.F., Wang, Z.W., Tang, Y.Y., and Zhang, X.S.** (2017). Type-B ARABIDOPSIS RESPONSE REGULATORS Specify the Shoot Stem Cell Niche by Dual Regulation of WUSCHEL. *Plant Cell* **29**: 1357–1372.
- Meyerowitz, E.M.** (1989). Arabidopsis, a useful weed. *Cell* **56**: 263–269.
- Miller, C.O., Skoog, F., Von Saltza, M.H., and Strong, F.M.** (1955). KINETIN, A CELL DIVISION FACTOR FROM DEOXYRIBONUCLEIC ACID ¹. *J. Am. Chem. Soc.* **77**: 1392–1392.
- Mirabet, V., Besnard, F., Vernoux, T., and Boudaoud, A.** (2012). Noise and robustness in phyllotaxis. *PLoS Comput. Biol.* **8**: e1002389.
- Mochizuki, N., Brusslan, J.A., Larkin, R., Nagatani, A., and Chory, J.** (2001). Arabidopsis genomes uncoupled 5 (GUN5) mutant reveals the involvement of Mg-chelatase H subunit in plastid-to-nucleus signal transduction. *Proc. Natl. Acad. Sci.* **98**: 2053–2058.
- Mochizuki, N., Tanaka, R., Tanaka, A., Masuda, T., and Nagatani, A.** (2008). The steady-state level of Mg-protoporphyrin IX is not a determinant of plastid-to-nucleus signaling in Arabidopsis. *Proc. Natl. Acad. Sci.* **105**: 15184–15189.
- Motte, H., Vercauteren, A., Depuydt, S., Landschoot, S., Geelen, D., Werbrouck, S., Goormachtig, S., Vuylsteke, M., and Vereecke, D.** (2014a). Combining linkage and association mapping identifies RECEPTOR-LIKE PROTEIN KINASE1 as an essential Arabidopsis shoot regeneration gene. *Proc. Natl. Acad. Sci.* **111**: 8305–8310.
- Motte, H., Vereecke, D., Geelen, D., and Werbrouck, S.** (2014b). The molecular path to in vitro shoot regeneration. *Biotechnol. Adv.* **32**: 107–121.
- Müller, R., Bleckmann, A., and Simon, R.** (2008). The receptor kinase CORYNE of Arabidopsis transmits the stem cell-limiting signal CLAVATA3 independently of CLAVATA1. *Plant Cell* **20**: 934–46.
- Nakano, T., Suzuki, K., Fujimura, T., and Shinshi, H.** (2006). Genome-wide analysis of the ERF gene family in Arabidopsis and rice. *Plant Physiol.* **140**: 411–432.
- Naumova, N., Imakaev, M., Fudenberg, G., Zhan, Y., Lajoie, B.R., Mirny, L.A., and Dekker, J.** (2013). Organization of the mitotic chromosome. *Science* **342**: 948–53.
- Ogas, J., Cheng, J.C., Sung, Z.R., and Somerville, C.** (1997). Cellular differentiation regulated by gibberellin in the Arabidopsis thaliana pickle mutant. *Science* **277**: 91–94.
- Ogata, T., Kida, Y., Tochigi, M., and Matsushita, Y.** (2013). Analysis of the cell death-inducing ability of the

- ethylene response factors in group VIII of the AP2/ERF family. *Plant Sci.* **209**: 12–23.
- Oh, E., Zhu, J.-Y., Ryu, H., Hwang, I., and Wang, Z.-Y.** (2014). TOPLESS mediates brassinosteroid-induced transcriptional repression through interaction with BZR1. *Nat. Commun.* **5**: 383–389.
- Ohme-Takagi, M. and Shinshi, H.** (1995). Ethylene-inducible DNA binding proteins that interact with an ethylene-responsive element. *Plant Cell* **7**: 173–182.
- Ohta, M., Matsui, K., Hiratsu, K., Shinshi, H., and Ohme-Takagi, M.** (2001). Repression domains of class II ERF transcriptional repressors share an essential motif for active repression. *Plant Cell* **13**: 1959–1968.
- Ohyama, K., Shinohara, H., Ogawa-Ohnishi, M., and Matsubayashi, Y.** (2009). A glycopeptide regulating stem cell fate in *Arabidopsis thaliana*. *Nat. Chem. Biol.* **5**: 578–580.
- Ojolo, S.P., Cao, S., Priyadarshani, S.V.G.N., Li, W., Yan, M., Aslam, M., Zhao, H., and Qin, Y.** (2018). Regulation of Plant Growth and Development: A Review From a Chromatin Remodeling Perspective. *Front. Plant Sci.* **9**: 1232.
- Pandey, R., Müller, A., Napoli, C.A., Selinger, D.A., Pikaard, C.S., Richards, E.J., Bender, J., Mount, D.W., and Jorgensen, R.A.** (2002). Analysis of histone acetyltransferase and histone deacetylase families of *Arabidopsis thaliana* suggests functional diversification of chromatin modification among multicellular eukaryotes. *Nucleic Acids Res.* **30**: 5036–5055.
- Patra, B., Pattanaik, S., and Yuan, L.** (2013). Proteolytic degradation of the flavonoid regulators, TRANSPARENT TESTA8 and TRANSPARENT TESTA GLABRA1, in *Arabidopsis* is mediated by the ubiquitin/26Sproteasome system. *Plant Signal. Behav.* **8**: e25901.
- Perianez-Rodriguez, J., Manzano, C., and Moreno-Risueno, M.A.** (2014). Post-embryonic organogenesis and plant regeneration from tissues: two sides of the same coin? *Front. Plant Sci.* **5**: 219.
- Peter, E. and Grimm, B.** (2009). GUN4 is required for posttranslational control of plant tetrapyrrole biosynthesis. *Mol. Plant* **2**: 1198–210.
- Pikaard, C.S. and Scheid, O.M.** (2014). Epigenetic regulation in plants. *Cold Spring Harb. Perspect. Biol.* **6**: a019315.
- Prigge, M.J., Otsuga, D., Alonso, J.M., Ecker, J.R., Drews, G.N., and Clark, S.E.** (2005). Class III homeodomain-leucine zipper gene family members have overlapping, antagonistic, and distinct roles in *Arabidopsis* development. *Plant Cell* **17**: 61–76.
- Reynolds, N., O’Shaughnessy, A., and Hendrich, B.** (2013). Transcriptional repressors: multifaceted regulators of gene expression. *Development* **140**: 505–512.
- Richmond, A.E. and Lang, A.** (1957). Effect of Kinetin on Protein Content and Survival of Detached Xanthium Leaves. *Science* **125**: 650–651.
- Riefler, M., Novak, O., Strnad, M., and Schmülling, T.** (2006). *Arabidopsis* cytokinin receptor mutants reveal functions in shoot growth, leaf senescence, seed size, germination, root development, and cytokinin metabolism. *Plant Cell* **18**: 40–54.
- Rim, Y., Huang, L., Chu, H., Han, X., Cho, W.K., Jeon, C.O., Kim, H.J., Hong, J.C., Lucas, W.J., and Kim, J.Y.** (2011). Analysis of *Arabidopsis* transcription factor families revealed extensive capacity for cell-to-cell movement as well as discrete trafficking patterns. *Mol. Cells* **32**: 519–526.
- Rim, Y., Jung, J.-H., Chu, H., Cho, W.K., Kim, S.-W., Hong, J.C., Jackson, D., Datla, R., and Kim, J.-Y.** (2009). A non-cell-autonomous mechanism for the control of plant architecture and epidermal differentiation involves intercellular trafficking of BREVIPEDICELLUS protein. *Funct. Plant Biol.* **36**: 280.
- Rojo, E., Sharma, V.K., Kovaleva, V., Raikhel, N. V., and Fletcher, J.C.** (2002). CLV3 is localized to the extracellular space, where it activates the *Arabidopsis* CLAVATA stem cell signaling pathway. *Plant Cell* **14**: 969–977.
- Romanov, G.A., Lomin, S.N., and Schmülling, T.** (2018). Cytokinin signaling: from the ER or from the PM? That is the question! *New Phytol.* **218**: 41–53.
- Rosa, S., Ntoukakis, V., Ohmido, N., Pendle, A., Abranches, R., and Shaw, P.** (2014). Cell Differentiation and Development in *Arabidopsis* Are Associated with Changes in Histone Dynamics at the Single-Cell Level. *Plant Cell Online* **26**: 4821–4833.

- Rosspopoff, O., Chelysheva, L., Saffar, J., Lecorgne, L., Gey, D., Caillieux, E., Colot, V., Roudier, F., Hilson, P., Berthomé, R., Da Costa, M., and Rech, P.** (2017). Direct conversion of root primordium into shoot meristem relies on timing of stem cell niche development. *Development* **144**: 1187–1200.
- Ryu, H., Cho, H., Bae, W., and Hwang, I.** (2014). Control of early seedling development by BES1/TPL/HDA19-mediated epigenetic regulation of ABI3. *Nat. Commun.* **5**: 755–766.
- Sabatini, S., Heidstra, R., Wildwater, M., and Scheres, B.** (2003). SCARECROW is involved in positioning the stem cell niche in the Arabidopsis root meristem. *Genes Dev.* **17**: 354–358.
- Sakuma, Y., Liu, Q., Dubouzet, J.G., Abe, H., Shinozaki, K., and Yamaguchi-Shinozaki, K.** (2002). DNA-Binding Specificity of the ERF/AP2 Domain of Arabidopsis DREBs, Transcription Factors Involved in Dehydration- and Cold-Inducible Gene Expression. *Biochem. Biophys. Res. Commun.* **290**: 998–1009.
- Salehin, M., Bagchi, R., and Estelle, M.** (2015). SCFTIR1/AFB-based auxin perception: mechanism and role in plant growth and development. *Plant Cell* **27**: 9–19.
- Sarkar, A.K., Luijten, M., Miyashima, S., Lenhard, M., Hashimoto, T., Nakajima, K., Scheres, B., Heidstra, R., and Laux, T.** (2007). Conserved factors regulate signalling in Arabidopsis thaliana shoot and root stem cell organizers. *Nature* **446**: 811–814.
- Satina, S., Blakeslee, A.F., and Avery, A.G.** (1940). Demonstration of the Three Germ Layers in the Shoot Apex of *Datura* by Means of Induced Polyploidy in Periclinal Chimeras on JSTOR. *Am. J. Bot.* **27**: 895–905.
- Scharfenberg, M., Mittermayr, L., von Roepenack-Lahaye, E., Schlicke, H., Grimm, B., Leister, D., and Kleine, T.** (2015). Functional characterization of the two ferrochelatases in Arabidopsis thaliana. *Plant. Cell Environ.* **38**: 280–298.
- Schubert, V., Lermontova, I., and Schubert, I.** (2013). The Arabidopsis CAP-D proteins are required for correct chromatin organisation, growth and fertility. *Chromosoma* **122**: 517–533.
- Scofield, S., Murison, A., Jones, A., Fozard, J., Aida, M., Band, L.R., Bennett, M., and Murray, J.A.H.** (2018). Coordination of meristem and boundary functions by transcription factors in the SHOOT MERISTEMLESS regulatory network. *Development* **145**: dev.157081.
- Serafini, M. and Verfaillie, C.** (2006). Pluripotency in Adult Stem Cells: State of the Art. *Semin. Reprod. Med.* **24**: 379–388.
- Shinohara, H. and Matsubayashi, Y.** (2015). Reevaluation of the CLV3-receptor interaction in the shoot apical meristem: dissection of the CLV3 signaling pathway from a direct ligand-binding point of view. *Plant J.* **82**: 328–336.
- Shu, K. and Yang, W.** (2017). E3 Ubiquitin Ligases: Ubiquitous Actors in Plant Development and Abiotic Stress Responses. *Plant Cell Physiol.* **58**: 1461–1476.
- Sitaraman, J., Bui, M., and Liu, Z.** (2008). LEUNIG_HOMOLOG and LEUNIG Perform Partially Redundant Functions during Arabidopsis Embryo and Floral Development. *PLANT Physiol.* **147**: 672–681.
- Skoog, F. and Miller, C.O.** (1957). Chemical regulation of growth and organ formation in plant tissues cultured in vitro. *Symp. Soc. Exp. Biol.* **11**: 118–130.
- Snipes, S.A., Rodriguez, K., DeVries, A.E., Miyawaki, K.N., Perales, M., Xie, M., and Reddy, G.V.** (2018). Cytokinin stabilizes WUSCHEL by acting on the protein domains required for nuclear enrichment and transcription. *PLoS Genet.* **14**: e1007351.
- Soldatova, O., Apchelimov, A., Radukina, N., Ezhova, T., Shestakov, S., Ziemann, V., Hedtke, B., and Grimm, B.** (2005). An Arabidopsis mutant that is resistant to the protoporphyrinogen oxidase inhibitor acifluorfen shows regulatory changes in tetrapyrrole biosynthesis. *Mol. Genet. Genomics* **273**: 311–318.
- Somssich, M., Je, B. II, Simon, R., and Jackson, D.** (2016). CLAVATA-WUSCHEL signaling in the shoot meristem. *Development* **143**: 3238–3248.
- Song, C.-P., Agarwal, M., Ohta, M., Guo, Y., Halfter, U., Wang, P., and Zhu, J.-K.** (2005). Role of an Arabidopsis AP2/EREBP-type transcriptional repressor in abscisic acid and drought stress responses. *Plant Cell* **17**: 2384–2396.
- Song, C.-P. and Galbraith, D.W.** (2006). AtSAP18, An Orthologue of Human SAP18, is Involved in the Regulation of Salt Stress and Mediates Transcriptional Repression in Arabidopsis. *Plant Mol. Biol.* **60**: 241–257.

- Sonoda, Y., Yao, S.-G., Sako, K., Sato, T., Kato, W., Ohto, M., Ichikawa, T., Matsui, M., Yamaguchi, J., and Ikeda, A.** (2007). SHA1, a novel RING finger protein, functions in shoot apical meristem maintenance in *Arabidopsis*. *Plant J.* **50**: 586–596.
- Spinelli, S. V., Martin, A.P., Viola, I.L., Gonzalez, D.H., and Palatnik, J.F.** (2011). A Mechanistic Link between STM and CUC1 during *Arabidopsis* Development. *PLANT Physiol.* **156**: 1894–1904.
- Stiegler, J.C., Bell, G.E., and Maness, N.O.** (2005). Comparison of Acetone and *N,N*-Dimethylformamide for Pigment Extraction in Turfgrass. *Commun. Soil Sci. Plant Anal.* **35**: 1801–1813.
- Stifani, S., Blaumueller, C.M., Redhead, N.J., Hill, R.E., and Artavanis-Tsakonas, S.** (1992). Human homologs of a *Drosophila* Enhancer of Split gene product define a novel family of nuclear proteins. *Nat. Genet.* **2**: 119–127.
- Sugimoto, K., Jiao, Y., and Meyerowitz, E.M.** (2010). *Arabidopsis* Regeneration from Multiple Tissues Occurs via a Root Development Pathway. *Dev. Cell* **18**: 463–471.
- Susek, R.E., Ausubel, F.M., and Chory, J.** (1993). Signal transduction mutants of *Arabidopsis* uncouple nuclear CAB and RBCS gene expression from chloroplast development. *Cell* **74**: 787–99.
- Szemenyei, H., Hannon, M., and Long, J.A.** (2008). TOPLESS Mediates Auxin-Dependent Transcriptional Repression During *Arabidopsis* Embryogenesis. *Science* **319**: 1384–1386.
- Tanaka, R., Kobayashi, K., and Masuda, T.** (2011). Tetrapyrrole Metabolism in *Arabidopsis thaliana*. *Arab. B.* **9**: e0145.
- Terry, M.J. and Smith, A.G.** (2013). A model for tetrapyrrole synthesis as the primary mechanism for plastid-to-nucleus signaling during chloroplast biogenesis. *Front. Plant Sci.* **4**: 14.
- Tian, Z., He, Q., Wang, H., Liu, Y., Zhang, Y., Shao, F., and Xie, C.** (2015). The Potato ERF Transcription Factor StERF3 Negatively Regulates Resistance to *Phytophthora infestans* and Salt Tolerance in Potato. *Plant Cell Physiol.* **56**: 992–1005.
- Tiwari, S.B.** (2004). Aux/IAA Proteins Contain a Potent Transcriptional Repression Domain. *PLANT CELL ONLINE* **16**: 533–543.
- To, J.P.C., Haberer, G., Ferreira, F.J., Deruère, J., Mason, M.G., Schaller, G.E., Alonso, J.M., Ecker, J.R., and Kieber, J.J.** (2004). Type-A *Arabidopsis* Response Regulators Are Partially Redundant Negative Regulators of Cytokinin Signaling. *PLANT CELL ONLINE* **16**: 658–671.
- To, J.P.C. and Kieber, J.J.** (2008). Cytokinin signaling: two-components and more. *Trends Plant Sci.* **13**: 85–92.
- Tsuzuki, T., Takahashi, K., Inoue, S., Okigaki, Y., Tomiyama, M., Hossain, M.A., Shimazaki, K., Murata, Y., and Kinoshita, T.** (2011). Mg-chelatase H subunit affects ABA signaling in stomatal guard cells, but is not an ABA receptor in *Arabidopsis thaliana*. *J. Plant Res.* **124**: 527–538.
- Valvekens, D., Montagu, M. V., and Lijsebettens, M. V.** (1988). *Agrobacterium tumefaciens*-mediated transformation of *Arabidopsis thaliana* root explants by using kanamycin selection. *Proc. Natl. Acad. Sci.* **85**: 5536–5540.
- Vandesompele, J., De Preter, K., Pattyn, I., Poppe, B., Van Roy, N., De Paepe, A., and Speleman, R.** (2002). Accurate normalization of real-time quantitative RT-PCR data by geometric averaging of multiple internal control genes. *Genome Biol.* **3**: research0034.1–0034.11.
- Verdeil, J.-L., Alemanno, L., Niemenak, N., and Tranbarger, T.J.** (2007). Pluripotent versus totipotent plant stem cells: dependence versus autonomy? *Trends Plant Sci.* **12**: 245–252.
- Vierstra, R.D.** (2009). The ubiquitin–26S proteasome system at the nexus of plant biology. *Nat. Rev. Mol. Cell Biol.* **10**: 385–397.
- Vojta, P., Kokáš, F., Husičková, A., Grúz, J., Bergougnoux, V., Marchetti, C.F., Jiskrová, E., Ježilová, E., Mik, V., Ikeda, Y., and Galuszka, P.** (2016). Whole transcriptome analysis of transgenic barley with altered cytokinin homeostasis and increased tolerance to drought stress. *N. Biotechnol.* **33**: 676–691.
- Wang, J., Meng, X., Yuan, C., Harrison, A.P., and Chen, M.** (2016). The roles of cross-talk epigenetic patterns in *Arabidopsis thaliana*. *Brief. Funct. Genomics* **15**: 278–287.
- Wang, L., Kim, J., and Somers, D.E.** (2013). Transcriptional corepressor TOPLESS complexes with

pseudoresponse regulator proteins and histone deacetylases to regulate circadian transcription. *Proc. Natl. Acad. Sci.* **110**: 761–766.

- Warren, C.R.** (2008). Rapid Measurement of Chlorophylls with a Microplate Reader. *J. Plant Nutr.* **31**: 1321–1332.
- Weber, H., Bernhardt, A., Dieterle, M., Hano, P., Mutlu, A., Estelle, M., Genschik, P., and Hellmann, H.** (2005). Arabidopsis AtCUL3a and AtCUL3b form complexes with members of the BTB/POZ-MATH protein family. *Plant Physiol.* **137**: 83–93.
- Weber, H. and Hellmann, H.** (2009). Arabidopsis thaliana BTB/POZ-MATH proteins interact with members of the ERF/AP2 transcription factor family. *FEBS J.* **276**: 6624–6635.
- Weisshart, K., Fuchs, J., and Schubert, V.** (2016). Structured Illumination Microscopy (SIM) and Photoactivated Localization Microscopy (PALM) to Analyze the Abundance and Distribution of RNA Polymerase II Molecules on Flow-Sorted Arabidopsis Nuclei. *BIO-PROTOCOL* **6**.
- Williams, F.E. and Trumbly, R.J.** (1990). Characterization of TUP1, a mediator of glucose repression in *Saccharomyces cerevisiae*. *Mol Cell Biol* **10**: 6500–6511.
- Williams, L., Grigg, S.P., Xie, M., Christensen, S., and Fletcher, J.C.** (2005). Regulation of Arabidopsis shoot apical meristem and lateral organ formation by microRNA miR166g and its AtHD-ZIP target genes. *Development* **132**: 3657–3668.
- Woodson, J.D., Joens, M.S., Sinson, A.B., Gilkerson, J., Salomé, P.A., Weigel, D., Fitzpatrick, J.A., and Chory, J.** (2015). Ubiquitin facilitates a quality-control pathway that removes damaged chloroplasts. *Science* **350**: 450–454.
- Woodson, J.D., Perez-Ruiz, J.M., and Chory, J.** (2011). Heme synthesis by plastid ferrochelatase I regulates nuclear gene expression in plants. *Curr. Biol.* **21**: 897–903.
- Xie, M., Chen, H., Huang, L., O’Neil, R.C., Shokhirev, M.N., and Ecker, J.R.** (2018). A B-ARR-mediated cytokinin transcriptional network directs hormone cross-regulation and shoot development. *Nat. Commun.* **9**: 1604.
- Xu, L., Wei, Y., Reboul, J., Vaglio, P., Shin, T.-H., Vidal, M., Elledge, S.J., and Harper, J.W.** (2003). BTB proteins are substrate-specific adaptors in an SCF-like modular ubiquitin ligase containing CUL-3. *Nature* **425**: 316–321.
- Xu, T.-T., Song, X.-F., Ren, S.-C., and Liu, C.-M.** (2013). The sequence flanking the N-terminus of the CLV3 peptide is critical for its cleavage and activity in stem cell regulation in Arabidopsis. *BMC Plant Biol.* **13**: 225.
- Yadav, R.K., Perales, M., Gruel, J., Girke, T., Jönsson, H., and Venugopala Reddy, G.** (2011). WUSCHEL protein movement mediates stem cell homeostasis in the Arabidopsis shoot apex. *Genes Dev.* **25**: 2025–2030.
- Yamamuro, C., Zhu, J.-K., and Yang, Z.** (2016). Epigenetic Modifications and Plant Hormone Action. *Mol. Plant* **9**: 57–70.
- Yanai, O., Shani, E., Dolezal, K., Tarkowski, P., Sablowski, R., Sandberg, G., Samach, A., and Ori, N.** (2005). Arabidopsis KNOXI proteins activate cytokinin biosynthesis. *Curr. Biol.* **15**: 1566–1571.
- Yang, S., Poretska, O., and Sieberer, T.** (2018). ALTERED MERISTEM PROGRAM1 Restricts Shoot Meristem Proliferation and Regeneration by Limiting HD-ZIP III-Mediated Expression of RAP2.6L. *Plant Physiol.* **177**: 1580–1594.
- Yang, S., Wang, S., Liu, X., Yu, Y., Yue, L., Wang, X., and Hao, D.** (2009). Four divergent Arabidopsis ethylene-responsive element-binding factor domains bind to a target DNA motif with a universal CG step core recognition and different flanking bases preference. *FEBS J.* **276**: 7177–7186.
- Yang, Z., Tian, L., Latoszek-Green, M., Brown, D., and Wu, K.** (2005). Arabidopsis ERF4 is a transcriptional repressor capable of modulating ethylene and abscisic acid responses. *Plant Mol. Biol.* **58**: 585–596.
- Yu, C.-W., Liu, X., Luo, M., Chen, C., Lin, X., Tian, G., Lu, Q., Cui, Y., and Wu, K.** (2011). HISTONE DEACETYLASE6 Interacts with FLOWERING LOCUS D and Regulates Flowering in Arabidopsis. *PLANT Physiol.* **156**: 173–184.
- Zhang, T.-Q., Lian, H., Zhou, C.-M., Xu, L., Jiao, Y., and Wang, J.-W.** (2017). A Two-Step Model for de Novo Activation of WUSCHEL during Plant Shoot Regeneration. *Plant Cell* **29**: 1073–1087.

- Zhang, W. and Yu, R.** (2014). Molecule mechanism of stem cells in Arabidopsis thaliana. *Pharmacogn. Rev.* **8**: 105–12.
- Zhang, X., Henriques, R., Lin, S.S., Niu, Q.W., and Chua, N.H.** (2006). Agrobacterium-mediated transformation of Arabidopsis thaliana using the floral dip method. *Nat. Protoc.* **1**: 641–646.
- Zhang, Y., Iratni, R., Erdjument-Bromage, H., Tempst, P., and Reinberg, D.** (1997). Histone Deacetylases and SAP18, a Novel Polypeptide, Are Components of a Human Sin3 Complex. *Cell* **89**: 357–364.
- Zhao, X. et al.** (2017). RETINOBLASTOMA RELATED1 mediates germline entry in Arabidopsis. *Science* **356**: eaaf6532.
- Zhao, Z., Andersen, S.U., Ljung, K., Dolezal, K., Miotk, A., Schultheiss, S.J., and Lohmann, J.U.** (2010). Hormonal control of the shoot stem-cell niche. *Nature* **465**: 1089–1092.
- Zhou, X., Zhang, Z.-L., Yusuke, J., Qiu, K., Park, J., Nam, E.A., Lumba, S., Desveaux, D., McCourt, P., Kamiya, Y., Tyler, L., and Sun, T.-P.** (2016). ERF11 Promotes Internode Elongation by Activating Gibberellin Biosynthesis and Signaling Pathways in Arabidopsis. *Plant Physiol.* **171**: 2760–2770.
- Zhu, Z. et al.** (2011). Derepression of ethylene-stabilized transcription factors (EIN3/EIL1) mediates jasmonate and ethylene signaling synergy in Arabidopsis. *Proc. Natl. Acad. Sci. U. S. A.* **108**: 12539–12544.
- Zhu, Z., Xu, F., Zhang, Y., Cheng, Y.T., Wiermer, M., Li, X., and Zhang, Y.** (2010). Arabidopsis resistance protein SNC1 activates immune responses through association with a transcriptional corepressor. *Proc. Natl. Acad. Sci.* **107**: 13960–13965.
- Zuo, J., Niu, Q.-W., and Chua, N.-H.** (2000). An estrogen receptor-based transactivator XVE mediates highly inducible gene expression in transgenic plants. *Plant J.* **24**: 265–273.

Abbreviations

2,4-D – 2,4-Dichlorophenoxyacetic acid

2ip – isopentenyl adenosine

AD – activation domain

ahk3 – *arabidopsis histidine kinase 3*

AMP – adenosine monophosphate

AMP1– altered meristem program 1

AP2/EREBP – apetala2/ethylene-responsive element binding protein

AP2/ERF – apetala2/ethylene responsive factor

APC – anaphase promoting complex/cyclosome

ARF – auxin response factor

ARR – arabidopsis response regulator

ATHB8 – arabidopsis thaliana homeobox8

ATP – adenosine triphosphate

AUX/IAA – auxin/indole acetic acid

BAM 1, 2, 3 – barely any meristem 1, 2 ,3

BD – binding domain

BPM – BTB/POZ-MATH

BTB/POZ – bric-a-brac – tramtrack – broadcomplex/pox virus and zinc finger

CaMV35S – cauliflower Mosaic Virus 35S promoter

CAPS – cleaved amplified polymorphic sequence

cDNA – complementary DNA

ChIP – chromatin immunoprecipitation

CHLD – magnesium chelatase-d

chlh – magnesium chelatase h

CHLI1– magnesium chelatase i1

CHX – cycloheximid

CIM – callus induction medium

CK – cytokinin

CLH – chlorophyllase

CLV – clavata

CLV3p – clavata peptide

CNA – CORONA
Col-0 – columbia-0
CRD1 – copper response deficient 1
CRE1/AHK4 – cytokinin response 1/arabidopsis histidine kinase 4
CRL – cullin – ring ligase
CRN/SOL2 – coryne/suppressor of llp1 2
CSC – columella stem cells
CUC 1, 2, 3 – cup-shaped cotyledon 1, 2, 3
CZ – central zone
DDB – dna damage-binding
DMF – N,N-dimethyl-formamide
DMSO – dimethyl sulfoxide
DNA – deoxyribonucleic acid
EAR – ERF-associated amphiphilic repression
EAR-like – ERF-associated amphiphilic repression-LIKE
EM – estradiol receptor fused with 4xmyc tag
ER – estradiol binding receptor motif
ERBS – EAR repressor binding site
ERF – ethylene responsive factor
ESR1,2 – enhancer of shoot regeneration 1, 2
FC2 – protoporphyrin ix ferrochelatase 2
gDNA – genomic DNA
GFP – green fluorescence protein
Gro/TLE – groucho/transducin-like enhancer of split
GUN3; GUN4 – genome uncoupled 3; 4
HAG1 – histone acetyltransferase GCN1 gene
HD2 – histone deacetylase-2
HAD – histone deacetylase
HECT – homologous to the e6ap carboxyl terminus
HPT – hygromycin b resistance cassette
hy1 – heme oxygenase/long hypocotyl 1
IAA – indole-3-acetic acid

IPA – isopentenyladenosine
KNOX – knotted1-like homeobox
Leu – leucine
LRM – lateral root meristem
LRP – lateral root primordia
LSCM – laser scanning confocal microscopy
LUG – leunig
MATH – meprin and traf (tumor necrosis factor receptor-associated factor) homology
mCherry – monomeric mCherry
MES – 2-(N-morpholino)ethanesulfonic acid
MS – Murashige and Skoog
Myc – c-Myc protein epitope tag
Na₂EDTA – disodium ethylenediaminetetraacetate dihydrate
NASC – european nottingham arabidopsis stock centre
NLS – nuclear localization signal
OC – organizing center
ORF – open reading frame
PAM – protospacer adjacent motif
PBS – phosphate-buffered saline
PCR – polymerase chain reaction
PHB – phabulosa
PHV – phavulota
PKL/CHK2 – pickle/cytokinin hypersensitive 2
PLT – plethora
polyUBQ – polyubiquitination
PPi – pyrophosphate
PZ – peripheral zone
QC – quiescence center
qRT-PCR – quantitative RT-PCR analysis
RAV – related to abi3/vp1
RBX1 – ring-box1
REV – revoluta

RIM – root induction medium

RING – really interesting new gene

RNA – ribonucleic acid

RNAPII inactive – RNA polymerase II inactive

RNAPIISer2ph – RNA polymerase II phosphorylated on serine 2

RPD3/HDA1 – reduced potassium dependency-3/histone deacetylase-1

RPK2/TOAD2 – receptor-like protein kinase 2/toadstool2

RT-PCR – reverse transcription polymerase chain reaction

RUB1 – related to ubiquitin

SAM – shoot apical meristem

SAP18 – Sin-associated polypeptide 18

SCF – s phase kinase-associated protein1 – cullin1 – f-box

SCR – scarecrow

semi-quantitative RT-PCR/semi-q RT-PCR – semi-quantitative reverse transcription PCR

SHR – shortroot

SIM – shoot induction medium

SIR2 – silent information regulator 2

SSLP – simple sequence length polymorphism analysis

STM – shoot meristemless

T-DNA – transfer dna

TIR1/AFB – transport inhibitor resistant1/auxin signaling f-box

TPL – topless

TPR – topless-related

Trp – tryptophan

TUB – tubulin

UPS – ubiquitin-26 proteasome system

UTR – untranslated region

WOX – wuschel-related homeobox

WSIP – wuschel-interacting protein

WT – wild type

WUS – wuschel

Y2H – Yeast Two-Hybrid System

Curriculum vitae

Ivona Kubalová

ORCID iD [0000-0002-5673-9715](https://orcid.org/0000-0002-5673-9715)

Date of Birth 20th May 1989

Nationality Slovak

Education:

2013-present Ph.D. program in Biochemistry, Palacký University in Olomouc
Research project: Genetic control of pluripotency in plant

2013 MSc. in Genetics, Comenius University in Bratislava, Slovak Republic

2011 BSc. in Biology, Comenius University in Bratislava, Slovak Republic

Professional career:

Since 2018 Researcher, Leibniz Institute of Plant Genetics and Crop Plant Research (IPK) Gatersleben, Germany

2013-2018 Student research assistant, Centre of the Region Haná for Biotechnological and Agricultural Research, Faculty of Science, Palacký University in Olomouc, Czech Republic

Professional interests

Molecular genetics, plant pluripotency, and regeneration, *Arabidopsis thaliana*, epigenetics, cell biology, plant transformation techniques, plant physiology, cytokinin signaling pathways

Key skills/knowledge

Broad knowledge in the field of molecular genetics

Experience in experiments planning, evaluating, and presenting results

Experience in molecular, biochemical, and contemporary DNA cloning techniques

Experience in protein expression in *E. coli*, protein purification, and analysis (SDS-PAGE, Western blotting)

Knowledge of laser scanning confocal microscopy (LSCM)

Immunofluorescence and Fluorescent *in situ* hybridization (FISH)

Experience in the field of genotoxicology, comet assay

Jiskrová E., Kubalová I., Ikeda Y. (2015) What turns on and off the cytokinin metabolism and beyond. In: Poltronieri P., Hong Y. (eds) Applied Plant Genomics and Biotechnology, Elsevier, pp 20-36. ISBN: 978-0-08-100068-7.

Selected conferences

2014 Genetic Control of Pluripotency

Ivona Kubalová, presentation

Konference Nové biotechnologie ve farmacii, biologii a medicíně 2014, Kouty nad Desnou, Česká republika

Impact of ESR2 on Auxin and Cytokinin Crosstalks during Shoot Development

Yoshihisa Ikeda and Ivona Kubalová, poster presentation

Plant science student conference (PSSC), IPK Gatersleben, Germany

Impact of ESR2 on Auxin and Cytokinin Crosstalks during Shoot Regeneration

Yoshihisa Ikeda and Ivona Kubalová, poster presentation

International Symposium on Auxins and Cytokinins in Plant Development – ACPD, Prague, Czech Republic

2018 Mutations in Tetrapyrrole Biosynthesis Pathway Uncouple Nuclear *Wuschel* Expression from *De Novo* Shoot Development in *Arabidopsis*

Ivona Kubalová, David Zalabák, Alžbeta Mičúchová, and Yoshihisa Ikeda, poster presentation

International Plant Molecular Biology 2018 (IPMB), Montpellier, France

Supplements

A) Chlorophyll Measurement as a Quantitative Method for the Assessment of Cytokinin-Induced Green Foci Formation in Tissue Culture

Research article

Ivona Kubalová, Yoshihisa Ikeda

Journal of Plant Growth Regulation, 2017 vol. 36 (2) pp: 516-521

Doi: 10.1007/s00344-016-9637-7

Impact Factor: 2.047

Chlorophyll Measurement as a Quantitative Method for the Assessment of Cytokinin-Induced Green Foci Formation in Tissue Culture

Ivona Kubalová¹ · Yoshihisa Ikeda¹

Received: 27 May 2016 / Accepted: 11 August 2016 / Published online: 27 October 2016
© Springer Science+Business Media New York 2016

Abstract Tissue culture systems have long been exploited to study the process of organogenesis. In response to externally applied cytokinins, pluripotent cells proliferate into green calli and subsequently regenerate shoots. Conventionally, the cytokinin-induced greening phenotype has been evaluated by counting numbers of green foci or to present photographic evidence of morphological changes. However, because the structure of calli is disorganized and the development of pigmentation takes place gradually from pale white through yellow to green, adequately defining and counting green foci remains difficult. In this study, we employed chlorophyll measurement as an alternative method to statistically assess the greening phenotype in tissue culture material. We found that *N,N*-dimethylformamide was the most effective solvent for the extraction of chlorophylls from callus tissue and that bead disruption of the structured tissue improved solvent penetration and the consistency of results. The sensitivity of the method facilitated the quantification of chlorophylls in single-cultured root explants and the use of a spectrophotometer increased the efficiency of measuring multiple samples. Our measurements showed that chlorophyll contents from calli of wild-type and altered cytokinin response mutants (*cre1*; *ahk3*, or *cytokinin hypersensitive 2 (ckh2)/pickle (pkl)*) were statistically distinguishable, validating the

method. Our proposed procedure represents gains in efficiency and precision and leads to more robust standardization than the conventionally used counting of green foci.

Keywords Chlorophyll measurement · Tissue culture · Green foci · *Arabidopsis thaliana* · Cytokinin

Introduction

Since the establishment of the *in vitro* tissue culture system by Skoog and Miller 1957, plant *de novo* organogenesis has been well documented. In principle, plant cell identity is manipulated by the defined cytokinin-to-auxin ratio in an *in vitro* tissue culture. The most widely used *in vitro* tissue culture system for *de novo* organogenesis in *Arabidopsis* was developed in 1988 (Valvekens and others 1988). It is composed of two subsequent steps—the first step involves pre-incubation of explants on auxin-rich callus-inducing medium (CIM) to induce a mass of growing cells, termed callus, that emerge from explants. The second step involves the culture of induced callus on shoot-inducing medium (SIM) in which a high cytokinin-to-auxin ratio is applied. This second medium promotes the nascent development of green foci. Live-imaging cell biology for visualizing marker gene expression and transcriptome analyses have shown that callus formation during CIM incubation is the differentiation of xylem pole-associated pericycle or pericycle-like cells toward root meristem-like tissue and that shoot regeneration is cytokinin-induced transdifferentiation of early lateral root meristems into shoot apical meristems (Atta and others 2009; Sugimoto and others 2010). These processes are summarized in detail in a number of review articles (Motte and others 2014b; Perianez-Rodriguez and others 2014). Lateral organ (shoot) differentiation takes

Electronic supplementary material The online version of this article (doi:10.1007/s00344-016-9637-7) contains supplementary material, which is available to authorized users.

✉ Yoshihisa Ikeda
yoshihisa.ikeda@upol.cz

¹ Faculty of Science, Centre of the Region Haná for Biotechnological and Agricultural Research, Palacký University, Šlechtitelů 27, 783 71 Olomouc, Czech Republic

place from the developed green foci in later stages of SIM incubation. An analysis of 88 *Arabidopsis* accessions revealed no correlation between green foci formation and subsequent shoot regeneration efficiencies, indicating that greening and the subsequent differentiation of lateral organs are distinct phenomena that are under genetic control (Motte and others 2014a). To obtain a better understanding of organogenesis, these two different processes must be evaluated independently.

To study the cytokinin response during organogenesis, two methods are commonly used to evaluate green foci formation. One is to count the number of green foci and the second is to present photographic evidence of morphological changes. The greening takes place gradually and no defined criteria exist. Determination of the number of green foci has largely been a subjective method, based on the observer's determination. Regardless of the chosen determination, the size and the degree of greening are not considered in the results. It is also difficult to count green foci that have developed downward and grown into the medium. A quantitative analysis of the greening phenotype is required to gain insights into cytokinin actions in a tissue culture system.

Materials and Methods

Plant Material and Growth Conditions

Arabidopsis thaliana accession Columbia-0 (Col-0) was used as wild-type. Seeds of *long hypocotyl 1 (hyl)* (Gabi Kat034B01), *genome uncoupled 4 (gun4)* (SALK_026911), *pickle-1 (pkl-1)* (WisDsLox407C12), and *arabidopsis histidine kinase 3(ahk3)* (Gabi Kat 754H09) were obtained from the European nottingham *Arabidopsis* stock centre (NASC). The *cytokinin response 1-2 (cre1-2)* mutant was kindly provided by Tatsuo Kakimoto at Osaka University. The original *hyl* and *gun4* mutants were backcrossed once, and *pkl-1* and *ahk3* were backcrossed three times with wild-type plants prior to characterization. The primers used for genotyping by PCR are listed in Appendix S1.

Arabidopsis plants were grown in a photoperiod of 16-h light (approximately $60 \mu\text{mol m}^{-2} \text{s}^{-1}$) and 8-h dark at 21 °C with 70 % humidity. The conditions for seed surface sterilization and growth on MS plates, CIM pre-incubation and subsequent SIM culture were as previously described (Ikeda and others 2006). In brief, *Arabidopsis* seeds were surface sterilized with 50 % sodium hypochlorite (VWR Chemicals), washed with sterilized water 3 times and stored for 3 days at 4 °C in the dark. Seedlings were grown on MS + 1 % sucrose (pH 5.7) containing 0.8 % phytagel plate in vertical orientation. Five days after germination,

roots were excised into intervals of approximately 8 mm in length and excised root explants that did not contain RAM were transferred onto CIM for 4 days for pre-incubation. Subsequently, root explants were transferred onto SIM for 10 days and subjected to chlorophyll extraction. For the CIM incubation, CIM containing $0.22 \mu\text{M}$ 2, 4-D and $1.16 \mu\text{M}$ kinetin was prepared and root explants were cultured for 36 days.

Semi Quantitative RT-PCR Analysis

Total RNA was extracted from root explants cultured on SIM for 10 days by an RNAqueous phenol-free total RNA isolation kit (Ambion). Conditions for RNA extraction, first strand cDNA synthesis, PCR and agarose gel electrophoresis were described (Ikeda and others 2006). Primers used for RT-PCR are listed in Supplementary material. Cycles used for detection of *WUS* or *TUB* are 38 or 18 cycles, respectively.

Chlorophyll Extraction, Measurement, and Statistical Analysis

Root explants cultured for either 10 days on SIM or 36 days on CIM were used in chlorophyll extraction. Individual root explants were transferred to 1.5-ml Safe-Lock Eppendorf tubes containing 60 μL solvent (80 % acetone, DMF or DMSO) and a tungsten carbide bead (3 mm QIAGEN). Tissue was disrupted by a Mixer Mill (Retsch MM 400) at 25 Hz for 20 s. Samples were left for 5 min before centrifugation at 14,000 rpm for 3 min at room temperature. Supernatants were transferred to 8-strip PCR tubes and centrifuged again to remove debris hindering absorptions. Forty microliters of solution were carefully transferred to wells of a 96-well glass plate (CORNING High Content Imaging Plate Black with 0.2-mm glass bottom cyclin olefin co-polymer). The following equations were used to determine chlorophyll contents. 80 % acetone: Chl a (mg l^{-1}) = $12.63 [A_{664-A750}] - 2.52 [A_{647-A750}]$; Chl b (mg l^{-1}) = $20.47 [A_{647-A750}] - 4.73 [A_{664-A750}]$ DMF: Chl a (mg l^{-1}) = $12.70 [A_{664-A750}] - 2.79 [A_{647-A750}]$; Chl b (mg l^{-1}) = $20.70 [A_{647-A750}] - 4.62 [A_{664-A750}]$ (Inskeep and Bloom 1985). DMSO: Chl a (mg l^{-1}) = $14.85 [A_{665-A750}] - 5.14 [A_{648-A750}]$; Chl b (mg l^{-1}) = $25.48 [A_{648-A750}] - 7.36 [A_{665-A750}]$ (Barnes and others 1992). A wavelength of 750 nm was used as a blank. The Gen5 software on the Synergy H4 microplate reader (BioTek) was used for measurements (Warren 2008). Results obtained from thirty root explants per genotype were subjected to a Student's *t* test (http://www.physics.csbsju.edu/stats/t-test_bulk_form.html) with biological triplicates. *P*-values were as presented.

Results and Discussion

Employment of Bead Disruption For Efficient And Consistent Chlorophyll Extraction from Cultured Tissue

To compare the extraction efficiency of chlorophylls from root explants, commonly used solvents, 80 % acetone, DMF and DMSO, were compared by following the equations for chlorophyll a and chlorophyll b determination as previously described (Barnes and others 1992; Inskeep and Bloom 1985). Glass plates were used for the measurements as DMF is an aggressive solvent that is not compatible with commonly used polystyrene plates. For the convenience of cutting roots, seedlings were grown in the vertical orientation on a relatively solid MS medium containing 0.8 % Phytigel. Five days after germination, root explants were excised and transferred onto CIM for 4 days (CIM pre-incubation), followed by transfer onto SIM. To prepare the same starting materials, two surgical blades were joined with an 8 mm gap separating the two blades. To consider variations in growth and cytokinin response, 30 root explants per solvent were randomly collected and subjected to chlorophyll extraction on day 10 of the SIM incubation. No lateral organs (shoot regeneration) were observed at this time. In agreement with previous reports (Inskeep and Bloom 1985; Stiegler and others 2004), DMF was the most effective solvent for extracting chlorophylls (Fig. 1a–c). When extracted in 80 % acetone, 30-min incubation was not sufficient to reach equilibrium (Fig. 1a), whereas it took around 15 min for DMF or DMSO to reach maximum levels (Fig. 1b, c). DMF extracted chlorophylls more efficiently than DMSO ($p = 0.0082$ at 5 min). During tissue culture, some root explants spontaneously developed wound-induced callus (Ikeuchi and others 2013) (Fig. 1d),

compromising efficient chlorophyll extraction when tissue was not disrupted, resulting in an underestimation of the chlorophyll content. This was particularly the case in *pkl-1* (data not shown). To tackle this difficulty, we applied tungsten bead disruption of all root explants. This procedure resulted in a chlorophyll recovery equivalent to the equilibrium of the corresponding solvents examined for the time-course experiments and an improved extraction in the case of 80 % acetone (Fig. 1e and compare to Fig. 1a), which is an advantage when glass plates are not available. Heat treatment was reported to prevent chlorophyll degradation by inhibiting the chlorophyll hydrolyzing enzyme, chlorophyllase (CLH) (Hu and others 2013); however, no degradation was observed in our conditions (data not shown). Thus, for all subsequent experiments extraction of chlorophylls in DMF with bead disruption and no pre-heat treatment was applied.

Validation of Chlorophyll Measurement as an Objective Greening Phenotype Analysis Method in Tissue Culture

To verify the reliability and reproducibility of quantifying chlorophylls from cultured root explants as a measure for their greening phenotype, mutants reported to have reduced chlorophyll contents were collected (Chory and others 1989; Peter and Grimm 2009). They were used as technical negative controls for chlorophyll quantifications. We obtained *hy1* (GK-034B01) and *gun4* (SALK_026911) mutants. GK-034B01 was referred to as *hy1-3* and SALK_026911 as *gun4-3*, respectively. We confirmed the position of the T-DNA insertion of *hy1-3* in the first exon of the annotated At2g26670.1 transcript, a longer version of splice variant. The *gun4-3* appeared to be null as no detectable GUN4 proteins were observed in the mutant

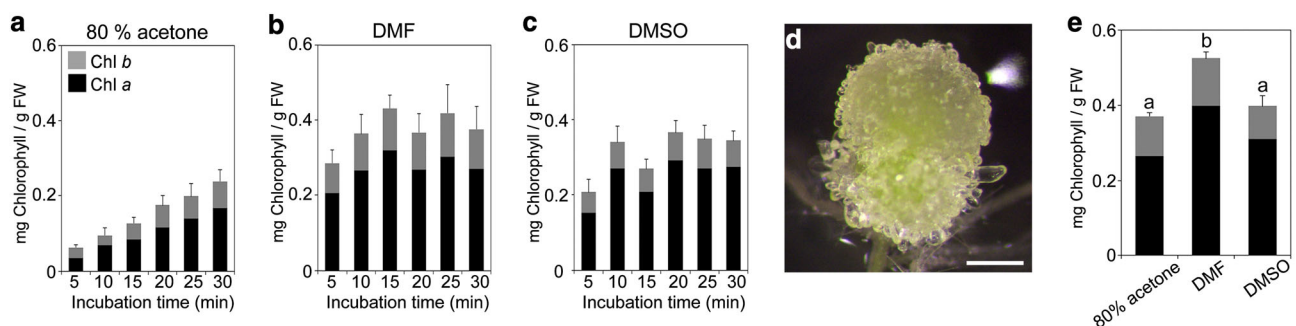


Fig. 1 Effect of bead disruption and solvent on chlorophyll extraction from cultured root explants. **a–c** Chlorophyll contents of wild-type root explants cultured on SIM for 10 days extracted by 80% acetone (**a**), DMF (**b**), and DMSO (**c**) without bead disruption. Chlorophyll a and chlorophyll b contents were measured at different time points (min) and indicated in *black* and *gray bars*, respectively. **d** Wound-induced callus formed at the cutting sites covers green

tissue in Col-0 root explant on SIM for 12 days. **e** Chlorophyll contents of wild-type root explants cultured on SIM for 10 days extracted for 5 min with bead disruption in corresponding solvents. Values marked with *different letters* are significantly different between solvents ($p \leq 0.01$) as determined by student's *t* tests. Data shown are the mean \pm SD of biological triplicates ($n = 30$). *Bar* = 0.5 mm (**d**)

(Peter and Grimm 2009). *HY1* encodes monooxygenase and *GUN4* encodes an adaptor protein positively regulating Mg^{2+} chelatase activity (Davis and others 1999; Peter and Grimm 2009). We found that, although the color of mutant calli was paler than that of wild-type (Fig. 2a), *hy1-3* and *gun4-3* root explants could form the disorganized structures (Fig. 2b, c), indicating that tetrapyrrole biosynthesis was not required for cell outgrowth. Therefore, the cytokinin-induced greening phenotype cannot be assessed by counting green foci or by chlorophyll measurements in these mutants. As expected, chlorophyll amounts extracted from the *hy1-3* or *gun4-3* root explants were significantly lower than that of wild-type ($p \leq 0.0001$ in both cases, Fig. 2d), indicating that our method is able to determine differences in chlorophyll content from a single root explant.

Cytokinin was essential for nascent SAM formation and greening. This suggests that, similarly to the *hy1-3* and *gun4-3*, mutants with an altered cytokinin response should have different chlorophyll levels. *pickle* (*pkl*)/*cytokinin hypersensitive 2* (*chk2*), in which a CHD3 SWI/SNF2 chromatin remodeling factor gene was disrupted, exhibited cytokinin hypersensitivity in tissue culture (Furuta and

others 2011). *pkl/chk2* was employed as a positive control. As the *cre1-2* and *ahk3* single mutants in the Col-0 background did not exhibit cytokinin-insensitive phenotypes (Riefler and others 2006), the cytokinin receptor double mutant, *cre1-2; ahk3*, was created as a negative control for reduced greening phenotype. We obtained the T-DNA insertion mutant line (Gabi-Kat 754H09), in which a T-DNA was inserted in the second exon of *AHK3*, resulting in no detectable transcript accumulation (data not shown). GK-754H09 appeared to be a null mutant and we referred to it as *ahk3-8* hereafter. The *cre1-2; ahk3-8* double mutant had reduced green foci formation (Fig. 2e), whereas *pkl-1* retained the capacity for pronounced greening phenotype (Fig. 2f). We evaluated accumulated chlorophylls per root explant because *pkl-1* exhibited increased growth with roots penetrating the agar medium. The increased mass due to pronounced *de novo* root development resulted in the underestimation of chlorophyll accumulation in *pkl-1* when chlorophylls were evaluated per fresh weight (data not shown). Besides, we found it inaccurate to measure fresh weight of individual 8-mm root explants developing *de novo* roots into medium (30 roots per genotype). Using

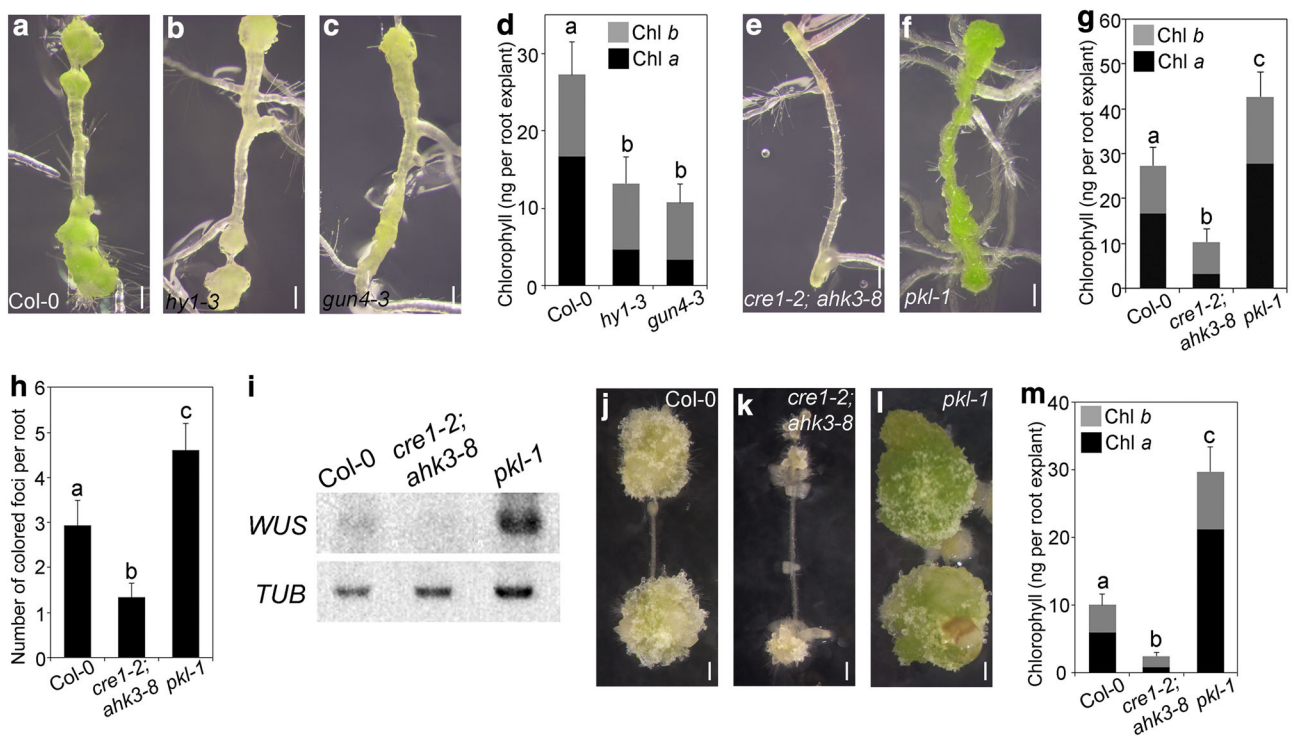


Fig. 2 Statistical evaluation of greening phenotype by chlorophyll measurements. **a–c, e, f** Root explant cultured on SIM for 10 days of Col-0 (**a**), *hy1-3* (**b**), *gun4-3* (**c**), *cre1-2; ahk3-8* (**e**), and *pkl-1* (**f**). **d** Chlorophyll contents of Col-0, *hy1-3* or *gun4-3* root explants cultured on SIM for 10 days. **g** Chlorophyll contents of Col-0, *cre1-2; ahk3-8* or *pkl-1* root explants cultured on SIM for 10 days. **h** Number of pigmented foci per root explant of Col-0, *cre1-2; ahk3-8* or *pkl-1*. **i** Expression of *WUS* on day 10 SIM incubation. **j–l** Root explant

cultured on CIM for 36 days of Col-0 (**j**), *cre1-2; ahk3-8* (**k**) or *pkl-1* (**l**). **m** Chlorophyll contents of Col-0, *cre1-2; ahk3-8*, and *pkl-1* root explants cultured on CIM for 36 days. Chlorophyll a and chlorophyll b contents are indicated in *black* and *gray bars*, respectively (**d, g, m**). Values marked with *different letters* are significantly different between genotypes ($p \leq 0.0001$) as determined by student's *t* tests. Data shown are the mean \pm SD of biological triplicates ($n = 30$). Bars = 0.5 mm (**a–c, e, f, j–l**)

chlorophyll measurements, we were able to statistically distinguish *cre1-2*; *ahk3-8* or *pkl-1* from wild-type ($p \leq 0.0001$ in both cases, Fig. 2g). When the number of green or yellow colored foci developed from *cre1-2*; *ahk3-8* and from *pkl-1* were counted, we obtained similar results to those by the chlorophyll measurements (Fig. 2h), indicating that chlorophyll measurement can be used as an alternative way to evaluate cytokinin-induced greening phenotype. Because greening tissue does not essentially indicate nascent SAM formation, the expression of *WUSCHEL* (*WUS*), encoding a homeodomain transcription factor required for stem cell niche maintenance, was examined. We found positive correlation of *WUS* expression with chlorophyll accumulation (Fig. 2i). The cytokinin-promoted greening of cultured tissue on CIM incubated material was more suitable than material from SIM incubation because no lateral organ differentiation took place in the CIM culture. Instead, outgrowth of calli persisted (Fig. 2j–l). Chlorophyll measurements were made on CIM-induced calli for assessing tissue greening stimulated by the higher kinetin to 2, 4-D ratio in CIM. Similar to the SIM incubation, significant differences in chlorophyll contents could be determined between the two mutants and the wild-type ($p \leq 0.0001$ in both cases, Fig. 2m).

In summary, although chlorophyll accumulation in cultured root explants is not as abundant as it is in leaves and spontaneous wound-induced callus hinders solvent penetration, we developed a method to quantify chlorophylls from a single cultured root explant (8 mm) by applying bead disruption in diverse solvents. The major advantages of our procedure over counting green foci are: (1) chlorophyll levels are a measurable parameter not depending on subjective observations; (2) because the extinction coefficients of chlorophylls are well defined, the results of different experiments are comparative; (3) considerable number of samples can be measured simultaneously by using 96-well glass plates with a conventional microplate reader; (4) the method is sensitive enough to assess a greening phenotype in root explants of 5 mm in length (data not shown), which is helpful for mutants exhibiting a short root phenotype; (5) all green foci are taken into account, including those that develop at sites inaccessible to the eye or image analysis software. Additionally, our methodology does not require parameter setting, which is crucial in the image analysis software when considering pale explants, so objective rather than relative data are obtained. The main disadvantage of our procedure is its destructive nature whereas taking photographs of calli has advantages as it can give insights into morphologic changes over time. Trans-differentiation of RAM into SAM triggered by cytokinins on SIM can be studied by analyzing available SAM-related markers, although introducing the markers in the desired genetic background takes time.

Thus, chlorophyll measurements are a concise and sensitive method that combined with complementary approaches such as taking photographs and SAM-related marker analysis for *de novo* SAM development give a whole view of the responsiveness of explants in tissue culture.

Acknowledgments This work was supported by grant LO1204 from the National Program of Sustainability I from the Ministry of Education, Youth and Sports, Czech Republic. We thank European Arabidopsis Stock Centre (NASC) and Tatsuo Kakimoto for providing mutant seeds, Brian Jones and Jun'ichi Mano for critical reading of manuscript.

Compliance with Ethical Standards

Conflict of interest The authors declare that they have no conflict of interest.

References

- Atta R, Laurens L, Boucheron-Dubuisson E, Guivarc'h A, Carnero E, Giraudat-Pautot V, Rech P, Chriqui D (2009) Pluripotency of *Arabidopsis xylem* pericycle underlies shoot regeneration from root and hypocotyl explants grown in vitro. *Plant J* 57:626–644
- Barnes JD, Balaguer L, Manrique E, Elvira S, Davison AW (1992) A reappraisal of the use of DMSO for the extraction and determination of chlorophylls a and b in lichens and higher plants. *Environ Exp Bot* 32:85–100
- Chory J, Peto CA, Ashbaugh M, Saganich R, Pratt L, Ausubel F (1989) Different Roles for Phytochrome in Etiolated and Green Plants Deduced from Characterization of *Arabidopsis thaliana* Mutants. *Plant Cell* 1:867–880
- Davis SJ, Kurepa J, Vierstra RD (1999) The *Arabidopsis thaliana* *HY1* locus, required for phytochrome-chromophore biosynthesis, encodes a protein related to heme oxygenases. *Proc Natl Acad Sci USA* 96:6541–6546
- Furuta K, Kubo M, Sano K, Demura T, Fukuda H, Liu YG, Shibata D, Kakimoto T (2011) The CKH2/PKL chromatin remodeling factor negatively regulates cytokinin responses in *Arabidopsis calli*. *Plant Cell Physiol* 52:618–628
- Hu X, Tanaka A, Tanaka R (2013) Simple extraction methods that prevent the artifactual conversion of chlorophyll to chlorophyllide during pigment isolation from leaf samples. *Plant Methods* 9:19. doi:10.1186/1746-4811-9-19
- Ikeda Y, Banno H, Niu QW, Howell SH, Chua NH (2006) The *ENHANCER OF SHOOT REGENERATION 2* gene in *Arabidopsis* regulates *CUP-SHAPED COTYLEDON 1* at the transcriptional level and controls cotyledon development. *Plant Cell Physiol* 47:1443–1456
- Ikeuchi M, Sugimoto K, Iwase A (2013) Plant callus: mechanisms of induction and repression. *Plant Cell* 25:3159–3173
- Inskeep WP, Bloom PR (1985) Extinction coefficients of chlorophyll a and B in *n*, *n*-dimethylformamide and 80 % acetone. *Plant Physiol* 77:483–485
- Motte H, Vercouteren A, Depuydt S, Landschoot S, Geelen D, Werbrouck S, Goormachtig S, Vuylsteke M, Vereecke D (2014a) Combining linkage and association mapping identifies *RECEPTOR-LIKE PROTEIN KINASE1* as an essential *Arabidopsis* shoot regeneration gene. *Proc Natl Acad Sci USA* 111:8305–8310
- Motte H, Vereecke D, Geelen D, Werbrouck S (2014b) The molecular path to in vitro shoot regeneration. *Biotechnol Adv* 32:107–121

- Perianez-Rodriguez J, Manzano C, Moreno-Risueno MA (2014) Post-embryonic organogenesis and plant regeneration from tissues: two sides of the same coin? *Front Plant Sci* 5:219. doi:[10.3389/fpls.2014.00219](https://doi.org/10.3389/fpls.2014.00219)
- Peter E, Grimm B (2009) GUN4 is required for posttranslational control of plant tetrapyrrole biosynthesis. *Mol Plant* 2:1198–1210
- Riefler M, Novak O, Strnad M, Schmulling T (2006) *Arabidopsis* cytokinin receptor mutants reveal functions in shoot growth, leaf senescence, seed size, germination, root development, and cytokinin metabolism. *Plant Cell* 18:40–54
- Skoog F, Miller CO (1957) Chemical regulation of growth and organ formation in plant tissues cultured in vitro. *Symp Soc Exp Biol* 11:118–130
- Stiegler JC, Bell GE, Maness NO (2004) Comparison of acetone and *N, N*-dimethylformamide for pigment extraction in turfgrass. *Commun Soil Sci Plant Anal* 35:1801–1813
- Sugimoto K, Jiao Y, Meyerowitz EM (2010) *Arabidopsis* regeneration from multiple tissues occurs via a root development pathway. *Dev Cell* 18:463–471
- Valvekens D, Montagu MV, Van Lijsebettens M (1988) *Agrobacterium tumefaciens*-mediated transformation of *Arabidopsis thaliana* root explants by using kanamycin selection. *Proc Natl Acad Sci USA* 85:5536–5540
- Warren CR (2008) Rapid measurement of chlorophylls with a microplate reader. *J Plant Nutri* 31:1321–1332

B) Mutations in Tetrapyrrole Biosynthesis Pathway Uncouple Nuclear *WUSCHEL* Expression from *de novo* Shoot Development in *Arabidopsis*.

Research article

Ivona Kubalová, David Zalabák, Alžbeta Mičúchová, and Yoshihisa Ikeda

Plant Cell, Tissue and Organ Culture (PCTOC), 2019, pp: 1-7

DOI: 10.1007/s11240-019-01680-w

Impact Factor: 2.2



Mutations in tetrapyrrole biosynthesis pathway uncouple nuclear *WUSCHEL* expression from de novo shoot development in *Arabidopsis*

Ivona Kubalová¹ · David Zalabák¹ · Alžbeta Mičúchová¹ · Yoshihisa Ikeda¹

Received: 16 January 2019 / Accepted: 24 August 2019
© Springer Nature B.V. 2019

Abstract

Plant de novo organogenesis in tissue culture systems has long been exploited to study the plasticity of pluripotency. External application of high cytokinin-to-auxin ratio in cultured medium stimulates greening of tissue and promotes nascent shoot apical meristem (SAM) formation. The stem cell niche in SAM is maintained by a negative feedback loop between *CLAVATA* and *WUSCHEL* (*WUS*) signaling. The fact that cytokinin is able to induce expression of SAM master regulator *WUS* suggests that the capacity of de novo shoot development is largely dependent on *WUS* activity. However, the molecular mechanism of *WUS* expression remains obscure. Here we found that *WUS* expression during de novo SAM formation is affected by the altered tetrapyrrole metabolism catalyzed in the plastid. Loss-of-function mutations in *HEME OXYGENASE/LONG HYPOCOTYL 1* (*hy1*), *Mg-CHELATASE H* (*chlh*), *Mg-CHELATASE II* (*chli1*), and the regulator of *Mg-CHELATASE*, *GENOME-UNCOUPLED 4* (*gun4*), result in elevated *WUS* expression but shoot regeneration efficiency is decreased whereas loss-of-function mutation in *PROTOPORPHYRIN IX FERROCHELATASE 2* (*fc2*) exhibits compromised *WUS* expression with a reduced number of shoots when mutant root explants are cultured on shoot induction medium. Our genetic results show that nuclear *WUS* expression is affected by tetrapyrrole intermediate(s) under the varying plastid status stimulated by external cytokinin treatment during de novo organogenesis.

Key Message

We propose novel regulatory mechanism of nuclear *WUS* expression that is likely modulated by tetrapyrrole intermediate(s) under the varying plastid status stimulated by external cytokinin treatment during de novo organogenesis.

Keywords *Arabidopsis thaliana* · Cytokinin · Retrograde signaling · Shoot apical meristem · Tetrapyrrole biosynthesis · *WUSCHEL*

Abbreviations

ahk3 Arabidopsis histidine kinase 3
ckh2 Cytokinin hypersensitive 2
cre1 Cytokinin response 1
fc2 Protoporphyrin IX ferrochelatase 2
gun Genome uncoupled

hy Long hypocotyl
pkl Pickle
SIM Shoot induction medium
wus Wuschel

Introduction

Since its discovery over 60 years ago, cytokinin, in concert with auxin, has been shown to promote cell division and shoot development in an in vitro tissue culture system (Miller et al. 1955; Skoog and Miller 1957). Cytokinin application renders dark grown plants a series of light-grown traits, such as inhibition of hypocotyl elongation, development of leaves, and etioplast-to-chloroplast transition (Chory et al. 1994; Cortleven et al. 2016). The in vitro tissue culture system has been employed to study pluripotency and de novo

Communicated by Jochen Kumlehn.

Electronic supplementary material The online version of this article (<https://doi.org/10.1007/s11240-019-01680-w>) contains supplementary material, which is available to authorized users.

✉ Yoshihisa Ikeda
yoshihisa.ikeda@upol.cz

¹ Centre of the Region Haná for Biotechnological and Agricultural Research, Faculty of Science, Palacký University, Olomouc, Czech Republic

organogenesis. The shoot regeneration system is composed of two subsequent steps—the first step involves pre-incubation of explants on auxin-rich callus inducing medium (CIM) to induce a mass of growing cells, termed callus (Valvekens et al. 1988). The second step stimulates greening of foci when induced calli are cultured on shoot-inducing medium (SIM) in which a high cytokinin-to-auxin ratio is given. In the late stage of SIM incubation, shoot development takes place from green foci. Recent studies have shown that callus formation during CIM pre-culture is the differentiation of xylem-pole associated pericycle toward root meristem-like tissue and that shoot regeneration is cytokinin-induced transdifferentiation of early lateral root meristem into SAM (Atta et al. 2009; Sugimoto et al. 2010). These processes are summarized in detail in a number of review articles (Motte et al. 2014b; Perianez-Rodriguez et al. 2014). An analysis of 88 *Arabidopsis* accessions revealed no correlation between green foci formation and subsequent shoot regeneration efficiencies, indicating that greening and the subsequent differentiation of lateral organs are distinct phenomena that are under genetic control (Motte et al. 2014a).

External application of cytokinins induces *WUS* expression probably via direct activation by B-type *Arabidopsis* RESPONSE REGULATORS (ARR1, ARR2, ARR10, and ARR12), which are involved in primary cytokinin signaling (Meng et al. 2017; Zhang et al. 2017). It appears that *WUS* expression is more tightly linked to shoot regeneration. Although cytokinin-stimulated phenotypes observed in tissue culture system (greening of tissue, *WUS* expression, and de novo SAM development) have been extensively studied, little is known about how such phenotypes are co-related together as a whole. In this study, we investigate the relationship among them by employing loss-of-function mutants defective in cytokinin perception, de novo SAM formation, and chlorophyll biosynthesis.

Materials and methods

Plant material

The *Arabidopsis thaliana* accession Columbia-0 (Col-0) was used as wild-type. Seeds described below are obtained from the European Nottingham Arabidopsis Stock Centre (NASC) and have been previously described; *pkl-1* (Ogas et al. 1997), *ahk3-8* (Gabi Kat 754_H09) (Kubalová and Ikeda 2017), *wus-101* (Gabi Kat 870_H12) (Zhao et al. 2017), *fc2-1* (Gabi Kat 766_H08) (Woodson et al. 2011), *hy1-3* (Gabi Kat 034_B01) (Kubalová and Ikeda 2017), *gun4-2* (SALK_026911) (Larkin et al. 2003; Peter and Grimm 2009), *chli1* (Sail_230_D11) (Huang and Li 2009; Tsuzuki et al. 2011), *chlh/gun5* (SALK_062726) (Huang and Li 2009), and *crd1* (SALK_009052) (Mochizuki et al.

2008). The *cre1-2* mutant was obtained from Tatsuo Kaki-moto (Inoue et al. 2001). The primers used for genotyping by PCR are listed in Supplemental Table 1. Transcript levels of *GUN3* in *gun3-3* (SALK_104923) (Cheng et al. 2011) or *CHLD* in *chld* (SALK_048878) T-DNA insertion lines are shown in Supplementary Fig. 1.

Growth conditions

The *Arabidopsis* plants and root explants in vitro tissue culture were grown in a photoperiod of 16 h light (approximately $60 \mu\text{mol m}^{-2} \text{s}^{-1}$) and 8 h dark at 21 °C with 70% humidity. The conditions for seed surface sterilization and growth on MS plates, CIM pre-incubation, and subsequent SIM culture were as previously described (Kubalová and Ikeda 2017). In brief, seedlings were grown on MS + 1% sucrose (pH 5.7) containing 1.0% gellan gum (Thermo Fisher Scientific) plate in a vertical orientation. Five days after germination, roots were excised into intervals of approximately 8 mm in length and excised root explants were transferred onto CIM and incubated for 4 days. Subsequently, root explants pre-incubated on CIM were transferred onto SIM for the indicated period and subjected to chlorophyll extraction or RNA extraction.

Chlorophyll measurement

In each replicate, at least 12 root explants per genotype, cultured on SIM at the indicated time period, were used for measurements. Chlorophyll contents in 8 mm SIM cultured root explant per genotype were determined as described previously (Kubalová and Ikeda 2017).

Shoot regeneration assay

As described previously (Li et al. 2011), nascent shoots that could develop true leaves were counted under a stereomicroscope at indicated time points. In each replicate, at least 40 root explants per genotype were examined and the frequency of explants developing shoots was determined. Average number of shoots per root explant was determined in the same manner.

Quantitative RT-PCR analysis (qRT-PCR)

Total RNA was extracted from root explants cultured on SIM for 5 days by RNAqueous phenol-free total RNA isolation kit (Ambion). Conditions for RNA extraction and first strand cDNA synthesis were described (Kubalová and Ikeda 2017). Using gb SG PCR Master Mix (Generi Biotech), real-time PCR reactions were performed on a StepOnePlus™ Real-Time PCR System (Life Technologies). Primers used for detecting *WUS* by qRT-PCR were described (Lee et al.

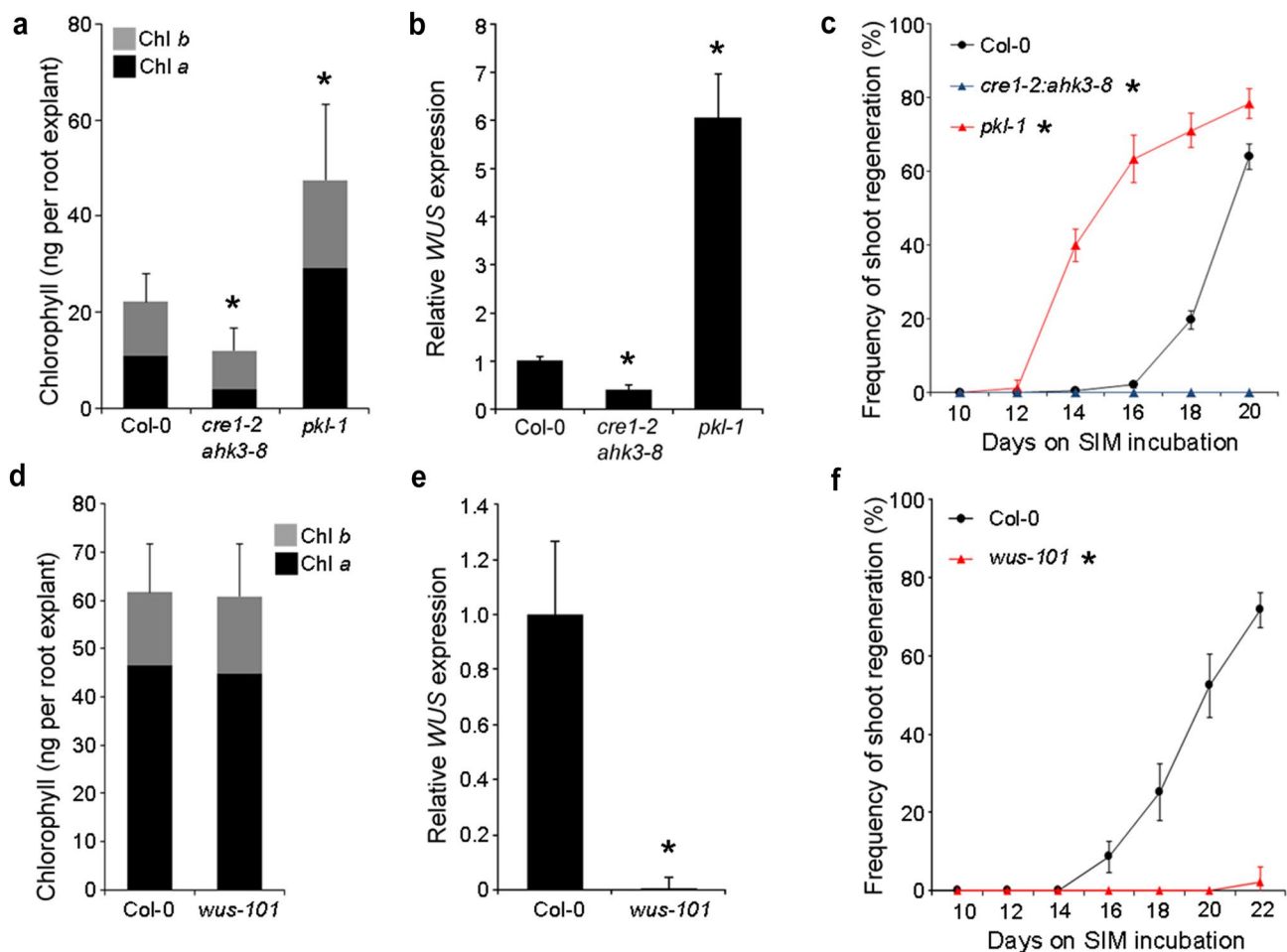


Fig. 1 *WUS* expression and de novo SAM formation are coupled in altered cytokinin response mutants. **a** Chlorophyll contents of Col-0, *cre1-2; ahk3-8*, and *pk1-1* root explants cultured on SIM for 8 days. **b** Relative *WUS* expression in Col-0, *cre1-2; ahk3-8*, and *pk1-1* root explants cultured on SIM for 5 days quantified by qRT-PCR. **c** Shoot regeneration frequency in Col-0, *cre1-2; ahk3-8*, and *pk1-1* root explants cultured at indicated time-points on SIM. **d** Chlorophyll contents of Col-0 and *wus-101* root explants cultured on SIM

for 12 days. **e** Relative *WUS* expression in 7-day-old Col-0 and *wus-101* shoots quantified by qRT-PCR. **f** Shoot regeneration frequency in Col-0 and *wus-101* root explants cultured at indicated time-points on SIM. Chlorophyll *a* and *b* contents are indicated in black and gray bars, respectively (**a**, **d**). Data shown are the mean \pm SD of biological triplicates and statistical significance was determined by student's *t* test ($*p < 0.05$)

2016). Ct values obtained from three biological replicates were normalized to *TUBULIN3* and *ELONGATION FACTOR 1a* as a reference. Relative expression values were determined as reported (Vandesompele et al. 2002).

Results

WUS expression and de novo SAM formation are coupled in altered cytokinin response mutants

We previously showed that loss-of-function mutants with altered cytokinin responses have a positive correlation among greening of calli, SAM marker expression and de novo shoot formation observed in the tissue culture system.

Cytokinin receptor double mutant, *cre1-2; ahk3-8*, had reduced sensitivity to cytokinin, thus showing substantially reduced chlorophyll contents, compromised *WUS* expression, and reduced shoot regeneration efficiency (Kubalová and Ikeda 2017). On the contrary, *pickle (pk1)/cytokinin hypersensitive 2 (ckh2)* mutant, in which a CHD3 SWI/SNF2 chromatin remodeler is disrupted, exhibited cytokinin hypersensitivity in CIM (Furuta et al. 2011), as well as in SIM culture (Kubalová and Ikeda 2017). In this study, we assessed these phenotypes by employing quantitative RT-PCR for examining *WUS* expression and by counting regenerated shoots from day 10 to 22 SIM incubation. *cre1-2; ahk3-8* root explants accumulated 54% of chlorophyll contents relative to that in the wild-type (Fig. 1a), reduced *WUS* expression (Fig. 1b) and never regenerated shoots

during SIM incubation (Fig. 1c). On the other hand, *pkl-1* root explants accumulated chlorophylls by 2.1 fold (Fig. 1a), had 6.03 fold higher *WUS* expression (Fig. 1b), and developed shoots earlier and more effectively (Fig. 1c). Thus, we could confirm the positive correlation between cytokinin perception and all cytokinin-related phenotypes observed in SIM culture. Next, we explored the relationship between greening of calli and nascent SAM development by employing *wus-101*. Chlorophyll accumulation was not affected by *wus-101* mutation (Fig. 1d). The transcript level of *WUS* in *wus-101* was undetectable (Fig. 1e). Consistent with the previous report (Zhang et al. 2017), shoot regeneration efficiency was substantially reduced in *wus-101* (Fig. 1f). These results suggest that chlorophyll accumulation is independent of *WUS* activity whereas *WUS* expression and shoot regeneration appear to be more tightly coupled with each other.

***WUS* expression is not correlated with de novo SAM formation in mutants defective in tetrapyrrole biosynthesis**

We further explored the relationship between chlorophyll accumulation and *WUS* expression by employing

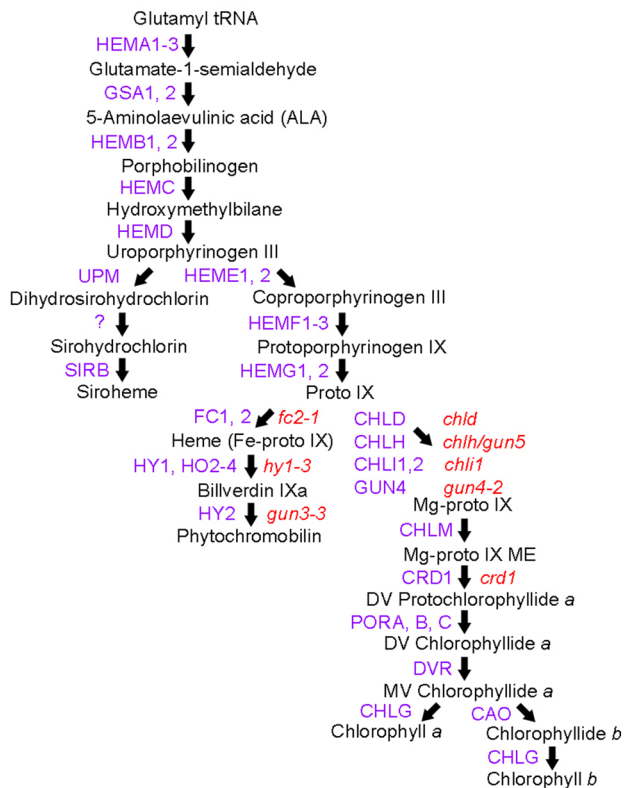


Fig. 2 Tetrapyrrole biosynthesis pathway. The tetrapyrrole biosynthesis pathway is adapted from Tanaka et al. (2011). Names of precursors and end products are indicated with black. Names of enzymes and mutants used in this study are highlighted in purple and red, respectively. (Color figure online)

loss-of-function mutants defective in tetrapyrrole biosynthesis; *fc2-1*, *hyl-3*, *gun3-3*, *gun4-2*, *chld*, *chlh*, *chli1*, and *crd1* (Fig. 2). In uncharacterized novel T-DNA insertion alleles, *chld* and *gun3-3*, endogenous *CHLD* or *GUN3* mRNA in the respective mutant was undetectable, suggesting that they are likely null alleles (Supplemental Fig. 1). FERROCHELATASE 2 (FC2), LONG HYPOCOTYL 1 (HY1), and GENOME-UNCOUPLED 3 (GUN3) belong to the heme/bilin branch. MAGNESIUM CHELATASE-D (CHLD), -H (CHLH), -I1 (CHLI1) subunits, GENOME-UNCOUPLED 4 (GUN4), and COPPER RESPONSE DEFICIENT 1 (CRD1) belong to the chlorophyll branch (Fig. 2). As reported previously, we found significantly reduced chlorophyll contents in all mutant root explants on day 15 of SIM culture, especially for those defective in chlorophyll branch (Fig. 3a). Surprisingly, the level of *WUS* transcripts in *hyl-3*, *gun4-2*, *chlh*, and *chli1* was elevated (Fig. 3b), although the shoot regeneration efficiency is substantially declined (Fig. 3c–f). *fc2-1* was the only one among mutants defective in tetrapyrrole biosynthesis exhibiting the decreased *WUS* expression with compromised shoot regeneration (coupled phenotype) when the number of developed shoots producing true leaves was counted at various time points during SIM incubation (Fig. 3c, d). Shoot regeneration efficiency, as well as an average number of shoots per root explants, were reduced in all tetrapyrrole mutants (Fig. 3c–f), suggesting that chlorophyll accumulation appeared to be important for sustaining shoot regeneration capacity. Thus, in *hyl-3*, *gun4-2*, *chlh*, and *chli1* mutant root explants the *WUS* expression is not related to shoot regeneration.

Discussion

Given the fact that cytokinin-related phenotypes observed at an early phase in SIM culture (greening of tissue, gene expression, and shoot regeneration) have been studied individually, we exerted our efforts on addressing how such phenotypes are coordinated as a whole. In fact, our genetic evidence confirmed that cytokinin-stimulated phenotypes are coupled to cytokinin perception (Fig. 1). In this study, we found that chlorophyll accumulation does not require *WUS* activity. This is in agreement with the finding that *WUS* expression is confined within the organizing center of developing SAM whereas greening takes place in much wider region of cultured root explant. On the other hand, the finding that all the tetrapyrrole mutants with reduced chlorophyll contents had compromised shoot regeneration efficiency suggests that the level of chlorophyll contents and shoot regeneration are moderately related to each other (Fig. 3). Loss-of-function mutants in Heme branch are deficient in a wide range of phytochrome-mediated responses and those in chlorophyll branch have impaired photosynthesis activities,

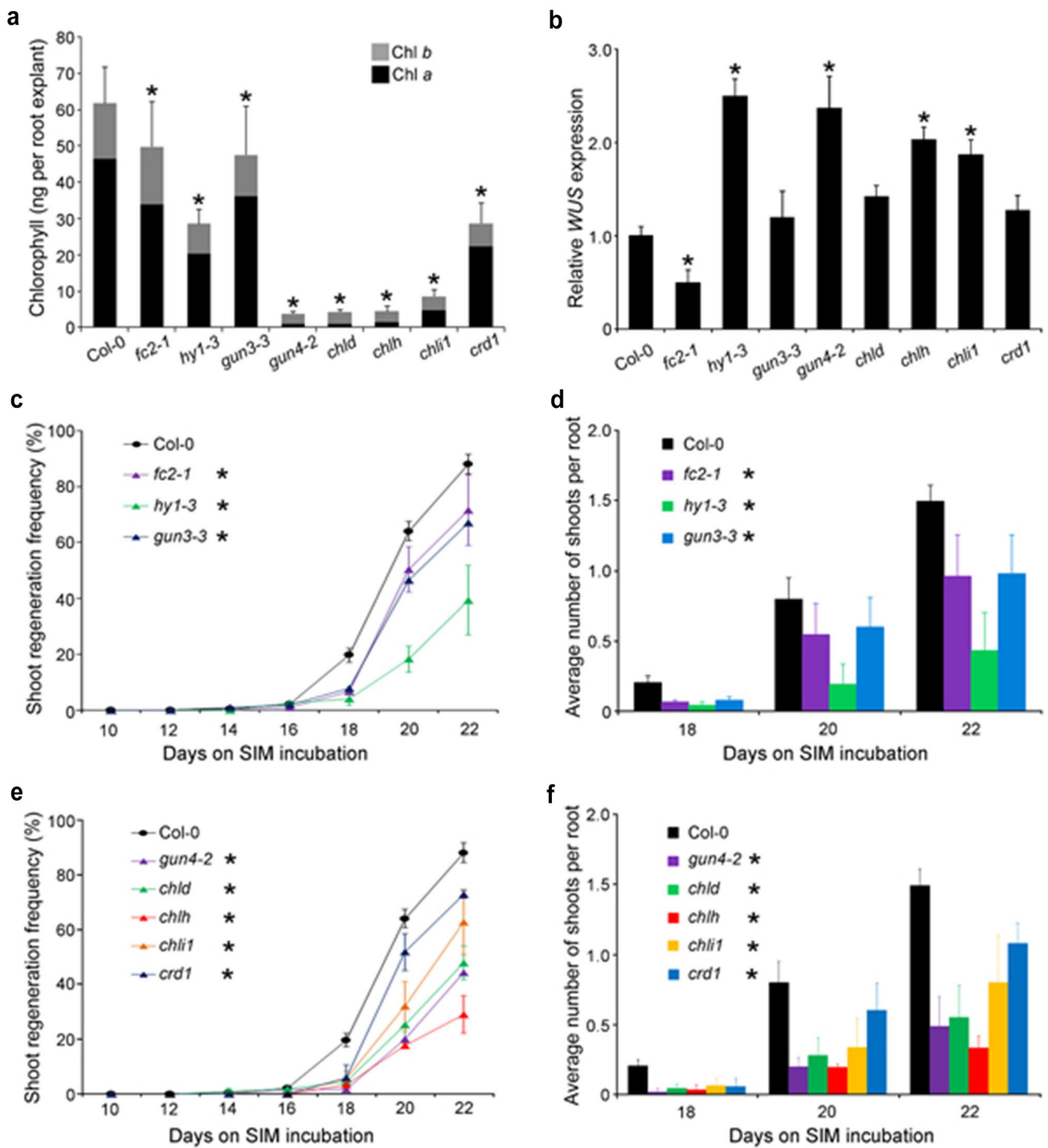


Fig. 3 *WUS* expression and *de novo* SAM formation are uncoupled in altered tetrapyrrole mutants. **a** Chlorophyll contents of Col-0, *fc2-1*, *hy1-3*, *gun3-3*, *gun4-2*, *chld*, *chlh*, *chli1*, and *crd1* root explants cultured on SIM for 15 days. **b** Relative *WUS* expression in Col-0, *fc2-1*, *hy1-3*, *gun3-3*, *gun4-2*, *chld*, *chlh*, *chli1*, and *crd1* root explants cultured on SIM for 5 days quantified by qRT-PCR. **c** Shoot regeneration frequency in Col-0, *fc2-1*, *hy1-3*, and *gun3-3* root explants cultured at indicated time-points on SIM. **d** Shoot regeneration frequency in

Col-0, *gun4-2*, *chld*, *chlh*, *chli1*, and *crd1* root explants cultured at indicated time-points on SIM. **e** Average number of shoots per root explant in Col-0, *fc2-1*, *hy1-3*, and *gun3-3*. **f** Average number of shoots per root explant in Col-0, *gun4-2*, *chld*, *chlh*, *chli1*, and *crd1*. Chlorophyll *a* and *b* contents are indicated in black and gray bars, respectively (**a**). Data shown are the mean \pm SD of biological triplicates and statistical significance was determined by student's *t* test ($*p < 0.05$)

which accounts for reduced shoot regeneration. It is widely recognized that de novo SAM development is coupled to *WUS* activity. Indeed, we confirmed it in mutants with altered cytokinin perception as well as in *wus-101* (Fig. 1). However, to our surprise, four out of eight tetrapyrrole mutants examined in this study exhibited increased *WUS* expression in a reduced number of SAM (Fig. 3c–f).

Plastid-to-nucleus communication, termed retrograde signaling, has been known to regulate gene expression, RNA turnover and splicing (reviewed in Chan et al. 2016; Larkin 2016). Nuclear-encoded genes involved in photosynthesis, stress, and ABA have been shown to be under the control of retrograde signaling (Larkin 2016). In the case of *gun* mutant screens, photosynthesis-related nuclear gene expression is monitored when chloroplast biogenesis is blocked by norflurazon treatment (Susek et al. 1993; Mochizuki et al. 2001; Larkin et al. 2003; Woodson et al. 2011). We monitored nuclear *WUS* expression when the etioplast-to-chloroplast transition is stimulated by cytokinin supplied in SIM culture. It is noteworthy that, although cytokinin treatment has an opposite effect to that of norflurazon on plastid development, three out of four mutants exhibiting increased *WUS* expression in reduced number of de novo SAM are *gun* mutants (*hyl/gun2*, *gun4*, *chlh/gun5*). We found that *hyl-3* exhibited the most contrasting responses to cytokinin—the highest *WUS* expression and the lowest shoot regeneration (Fig. 3). The positive and tight correlation between *WUS* expression and SAM activity has been documented by numerous studies. Our genetic analyses suggest that such coordination is, in part, through the regulation of tetrapyrrole pathway. Further studies such as histological analyses of de novo SAM in the mutants and measurements of tetrapyrrole intermediates are within our reach.

Acknowledgements This work was supported by Grant Agency in the Czech Republic (GAČR17-23702S and GAČR 18-23972Y) and the European Regional Development Fund (ERDF) Project (No. CZ.02.1.01/0.0/0.0/16_019/0000827). We thank European Arabidopsis Stock Centre (NASC) and Tatsuo Kakimoto for providing *cre1-2* mutant seeds.

Author contributions IK, DZ, AM, and YI carried out experiments and wrote the manuscript.

Compliance with ethical standards

Conflict of interest The authors declare that they have no conflict of interest.

References

Atta R, Laurens L, Boucheron-Dubuisson E, Guivarc'h A, Carnero E, Giraudat-Pautot V, Rech P, Chriqui D (2009) Pluripotency of

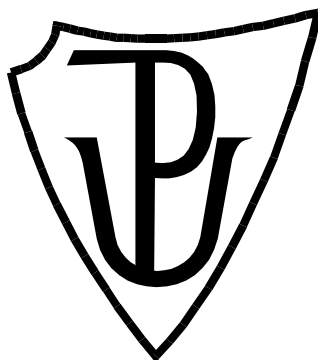
- Arabidopsis* xylem pericycle underlies shoot regeneration from root and hypocotyl explants grown in vitro. *Plant J* 57:626–644
- Chan KX, Phua SY, Crisp P, McQuinn R, Pogson BJ (2016) Learning the languages of the chloroplast: retrograde signaling and beyond. *Annu Rev Plant Biol* 67:25–53
- Cheng J, He CX, Zhang ZW, Xu F, Zhang DW, Wang X, Yuan S, Lin HH (2011) Plastid signals confer *Arabidopsis* tolerance to water stress. *Z Naturforsch C* 66:47–54
- Chory J, Reinecke D, Sim S, Washburn T, Brenner M (1994) A role for cytokinins in de-etiolation in *Arabidopsis* (det mutants have an altered response to cytokinins). *Plant Physiol* 104:339–347
- Cortleven A, Marg I, Yamburenko MV, Schlicke H, Hill K, Grimm B, Schaller GE, Schmulling T (2016) Cytokinin regulates the etioplast-chloroplast transition through the two-component signaling system and activation of chloroplast-related genes. *Plant Physiol* 172:464–478
- Furuta K, Kubo M, Sano K, Demura T, Fukuda H, Liu YG, Shibata D, Kakimoto T (2011) The CKH2/PKL chromatin remodeling factor negatively regulates cytokinin responses in *Arabidopsis calli*. *Plant Cell Physiol* 52:618–628
- Huang YS, Li HM (2009) Arabidopsis CHLI2 can substitute for CHLI1. *Plant Physiol* 150:636–645
- Inoue T, Higuchi M, Hashimoto Y, Seki M, Kobayashi M, Kato T, Tabata S, Shinozaki K, Kakimoto T (2001) Identification of CRE1 as a cytokinin receptor from *Arabidopsis*. *Nature* 409:1060–1063
- Kubalová I, Ikeda Y (2017) Chlorophyll measurement as a quantitative method for the assessment of cytokinin-induced green foci formation in tissue culture. *J Plant Growth Regul* 36:516–521
- Larkin RM (2016) Tetrapyrrole signaling in plants. *Front Plant Sci* 7:1586. <https://doi.org/10.3389/fpls.2016.01586>
- Larkin RM, Alonso JM, Ecker JR, Chory J (2003) GUN4, a regulator of chlorophyll synthesis and intracellular signaling. *Science* 299:902–906
- Lee DK, Parrott DL, Adhikari E, Fraser N, Sieburth LE (2016) The mobile bypass signal arrests shoot growth by disrupting shoot apical meristem maintenance, cytokinin signaling, and *WUS* transcription factor expression. *Plant Physiol* 171:2178–2190
- Li W, Liu H, Cheng ZJ, Su YH, Han HN, Zhang Y, Zhang XS (2011) DNA methylation and histone modifications regulate de novo shoot regeneration in *Arabidopsis* by modulating WUSCHEL expression and auxin signaling. *PLoS Genet* 7:e1002243. <https://doi.org/10.1371/journal.pgen.1002243>
- Meng WJ, Cheng ZJ, Sang YL, Zhang MM, Rong XF, Wang ZW, Tang YY, Zhang XS (2017) Type-B *Arabidopsis* response regulators specify the shoot stem cell niche by dual regulation of WUSCHEL. *Plant Cell* 29:1357–1372
- Miller C, Skoog F, Von Saltza M, Strong F (1955) Kinetin, a cell division factor from deoxyribonucleic acid. *J Am Chem Soc* 77:1392
- Mochizuki N, Brusslan JA, Larkin A, Nagatani A, Chory J (2001) Arabidopsis genomes uncoupled 5 (GUN5) mutant reveals the involvement of Mg-chelatase H subunit in plastid-to-nucleus signal transduction. *Proc Natl Acad Sci USA* 98:2053–2058
- Mochizuki N, Tanaka R, Tanaka A, Masuda T, Nagatani A (2008) The steady-state level of Mg-protoporphyrin IX is not a determinant of plastid-to-nucleus signaling in *Arabidopsis*. *Proc Natl Acad Sci USA* 105:15184–15189
- Motte H, Vercauteren A, Depuydt S, Landschoot S, Geelen D, Werbrouck S, Goormachtig S, Vuylsteke M, Vereecke D (2014a) Combining linkage and association mapping identifies receptor-like protein kinase1 as an essential *Arabidopsis* shoot regeneration gene. *Proc Natl Acad Sci USA* 111:8305–8310
- Motte H, Vereecke D, Geelen D, Werbrouck S (2014b) The molecular path to in vitro shoot regeneration. *Biotechnol Adv* 32:107–121
- Ogas J, Cheng JC, Sung ZR, Somerville C (1997) Cellular differentiation regulated by gibberellin in the *Arabidopsis thaliana* pickle mutant. *Science* 277:91–94

- Perianez-Rodriguez J, Manzano C, Moreno-Risueno MA (2014) Post-embryonic organogenesis and plant regeneration from tissues: two sides of the same coin? *Front Plant Sci* 5:219. <https://doi.org/10.3389/fpls.2014.00219>
- Peter E, Grimm B (2009) GUN4 is required for posttranslational control of plant tetrapyrrole biosynthesis. *Mol Plant* 2:1198–1210
- Skoog F, Miller CO (1957) Chemical regulation of growth and organ formation in plant tissues cultured in vitro. *Symp Soc Exp Biol* 11:118–130
- Sugimoto K, Jiao Y, Meyerowitz EM (2010) Arabidopsis regeneration from multiple tissues occurs via a root development pathway. *Dev Cell* 18:463–471
- Susek RE, Ausubel FM, Chory J (1993) Signal transduction mutants of Arabidopsis uncouple nuclear CAB and RBCS gene expression from chloroplast development. *Cell* 74:787–799
- Tanaka R, Kobayashi K, Masuda T (2011) Tetrapyrrole metabolism in *Arabidopsis thaliana*. *Arabidopsis Book* 9:e0145. <https://doi.org/10.1199/tab.0145>
- Tsuzuki T, Takahashi K, Inoue S, Okigaki Y, Tomiyama M, Hossain MA, Shimazaki K, Murata Y, Kinoshita T (2011) Mg-chelatase H subunit affects ABA signaling in stomatal guard cells, but is not an ABA receptor in *Arabidopsis thaliana*. *J Plant Res* 124:527–538
- Valvekens D, Montagu MV, Van Lijsebettens M (1988) *Agrobacterium tumefaciens*-mediated transformation of *Arabidopsis thaliana* root explants by using kanamycin selection. *Proc Natl Acad Sci USA* 85:5536–5540
- Vandesompele J, De Preter K, Pattyn F, Poppe B, Van Roy N, De Paepe A, Speleman F (2002) Accurate normalization of real-time quantitative RT-PCR data by geometric averaging of multiple internal control genes. *Genome Biol* 3:0034
- Woodson JD, Perez-Ruiz JM, Chory J (2011) Heme synthesis by plastid ferrochelatase 1 regulates nuclear gene expression in plants. *Curr Biol* 21:897–903
- Zhang TQ, Lian H, Zhou CM, Xu L, Jiao Y, Wang JW (2017) A two-step model for de novo activation of WUSCHEL during plant shoot regeneration. *Plant Cell* 29:1073–1087
- Zhao X, Bramsiepe J, Van Durme M, Komaki S, Prusicki MA, Maruyama D, Forner J, Medzihradzky A, Wijnker E, Harashima H, Lu Y, Schmidt A, Guthorl D, Logrono RS, Guan Y, Pochon G, Grossniklaus U, Laux T, Higashiyama T, Lohmann JU, Nowack MK, Schnittger A (2017) Retinoblastoma Related1 mediates germline entry in *Arabidopsis*. *Science*. <https://doi.org/10.1126/science.aaf6532>

Publisher's Note Springer Nature remains neutral with regard to jurisdictional claims in published maps and institutional affiliations.

PALACKÝ UNIVERSITY OLMOUC

Faculty of Science



SUMMARY OF THE DOCTORAL THESIS

Genetic Control of Pluripotency in Plant

P1406-Biochemistry

Ivona Kubalová

Olomouc 2019

The experiments included in this Ph.D. thesis have been performed in the laboratories of Department of Molecular Biology, Centre of the Region Haná for Biotechnological and Agricultural Research (Palacký University Olomouc) under the supervision of Dr. Yoshihisa Ikeda in the period September 2013-September 2018.

Ph.D. candidate: Mgr. Ivona Kubalová
Department of Biochemistry,
Centre of the Region Haná for Biotechnological and Agricultural Research,
Faculty of Science, Palacký University Olomouc
Šlechtitelů 27, 78371 Olomouc, Czech Republic
e-mail: ivona.kubalova@upol.cz

Supervisor: Yoshihisa Ikeda, Ph.D.
Centre of the Region Haná for Biotechnological and Agricultural Research,
Faculty of Science, Palacký University Olomouc
Šlechtitelů 27, 78371 Olomouc, Czech Republic
e-mail: yoshihisa.ikeda@upol.cz

Reviewers: Prof. Andreas Houben
Institute of Plant Genetics and Crop Plant Research (IPK)
Chromosome Structure and Function
Corrensstrasse 3, D-06466 Gatersleben, Germany
e-mail: houben@ipk-gatersleben.de

Prof. Takashi Aoyama
Institute for Chemical Research
Kyoto University, Gokasho
Uji, Kyoto, 611-0011, Japan
e-mail: aoyama@scl.kyoto-u.ac.jp

Table of Contents

Abstract	4
Abstrakt	5
Aims of Work	6
Introduction	7
PART I – Placing ERF transcriptional repressors into genetic framework regulating Shoot Apical Meristem development	8
1 Introduction.....	8
2 Material and Methods.....	12
3 Results	12
3.1 Selection of T-DNA insertion lines of <i>ERF</i> and <i>BPM</i> genes.....	12
3.2 Proteolysis is essential for the correct development.....	12
3.3 ERF proteins can interact with BPM adaptor proteins of E3 ligase.....	13
3.4 Evaluation of shoot regeneration in higher-order mutants.....	14
3.5 Quadruple mutant in <i>ERF</i> genes could partially rescue aberrant SAM in <i>wuschel</i> mutant	15
3.6 Higher-order <i>erf</i> mutants show display alteration in relative <i>CUC1</i> and <i>STM</i> gene expression	15
3.7 Expression pattern and sub-cellular localization of ERF4.....	16
3.8 ERF4 is more often associated with the active than with inactive RNAPoIII variant	16
3.9 The impact of ERF4 on the acetylation of histone H3.....	17
4 Discussion.....	19
4.1 Proper proteolysis of transcriptional factors is essential for correct plant development	19
4.2 <i>WUSCHEL</i> -independent pathway	20
4.3 Role of ERF4 in gene expression regulation	21
PART II – Chlorophyll Measurement as a Quantitative Method for the Assessment of Cytokinin-Induced Green Foci Formation in Tissue Culture	23
5 Introduction.....	23
6 Materials and methods	23
7 Results	23
8 Discussion.....	26
PART III – Mutations in Tetrapyrrole Biosynthesis Pathway Uncouple Nuclear <i>WUSCHEL</i> Expression from <i>de novo</i> Shoot Development in <i>Arabidopsis</i>	27
9 Introduction.....	27
10 Materials and Methods	27
11 Results	27

11.1	WUS expression and de novo SAM formation are coupled in altered cytokinin response mutants	27
11.2	WUS expression is uncoupled from de novo SAM formation in mutants defective in tetrapyrrole biosynthesis	29
12	Discussion	31
	Conclusions	32
	References	34
	Curriculum vitae	37

Abstract

People were fascinated by immortality accompanied by renewal of old and sick tissue since ancient times. Plants are a shining example of regeneration ability. Their competence to produce new cells, tissues and thus replenish the old organs throughout plant lifespan is of interest for science. Just a few decades ago the molecular mechanisms behind these processes started to be unveiled and *WUSCHEL* being the key player.

Here we elaborated a *WUSCHEL*-independent pathway of shoot apical meristem (SAM) positioning and maintenance and proposed ETHYLENE RESPONSIVE FACTOR (ERF) transcriptional repressors as novel components regulating this pathway. The quintuple *wus;erf4-1;8;9-1;10;11-2;12* could restore the SAM formation throughout the vegetative growth in *wus* mutant background. The expression profile of *CUC1*, *STM*, *ESR1*, and *ESR2* in *erf4-1;8;9-1;11-2;12* and *erf4-1;8;9-1;10;12* mutants was also investigated. The elevated relative expression of these SAM regulators was detected.

Further, we showed that ERF4 is predominantly localized in nuclear euchromatin and it is excluded from heterochromatin. ERF4 did not localize in nuclear bodies. Also, we have found out that ERF4 might influence the histone 3 acetylation status of its target genes.

Turnover of ERF proteins is essential for the accurate activity of this pathway. Ubiquitin-mediated protein degradation seems to be the limiting step regulating the ERF's function.

Additionally, we extended our recent knowledge of *WUSCHEL* regulation as we showed the importance of plastid-to-nucleus communication on nuclear *WUSCHEL* expression. Therefore, we established a new high-throughput method for chlorophyll quantification from single root explants. Using different mutants in tetrapyrrole biosynthesis we identified Heme as a plausible candidate molecule of retrograde signaling.

Abstrakt

Nesmrtelnosť spojená s obnovou starých a poškodených tkanív fascinovala ľudí od nepamäti. Žiarivým príkladom regenerácie sú rastliny. Ich schopnosť nahrádzať staré orgány novými bunkami a pletivami stojí dlhodobo v pozornosti vedy. Len pred niekoľkými desaťročiami odhalilo štúdium zamerané na molekulárne mechanizmy podmieňujúce regeneračný proces WUSCHEL proteín ako kľúčový komponent.

V tejto práci sme rozvinuli WUSCHEL nezávislú dráhu, ktorá prispieva k správne umiestneniu a udržiavaniu apikálneho meristému stonky. Navrhli sme ETHYLENE RESPONSIVE FACTOR (ERF) transkripčné faktory ako nové komponenty regulujúce túto dráhu. Štvornásobný *wus;erf4-1;8;9-1;10;11-2;12* mutant dokázal produkovať apikálny meristém stonky počas vegetatívnej fázy rastu aj napriek chýbajúcemu WUS. Tiež sme analyzovali expresný profil *CUC1*, *STM*, *ESR1* a *ESR2* génov v *erf4-1;8;9-1;11-2;12* a *erf4-1;8;9-1;10;12* mutantnej línii a zistili sme zvýšenú relatívnu expresiu meristemických regulátorov.

Následne sme ukázali, že ERF4 lokalizuje v euchromatíne v rámci jadra a je vylúčený z heterochromatínu. ERF4 nie je umiestnený v jadrových telieskach. Tiež sme zistili, že ERF4 môže ovplyvniť acetylačný stav svojich cieľových génov.

Optimálna aktivita tejto dráhy závisí od vzniku a zániku ERF proteínov. Ubikvitínom sprostredkovaná proteínová degradácia je pravdepodobne krok, ktorý limituje funkciu ERF proteínov.

Zároveň sme rozšírili súčasnú problematiku regulácie WUSCHEL a ukázali sme dôležitosť komunikácie z plastidov do jadra a jej vplyv na expresiu WUSCHEL. Stanovili sme novú metódu na rýchlu kvantifikáciu chlorofylu z jedného koreňového odrezku. Analýzou rozličných mutančných línii v biosyntéze tetrapyrolu sme identifikovali hem ako možnú kandidátnu molekulu retrográdnej signalizácie.

Aims of Work

- literature review
- preparation of higher-order mutants and evaluation of their shoot regeneration efficiency phenotype
- placing ERF transcriptional repressors into the regulatory network of the shoot apical meristem development
- sub-cellular localization of ERF4 and monitoring the acetylation status of histone H3 in cells overexpressing *ERF4*
- establishment of a high-throughput method for chlorophyll measurements from single root explants
- study of WUSCHEL regulation in tetrapyrrole mutants

Introduction

Plants as sessile organisms had to evolve an effective system of how to cope with changing environmental cues. In contrast to animals, that usually lack the pluripotent stem cells after establishment of their body; plants retain pluripotent stem cells and therefore are able to produce new tissue and organs through their whole lifespan. The source for new organs and tissues are pluripotent stem cells which can replenish any given type of plant cells. They are located in a specialized microenvironment called stem cell niche, which is a part of a meristem, a place where all new organs and tissues are established. There are three different meristem types: shoot, root, and vasculature meristems. Shoot and root meristems are situated at opposite ends of the plant body, therefore known as a shoot apical meristem (SAM) and a root apical meristem (RAM) (Heidstra and Sabatini, 2014).

Phytohormones play an eminent role in mediating responses to the external and internal stimuli as well as in coordinating plant development. The key players in this process are auxin (AUX) and cytokinin (CK). An effective approach to study plant development, including regeneration and gene expression profiling, is an *in vitro* tissue culture system manipulated by phytohormones. Tissue culture systems are broadly used in the laboratories. The employment of this tool can help to better understand the pluripotency and regeneration programs *in planta*.

Gene expression is controlled by transcription factors which can act in a positive or negative manner. Negative regulators, so-called transcriptional repressors, often form complexes with co-repressors and thus moderate the expression of the target genes. Fine-tuning of gene expression is mediated by epigenetic modification of chromatin, including conformational changes (chromatin remodeling) or chemical modification of DNA (methylation) or histones (histone acetylation, methylation, and phosphorylation) (Reynolds et al., 2013; Wang et al., 2016). Additionally, the non-coding RNAs were shown to contribute to the epigenetic regulation of gene transcription (Heo and Sung, 2011; Deforges et al., 2019). An important factor influencing the ability to repress gene expression is the repressor stability and its accumulation.

Master key regulator of the regeneration is the transcription factor WUSCHEL (WUS) and its regulation seems to be crucial for a correct SAM development (Laux et al., 1996). The proper spatial-temporal gene expression plays an important role during plant development.

However, increasing evidence strongly implies the existence of WUSCHEL-independent pathways regulating SAM positioning and maintenance. Despite the fact that the WUS-dependent pathway is of main interest for several decades (Laux et al., 1996; Baurle, 2005; Snipes et al., 2018), the WUS regulation is still not completely understood. *De novo* shoot regeneration is induced by a higher concentration of cytokinins. It is well known that cytokinins affect plant development in three aspects 1) by promoting shoot regeneration, 2) by etioplast to chloroplast transition, and 3) by changing nuclear gene expression. Although it was previously shown that plastid-to-nucleus signalization controls the expression of genes involved in photosynthesis (Susek et al., 1993; Woodson et al., 2011) little is known whether and how plastid-to-nucleus signaling is involved in the regulation of genes responsible for the SAM development.

PART I – Placing ERF transcriptional repressors into genetic framework regulating Shoot Apical Meristem development

1 Introduction

The adult body consists of stem cells sustaining different levels of regeneration capacity. The classification based on animal stem cell research recognizes totipotent, pluripotent, multipotent, and pluripotent stem cells. Definition of plant stem cells is taken from the animal terminology, hence it does not fit perfectly. Meristematic plant stem cells can give rise to all cell types of above-ground tissue and root but their behavior resembles more multipotent animal stem cells (Gaillochet and Lohmann, 2015). Verdail et al. (2007) proposed an extended plant stem cell concept. In accordance with this concept, single somatic cells can de-differentiate to a totipotent embryonic cell under certain conditions. Thus, a totipotent cell can lead to the whole plant body through somatic embryogenesis.

Tissue culture under controlled sterile conditions represents an elegant system for plant regeneration. Excised plant tissues are cultivated on a growth medium with a defined composition. This system is based on the ability of phytohormones to determine plant cell fate (Kumar and Loh, 2012). In principle, the plant cell identity can be manipulated by different ratios of two plant hormones; auxin and cytokinin. The tissue culture system became a powerful tool for studying plant development since its establishment in the 1950s (Valvekens et al., 1988)

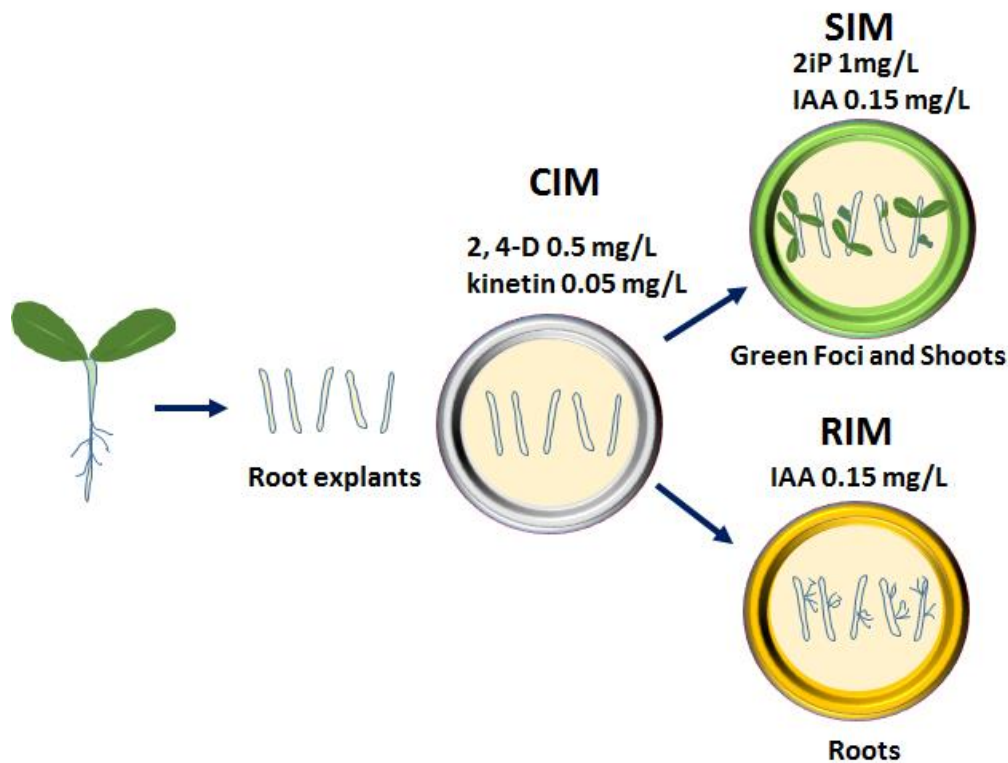


Figure 1 Tissue culture system.

Interestingly, xylem pericycle, but not phloem pericycle, could give rise to shoots without prior callus inducing medium (CIM) incubation, when grown on CK rich medium (Atta et al., 2009). This indicates that pericycle cells sustain pluripotency. Moreover, pericycle cells retain a diploid status and do not undergo multiple rounds of endoreduplication. This attribute allows them to re-enter the cell cycle and to regenerate meristems (Atta et al., 2009). The protuberances emerging from the root and hypocotyl explants cultivated on CIM resemble a lateral root meristem (LRM). After transfer to shoot inducing medium (SIM), the LRM-like structures develop into shoots. Thus the authors proposed that SAM regeneration during shoot regeneration process is a result of re-determination of LRM-like primordia and not de-differentiation process (reprogramming process back to an undifferentiated stage) (Atta et al., 2009).

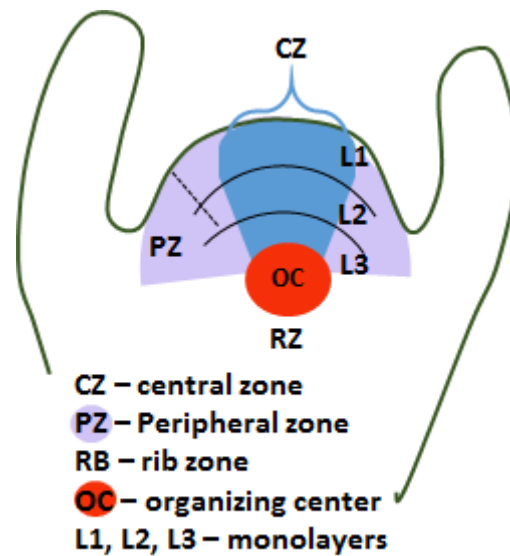


Figure 2: Schematic representation of the shoot apical meristem (SAM).

Each zone in the shoot apical meristem (SAM) is specified by a different composition of hormones and regulatory components. The ability to maintain a balance between the differentiated and stem cells requires precise control. Key components of this process are two homeobox-containing transcription factors *WUSCHEL* and *SHOOT MERISTEMLESS (STM)*.

WUSCHEL encodes a homeodomain-containing transcription factor and is a founder member of the *WUSCHEL-RELATED HOMEODOMAIN (WOX)* gene subfamily (Mayer et al., 1998; Haecker et al., 2004). Loss of function mutation of *WUS* leads to the developmental defects in the shoot and floral meristems (Laux et al., 1996). *WUS* is specifically expressed in the organizing center (OC) and is responsible for maintaining the stem cell niche (Mayer et al., 1998). *WUS* protein acts cell-non-autonomously and moves to stem cells where it triggers the so-called CLAVATA (CLV) pathway which restricts *WUS* expression. The *WUS* – CLV negative feedback has an important impact on maintaining SAM size and stem cells number (Yadav et al., 2011).

STM is a member of the class I *KNOTTED1*-like homeobox (*KNOX*) gene family. Unlike *WUS*, which is expressed only in a distinct zone, the *STM* is expressed all over the SAM (Long et al., 1996). *STM* is a small protein moving from cell to cell. Even though there is no difference between mRNA and *STM*

protein localization, the movement has been shown to be essential for its proper function to maintain meristem and to define the meristem-organ boundary zone (Balkunde et al., 2017).

Members of the *ETHYLENE RESPONSIVE FACTOR (ERF)* gene family create a big group of transcription factors. They are part of the *APETALA2/ETHYLENE RESPONSIVE FACTOR (AP2/ERF)* superfamily. Each member contains at least one copy of the AP2/ERF domain at the N-terminus. This DNA binding domain recognizes CGGCGG cis-element (GCC-box) in the sequence of the target loci (Nakano et al., 2006; Ohme-Takagi and Shinshi, 1995).

Proper development requires maintenance of an internal environment of the organism in a balanced state. This process is known as homeostasis and includes also a mechanism specialized for proteins, referred to as proteostasis. It includes protein synthesis, folding, trafficking, interaction, and proteolysis. There are two ways of how proteins can be degraded. While long-living proteins tend to be degraded in the lysosomes, short-living proteins are eliminated through the Ubiquitin-26S Proteasome System (UPS)(Figure3) (Jackson and Hewitt, 2016)

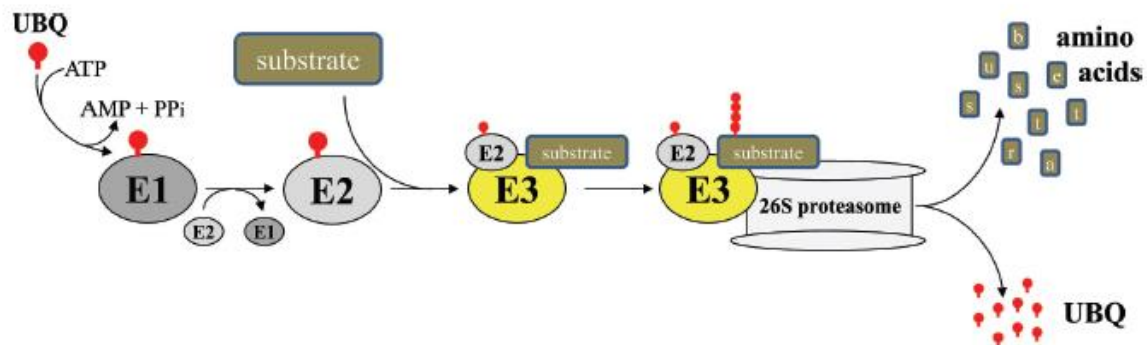


Figure 3: Schematic model of the polyubiquitination mediated proteasomal degradation.

In recent years, few studies tried to shed light on the role of CUL3 – RING E3s complex (Mazzucotelli et al., 2006; Chen et al., 2013). In *Arabidopsis*, there are two *CUL3* genes with redundant function, *CUL3A*, and *CUL3B*. They share 88 % similarity and at least one gene is required for proper embryo development. Loss of function mutation of both genes is embryonic-lethal (Figuroa et al., 2005). CUL3 interacts *via* its C-terminal region with RBX1. The N-terminus is responsible for binding BTB/POZ domain-containing proteins (Figuroa et al., 2005; Gingerich et al., 2005). This domain is localized at the C-terminal end of the protein and additionally can serve for BTBs assembling into homo- or heterodimers. Moreover, BTB proteins can contain additional domains or motifs at the N-terminus, which act as a substrate-specific adaptor (Figure 4). Together, they form twelve subgroups. One of these groups contains the MEPRIN and IRAF (TUMOR NECROSIS FACTOR RECEPTOR-ASSOCIATED FACTOR) HOMOLOGY (MATH) at the N-terminus (Gingerich et al., 2007).

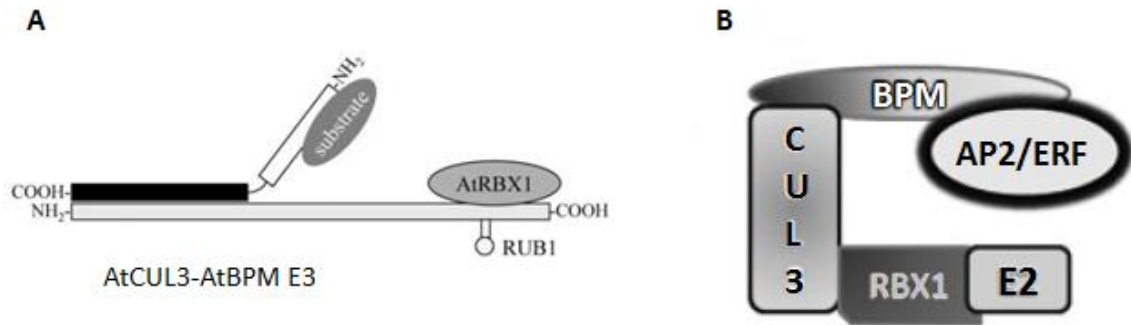


Figure 4: Schematic model of CUL3 based E3 ligase degradation of AP2/ERF proteins. Modified from Weber and Hellmann (2009).

Histones are positively charged and have a strong affinity to negatively charged DNA. Acetylation of lysine at the N-terminus neutralizes the positive charge, and thus histone-DNA binding is weakened. The relaxed chromatin structure allows easy access for components of the transcription machinery, such as RNA polymerase II, to promoter regions of genes. Highly acetylated histones are associated with actively transcribed genes, whereas hypoacetylated histones mark transcriptionally silenced loci. Several sites of histone H3 are known to be acetylated at K9, K14, K18, K23, K27, and K36. Histone acetyltransferases (HATs) add the acetyl group to lysine residues and histone deacetylases (HDAs) remove the acetyl group from the lysine residue (Pandey et al., 2002).

The mechanism by which HDAs facilitate transcriptional repression is complex. TFs, specifically recognizing cis-regulating elements in their target genes, interact with co-repressor proteins which in turn bind to HDA and thus recruit deacetylation machinery to the target loci (Figure 5)(Kagale and Rozwadowski, 2011).

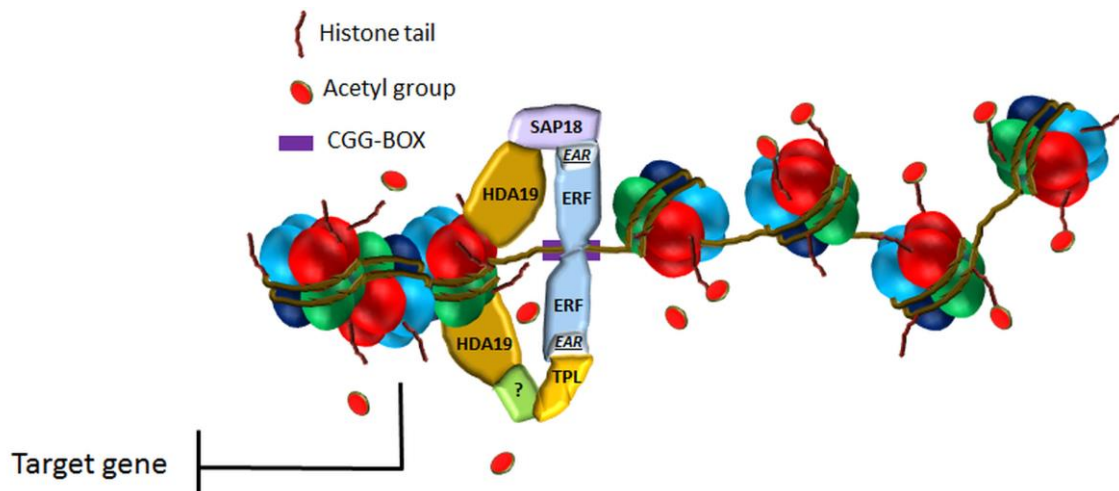


Figure 5: Model of EAR and HDA mediated repression of a target locus. Transcriptional repressor upon different signals binds to its target locus and conducts transcriptional repression through its EAR motif. Repressor binds through EAR motif to SAP18 and thus recruits co-repressor complex to the target loci. SAP 18 directly interacts with HDA19 which deacetylates histones. As a result, chromatin is closed and transcription is stopped or repressor binds through EAR motif to TPL which indirectly interacts with HDA19 through the putative adaptor. HDA deacetylates histones and gene expression is stopped.

2 Material and Methods

All used material and methods are described in detail in the Ph.D. thesis.

3 Results

3.1 Selection of T-DNA insertion lines of *ERF* and *BPM* genes

To shed a light on the role of ERF transcriptional repressors in developmental processes different mutant lines of *ERF* and *BPM* genes were used *Arabidopsis* lines mutated in *ERF* and *BPM* genes obtained from NASC were three times backcrossed with wild-type (WT) plants of Col-0 background to remove additional non-specific mutations. Each line was genotyped and then sequenced to identify the exact position of T-DNA insertion.

The expression status of the gene was estimated using semi-quantitative RT-PCR. No PCR product was detected in most of the analyzed *erf* mutant lines. Mutant lines of *erf4* (SALK_073394) denoted as *erf4-1*, *erf8* (FLAG_157D10), *erf9* (SALK_043407) denoted as *erf9-1*, *erf10* (GK-170C02), *erf11* (SALK116053) denoted as *erf11-1*, and *erf12* (SAIL_873_D11) were used for further experiments.

In the case of *BPM* genes, *bpm1* SALK_125026 and SALK_31057 lines were shown not to be knock-out lines. Interestingly, based on semi-quantitative RT-PCR, the SALK_31057 line appeared to be an overexpressor. On the other hand, *bpm2* GK-391E4 and *bpm3* GB-436E12 mutant lines were confirmed to be a complete knock-out; and *bpm3* SALK_72848 line as a knock-down line.

Higher-order mutant combinations were obtained by crossing individual single mutants followed by self-pollination. Due to the linkage of *ERF11* (At1g28370) and *ERF12* (At1g28360) genes, it was impossible to obtain double mutant using traditional crossing approach. To overcome this issue, CRISPR/Cas9 system was employed to engineer the *ERF11* gene. Since *ERF11* does not contain introns such deletion affects the coding region and results in truncation of *ERF11* protein at 25 amino acids position which is likely to be non-functional.

Because *bpm1* SALK_31057 and *bpm1* SALK_125026 mutant lines did not display complete gene disruption the CRISPR/Cas9 system was employed as well. No obvious deletion/insertion was observed in T1 transgenic plants after the PCR amplification of the sequence with the putative mutated site. The CAPS analysis did not reveal any change in sensitivity to cleavage by selected restriction enzymes. The CAPS analysis of T2 generation revealed plants partially resistant to cleavage by *EcoRI*, these plants were propagated to the next generation and sequenced to verify the homozygous state. Sequencing confirmed the one base-pair insertion in the first exon. The homozygous *bpm1* mutant plant was crossed with *bpm2* and *bpm3* mutant lines to prepare a triple mutant.

3.2 Proteolysis is essential for the correct development

Before the genetic analysis of *erf* and *bmp* higher-order mutant was carried out, a chemical treatment was conducted first to monitor the global impact of proteolysis on development. Root explants prepared from 6 day-old WT Col-0 seedlings were incubated on medium (MS, CIM, SIM) with or without MG132 proteasome inhibitor and the shoot regeneration phenotype was observed (Figure 6a). Explants grown on medium without MG132 started to green and expand their size when

transferred on SIM. After 10 days on SIM incubation first shoots started to emerge. From such regenerated explants, new roots penetrated into the medium (Figure 6c). Interestingly, no shoot regeneration was observed when explants were grown on medium with MG132. The explants were yellowish and smaller than explants grown on medium without MG132 (Figure 6b). Application of proteasome inhibitor had a clear impact on shoot regeneration and development itself. This result indicates that protein degradation is essential for the proper development of plants.

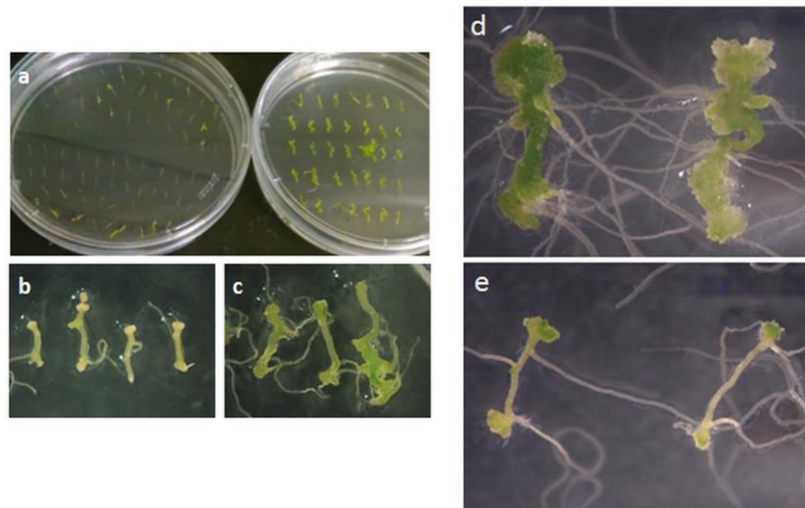


Figure 6: (a-c) Pharmacological treatment of Col-0 root explants with MG132 reduces *de novo* organogenesis (d-e) BPM E3-ligases are positive regulators of organogenesis. d) WT Col-0 e) *bmp;bpm2* double mutant

BPM proteins mediate the substrate specificity of CUL3 based E3 ligase that targets proteins for degradation *via* 26S proteasome (Gingerich et al., 2007). The previous experiment showed that impaired proteolysis has a severe effect on plant development. To investigate the role of BPM proteins in this process, *Arabidopsis bpm* mutant lines were examined in terms of shoot regeneration efficiency. Mutation in a single *BPM* gene did not cause change in phenotype (not shown), indicating gene redundancy. Therefore, the double *bpm1;bpm2* mutant was assessed in the shoot regeneration assay. In the early phase on SIM incubation explants showed altered phenotype from WT Col-0. Explants were pale, shoot formation frequency was reduced, and explants exhibited also weak lateral root system (Figure 6e). The shoot regeneration capacity was notably reduced. Root explants prepared from WT Col-0 developed normally, including greening, shoot development and large root system (Figure 14d). Double mutant phenotype partially resembled the phenotype of root explants treated with MG132.

3.3 ERF proteins can interact with BPM adaptor proteins of E3 ligase

Another task was to identify key players connecting protein degradation with target gene repression together in developmental processes. BPMs, part of E3 CUL^{BPM} complex, were shown to be positive regulators of shoot regeneration. Therefore the ERF proteins, negative regulators of gene expression, were tested to be the substrate proteins for BPMs and be targeted for protein degradation *via* 26S proteasome. Analysis of the physical interaction of ERF repressors with E3 substrate-specific E3 ligases BPMs in yeast revealed that only ERF4 and ERF8 were able to interact with BPM1 and BPM3. The ERF4dC mutant version lacking the central domain (dC) was unable to interact with E3 ligases.

Suggesting the central domain of repressors is responsible for binding to E3 ligase. ERF9, ERF10, ERF11, and ERF12 did not associate with any BPMs (Figure 7).

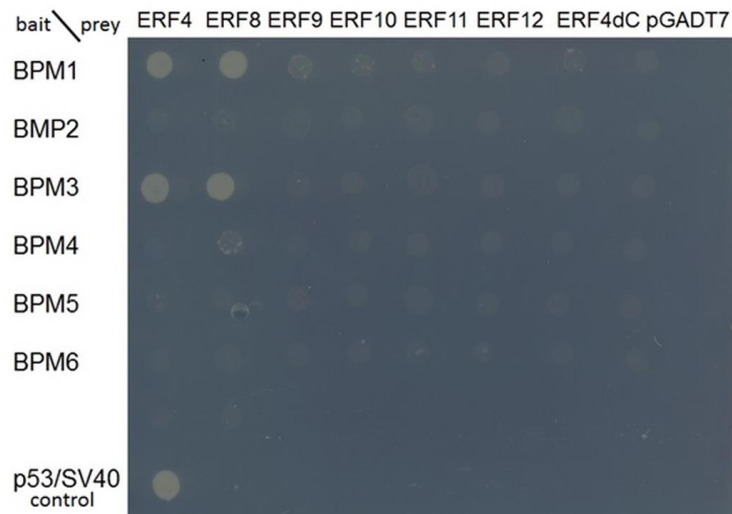


Figure 7: Interaction studies between ERF repressors and BPM E3 ligases by Y2H assays.

RNA-seq analysis revealed upregulation of 16 candidate direct-downstream target genes of *N4C2-ER* showing at least 2-fold change. Since the *N4C2-ER* is the active form of ERF4 repressor it can be assumed that these upregulated genes represent the target genes repressed by canonical ERF4. One-third of these genes are members of the AP2/ERF transcription factor family, including *ERF4*, *ERF8*, *ERF9*, and *ERF12*.

In the root explants harboring *35S::ESR2-ER*, a set of 30 genes showed at least 2-fold change; including *ERF8*, *ERF9*, and *ERF12*. The SAM marker gene *CUC1* was upregulated 2.3-fold. In comparison, the Affymetrix Arabidopsis GeneChips analysis showed 3-fold upregulation of *CUC1* in *35S::ESR2-ER* (Ikeda et al., 2006). It is likely that ESR2 directly activates *CUC1* gene.

Based on the results obtained from RNA-seq, semi-RT PCR was carried out to show changed expression of selected *ERF* genes. The cDNA prepared from five replicates of root explants harboring *35S::N4C2-ER*, *35S::ESR2-ER*, and *35S::GFP-ER* treated with β -estradiol and CHX was used. From five tested genes only *ERF9* and *ERF12* responded to ERF4 and ESR2 accumulation.

3.4 Evaluation of shoot regeneration in higher-order mutants

Higher-order mutants were subjected to shoot regeneration analysis. Root explants were incubated on SIM and *de novo* developed shoots were counted at indicated time points. First shoots started to emerge after 14 days on SIM incubation in case of WT Col-0 and sextuple mutant *erf4-1;8;9-1;10;11-2;12*. Over time the shoot regeneration frequency gradually rose and reached up to 84.86 % and 85.14 %, respectively. The mutant in the SAM master regulator, *wus*, could not regenerate shoots in the early time points, after the 26 days on SIM the shoot regeneration frequency remained still below the 10 %. The septuple *wus;erf4-1;8;9-1;10;11-2;12* mutant showed similar shoot regeneration frequency to *wus*.

To investigate the role of BPMs, the substrate-specific adaptors for E3 ligases, in shoot regeneration *6xami_bpm* (the micro RNA silencing line of *BPM 1 – 6* genes) and the *bpm1;2;3* triple mutant were examined in the shoot regeneration assay. Further, a double mutant in ERF transcriptional repressors *erf4-1;8*, the substrate of BPM proteins, and quintuple *erf4-1;8;bpm1;2;3* mutant were tested.

Four out of five genotypes started to produce shoot on day 14 on SIM, only *bpm1;2;3* mutant started to regenerate from day 16. The regeneration rate of all above-mentioned genotypes seemed to be same up to day 18 on SIM. Col-0 and *bpm1;2;3* produced more shoots from day 20 than the remaining genotypes with regeneration frequency up to 73 % after 22 days on SIM. *6xami_bpm1;2;3* displayed the slightly reduced number of shoots from Col-0 and *bpm1;2;3* but still produced more shoots than *erf4-1;8* and *erf4-1;8;bpm1;2;3*. Reduced shoot regeneration frequency from Col-0 was observed in *erf4-1;8* and *erf4-1;8;bpm1;2;3* mutant lines. *erf4-1;8* showed significantly decreased shoot regeneration frequency from Col-0 after 22 days on SIM (46.7 %), whereas *erf4-1;8;bpm1;2;3* displayed significantly reduced shoot regeneration frequency after day 20 on SIM (up to 44.86 % after 22 days on SIM), $p < 0.05$. No significant differences were observed between *erf4-1;8;bpm1;2;3* and *erf4-1;8*.

Next, another negative regulator of gene expression, HDA6, was also examined in shoot regeneration assay to test the impact of histone deacetylation on shoot development. Mutation in histone deacetylase HDA6 positively affected shoot regeneration. *hda6-6* mutant showed higher shoot regeneration efficiency than Col-0, statistically significant differences were observed from day 16 on SIM incubation and the mutant reached up to 91 % regeneration capacity ($p < 0.5$) whereas Col-0 reached up to 73 %. *bpm1;2;3* started to regenerate shoots later (day 16) than remaining genotypes (day 14). The shoot regeneration efficiency from day 18 on SIM was similar to WT Col-0. Quadruple *hda6-6;bpm1;2;3* mutant produced more shoots than *bpm1;2;3* and Col-0 but less than single *hda6-6* mutant.

3.5 Quadruple mutant in *ERF* genes could partially rescue aberrant SAM in *wuschel* mutant

Mutation in the *WUS* gene causes aberrant SAM and inflorescence meristem development resulting in plant sterility (Laux et al., 1996). When assessing *wus-101* mutant phenotype, no true leaves development was observed 9 days after germination (dag). The quadruple mutant *erf4-1;8;9-1;12* produced slightly more leaves than WT Col-0. Despite no significant changes in phenotype were observed in tissue culture system between *wus* single mutant and *wus;erf4-1;8;9-1;10;11-2;12* mutant, in intact seedling the mutation in *ERF4*, *ERF8*, *ERF9*, and *ERF12* gene partially rescued the *wuschel* phenotype in early days of germination (9 dag).

3.6 Higher-order *erf* mutants show display alteration in relative *CUC1* and *STM* gene expression

To monitor the impact of ERFs on expression of SAM marker genes two quintuple mutant lines (*erf4-1;8;9-1;11-2;12* and *erf4-1;8;9-1;10;12*) were examined and relative *CUC1* and *STM* gene expression was compared to WT Col-0.

In both mutant lines, the strongest *CUC1* expression was detected after 3 days on SIM incubation. *erf4-1;8;9-1;11-2;12* mutant line displayed 4.7 times higher relative *CUC1* expression than Col-0

whereas *erf4-1;8;9-1;10;12* accumulated *CUC1* transcripts only 3.3 times more than Col-0. Therefore, the aberrant ERF11 gene has a bigger impact on *CUC1* relative expression than ERF10. In contrast to the *CUC1* expression profile, STM seems to oscillate in both quintuple mutants. Similarly to effect on *CUC1* expression, the *erf4-1;8;9-1;11-2;12* mutant line displayed stronger impact on STM transcripts accumulation than *erf4-1;8;9-1;10;12* mutant line. According to this qRT-PCR analysis, it is tempting to speculate that ERF11 is a negative regulator of putative activator controlling STM gene expression.

3.7 Expression pattern and sub-cellular localization of ERF4

To analyze the expression domain of ERF4, transgenic plants, harboring the *pERF4::ERF4-GUS* construct, were analyzed by GUS-staining. Strong signals were observed in pericycle cells and mostly in lateral root primordia (LRP) (Figure 8a). Live-cell imaging of transgenic plants harboring the *pBIB-UAS-ERF4-mCherry-tNOS* construct showed a similar pattern (Figure 8b). Nuclei of LRP were positive for the presence of the ERF4-mCherry fusion protein.

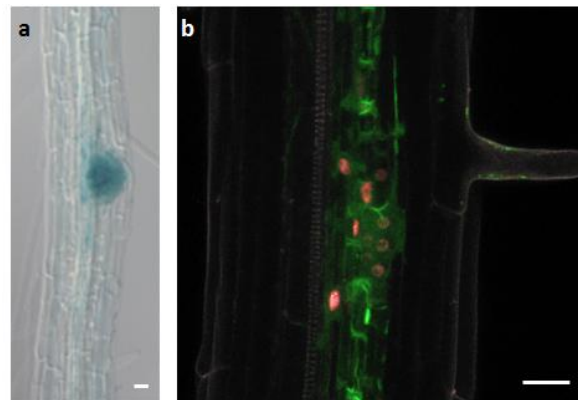


Figure 8: a) Transgenic plants harboring *pERF4::ERF4-GUS* show the accumulation of the ERF4-GUS fusion protein predominantly in LRP b) Transgenic plants harboring the *pBIB-UAS-ERF4-mCherry-tNOS* construct. Scale bar represents 20 μm.

3.8 ERF4 is more often associated with the active than with inactive RNAPoIII variant

Afterward, widefield live-cell imaging super-resolution microscopy was employed to examine the ERF4 protein distribution inside the nucleus more in detail. In addition, the co-localization of ERF4 with inactive RNAPoIII and the active variant RNAPoIIISer2ph (phosphorylated at serine 2) has been quantified. The ERF4-mCherry fusion protein was present in euchromatin but absent from heterochromatin and the nucleolus (Figure 9a, c, d, e, g, h), where also RNAPoIII was localized in a network-like manner. The inactive RNAPoIII formed compacter structures (Figure 9b) when compared to the active variant (Figure 9f). ERF4-mCherry co-localized more often to RNAPoIIISer2ph (Figure 9a, b) than to the inactive variant (Figure 9e, f).

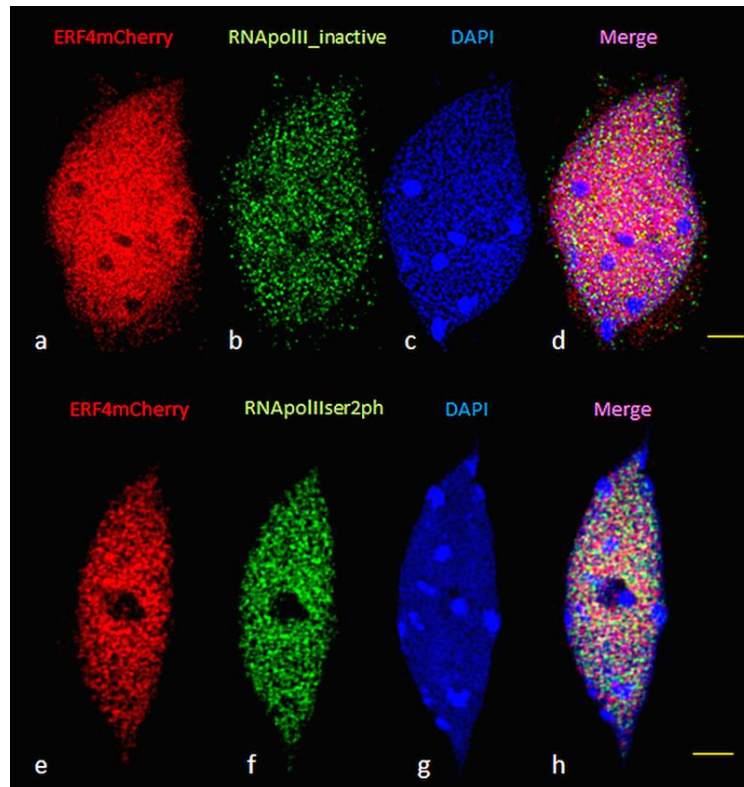


Figure 9: Co-localization of ERF4-mCherry with inactive RNAPolIII (a-d) and the active variant RNAPolIIIser2ph (e-h). Scale bars represent 2 μ m.

3.9 The impact of ERF4 on the acetylation of histone H3

Because the expression of ERF4-mCherry under the control of native *ERF4* regulation elements was very low and tissue-specific, plants harboring the *ERF4-Myc* expression cassette under the control of the strong estradiol inducible promoter (XVE) were selected for further analysis. First, the functionality of the construct was tested using β -estradiol treatment. Seedlings treated with β -estradiol showed severe pleiotropic phenotypes, obviously suffering from *ERF4-Myc* overexpression, and were vastly dwarfed when compared to non-treated seedlings (Figure 10a). The overexpressing lines showing the strongest deviating phenotype were selected for further experiments. To detect the fused ERF4-Myc protein Western blot analysis was carried out. Although the construct was driven under the inducible promoter and the expression was supposed to be massive only very weak signal was detected (data not shown). Presumably, this could be due to protein degradation. Western blotting seems not to be sensitive enough to detect such an unstable protein. Instead, the presence of the ERF4-Myc fusion protein was detected using a whole-mount approach (Figure 10b). ERF4-Myc fusion protein was detected using a specific anti-Myc antibody. The signals were observed in nuclei and no distinct structures within the nucleus were found. Assuming that ERF4 takes part in a co-repressor mediated expression attenuation, the acetylation status of nuclei expressing ERF4-Myc was monitored.

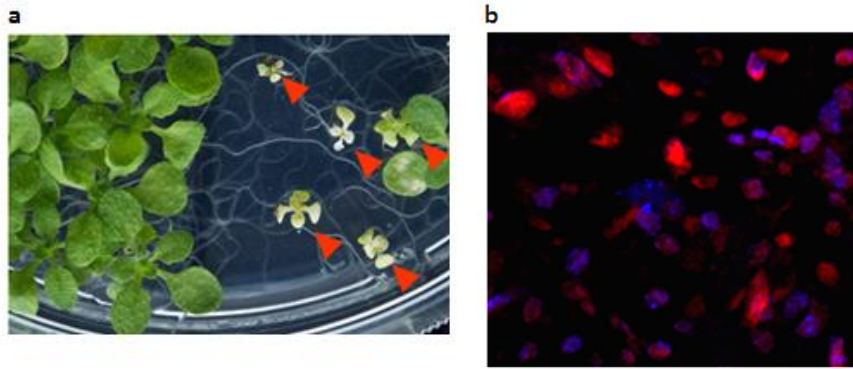


Figure 10: Inducible expression of *ERF4-Myc* after β -estradiol treatment.

To analyze changes in the acetylation status of histone 3 (H3) at different lysine residues transgenic plants harboring an estradiol-inducible *XVE::ERF4Myc* expression cassette were treated with β -estradiol overnight. Nuclei from whole 5 day-old seedlings were isolated and immediately flow-sorted according to their ploidy level. Within the population of isolated nuclei, the nuclei accumulating ERF4-Myc fused protein and nuclei without ERF4-Myc were found. The 8C fraction of sorted nuclei was subjected to super-resolution microscopy (SIM) analysis to achieve a higher resolution. The fluorescence signals of nuclei expressing the ERF4-Myc fusion protein were detected in euchromatin, similar to the localization pattern observed in nuclei prepared from plants harboring the *pBIB-UAS-ERF4-mCherry-tNOS* construct (Figure 10). No fluorescence signals were observed in the nucleoli and chromocenters (heterochromatin). As expected, nuclei without ERF4-Myc expression showed no fluorescence signals when stained with anti-Myc antibody. Similarly, no signals for Myc were detected in the two controls, WT Col-0 and plants harboring the empty vector pER10 after β -estradiol treatment. The fluorescence signals of H3K9 were detected in euchromatin in the whole nucleus and were excluded from the nucleolus and heterochromatin. A similar signal distribution was observed also for H3K14, H3K23, and H3K9, H3K14, H3K23, H3K27 epigenetic marks.

Although the analyzed nuclei displayed no changes in the acetylation pattern of H3K9, differences in the intensity of the fluorescence signals were observed. The intensity of H3K9 acetylation was clear and strong in the control nuclei (Col-0, pER10), and also in nuclei without the detection of ERF4-Myc. Interestingly, some ERF4-Myc-positive nuclei exhibited an altered signal intensity of H3K9. The fluorescence signals were apparently weaker, and in some nuclei only background noise was visible. This suggests that the acetylation of H3K9 was specifically reduced. This decrease was predominantly visible in nuclei with ERF4-Myc expression. To classify nuclei showing various acetylation intensities three distinct categories were created. The first category denotes the nuclei with the lowest H3K9 fluorescence signals (Figure 11a), the second category represents intermediate intensities (Figure 11b), and the third one stands for the strongest signals observed in nuclei without ERF4-Myc expression (Figure 11c). No negative correlation between ERF4-Myc expression and the H3K9 fluorescence signal intensity was observed.

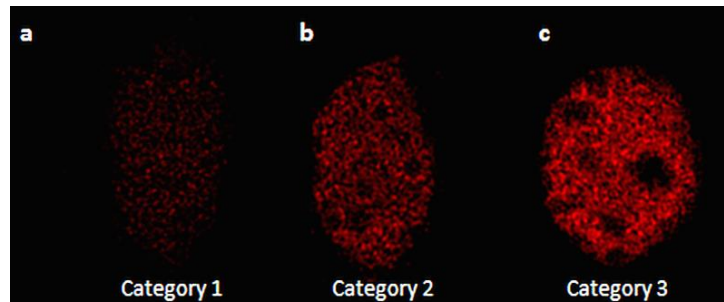


Figure 11: Categories of nuclei showing altered histone H3 acetylation intensity.

Among 8C nuclei expressing ERF4-Myc, the categories 1 and 2 of the H3K9 acetylation intensities (27 % and 37 %, respectively) were more abundant than in the control samples WT Col-0 and pER10-GFP. Here both categories reached only 5 %. The majority of nuclei in control samples fitted to category 3 (95 %), whereas the 8C fraction of ERF4-Myc nuclei contained only 43 % of category 3. To investigate whether this acetylation variation was caused by the ploidy level, or whether it is a global phenomenon, a mixture of isolated (not flow-sorted) nuclei was used to count the number of nuclei belonging into the three distinct categories. No significant differences between the mixed and the flow-sorted nuclei were detected. The obtained values were almost identical.

Similar trends were found for acetylated H3K14; H3K18; and H3K9, H3K14, H3K18, H3K23, H3K27, where categories 1 and 2 were more abundant in ERF4-Myc positive nuclei than in the control samples.

4 Discussion

4.1 Proper proteolysis of transcriptional factors is essential for correct plant development

The impaired proteolysis causing severe plant defects clearly shows that not only the proteosynthesis but also protein degradation play an essential role in normal plant growth and development (Sonoda et al., 2007; Gallois et al., 2009). Except for the pharmacological treatment, we affirmed the crucial role of proteolysis on the development of shoots by employing a genetic approach. WT Col-0 root explants treated with the proteasome inhibitor MG132 were defective in shoot development (Figure 6a-c). This pharmacological experiment proved the essential role of the proteasome in normal shoot development. A *bpm1;2 Arabidopsis* double mutant in genes encoding the E3 ligases *BPM1* and *BPM2*, which are key elements of proteasome-mediated protein degradation machinery, exhibited also reduced shoot regeneration efficiency.

Next, we elucidated the role of ERF repressors in the maintenance and specification of SAM as well as their impact on *CUC1* and *STM* gene expression. A general feature of transcriptional repressors is their fast degradation, usually mediated *via* 26S proteasome activity (Gray et al., 2001; Patra et al., 2013). Such a tightly controlled regulation allows for the prompt and transient accumulation of repressor and thus is essential for its proper function. Malfunction of components of the proteasome might cause accumulation of cellular proteins including transcriptional repressors such as ERFs. This assumption is greatly supported by positive protein-protein interaction results provided in this work. Although only ERF4 and ERF8 could interact with the components of E3 CUL^{BPM} ligase complex (Figure 7), the ERF interaction with other E3 ligases cannot be completely excluded. To this, protein-protein

interaction analysis in yeast showed the interaction of BPM1 and BPM3 with both ERF4 and ERF8. In the case of BPM2, ambiguous results were obtained.

Our results on BPMs and ERFs are pointing out the importance of protein degradation in gene expression regulation mediated by the ERF repressors playing an important developmental role. We assume that the stabilization of ERF repressor proteins leads to a greater rate of co-repressor assembly at actively transcribed loci. As a consequence of this process, adjacent histones undergo deacetylation. Thus, chromatin condenses and the access of the transcription machinery to the promoter is constrained. The employment of the TPL-EAR motif-containing a transcription factor involved in root and shoot meristem development was recently reported (Espinosa-Ruiz et al., 2017).

Because we showed that the ERF repressors can interact with BPM adaptor proteins which are components of E3 CUL^{BPM} ligase, we hypothesize that an impaired BPM synthesis leads to the accumulation of ERF. In turn, ERF can recruit a co-repressor complex to its target loci and thus HDA can execute histone deacetylation. Therefore, we favor the interpretation that HDA6 acts downstream from the BPMs but an opposite role cannot be excluded.

4.2 WUSCHEL-independent pathway

Next objective of this work was to expand the current knowledge on plant development regulation focused on genes playing a key role in shoot regeneration. Plant development is a complex process involving several regulatory pathways. Some are acting synergistically while others antagonistically. These pathways usually consist of particular genes which act up- or downstream from each other and thus create a complex genetic framework. The best-studied pathway is the WUS/CLV pathway which regulates the specification of stem cells and maintenance of the shoot apical meristem (Baurle, 2005; Busch et al., 2010; Somssich et al., 2016). Apart from this pathway, other independent mechanisms were suggested to take part in SAM regulation.

Our results obtained by the genetic approach and the phenotypic manifestation of a quintuple *wus;erf4-1;8;9-1;12* mutant, that could partially rescue the *wuschel* phenotype, strongly suggest the importance of ERF transcriptional repressors in SAM maintenance acting independently from WUSCHEL. Interestingly, mutants lacking the WUS protein were able to produce recognizable SAM only when ERF repressors were impaired. Similarly to a *wus;phb;phv;cna* quadruple mutant described previously by Lee and Clark (2015), the rescue of the *wus* phenotype in a *wus;erf4-1;8;9-1;12* mutant was observed only within the vegetative growth stage. After the floral transition, the *wus;erf4-1;8;9-1;12* mutant showed a phenotype similar to *wus*, resulting in plant sterility.

Transcriptional repressors, ERFs, along with transcription activators, ESR1 and ESR2, recognize the GCC-box in the promoter region of their target genes. Thus, they can compete for binding to this element. Identification of candidate direct target genes of ERF4 using RNAseq revealed that 62 % of genes showing at least 2-fold change were found to be common for *N4C2-ER* and *ESR2-ER*. Likely, ESR2 and ERF4 share similar targets. Using a semi-quantitative RT-PCR, we showed that *ERF* genes with a GCC-box, only *ERF9* and *ERF12* respond to ERF4 and also ESR2. These findings can explain the reduced shoot regeneration efficiency of the *erf4-1;8* and *erf4-1;8;bpm1;2;3* mutant. We found that

ERF9 and *ERF12* are primary target genes of *ERF4*. In the mutant line with an impaired *ERF4* function, *ERF9* and *ERF12* repressors are no longer repressed or their repression is attenuated. Thus, they can exhibit their repression activity with shoot regeneration inhibition as a result.

Based on our gene expression analysis it can be hypothesized that the SAM development might be indirectly mediated through *CUC1* and *STM*. Mutant lines impaired in *ERF* repressors displayed an elevated time-dependent *CUC1* gene expression, similar to *STM*. Although *CUC1* does not contain GCC-box in its promoter, the neighboring gene sequence is enriched in the GC content that might mimic the *ERF*-binding site.

Surprisingly, apparent differences in the relative expression of *CUC1* and *STM* were observed in two mutant lines, *erf4-1;8;9-1;11-2;12* and *erf4-1;8;9-1;10;12*. These unexpected differences in relative *CUC1* and *STM* gene expression might be explained by the distinct spatiotemporal gene expression pattern of individual *ERF* genes in the time course of CIM and SIM incubation. Based on the publicly available data in the TAIR database (Che et al., 2002), we analyzed the expression pattern of *ERF* genes. Expression of *ERF4* was strongest among all studied *ERF* genes (*ERF4*, *ERF8*, *ERF9*, *ERF11*, and *ERF12* expression profile of *ERF10* was not monitored) at day 0 on CIM incubation and was gently decreasing up to day 4 on CIM incubation. After the transfer to SIM, the *ERF4* expression dropped more rapidly. *ERF11* also showed significant changes in the expression. Although, there is no information on *ERF* protein abundance it might be assumed that it correlates with the RNA level. The lack of the *ERF11* gene product has a big impact on the expression of *CUC1* as clearly demonstrated by our results obtained with the *erf* quintuple mutants

4.3 Role of *ERF4* in gene expression regulation

The sub-cellular localization of *ERFs* was for the first time shown by Yang et al., (2005). The authors overexpressed a *35S::AtERF4-GFP* construct in *Arabidopsis* protoplasts and found the GFP-fluorescence being localized to discrete nuclear bodies. Previously, it was shown that the ABI5 (abscisic acid insensitive 5), a key player in abscisic acid signaling, co-localized also in nuclear bodies when interacting with its negative regulator (Lopez-Molina et al., 2003). Since, the nuclear bodies contained a RING protein, a key component of 26S proteasome, these structures were proposed as sites for the proteasome-mediated protein degradation (Lopez-Molina et al., 2003). This finding inspired us to examine whether *ERF* repressors undergo the proteasome-mediated degradation within the nuclear bodies. To test this hypothesis, the transgenic *Arabidopsis* lines expressing an *ERF4-mCherry* fusion protein were prepared. The localization of the mCherry fluorescence was followed using live-cell confocal microscopy. Surprisingly, *ERF4-mCherry*-specific signals did not co-localized within the nuclear bodies but were spread all over the nucleus (Figure 9). The observed pattern seems to be specific since the control line expressing *mCherry-only* displayed red fluorescence signals throughout the cell.

As *ERF4* works as transcriptional repressor directly regulating expression of specific target genes, its co-localization with the transcription machinery was tested in this study. Interestingly, the *ERF4-mCherry* signals co-localized with the active RNAPolIIIser2ph better than with inactive RNAPolIII variant. Our findings thus support the recently described novel concept of transcriptional repressor

mode of activation; suggesting that repressors are more co-localizing with actively transcribed loci than with the silent loci (summarized in Reynolds et al., 2013).

ERF4 can interact with co-repressor components (Song and Galbraith, 2006). In parallel, we have shown that ERF4 co-localizes with RNApollser2 which occupies the sites of active gene transcription in the nucleus. Next, ERF4 is capable to recruit histone deacetylases to target loci and through their enzyme activity presumably to repress gene expression. To test this hypothesis, we investigated the acetylation pattern/status of five histone marks in the plant line over-expressing *ERF4-Myc*. We confirmed the localization of ERF4 within the nuclear euchromatin. This observation is in agreement with our observation with the ERF4-mCherry line (Figure 17a, e). Obtaining identical results using two independent constructs strongly implies that the observed pattern reflects the actual localization of ERF4 *in planta*. We assume that the weaker fluorescence signal of antibodies specific to histone marks mirrors the reduction of acetylation at histone H3 in response to ERF4 accumulation in the nucleus

As we showed, no accelerated shoot regeneration was observed in *erf4-1;8;9-1;10;11-1;12* sextuple mutant by using in vitro tissue culture system. Apart from the reasons for this result discussed above a new explanation emerged in light of the study by Rosa et al. (2014) study. The weak phenotype of *erf4-1;8;9-1;10;11-1;12* sextuple mutant in terms of shoot regeneration efficiency might be due to the retarded differentiation rate of the meristem tissue caused by hyperacetylation in the absence of ERF repressors. There are two possible scenarios explaining why we could not detect a higher number of regenerated shoots. 1) A number of *de novo* formed SAM is not affected but its enlargement is enhanced. 2) The number of *de novo* SAM is increased but their function is limited and some cannot develop true leaves. In our shoot regeneration assay, we considered already differentiated true leaves arising from the *de novo* developed SAM, instead of counting a number of all newly formed meristems. This approach, therefore, reflects only fully functional SAMs. Even though we could not detect higher shoot regeneration efficiency in *erf4-1;erf8;erf9-1;erf10;erf11-1;erf12* mutants when compared to the WT Col-0 using our system, we still cannot exclude the second scenario.

Taking into consideration the above-discussed results; it seems that the first scenario is more likely. In addition, the enlargement of SAM is supported not only by larger fluorescence meristems observed in the *erf4 1;8;9-1;12* quadruple mutant but also by the elevated relative gene expression of the SAM marker gene, *STM*, in *erf* mutants. Although those are just indirect evidence of SAM enlargement there is a strong indication that ERF repressors can regulate the size of SAM. This scenario might also explain why we could observe formation of SAM in the *wus;erf4-1;8;9-1;12* mutant *in planta*. To further examine this hypothesis, histological sections through SAM of *erf* mutants and WT need to be prepared to evaluate the SAM size.

PART II – Chlorophyll Measurement as a Quantitative Method for the Assessment of Cytokinin-Induced Green Foci Formation in Tissue Culture

Ivona Kubalová, Yoshihisa Ikeda

*Center of the Region Haná for Biotechnological and Agricultural Research, Faculty of Science, Palacký
University, Olomouc, Czech Republic*

5 Introduction

Tissue culture systems have long been exploited to study the process of organogenesis. In response to externally applied cytokinins, pluripotent cells proliferate into green calli and subsequently regenerate shoots. Conventionally, the cytokinin-induced greening phenotype has been evaluated by counting numbers of green foci or to present photographic evidence of morphological changes. However, because the structure of calli is disorganized and the development of pigmentation takes place gradually from pale white through yellow to green, adequately defining and counting green foci remains difficult. In this study, we employed chlorophyll measurement as an alternative method to statistically assess the greening phenotype in tissue culture material. We found that N,N-dimethyl-formamide was the most effective solvent for the extraction of chlorophylls from callus tissue and that bead disruption of the structured tissue improved solvent penetration and the consistency of results. The sensitivity of the method facilitated the quantification of chlorophylls in single-cultured root explants and the use of a spectrophotometer increased the efficiency of measuring multiple samples.

Our measurements showed that chlorophyll contents from calli of wild-type and altered cytokinin response mutants (*cre1*; *ahk3*, or cytokinin hypersensitive 2 (*ckh2*)/pickle (*pkl*) were statistically distinguishable, validating the method. Our proposed procedure represents gains in efficiency and precision and leads to more robust standardization than the conventionally used counting of green foci.

6 Materials and methods

Plant material and growth condition, Semi-quantitative RT-PCR analysis, Semi-quantitative RT-PCR analysis are described in detail in Kubalová and Ikeda (2017).

7 Results

To compare the extraction efficiency of chlorophylls from root explants, commonly used solvents, such as 80 % acetone, DMF, and DMSO were compared by following the equations for chlorophyll a and chlorophyll b determination as previously described (Inskeep and Bloom, 1985; Barnes et al., 1992). Glass plates were used for the measurements as DMF is an aggressive solvent that is not compatible with commonly used polystyrene plates. For the convenience of cutting roots, seedlings were grown in the vertical orientation on a relatively solid MS medium containing 0.8 % Phytigel. Five days after

germination, root explants were excised and transferred onto CIM for 4 days (CIM pre-incubation), followed by transfer onto SIM. In order to prepare the same starting materials, two surgical blades were joined with an 8 mm gap separating the two blades. To consider variations in growth and cytokinin response, 30 root explants per solvent were randomly collected and subjected to chlorophyll extraction on day 10 of the SIM incubation. No lateral organs (shoot regeneration) were observed at this time. In agreement with previous reports (Inskeep and Bloom, 1985; Stiegler et al., 2005), DMF was the most effective solvent for extracting chlorophylls (Figure 12a-c). When extracted in 80 % acetone, 30 min incubation was not sufficient to reach equilibrium (Figure 12a), whereas it took around 15 min for DMF or DMSO to reach maximum levels (Figure 12b-c). DMF extracted chlorophylls more efficiently than DMSO ($p = 0.0082$ at 5 min). During tissue culture, some root explants spontaneously developed wound-induced callus (Ikeuchi et al., 2013) (Figure 12d), compromising efficient chlorophyll extraction when tissue is not disrupted, resulting in an underestimation of the chlorophyll content. In order to tackle this difficulty, we applied tungsten bead disruption of all root explants. This procedure resulted in a chlorophyll recovery equivalent to the equilibrium of the corresponding solvents examined for the time-course experiments and an improved extraction in the case of 80 % acetone (Figure 12e and compare to Figure 12a), which is an advantage when glass plates are not available. Heat treatment was reported to prevent chlorophyll degradation by inhibiting the chlorophyll hydrolyzing enzyme, chlorophyllase (CLH) (Hu et al., 2013), however, no degradation was observed in our conditions (data not shown). Thus, for all subsequent experiments extraction of chlorophylls in DMF with bead disruption and no pre-heat treatment was applied.

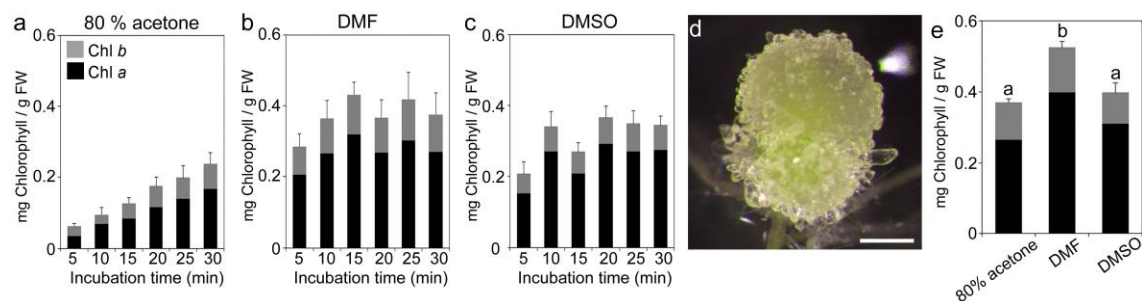


Figure 12: Effect of bead disruption and solvent on chlorophyll extraction from cultured root explants Chlorophyll contents of wild-type root explants cultured on SIM for 10 days extracted by 80 % acetone (a), DMF (b), and DMSO (c) without bead disruption. (d) Wound-induced callus formed at the cutting sites covers green tissue in Col-0 root explant on SIM for 12 days. (e) Chlorophyll contents of wild-type root explants cultured on SIM for 10 days extracted for 5 min with bead disruption in corresponding solvents. Scale bar represents 0.5 mm

To verify the reliability and reproducibility of quantifying chlorophylls from cultured root explants as a measure for their greening phenotype, *hy1* (GK-034B01) and *gun4* (SALK_026911) mutants reported to have reduced chlorophyll contents were collected (Chory et al., 1989; Peter and Grimm, 2009). They were used as technical negative controls for chlorophyll quantifications. We confirmed the position of the T-DNA insertion of *hy1-3* in the first exon of the annotated At2g26670.1 transcript, a longer version of splice variant. The *gun4-3* appeared to be null as no detectable GUN4 proteins were observed in the mutant (Peter and Grimm, 2009). *HY1* encodes monooxygenase and *GUN4* encodes an adaptor protein positively regulating Mg^{2+} chelatase activity (Davis et al., 1999; Peter and Grimm, 2009). We found that, although the color of mutant calli is paler than that of wild-type (Figure 13a), *hy1-3* and *gun4-3* root

explants could form the disorganized structures (Figure 13b and 13c), indicating that tetrapyrrole biosynthesis is not required for cell outgrowth. Therefore cytokinin-induced greening phenotype cannot be assessed by counting green foci or by chlorophyll measurements in these mutants. As expected, chlorophyll amounts extracted from the *hy1-3* or *gun4-3* root explants were significantly lower than that of wild-type (in both cases $p \leq 0.0001$ Figure 13d), indicating that our method is able to determine differences in chlorophyll content from a single root explant.

Cytokinin was essential for nascent SAM formation and greening. This suggests that similarly to the *hy1-3* and *gun4-3*, mutants with an altered cytokinin response should have different chlorophyll levels. The *pkl* (*pickle*)/*cytokinin hypersensitive 2* (*chk2*), in which a CHD3 SWI/SNF2 chromatin remodeling factor gene is disrupted, exhibited cytokinin hypersensitivity in tissue culture (Furuta et al., 2011). The *pkl/chk2* was employed as a positive control. As the *cre1-2* and *ahk3* single mutants in the Col-0 background did not exhibit cytokinin-insensitive phenotypes (Riefler et al., 2006), cytokinin receptor double mutant, *cre1-2;ahk3-8*, was created as a negative control for reduced greening phenotype.

The *cre1-2;ahk3-8* double mutant had reduced green foci formation (Figure 13e), whereas *pkl-1* retained the capacity for the pronounced greening phenotype (Figure 13f). We evaluated accumulated chlorophylls per root explant because *pkl-1* exhibited increased growth with root penetrating the agar medium. The increased mass due to pronounced *de novo* root development resulted in the underestimation of chlorophyll accumulation in *pkl-1* when chlorophylls were evaluated per fresh weight (data not shown). Besides, we found it inaccurate to measure fresh weight of individual 8 mm root explant developing *de novo* roots into medium (30 roots per genotype). Using chlorophyll measurements, we were able to statistically distinguish *cre1-2;ahk3-8* or *pkl-1* from wild-type (in both cases $p \leq 0.0001$ Figure 13g). When the number of green or yellow colored foci developed from *cre1-2;ahk3-8* and from *pkl-1* were counted, we obtained similar results to those by the chlorophyll measurements (Figure 13h), indicating that chlorophyll measurement can be used as an alternative way to evaluate cytokinin-induced greening phenotype. Since greening tissue does not essentially indicate nascent SAM formation, the expression of *WUS* was examined. We found a positive correlation of *WUS* expression with chlorophyll accumulation (Figure 13i). The cytokinin-promoted greening of cultured tissue on CIM incubated material was more suitable than material from SIM incubation because no lateral organ differentiation took place in the CIM culture. Instead, outgrowth of calli persisted (Figure 13j-l). Chlorophyll measurements were made on CIM-induced calli for assessing tissue greening stimulated by the higher kinetin to 2,4-D ratio in CIM. Similar to the SIM incubation, significant differences in chlorophyll contents could be determined between the two mutants and the wild-type (in both cases $p \leq 0.0001$ Figure 13m).

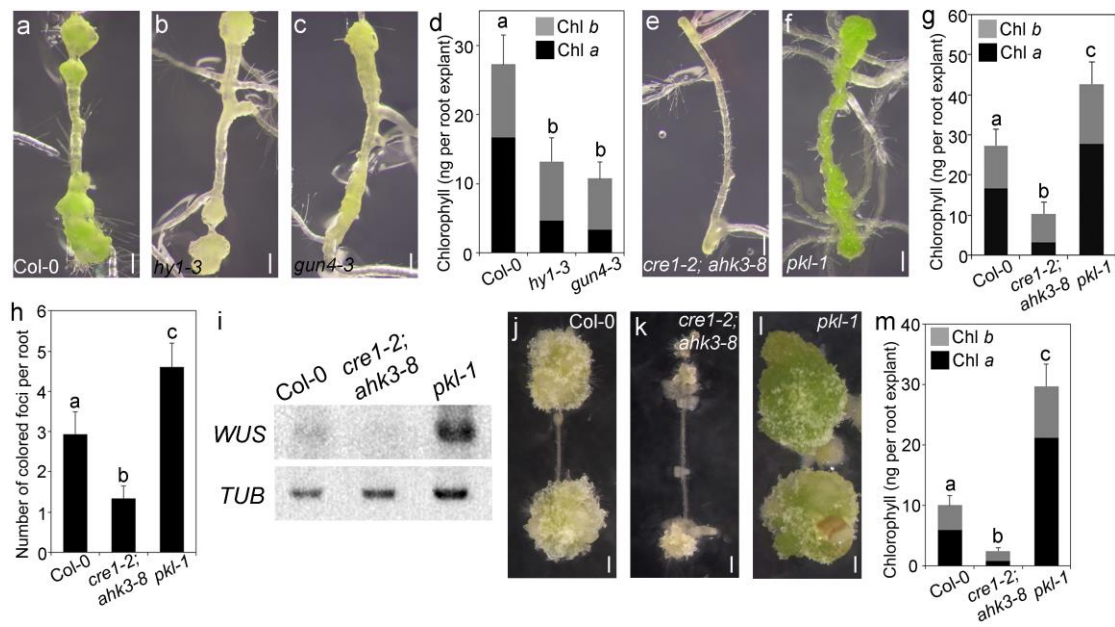


Figure 13: Statistical evaluation of greening phenotype by chlorophyll measurements. Root explant cultured on SIM for 10 days of Col-0 (a), *hy1-3* (b), *gun4-3* (c), *cre1-2;ahk3-8* (e), and *pk1-1* (f). (d) Chlorophyll contents of Col-0, *hy1-3* or *gun4-3* root explants cultured on SIM for 10 days. (g) Chlorophyll contents of Col-0, *cre1-2;ahk3-8* or *pk1-1* root explants cultured on SIM for 10 days. (h) A number of pigmented foci per root explant of Col-0, *cre1-2;ahk3-8* or *pk1-1*. (i) Expression of *WUS* on day 10 SIM incubation. (j - l) Root explant cultured on CIM for 36 days of Col-0 (j), *cre1-2;ahk3-8* (k) or *pk1-1* (l). (m) Chlorophyll contents of Col-0, *cre1-2;ahk3-8*, and *pk1-1* root explants cultured on CIM for 36 days. Scale bars represent 0.5 mm

8 Discussion

In summary, although chlorophyll accumulation in cultured root explants is not as abundant as it is in leaves and spontaneous wound-induced callus hinders solvent penetration, we developed a method to quantify chlorophylls from a single cultured root explant (8 mm) by applying bead disruption in diverse solvents. Major advantage of our procedure over counting green foci are: 1) chlorophyll levels are a measurable parameter not depending on subjective observations; 2) since the extinction coefficients of chlorophylls are well-defined, the results of different experiments are comparable; 3) considerable number of samples can be measured simultaneously using 96-well glass plates with a conventional microplate reader; 4) the method is sensitive enough to assess a greening phenotype in root explants of 5 mm in length which is helpful for mutants exhibiting a short root phenotype; 5) all green foci are taken into account, including those that develop at sites inaccessible to the eye or image analysis software. Additionally, our methodology does not require parameter setting, which is crucial in the image analysis software when considering pale explants, so objective rather than relative data are obtained. The main disadvantage of our procedure is its destructive nature whereas taking photographs of calli has an advantage in giving insights into morphologic changes over time. Trans-differentiation of RAM into SAM triggered by cytokinins on SIM can be studied by analyzing available SAM-related markers, although introducing the markers in the desired genetic background takes time. Thus, chlorophyll measurements are a concise and sensitive method that combined with complementary approaches such as taking photographs and SAM-related marker analysis for *de novo* SAM development give a whole view of the responsiveness of explants in tissue culture.

PART III – Mutations in Tetrapyrrole Biosynthesis Pathway Uncouple Nuclear *WUSCHEL* Expression from *de novo* Shoot Development in *Arabidopsis*

Ivona Kubalová, David Zalabák, Alžbeta Mičúchová, and Yoshihisa Ikeda

Center of the Region Haná for Biotechnological and Agricultural Research, Faculty of Science, Palacký University, Olomouc, Czech Republic

9 Introduction

Plant *de novo* organogenesis in tissue culture systems has long been exploited to study the plasticity of pluripotency. External application of high cytokinin-to-auxin ratio in cultured medium stimulates greening of calli and promotes nascent shoot apical meristem (SAM) formation. The stem cell niche in SAM is maintained by a negative feedback loop between CLAVATA-WUSCHEL (WUS) signaling. Cytokinin being known to induce *WUS* expression, the capacity of *de novo* shoot development is largely dependent on *WUS* activity. However, the molecular mechanism of *WUS* expression remains obscure. Here we provide a novel regulatory mechanism of *WUS* expression during *de novo* SAM formation that is affected by the altered tetrapyrrole metabolism catalyzed in the plastid. Loss-of-function mutations in *HEME OXYGENASE/LONG HYPOCOTYL 1* (*hy1*), *Mg-CHELATASE H* (*chlh*), *Mg-CHELATASE I1* (*chli1*) and the regulator of Mg-CHELATASE, *GENOME-UNCOUPLED 4* (*gun4*), result in elevated *WUS* expression but the shoot regeneration efficiency is decreased whereas loss-of-function mutation in *PROTOPORPHYRIN IX FERROCHELATASE 2* (*fc2*) exhibits compromised *WUS* expression with reduced number of shoots when mutant root explants are cultured on shoot induction medium. Our results suggest that plastid-to-nucleus communication takes place to coordinate cytokinin-stimulated etioplast-to-chloroplast transition with *de novo* organogenesis through fine-tuning a nuclear gene expression of the master SAM regulator.

10 Materials and Methods

Plant material, growth condition, chlorophyll measurement, shoot regeneration assay Quantitative RT-PCR analysis (qRT-PCR) are described in (Kubalová et al., 2019).

11 Results

11.1 *WUS* expression and *de novo* SAM formation are coupled in altered cytokinin response mutants

We previously showed that loss-of-function mutants with altered cytokinin responses have a positive correlation among greening of calli, SAM marker expression and *de novo* shoot formation observed in the tissue culture system. Cytokinin receptor double mutant, *cre1-2; ahk3-8*, had reduced sensitivity to cytokinin, thus showing substantially reduced chlorophyll contents, compromised *WUS* expression and reduced shoot regeneration efficiency (Kubalová and Ikeda, 2017). On the contrary, *pickle* (*pkl*)/*cytokinin*

hypersensitive 2 (ckh2) mutant, in which a CHD3 SWI/SNF2 chromatin remodeler is disrupted, exhibited cytokinin hypersensitivity in CIM (Furuta et al., 2011), as well as in SIM culture (Kubalová and Ikeda, 2017). In this study, we assessed these cytokinin related phenotypes by employing quantitative RT-PCR for examining *WUS* expression and by counting regenerated shoots from day 10 to 22 SIM incubation. *cre1-2; ahk3-8* root explants accumulated 54 % of chlorophyll contents relative to that in wild-type (Figure 14a), reduced *WUS* expression (Figure 14b) and they never regenerated shoots during SIM incubation (Figure 14c). On the other hand, *pk1-1* root explants accumulated chlorophylls by 2.1-fold (Figure 14a), had 6.03 fold higher *WUS* expression (Figure 14b), and developed shoots earlier and more effectively (Figure 14c). Thus, we could confirm the positive correlation between cytokinin perception and all cytokinin-related phenotypes observed in SIM culture. Next, we explored the relationship between greening of calli and nascent SAM development by employing *wus-101* with undetectable transcription of *WUS* (Figure 14e). Consistent with the previous report (Zhang et al., 2017), shoot regeneration efficiency was substantially reduced in *wus-101* (Figure 14f). These results suggest that chlorophyll accumulation is independent of *WUS* activity. This is in agreement with the finding that *WUS* expression is confined within the organizing center of developing SAM whereas greening takes place in a much wider region of cultured root explant. Taken together, *WUS* expression and shoot regeneration appear to be more tightly coupled with each other.

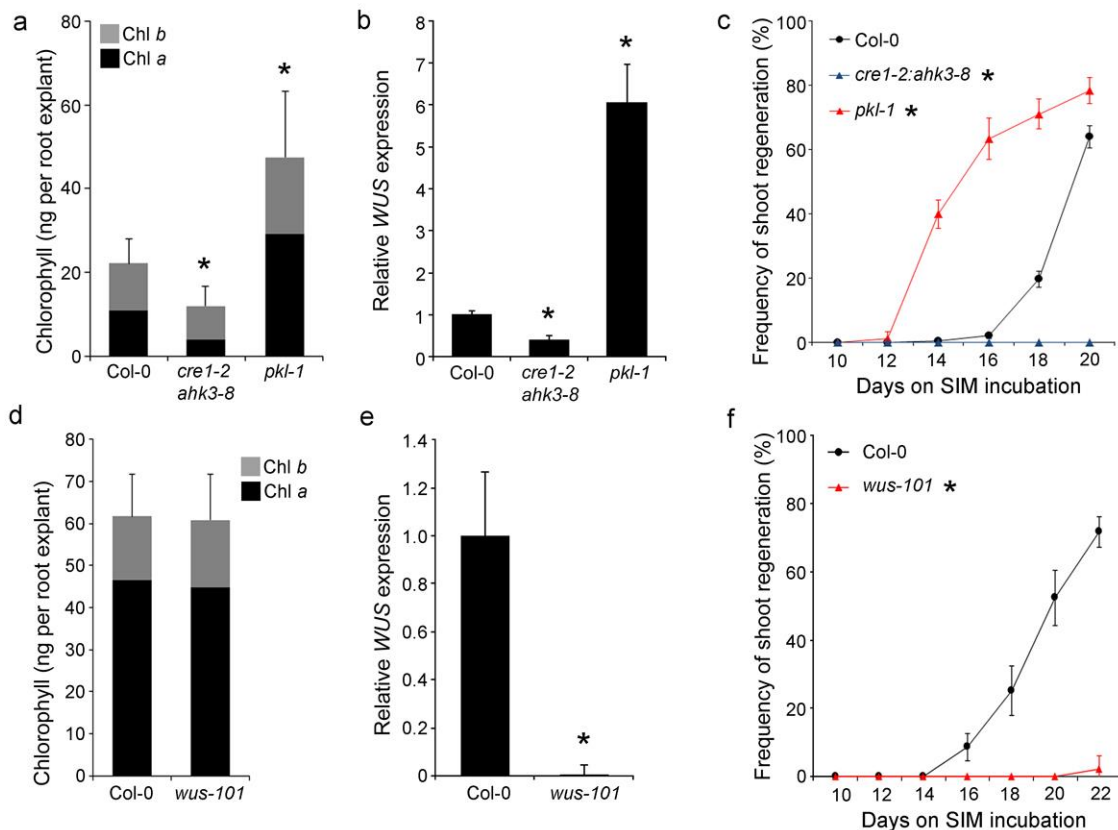


Figure14: *WUS* expression and *de novo* SAM formation are coupled in mutants with altered cytokinin response. (a) Chlorophyll contents of Col-0, *cre1-2;ahk3-8*, and *pk1-1* root explants cultured on SIM (b) Relative *WUS* expression in Col-0, *cre1-2;ahk3-8*, and *pk1-1* root explants cultured on SIM quantified by qRT-PCR (c) Shoot regeneration frequency in Col-0, *cre1-2;ahk3-8*, and *pk1-1* root explants cultured on SIM. (d) Chlorophyll contents of

Col-0 and *wus-101* root explants cultured on SIM (e) Relative *WUS* expression in seven-day-old Col-0 and *wus-101* shoots quantified by qRT-PCR (f) Shoot regeneration frequency in Col-0 and *wus-101* root explants cultured on SIM.

11.2 *WUS* expression is uncoupled from de novo SAM formation in mutants defective in tetrapyrrole biosynthesis

We further explored the relationship between chlorophyll accumulation and *WUS* expression by employing loss-of-function mutants defective in tetrapyrrole biosynthesis: *fc2-1*, *hy1-3*, *gun3-3*, *gun4-2*, *chld*, *chlh*, *chli1*, and *crd1* (Figure 15). As reported previously, we found significantly reduced chlorophyll contents in all mutant root explants, especially those defective in chlorophyll branch (Figure 16a). Surprisingly, the level of *WUS* transcripts in *hy1-3*, *gun4-2*, *chlh*, and *chli1* was elevated (Figure 16b), although the shoot regeneration efficiency is substantially declined (Figure 16c). *fc2-1* was the only mutant examined in this study exhibiting the decreased *WUS* expression with compromised shoot regeneration when the number of developed shoots producing true leaves was counted at various time points during SIM incubation (Figure 16c, d). Shoot regeneration efficiency, as well as an average number of shoots per root explants, were reduced in all tetrapyrrole mutants (Figure 16c-f), suggesting that chlorophyll accumulation appeared to be crucial for sustaining shoot regeneration capacity. Thus, in *hy1-3*, *gun4-2*, *chlh*, and *chli1* mutant root explants the *WUS* expression is not related to shoot regeneration.

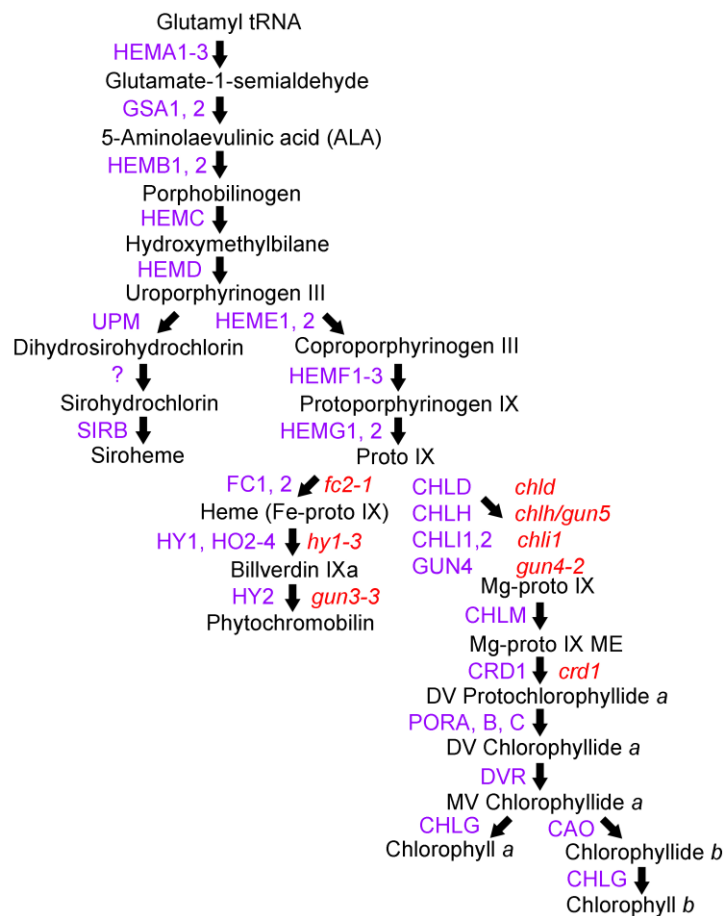


Figure 15: Tetrapyrrole biosynthesis pathway.

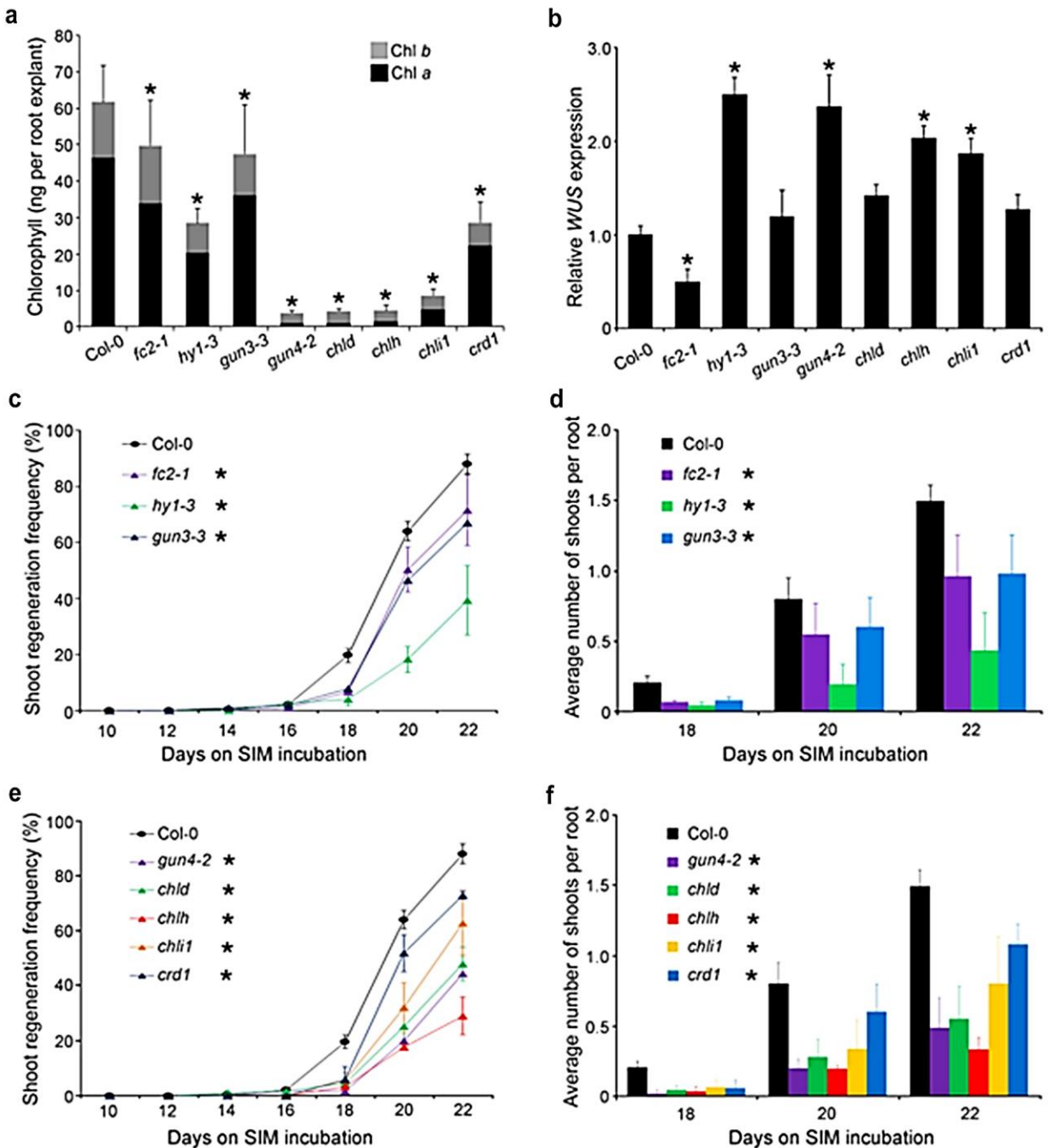


Figure 16: *WUS* expression and *de novo* SAM formation are uncoupled in altered tetrapyrrole mutants. (a) Chlorophyll contents of Col-0, *fc2-1*, *hy1-3*, *gun3-3*, *gun4-2*, *chld*, *chlh*, *chli1*, and *crd1* root explants cultured on SIM for 15 days (b) Relative *WUS* expression in Col-0, *fc2-1*, *hy1-3*, *gun3-3*, *gun4-2*, *chld*, *chlh*, *chli1*, and *crd1* root explants cultured on SIM for 5 days quantified by qRT-PCR (c) Shoot regeneration frequency in Col-0, *fc2-1*, *hy1-3*, and *gun3-3* root explants cultured at indicated time-points on SIM. (d) Shoot regeneration frequency in Col-0, *gun4-2*, *chld*, *chlh*, *chli1*, and *crd1* root explants cultured at indicated time-points on SIM. (e) An average number of shoots per root explant in Col-0, *fc2-1*, *hy1-3*, and *gun3-3*. (f) An average number of shoots per root explant in Col-0, *gun4-2*, *chld*, *chlh*, *chli1*, and *crd1*.

12 Discussion

Plastid-to-nucleus communication, termed retrograde signaling, has been known to regulate gene expression, RNA turnover and splicing (reviewed in Chan et al., 2016; Larkin, 2016). In the case of *gun* mutant screens, photosynthesis-related nuclear gene expression is monitored when chloroplast biogenesis is blocked by norflurazon treatment (Susek et al., 1993; Mochizuki et al., 2001; Larkin et al., 2003; Woodson et al., 2011). We monitored nuclear *WUS* expression when the etioplast-to-chloroplast transition is stimulated by cytokinin in SIM culture and found that *WUS* expression in *hy1-3*, *gun4-2*, *chlh*, and *chli1* is uncoupled from *de novo* SAM formation (Figure 58b). Although tetrapyrrole biosynthesis is controlled under complex regulation, it is reasonable to assume that precursor molecules accumulate as their further conversion is blocked in mutants where the catalytic enzyme gene is disrupted. Our results imply that the accumulation of either Proto IX or heme (or combination of both) takes place in *hy1-3*, *gun4-2*, *chlh*, and *chli1* mutant root explants to positively regulate *WUS* expression. In fact, the level of Proto IX is reported to be increased in *chlh* (Mochizuki et al., 2001), *fc2-1* (Woodson et al., 2015), and *aci5-3*, a semi-dominant loss-of-function mutation in *chli1* (Soldatova et al., 2005). However, Proto IX is unlikely to do so due to the fact that *fc2-1* exhibited compromised *WUS* expression (Figure 58b). It is tempting to speculate that heme, which is decreased in *fc2-1* but likely to be accumulated in the rest of above-mentioned mutants, in particular, *hy1-3*, is the plausible candidate molecule controlling *WUS* expression. Note that *hy1-3* exhibited the most contrasting responses to cytokinin (the highest *WUS* expression and the lowest shoot regeneration). This is in agreement with the previous reports revealing the increased steady-state level of non-covalently bound heme in *hy1* (Woodson et al., 2011) and *aci5-3* seedlings (Soldatova et al., 2005) and reduced steady-state level of heme in *fc2-1* (Scharfenberg et al., 2015; Woodson et al., 2015). It is crucial to explore the co-relationship between heme content and mutants with altered *WUS* expression by measuring tetrapyrrole intermediate molecules in the future. Besides, histological studies in nascent SAM in *hy1-3*, *gun4-2*, *chlh*, or *chli1* mutant root explants on SIM culture will give insights into the coordinated *WUS* expression of nascent SAM development modulated by plastid-to-nucleus communication. Novel regulatory mechanism modulating nuclear SAM master regulator gene expression in response to plastid developmental change stimulated by cytokinin during *de novo* organogenesis is proposed in this study.

Conclusions

For many people having weed in their garden is a kind of nightmare, mainly because of its fundamental attribute and that, its 'immortality' once it is germinated. This ability may be explained by an outstanding regeneration capacity of weed. Regeneration, by definition, is a capability to renew tissue. Arabidopsis, the most popular plant model organism also shares weed characteristics (Meyerowitz, 1989). Thus, for molecular biologists, Arabidopsis with its weed characteristics is a gift from heaven to study regeneration. Exploring the molecular mechanisms behind the great regeneration capacity can provide a powerful tool for the applied field in plant science.

Regeneration capacity depends on the ability to replenish old cells by the new ones. This would be impossible without meristem localized stem cells. The function of the meristem must be precisely controlled to avoid an excessive proliferation of meristematic cells, as well as to hinder the loss of stem cells. Proper regulation of these processes is the basis of the plant body plasticity.

WUSCHEL (WUS), the master key regulator of plant development, is studied for years. Its significance in development was shown in numerous studies (Laux et al., 1996; Leibfried et al., 2005; Yadav et al., 2011; Snipes et al., 2018). Although new regulatory mechanisms of WUS-dependent pathway controlling SAM are regularly emerging, this puzzle is not completely solved, yet. It is very likely that there are other players controlling WUS-dependent pathway and thus development itself.

As the first, we unveiled that the plastid-to-nucleus communication influences the expression of the master SAM regulator WUSCHEL. With our new high-throughput method for chlorophyll quantification from single root explants we evaluated the correlation between greening and shoot development; and between greening and nuclear gene expression. Based on our results we hypothesize that this new regulation pathway might be mediated by the Heme molecule. We are aware that additional experiments are required to test this hypothesis. However, we consider our findings as an important contribution to the current understanding of the WUSCHEL regulatory network.

Besides the WUS-dependent pathway, we also investigated an alternative WUS-independent pathway. In this work, we showed that ERF transcriptional repressors from the group VIII can regulate positioning and maintenance of SAM. We also showed that the quintuple mutant *wus;erf4-1;8;9-1;12* was able to produce SAM *in planta*, but interestingly failed to establish *de novo* meristems in a tissue culture system. These ambiguous results of SAM controlling through ERF repressors show that the development of a plant is a far more complex process and our understanding of the meristem regulatory network remains still elusive.

Our results help to expand the present model of the SAM regulatory network proposed by Lee and Clark (2015). In our extended regulatory network (Figure 17), we placed ERF repressors up-stream from *CUC* and *STM* genes and independently from the WUS-CLV pathway. Results obtained by our group showed that the double *esr1-1;wus* mutant displays an accelerated *wus* phenotype. This, together with further results presented in this work, strongly implies the existence of an additional pathway regulating the maintenance of SAM. Importantly, this novel pathway, especially ERF repressors; seems to be regulated

at the posttranslational level through proteasome-mediated ERF protein degradation, rather than *via* miRNA.

This study focused on the role of ERF repressor in the *de novo* meristem development and maintenance. Discrepancies with hitherto obtained results clearly demonstrate the urgent need for consecutive research in this field. We believe that our work is a novel and significant contribution to our current knowledge of plant development.

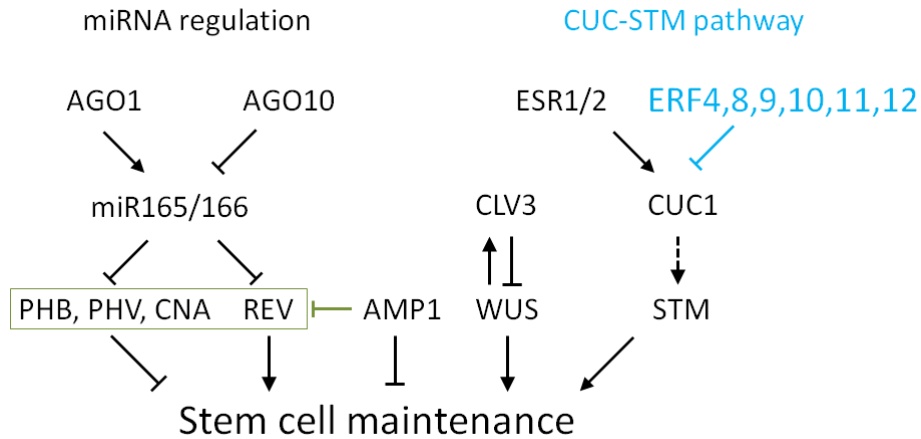


Figure 17: Model of the stem cell regulatory network. Stem cell maintenance is regulated *via* different pathways. 1) miRNA regulation. ARGONAUTE (AGO) proteins 1 and 10 are responsible for the processing of precursor miRNA into their mature form and act antagonistically. miR165/166 cleave their targets – HD-ZIP III TFs as PHABULOSA (PHB), PHAVOLUTA (PHV), CORONA (CNA), and REVOLUTA (REV). PHB, PHV, and CNA block stem cell maintenance whereas REV contributes to stem cell production. ALTERED MERISTEM PROGRAM 1 (AMP1) is also involved in miRNA regulation. AMP1 targets HD-ZIP III TFs but in contrast to miR165/166, AMP1 inhibits HD-ZIP III TFs on translation level. 2) WUSCHEL-CLAVATA regulation pathway, where WUS is a positive signal for stem cell maintenance and also induce CLV3 which in turn inhibits WUS expression. They act in negative-feedback loop. 3) CUC-STM pathway. Here WUS-independent pathway CUC1 induce STM which positively regulates stem cells. CUC1 is positively regulated by ESR1 and ESR2 (ENHANCER OF SHOOT REGENERATION1,2). Adapted from Lee and Clark (2015). On the other hand, CUC1 is repressed by ERF transcriptional repressors.

References

- Atta, R., Laurens, L., Boucheron-Dubuisson, E., Guivarc'h, A., Carnero, E., Giraudat-Pautot, V., Rech, P., and Chriqui, D.** (2009). Pluripotency of Arabidopsis xylem pericycle underlies shoot regeneration from root and hypocotyl explants grown in vitro. *Plant J.* **57**: 626–644.
- Balkunde, R., Kitagawa, M., Xu, X.M., Wang, J., and Jackson, D.** (2017). SHOOT MERISTEMLESS trafficking controls axillary meristem formation, meristem size and organ boundaries in Arabidopsis. *Plant J.* **90**: 435–446.
- Barnes, J.D., Balaguer, L., Manrique, E., Elvira, S., and Davison, A.W.** (1992). A reappraisal of the use of DMSO for the extraction and determination of chlorophylls a and b in lichens and higher plants. *Environ. Exp. Bot.* **32**: 85–100.
- Baurle, I.** (2005). Regulation of WUSCHEL Transcription in the Stem Cell Niche of the Arabidopsis Shoot Meristem. *PLANT CELL ONLINE* **17**: 2271–2280.
- Busch, W. et al.** (2010). Transcriptional Control of a Plant Stem Cell Niche. *Dev. Cell* **18**: 841–853.
- Chan, K.X., Phua, S.Y., Crisp, P., McQuinn, R., and Pogson, B.J.** (2016). Learning the Languages of the Chloroplast: Retrograde Signaling and Beyond. *Annu. Rev. Plant Biol.* **67**: 25–53.
- Che, P., Gingerich, D.J., Lall, S., and Howell, S.H.** (2002). Global and hormone-induced gene expression changes during shoot development in Arabidopsis. *Plant Cell* **14**: 2771–2785.
- Chen, L., Lee, J.H., Weber, H., Tohge, T., Witt, S., Roje, S., Fernie, A.R., and Hellmann, H.** (2013). Arabidopsis BPM proteins function as substrate adaptors to a cullin3-based E3 ligase to affect fatty acid metabolism in plants. *Plant Cell* **25**: 2253–2264.
- Chory, J., Peto, C.A., Ashbaugh, M., Saganich, R., Pratt, L., and Ausubel, F.** (1989). Different Roles for Phytochrome in Etiolated and Green Plants Deduced from Characterization of Arabidopsis thaliana Mutants. *Plant Cell* **1**: 867–880.
- Davis, S.J., Kurepa, J., and Vierstra, R.D.** (1999). The Arabidopsis thaliana HY1 locus, required for phytochrome-chromophore biosynthesis, encodes a protein related to heme oxygenases. *Proc. Natl. Acad. Sci. U. S. A.* **96**: 6541–6546.
- Deforges, J., Reis, R.S., Jacquet, P., Vuarambon, D.J., and Poirier, Y.** (2019). Prediction of regulatory long intergenic non-coding RNAs acting in trans through base-pairing interactions. *BMC Genomics* **20**: 601.
- Espinosa-Ruiz, A., Martínez, C., de Lucas, M., Fàbregas, N., Bosch, N., Caño-Delgado, A.I., and Prat, S.** (2017). TOPLESS mediates brassinosteroid control of shoot boundaries and root meristem development in Arabidopsis thaliana. *Development* **144**: 1619–1628.
- Figuroa, P., Gusmaroli, G., Serino, G., Habashi, J., Ma, L., Shen, Y., Feng, S., Bostick, M., Callis, J., Hellmann, H., and Deng, X.W.** (2005). Arabidopsis has two redundant Cullin3 proteins that are essential for embryo development and that interact with RBX1 and BTB proteins to form multisubunit E3 ubiquitin ligase complexes in vivo. *Plant Cell* **17**: 1180–1195.
- Furuta, K., Kubo, M., Sano, K., Demura, T., Fukuda, H., Liu, Y.G., Shibata, D., and Kakimoto, T.** (2011). The CKH2/PKL chromatin remodeling factor negatively regulates cytokinin responses in arabidopsis calli. *Plant Cell Physiol.* **52**: 618–628.
- Gaillochet, C. and Lohmann, J.U.** (2015). The never-ending story: from pluripotency to plant developmental plasticity. *Development* **142**: 2237–49.
- Gallois, J.-L., Guyon-Debast, A., Lecureuil, A., Vezon, D., Carpentier, V., Bonhomme, S., and Guerche, P.** (2009). The Arabidopsis Proteasome RPT5 Subunits Are Essential for Gametophyte Development and Show Accession-Dependent Redundancy. *PLANT CELL ONLINE* **21**: 442–459.
- Gingerich, D.J., Gagne, J.M., Salter, D.W., Hellmann, H., Estelle, M., Ma, L., and Vierstra, R.D.** (2005). Cullins 3a and 3b assemble with members of the broad complex/tramtrack/bric-a-brac (BTB) protein family to form essential ubiquitin-protein ligases (E3s) in Arabidopsis. *J. Biol. Chem.* **280**: 18810–21.
- Gingerich, D.J., Hanada, K., Shiu, S.-H., and Vierstra, R.D.** (2007). Large-scale, lineage-specific expansion of a bric-a-brac/tramtrack/broad complex ubiquitin-ligase gene family in rice. *Plant Cell* **19**: 2329–2348.
- Gray, W.M., Kepinski, S., Rouse, D., Leyser, O., and Estelle, M.** (2001). Auxin regulates SCFTIR1-dependent degradation of AUX/IAA proteins. *Nature* **414**: 271–276.
- Haecker, A., Groß-Hardt, R., Geiges, B., Sarkar, A., Breuninger, H., Herrmann, M., and Laux, T.** (2004). Expression dynamics of WOX genes mark cell fate decisions during early embryonic patterning in Arabidopsis thaliana. *Development* **131**: 657–668.

- Heidstra, R. and Sabatini, S.** (2014). Plant and animal stem cells: Similar yet different. *Nat. Rev. Mol. Cell Biol.* **15**: 301–312.
- Heo, J.B. and Sung, S.** (2011). Vernalization-mediated epigenetic silencing by a long intronic noncoding RNA. *Science* **331**: 76–9.
- Hu, X., Tanaka, A., and Tanaka, R.** (2013). Simple extraction methods that prevent the artifactual conversion of chlorophyll to chlorophyllide during pigment isolation from leaf samples. *Plant Methods* **9**: 1–13.
- Ikeda, Y., Banno, H., Niu, Q.-W., Howell, S.H., and Chua, N.-H.** (2006). The ENHANCER OF SHOOT REGENERATION 2 gene in Arabidopsis Regulates CUP-SHAPED COTYLEDON 1 at the Transcriptional Level and Controls Cotyledon Development. *Plant Cell Physiol.* **47**: 1443–1456.
- Ikeuchi, M., Sugimoto, K., and Iwase, A.** (2013). Plant Callus: Mechanisms of Induction and Repression. *Plant Cell* **25**: 3159–3173.
- Inskeep, W.P. and Bloom, P.R.** (1985). Extinction Coefficients of Chlorophyll a and b in N,N-Dimethylformamide and 80% Acetone. *PLANT Physiol.* **77**: 483–485.
- Jackson, M.P. and Hewitt, E.W.** (2016). Cellular proteostasis: degradation of misfolded proteins by lysosomes. *Essays Biochem.* **60**: 173–180.
- Kagale, S. and Rozwadowski, K.** (2011). EAR motif-mediated transcriptional repression in plants: An underlying mechanism for epigenetic regulation of gene expression. *Epigenetics* **6**: 141–146.
- Kubalová, I. and Ikeda, Y.** (2017). Chlorophyll Measurement as a Quantitative Method for the Assessment of Cytokinin-Induced Green Foci Formation in Tissue Culture. *J. Plant Growth Regul.* **36**: 516–521.
- Kubalová, I., Zalabák, D., Mičúchová, A., and Ikeda, Y.** (2019). Mutations in tetrapyrrole biosynthesis pathway uncouple nuclear WUSCHEL expression from de novo shoot development in Arabidopsis. *Plant Cell, Tissue Organ Cult.*: 1–7.
- Kumar, P.P. and Loh, C.S.** (2012). Plant tissue culture for biotechnology. In *Plant Biotechnology and Agriculture* (Academic Press), pp. 131–138.
- Larkin, R.M.** (2016). Tetrapyrrole Signaling in Plants. *Front. Plant Sci.* **7**: 1–17.
- Larkin, R.M., Alonso, J.M., Ecker, J.R., and Chory, J.** (2003). GUN4, a regulator of chlorophyll synthesis and intracellular signaling. *Science* **299**: 902–906.
- Laux, T., Mayer, K.F., Berger, J., and Jürgens, G.** (1996). The WUSCHEL gene is required for shoot and floral meristem integrity in Arabidopsis. *Development* **122**: 87–96.
- Lee, C. and Clark, S.E.** (2015). A WUSCHEL-independent stem cell specification pathway is repressed by PHB, PHV and CNA in Arabidopsis. *PLoS One* **10**: e0126006.
- Leibfried, A., To, J.P.C., Busch, W., Stehling, S., Kehle, A., Demar, M., Kieber, J.J., and Lohmann, J.U.** (2005). WUSCHEL controls meristem function by direct regulation of cytokinin-inducible response regulators. *Nature* **438**: 1172–1175.
- Long, J.A., Moan, E.I., Medford, J.I., and Barton, M.K.** (1996). A member of the KNOTTED class of homeodomain proteins encoded by the STM gene of Arabidopsis. *Nature* **379**: 66–69.
- Lopez-Molina, L., Mongrand, S., Kinoshita, N., and Chua, N.H.** (2003). AFP is a novel negative regulator of ABA signaling that promotes ABI5 protein degradation. *Genes Dev.* **17**: 410–418.
- Mayer, K.F.X., Schoof, H., Haecker, A., Lenhard, M., Jürgens, G., and Laux, T.** (1998). Role of WUSCHEL in regulating stem cell fate in the Arabidopsis shoot meristem. *Cell* **95**: 805–815.
- Mazzucotelli, E., Belloni, S., Marone, D., De Leonardi, A., Guerra, D., Di Fonzo, N., Cattivelli, L., and Mastrangelo, A.** (2006). The e3 ubiquitin ligase gene family in plants: regulation by degradation. *Curr. Genomics* **7**: 509–22.
- Meyerowitz, E.M.** (1989). Arabidopsis, a useful weed. *Cell* **56**: 263–269.
- Mochizuki, N., Brusslan, J.A., Larkin, R., Nagatani, A., and Chory, J.** (2001). Arabidopsis genomes uncoupled 5 (GUN5) mutant reveals the involvement of Mg-chelatase H subunit in plastid-to-nucleus signal transduction. *Proc. Natl. Acad. Sci.* **98**: 2053–2058.
- Nakano, T., Suzuki, K., Fujimura, T., and Shinshi, H.** (2006). Genome-wide analysis of the ERF gene family in Arabidopsis and rice. *Plant Physiol.* **140**: 411–432.
- Ohme-Takagi, M. and Shinshi, H.** (1995). Ethylene-inducible DNA binding proteins that interact with an ethylene-responsive element. *Plant Cell* **7**: 173–182.
- Pandey, R., Müller, A., Napoli, C.A., Selinger, D.A., Pikaard, C.S., Richards, E.J., Bender, J., Mount, D.W., and Jorgensen, R.A.** (2002). Analysis of histone acetyltransferase and histone deacetylase families of Arabidopsis thaliana suggests functional diversification of chromatin modification among multicellular eukaryotes. *Nucleic Acids Res.* **30**: 5036–5055.

- Patra, B., Pattanaik, S., and Yuan, L.** (2013). Proteolytic degradation of the flavonoid regulators, TRANSPARENT TESTA8 and TRANSPARENT TESTA GLABRA1, in Arabidopsis is mediated by the ubiquitin/26Sproteasome system. *Plant Signal. Behav.* **8**: e25901.
- Peter, E. and Grimm, B.** (2009). GUN4 is required for posttranslational control of plant tetrapyrrole biosynthesis. *Mol. Plant* **2**: 1198–210.
- Reynolds, N., O’Shaughnessy, A., and Hendrich, B.** (2013). Transcriptional repressors: multifaceted regulators of gene expression. *Development* **140**: 505–512.
- Riefler, M., Novak, O., Strnad, M., and Schmülling, T.** (2006). Arabidopsis cytokinin receptor mutants reveal functions in shoot growth, leaf senescence, seed size, germination, root development, and cytokinin metabolism. *Plant Cell* **18**: 40–54.
- Scharfenberg, M., Mittermayr, L., von Roepenack-Lahaye, E., Schlicke, H., Grimm, B., Leister, D., and Kleine, T.** (2015). Functional characterization of the two ferrochelatases in Arabidopsis thaliana. *Plant. Cell Environ.* **38**: 280–298.
- Snipes, S.A., Rodriguez, K., DeVries, A.E., Miyawaki, K.N., Perales, M., Xie, M., and Reddy, G.V.** (2018). Cytokinin stabilizes WUSCHEL by acting on the protein domains required for nuclear enrichment and transcription. *PLoS Genet.* **14**: e1007351.
- Soldatova, O., Apchelimov, A., Radukina, N., Ezhova, T., Shestakov, S., Ziemann, V., Hedtke, B., and Grimm, B.** (2005). An Arabidopsis mutant that is resistant to the protoporphyrinogen oxidase inhibitor acifluorfen shows regulatory changes in tetrapyrrole biosynthesis. *Mol. Genet. Genomics* **273**: 311–318.
- Somssich, M., Je, B. II, Simon, R., and Jackson, D.** (2016). CLAVATA-WUSCHEL signaling in the shoot meristem. *Development* **143**: 3238–3248.
- Song, C.-P. and Galbraith, D.W.** (2006). AtSAP18, An Orthologue of Human SAP18, is Involved in the Regulation of Salt Stress and Mediates Transcriptional Repression in Arabidopsis. *Plant Mol. Biol.* **60**: 241–257.
- Sonoda, Y., Yao, S.-G., Sako, K., Sato, T., Kato, W., Ohto, M., Ichikawa, T., Matsui, M., Yamaguchi, J., and Ikeda, A.** (2007). SHA1, a novel RING finger protein, functions in shoot apical meristem maintenance in Arabidopsis. *Plant J.* **50**: 586–596.
- Stiegler, J.C., Bell, G.E., and Maness, N.O.** (2005). Comparison of Acetone and *N,N*-Dimethylformamide for Pigment Extraction in Turfgrass. *Commun. Soil Sci. Plant Anal.* **35**: 1801–1813.
- Susek, R.E., Ausubel, F.M., and Chory, J.** (1993). Signal transduction mutants of Arabidopsis uncouple nuclear CAB and RBCS gene expression from chloroplast development. *Cell* **74**: 787–99.
- Valvekens, D., Montagu, M. V., and Lijsebettens, M. V.** (1988). Agrobacterium tumefaciens-mediated transformation of Arabidopsis thaliana root explants by using kanamycin selection. *Proc. Natl. Acad. Sci.* **85**: 5536–5540.
- Wang, J., Meng, X., Yuan, C., Harrison, A.P., and Chen, M.** (2016). The roles of cross-talk epigenetic patterns in *Arabidopsis thaliana*. *Brief. Funct. Genomics* **15**: 278–287.
- Weber, H. and Hellmann, H.** (2009). Arabidopsis thaliana BTB/POZ-MATH proteins interact with members of the ERF/AP2 transcription factor family. *FEBS J.* **276**: 6624–6635.
- Woodson, J.D., Joens, M.S., Sinson, A.B., Gilkerson, J., Salomé, P.A., Weigel, D., Fitzpatrick, J.A., and Chory, J.** (2015). Ubiquitin facilitates a quality-control pathway that removes damaged chloroplasts. *Science* **350**: 450–454.
- Woodson, J.D., Perez-Ruiz, J.M., and Chory, J.** (2011). Heme synthesis by plastid ferrochelatase I regulates nuclear gene expression in plants. *Curr. Biol.* **21**: 897–903.
- Yadav, R.K., Perales, M., Gruel, J., Girke, T., Jönsson, H., and Venugopala Reddy, G.** (2011). WUSCHEL protein movement mediates stem cell homeostasis in the Arabidopsis shoot apex. *Genes Dev.* **25**: 2025–2030.
- Yang, Z., Tian, L., Latoszek-Green, M., Brown, D., and Wu, K.** (2005). Arabidopsis ERF4 is a transcriptional repressor capable of modulating ethylene and abscisic acid responses. *Plant Mol. Biol.* **58**: 585–596.
- Zhang, T.-Q., Lian, H., Zhou, C.-M., Xu, L., Jiao, Y., and Wang, J.-W.** (2017). A Two-Step Model for de Novo Activation of WUSCHEL during Plant Shoot Regeneration. *Plant Cell* **29**: 1073–1087.

Curriculum vitae

Ivona Kubalová

ORCID iD [0000-0002-5673-9715](https://orcid.org/0000-0002-5673-9715)

Date of Birth 20th May 1989

Nationality Slovak

Education:

2013-present Ph.D. program in Biochemistry, Palacký University in Olomouc
Research project: Genetic control of pluripotency in plant

2013 MSc. in Genetics, Comenius University in Bratislava, Slovak Republic

2011 BSc. in Biology, Comenius University in Bratislava, Slovak Republic

Professional career:

Since 2018 Researcher, Leibniz Institute of Plant Genetics and Crop Plant Research (IPK)
Gatersleben, Germany

2013-2018 Student research assistant, Centre of the Region Haná for Biotechnological and
Agricultural Research, Faculty of Science, Palacký University in Olomouc, Czech
Republic

Research stays:

07.06.2016 – 19.10.2016 Research stay in the laboratory of Prof. Andreas Houben, Research
Group Chromosome Structure and Function, Leibniz-Institut für Pflanzengenetik und
Kulturpflanzenforschung (IPK).

04.04.2017 – 30.06.2017 Research stay in the laboratory of Prof. Andreas Houben, Research
Group Chromosome Structure and Function, Leibniz-Institut für Pflanzengenetik und
Kulturpflanzenforschung (IPK). The stay was supported by Erasmus+ fellowship.

List of publications

Kubalová I., Zalabák D., Mičúchová A. et al. (2019) Mutations in Tetrapyrrole Biosynthesis Pathway Uncouple Nuclear *WUSCHEL* Expression from *de novo* Shoot Development in *Arabidopsis*, Plant Cell Tiss Organ Cult
doi.org/10.1007/s11240-019-01680-w

Kubalová I., Ikeda Y. (2016) Chlorophyll measurement as a quantitative method for the assessment of cytokinin-induced green foci formation in tissue culture, J. Plant Growth Regul. 36, 516–521; [doi: 10.1007/s00344-016-9637-7](https://doi.org/10.1007/s00344-016-9637-7)

Jiskrová E., Kubalová I., Ikeda Y. (2015) What turns on and off the cytokinin metabolism and beyond. In: Poltronieri P., Hong Y. (eds) Applied Plant Genomics and Biotechnology, Elsevier, pp 20-36. ISBN: 978-0-08-100068-7.

Selected conferences

2014 Genetic Control of Pluripotency

Ivona Kubalová, oral presentation

Konference Nové biotechnologie ve farmacii, biologii a medicíně 2014, Kouty nad Desnou, Česká republika

Impact of ESR2 on Auxin and Cytokinin Crosstalks during Shoot Development

Yoshihisa Ikeda and Ivona Kubalová, poster presentation

Plant science student conference (PSSC), IPK Gatersleben, Germany

Impact of ESR2 on Auxin and Cytokinin Crosstalks during Shoot Regeneration

Yoshihisa Ikeda and Ivona Kubalová, poster presentation

International Symposium on Auxins and Cytokinins in Plant Development – ACPD, Prague, Czech Republic

2018 Mutations in Tetrapyrrole Biosynthesis Pathway Uncouple Nuclear *Wuschel* Expression from *De Novo* Shoot Development in *Arabidopsis*

Ivona Kubalová, David Zalabák, Alžbeta Mičúchová, and Yoshihisa Ikeda, poster presentation

International Plant Molecular Biology 2018 (IPMB), Montpellier, France